

PROBIOTICS, PREBIOTICS, POSTBIOTICS AND INTESTINAL BARRIER FUNCTION

EDITED BY: Huaxi Yi, Qixiao Zhai, Yanling Hao and Jiong-Wei Wang
PUBLISHED IN: *Frontiers in Immunology* and *Frontiers in Nutrition*





frontiers

Frontiers eBook Copyright Statement

The copyright in the text of individual articles in this eBook is the property of their respective authors or their respective institutions or funders. The copyright in graphics and images within each article may be subject to copyright of other parties. In both cases this is subject to a license granted to Frontiers.

The compilation of articles constituting this eBook is the property of Frontiers.

Each article within this eBook, and the eBook itself, are published under the most recent version of the Creative Commons CC-BY licence.

The version current at the date of publication of this eBook is CC-BY 4.0. If the CC-BY licence is updated, the licence granted by Frontiers is automatically updated to the new version.

When exercising any right under the CC-BY licence, Frontiers must be attributed as the original publisher of the article or eBook, as applicable.

Authors have the responsibility of ensuring that any graphics or other materials which are the property of others may be included in the CC-BY licence, but this should be checked before relying on the CC-BY licence to reproduce those materials. Any copyright notices relating to those materials must be complied with.

Copyright and source acknowledgement notices may not be removed and must be displayed in any copy, derivative work or partial copy which includes the elements in question.

All copyright, and all rights therein, are protected by national and international copyright laws. The above represents a summary only. For further information please read Frontiers' Conditions for Website Use and Copyright Statement, and the applicable CC-BY licence.

ISSN 1664-8714

ISBN 978-2-88974-719-1

DOI 10.3389/978-2-88974-719-1

About Frontiers

Frontiers is more than just an open-access publisher of scholarly articles: it is a pioneering approach to the world of academia, radically improving the way scholarly research is managed. The grand vision of Frontiers is a world where all people have an equal opportunity to seek, share and generate knowledge. Frontiers provides immediate and permanent online open access to all its publications, but this alone is not enough to realize our grand goals.

Frontiers Journal Series

The Frontiers Journal Series is a multi-tier and interdisciplinary set of open-access, online journals, promising a paradigm shift from the current review, selection and dissemination processes in academic publishing. All Frontiers journals are driven by researchers for researchers; therefore, they constitute a service to the scholarly community. At the same time, the Frontiers Journal Series operates on a revolutionary invention, the tiered publishing system, initially addressing specific communities of scholars, and gradually climbing up to broader public understanding, thus serving the interests of the lay society, too.

Dedication to Quality

Each Frontiers article is a landmark of the highest quality, thanks to genuinely collaborative interactions between authors and review editors, who include some of the world's best academicians. Research must be certified by peers before entering a stream of knowledge that may eventually reach the public - and shape society; therefore, Frontiers only applies the most rigorous and unbiased reviews.

Frontiers revolutionizes research publishing by freely delivering the most outstanding research, evaluated with no bias from both the academic and social point of view. By applying the most advanced information technologies, Frontiers is catapulting scholarly publishing into a new generation.

What are Frontiers Research Topics?

Frontiers Research Topics are very popular trademarks of the Frontiers Journals Series: they are collections of at least ten articles, all centered on a particular subject. With their unique mix of varied contributions from Original Research to Review Articles, Frontiers Research Topics unify the most influential researchers, the latest key findings and historical advances in a hot research area! Find out more on how to host your own Frontiers Research Topic or contribute to one as an author by contacting the Frontiers Editorial Office: frontiersin.org/about/contact

PROBIOTICS, PREBIOTICS, POSTBIOTICS AND INTESTINAL BARRIER FUNCTION

Topic Editors:

Huaxi Yi, Ocean University of China, China

Qixiao Zhai, Jiangnan University, China

Yanling Hao, China Agricultural University, China

Jiong-Wei Wang, National University of Singapore, Singapore

Citation: Yi, H., Zhai, Q., Hao, Y., Wang, J.-W., eds. (2022). Probiotics, Prebiotics, Postbiotics and Intestinal Barrier Function. Lausanne: Frontiers Media SA.
doi: 10.3389/978-2-88974-719-1

Table of Contents

- 04 A Novel Bacteriocin From *Lactobacillus Pentosus* ZFM94 and Its Antibacterial Mode of Action**
Mengdi Dai, Yanran Li, Luyao Xu, Danli Wu, Qingqing Zhou, Ping Li and Qing Gu
- 12 The Protection of *Lactiplantibacillus plantarum* CCFM8661 Against Benzopyrene-Induced Toxicity via Regulation of the Gut Microbiota**
Leilei Yu, Lingyu Zhang, Hui Duan, Ruohan Zhao, Yue Xiao, Min Guo, Jianxin Zhao, Hao Zhang, Wei Chen and Fengwei Tian
- 24 Consumption of Butylated Starch Alleviates the Chronic Restraint Stress-Induced Neurobehavioral and Gut Barrier Deficits Through Reshaping the Gut Microbiota**
Peijun Tian, Huiyue Zhu, Xin Qian, Ying Chen, Zheng Wang, Jianxin Zhao, Hao Zhang, Gang Wang and Wei Chen
- 32 Synergistic Protective Effect of Konjac Mannan Oligosaccharides and *Bacillus subtilis* on Intestinal Epithelial Barrier Dysfunction in Caco-2 Cell Model and Mice Model of Lipopolysaccharide Stimulation**
Lupeng Chen, Shuai Zhang, Shi Wu, Zhuqing Ren, Guoquan Liu and Jian Wu
- 45 Sodium Acetate Inhibit TGF- β 1-Induced Activation of Hepatic Stellate Cells by Restoring AMPK or c-Jun Signaling**
Weiwei Li, Mingjuan Deng, Jiahui Gong, Xiaoying Zhang, Shaoyang Ge and Liang Zhao
- 59 Short-Chain Fatty Acids Alleviate Hepatocyte Apoptosis Induced by Gut-Derived Protein-Bound Uremic Toxins**
Mingjuan Deng, Xingqi Li, Weiwei Li, Jiahui Gong, Xiaoying Zhang, Shaoyang Ge and Liang Zhao
- 71 *Lactobacillus plantarum* CCFM1143 Alleviates Chronic Diarrhea via Inflammation Regulation and Gut Microbiota Modulation: A Double-Blind, Randomized, Placebo-Controlled Study**
Bo Yang, Yue Yue, Yang Chen, Mengfan Ding, Bowen Li, Linlin Wang, Qun Wang, Catherine Stanton, R. Paul Ross, Jianxin Zhao, Hao Zhang and Wei Chen
- 83 Mannan Oligosaccharides Application: Multipath Restriction From *Aeromonas hydrophila* Infection in the Skin Barrier of Grass Carp (*Ctenopharyngodon idella*)**
Zhiyuan Lu, Lin Feng, Wei-Dan Jiang, Pei Wu, Yang Liu, Jun Jiang, Sheng-Yao Kuang, Ling Tang, Shu-Wei Li, Xiang-An Liu, Cheng-Bo Zhong and Xiao-Qiu Zhou
- 97 A Potential Probiotic for Diarrhea: *Clostridium tyrobutyricum* Protects Against LPS-Induced Epithelial Dysfunction via IL-22 Produced By Th17 Cells in the Ileum**
Zhiping Xiao, Lujie Liu, Xun Pei, Wanjing Sun, Yuyue Jin, Shang-Tian Yang and Minqi Wang
- 112 Evaluation of the Anti-Aging Effects of a Probiotic Combination Isolated From Centenarians in a SAMP8 Mouse Model**
Xin Fang, Mengyun Yue, Jing Wei, Yun Wang, Daojun Hong, Bo Wang, Xiaoting Zhou and Tingtao Chen



A Novel Bacteriocin From *Lactobacillus Pentosus* ZFM94 and Its Antibacterial Mode of Action

Mengdi Dai, Yanran Li, Luyao Xu, Danli Wu, Qingqing Zhou, Ping Li* and Qing Gu*

Key Laboratory for Food Microbial Technology of Zhejiang Province, College of Food Science and Biotechnology, Zhejiang Gongshang University, Hangzhou, China

OPEN ACCESS

Edited by:

Huaxi Yi,
Ocean University of China, China

Reviewed by:

Xin Lu,
Northwest A and F University, China

Fei Liu,

Northeast Agricultural

University, China

Gang Wang,
Jiangnan University, China

*Correspondence:

Ping Li
ping-biology@outlook.com
Qing Gu
guqing2002@hotmail.com

Specialty section:

This article was submitted to
Nutritional Immunology,
a section of the journal
Frontiers in Nutrition

Received: 17 May 2021

Accepted: 21 June 2021

Published: 23 July 2021

Citation:

Dai M, Li Y, Xu L, Wu D, Zhou Q, Li P
and Gu Q (2021) A Novel Bacteriocin
From *Lactobacillus Pentosus* ZFM94
and Its Antibacterial Mode of Action.
Front. Nutr. 8:710862.
doi: 10.3389/fnut.2021.710862

Bacteriocins are bioactive antimicrobial peptides synthesized in the ribosome of numerous bacteria and released extracellularly. Pentocin ZFM94 produced by *Lactobacillus pentosus* (*L. pentosus*) ZFM94, isolated from infant feces with strong antibacterial activity, was purified by ammonium sulfate precipitation, dextran gel chromatography, and reverse-phase high-performance liquid chromatography (RP-HPLC). The molecular mass of the purified bacteriocin was 3,547.74 Da determined by matrix-assisted laser desorption/ionization time-of-flight mass spectrometry (MALDI-TOF MS). Pentocin ZFM94 exhibited broad-spectrum antimicrobial activity against tested Gram-positive and Gram-negative bacteria, and the minimal inhibitory concentrations (MICs) of *Micrococcus luteus* (*M. luteus*) 10,209, *Staphylococcus aureus* (*S. aureus*) D48, and *Escherichia coli* (*E. coli*) DH5 α were 1.75, 2.00, and 2.50 μ m, respectively. Pentocin ZFM94 was heat-stable (30 min at 80°C) and showed inhibitory activity over a wide pH range (5.00–7.00). It could be degraded by trypsin and pepsin, but not by amylase, lysozyme, lipase, and ribonuclease A. Fluorescence leakage assay showed that pentocin ZFM94 induced disruption of the cell membrane and caused leakage of cellular content. Furthermore, lipid II was not an antibacterial target of pentocin ZFM94. This study laid the foundation for further development and utilization of *L. pentosus* ZFM94 and its bacteriocin.

Keywords: bacteriocin, purification, pentocin ZFM94, antibacterial activity, mode of action

INTRODUCTION

Bacteriocins are ribosomally synthesized peptides that in most cases they exhibit antibacterial activity against bacteria that are closely related to the producing bacteria. As for food corruption, the commonly used method is to add preservatives. Although, the toxicity of the preservatives now used is low, the toxicity accumulates and damages the body when taken in excess. Non-toxic natural preservatives solve this problem perfectly. The bacteriocins are of very high perspective because they may not only be used for food biopreservation but also have the potential to be utilized as antibiotics, exploited in animal healthcare and marine environment (1). Bacteriocins are usually divided into four groups (2). Class I bacteriocins, known as lantibiotic, generally have a molecular weight of <5 kDa (3), such as lantionine, β -12 methyllanthionine, dehydrobutyrine, dehydroalanine, and labyrinthine. Class I is further subdivided into class Ia (lantibiotics), class Ib (labyrinthopeptins), and class Ic (sanctibiotics). Nisin is a most popular class I bacteriocin (4). Class II bacteriocins are called non-lantibiotics with molecular weight <10 kDa (5), which contain

30–60 amino acids with thermal stability, and Class II bacteriocins can be further subdivided into class IIa (pediocin-like bacteriocins), class IIb (two-peptide unmodified bacteriocins), class IIc (circular bacteriocins), and class IId (unmodified, linear, and non-pediocin-like bacteriocins). Pediocin-like bacteriocins are the most dominant class IIa bacteriocins (4). Class III bacteriocins are non-lantibiotics with heat sensitivity, and their molecular weight is generally >30 kDa (6). Colicin is one of the examples of class III bacteriocins produced by *Escherichia coli*. Class III bacteriocins also include helveticin M, helveticin J, and enterolysin A produced by *Lactobacillus crispatus* and *Lactobacillus helveticus*, respectively (4). Class IV bacteriocins are comprised of lipid or carbohydrate groups (7). Besides, many bacteriocin-producing strains have been found, such as *Streptococcus lactis*, *Listeria monocytogenes* (*L. monocytogenes*), and *Staphylococcus aureus* (*S. aureus*) (4).

Lactic acid bacteria (LAB) are food-grade microorganisms recognized by the Food and Drug Administration (FDA). Recently, the isolation of bacteriocins has become a research hotspot. The most well-known bacteriocin produced by LAB is nisin (8). It is an FDA-approved and generally regarded as safe (GRAS) peptide with recognized potential for food preservation, which has been commercialized in more than 50 countries (9). Nisin was effective in the treatment of dental caries and ulcers in humans, and mastitis in cattle (8, 10).

Studies on the mode of action and target of bacteriocins can lay a foundation for its applications. The action mode of bacteriocins can generally be grouped into two types. The first one is acting on the cell membrane of the bacteria, which can be further divided into two subclasses: targeting cell membrane protein (11) and non-specific “membrane perforation.” Nisin can inhibit the growth of Gram-positive bacteria through two antibacterial mechanisms. Lipid II, as a membrane-anchored cell wall precursor, is essential for the biosynthesis of the bacterial cell wall. When nisin binds with lipid II, the biosynthesis of the cell wall is inhibited, resulting in the death of the bacteria (12). Nisin can also cause the loss of proton motive force (PMF) of the cell membrane through the formation of non-selective transmembrane pores at micromolar concentrations (13). The second type is directed to the destruction of non-membrane substances in cells, for example, the target of microcin B17 is DNA gyrase (14).

Although, bacteriocinogenic *Lactobacillus Pentosus* (*L. pentosus*) has been isolated from different products such as fermented meat and cereals, there are few reports on the purification of bacteriocin from *L. pentosus* (15–19). *Lactobacillus Pentosus* ZFM94 was isolated from the feces of a healthy infant with strong antibacterial activities and probiotic properties (20). In this study, a three-step method was established to purify a novel bacteriocin (pentocin ZFM94) from the cell-free supernatant (CFS) of *L. pentosus* ZFM94. The antibacterial spectrum and minimum inhibitory concentrations (MICs) of pentocin ZFM94 were determined. Meanwhile, the effects of temperature, pH, and enzyme on the stability of pentocin ZFM94 were studied. Finally, the leakage experiment and agar well-diffusion method were used to explore the action mode of pentocin ZFM94 and its binding site with lipid II.

MATERIALS AND METHODS

Strains and Culture Conditions

Lactobacillus pentosus ZFM94 was isolated from the feces of a healthy infant, deposited at the China Center for Type Culture Collection (CCTCC) with the strain number of CCTCC NO: M 2016632, and cultured in de Man, Rogosa, and Sharpe (MRS) broth at 37°C. The indicator strains are listed in **Table 1**.

Purification of Bacteriocin

A three-step method, including ammonium sulfate precipitation, Sephadex™ G-25, and reverse-phase high-performance liquid chromatography (RP-HPLC) were established to purify bacteriocin. Four liters of clarified MRS broth was inoculated (1%) with *L. pentosus* ZFM94 and incubated for 18–20 h at 37°C. The culture was centrifuged (Beckman, USA) at 8,000 rpm and 4°C for 20 min. The CFS was precipitated with saturated ammonium sulfate (gradient from 10 to 90%). The protein precipitations were collected by centrifugation (8,000 rpm, 4°C, 20 min), dissolved in 50 mm phosphate buffer saline (PBS, pH 3.69), and desalted by dialysis (1 kDa cutoff membrane, Sangon, China). The active fractions were purified by Sephadex G-25 (GE Healthcare, 1.6 × 80 cm) equilibrated and eluted with ultrapure water at 1 ml/min. The eluent was collected every 3 min until no absorbance was detected at 280 nm. Next, the active ingredient was concentrated by a vacuum rotary evaporator (Marin Christ, Germany). Subsequently, it was introduced into the RP-HPLC system (Waters, USA) equipped with a RP C18 column (YMC-Pack ODS-AQ, 150 × 20 mm L.D.). The buffer A was 0.05% trifluoroacetic acid (TFA)/distilled water (v/v), and buffer B was 0.05% TFA/acetonitrile (v/v). Gradient elution ranged from 95% buffer A to 95% buffer B, with a flow rate of 4.0 ml/min. Fractions with antibacterial activity were analyzed by an analytical RP-HPLC system (Waters 2489 Detector, USA) using RP C18 column (YMC-Pack ODS-AQ, 150 × 4.6 mm L.D., Japan) after removing acetonitrile by evaporation. Protein concentration was determined by a bicinchoninic acid (BCA) protein assay kit according to the instructions of the manufacturer (Takara, Dalian, China).

Determination of the Molecular Weight of Pentocin ZFM94

The rough molecular mass of sample fraction with antibacterial activity prepared by RP-HPLC was analyzed by Tricine-sodium dodecyl sulfate–polyacrylamide gel electrophoresis (SDS-PAGE) (5% concentrated glue and 18% separation glue). The antibacterial activity and a low molecular weight marker were run at 80 V for 30 min and 120 V during the rest of the separation. After completion of the run, the gel was stained with Coomassie Brilliant Blue G-250 and destained by ethyl alcohol acetic acid solution. Matrix-assisted laser desorption/ionization time-of-flight mass spectrometry (MALDI-TOF MS) (ABSciex 5800) was further used to determine the accurate molecular weight of this sample (21), which was operated in positive ion mode. The α -cyano-4-hydroxy-cinnamic acid (CHCA) solution was used as the matrix. In brief, 1 μ l of the sample was dried on

TABLE 1 | Inhibition spectrum of pentocin ZFM94 against different bacterial indicator strains.

Indicator strains	Growth condition	Antimicrobial activity	Sources
<i>Micrococcus luteus</i> 10209	LB at 30°C	+++	Laboratory preservation
<i>Staphylococcus aureus</i> D48	LB at 37°C	+++	Laboratory preservation
<i>Staphylococcus carnosus</i> pCA44	LB at 37°C	++	Laboratory preservation
<i>Staphylococcus carnosus</i> pot20	LB at 37°C	+	Laboratory preservation
<i>Listeria monocytogenes</i> LM1	LB at 37°C	+	Laboratory preservation
<i>Bacillus subtilis</i> BAS2	LB at 37°C	–	Laboratory preservation
<i>Escherichia coli</i> DH5 α	LB at 37°C	+++	Laboratory preservation
<i>Salmonella paratyphi</i> -A CMCC50093	LB at 37°C	–	National Center for Medical Culture Collections (CMCC)
<i>Salmonella paratyphi</i> -B CMCC50094	LB at 37°C	–	National Center for Medical Culture Collections (CMCC)
<i>Salmonella enterica</i> subsp. <i>enterica</i> ATCC14028	LB at 37°C	+	American Type Culture Collection (ATCC)
<i>Saccharomyces cerevisiae</i> SM190	YPD at 28°C	+	Laboratory preservation

Inhibitory zone diameter (mm): +++ 22–25, ++ 18–21, + 14–17, – 10–13, – no inhibition.

the sample target plate, and then 0.6 μ l of CHCA was added after natural drying for the MALDI analysis.

Antibacterial Spectrum and MICs of Pentocin ZFM94

The antibacterial spectrum of pentocin ZFM94 after purification was detected by the agar well-diffusion method (22). Soft agar of each medium was inoculated with 10^6 colony-forming units (CFU)/ml of each indicator strain (Table 1) and mixed well, and 8 mm diameter wells were punched with Oxford Cups in the plates. Every well was filled with 100 μ l of 10 μ M pentocin ZFM94, and the plates were incubated overnight at 37°C. The diameter of the inhibition zones (mm) around the wells was measured.

According to the results of the antibacterial spectrum, MICs of pentocin ZFM94 on *S. aureus* D48, *Micrococcus luteus* 10209, and *E. coli* DH5 α were determined by tube method (23). The concentration gradient was 0, 0.10, 0.20, 0.50, 0.875, 1.75, 2.00, 2.50, 3.00, and 10.00 μ M. The absorbance was measured by an ultraviolet spectrophotometer (OLYMPUS, Japan). Each concentration was carried out in triplicate.

Stability of Pentocin ZFM94 on pH, Heat, and Enzyme Conditions

Purified pentocin ZFM94 was prepared at a concentration of 15 μ g/m and was used for testing the effects of heat, pH, and enzymes. To determine thermal stability, the purified pentocin ZFM94 was heated to 50, 60, 70, 80, 90, 100, and 121°C for 30 min, respectively, and then cooled to room temperature. To evaluate the susceptibility of pentocin ZFM94 to different pH values, the pH of purified peptide solution was adjusted to 2–10 using 1 M hydrochloric acid (HCl) and 1 M sodium hydroxide (NaOH), respectively. The above samples were then incubated at 4°C for 2 h and adjusted to an initial pH of 3.69. For proteolytic enzyme treatments, pentocin ZFM94 was treated

with lysozyme, ribonuclease A, lipase, papain, α -amylase, α -chymotrypsin, pepsin, and trypsin at the final concentration of 1 mg/ml, under the optimal temperature and pH of each enzyme for 2 h, and then, the pH was adjusted to initial pH of 3.69. The activity of residual anti-*M. luteus* 10209 was calculated by the agar well-diffusion test. An untreated peptide sample was taken as a control.

Analysis of Transmembrane Electrical Potential

Fluorescence leakage test was used to measure transmembrane electrical potential ($\Delta\Psi$) (24), and the response value of the cell membrane probe [3, 3-dipropylthiadicarbocyanine iodide, DisC2(5)] was measured by a fluorescence spectrophotometer (Agilent, USA). Luria-Bertani (LB) broth (20 ml) was inoculated with a 1% overnight culture of *M. luteus* 10209. The inoculated broth was grown until it reached the exponential phase of growth ($OD_{600} = 0.6$ – 0.8). Cells were collected by centrifugation at 4,000 rpm and 4°C for 30 min, washed twice with buffer (250 mM glucose, 5 mM magnesium sulfate ($MgSO_4$), 10 mM tripotassium phosphate (K_3PO_4), and 100 mM potassium chloride (KCl), pH 7.0), and dissolved in 2 ml of the same buffer, by adding 20 μ l strain and 2 μ l DisC2(5) into 2 ml buffer in order. When the detected fluorescence value was stable, pentocin ZFM94 with final concentrations of 1.75 and 8.75 μ M was added, respectively. The same volume of 0.05% acetic acid was used as a negative control.

Study on the Binding of Pentocin ZFM94 to Lipid II

Studies have shown that lipid II was the target of nisin (25), and the combination of lipid II and nisin can mediate the formation of pores. Nisin and pentocin ZFM94 were mixed with lipid II, respectively. The final concentration of nisin or pentocin ZFM94 was 10 μ M, while the concentration of lipid II was 20 μ M. The

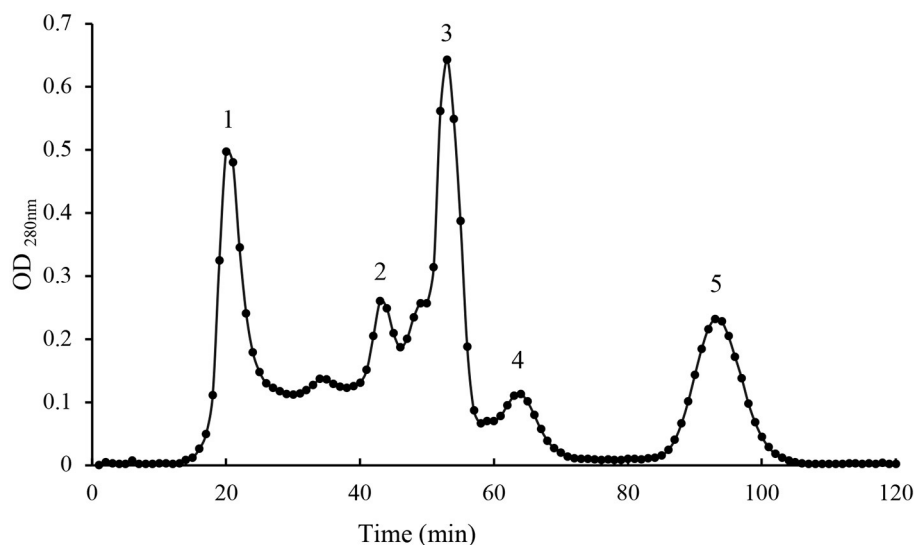


FIGURE 1 | Gel filtration chromatography peak of active fractions.

mixture was maintained at 4°C for 1 h. The changes in the antibacterial activity were detected by the agar well-diffusion method. *Micrococcus luteus* 10209 was used as the indicator. Then, the size of the inhibition zone was observed.

RESULTS

Purification of Bacteriocin

Pentocin ZFM94 was purified from a 4 L culture supernatant. The obtained precipitate had good antibacterial activity when the saturation of ammonium sulfate was 40%. Then, Sephadex G-25 was used to separate and acquire the range between 1 and 5 kDa. Ultrapure water was used as a buffer. When the sample was added to the dextran gel chromatography, it was separated according to the molecular weight. About 40% ammonium sulfate precipitation component can be well-separated from Sephadex G-25. Five peaks were obtained as shown in **Figure 1**. Only peak 3 had antibacterial activity against *M. luteus* 10209.

After purification by Sephadex G-25, RP-HPLC was used to purify the active ingredient. The active ingredient was obtained at a retention time of 22–23 min using the preparative C18 column. Analytical column C18 was used to analyze bacteriocin, and only a single peak at 34.129 min was observed, as shown in **Figure 2**. The purity of bacteriocin obtained by the area normalization method was 98.70%. The concentration of bacteriocin was 3.65 mg/L.

Molecular Weight Determination of Purified Bacteriocin

As we can see from the result of Sephadex G-25, the molecular weight of purified bacteriocin was <5 kDa. Tricine-SDS-PAGE analysis was performed with purified bacteriocin. The molecular mass determined by relative mobility was between 1.7 and 4.6 kDa. Purified bacteriocin had an accurate molecular mass of

3,547.74 Da by MALDI-TOF MS as shown in **Figure 3** and named pentocin ZFM94.

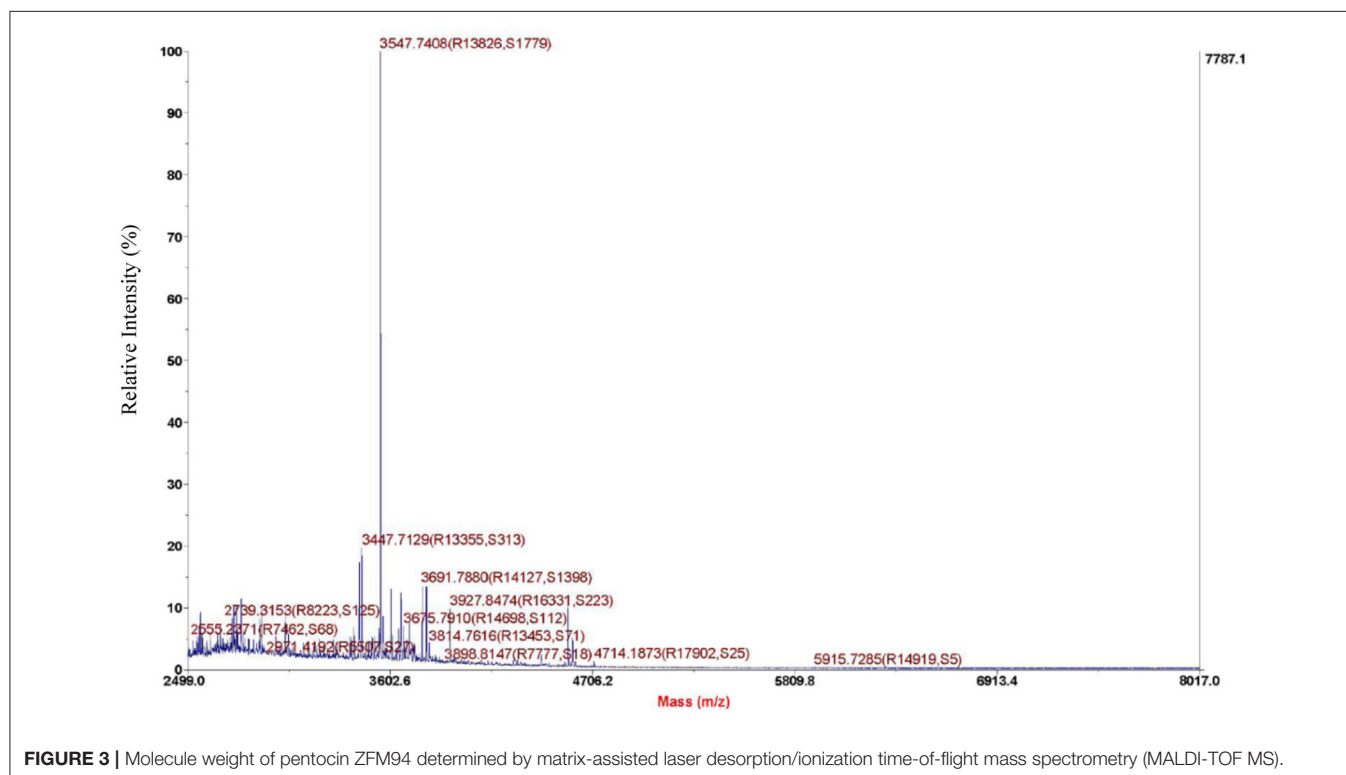
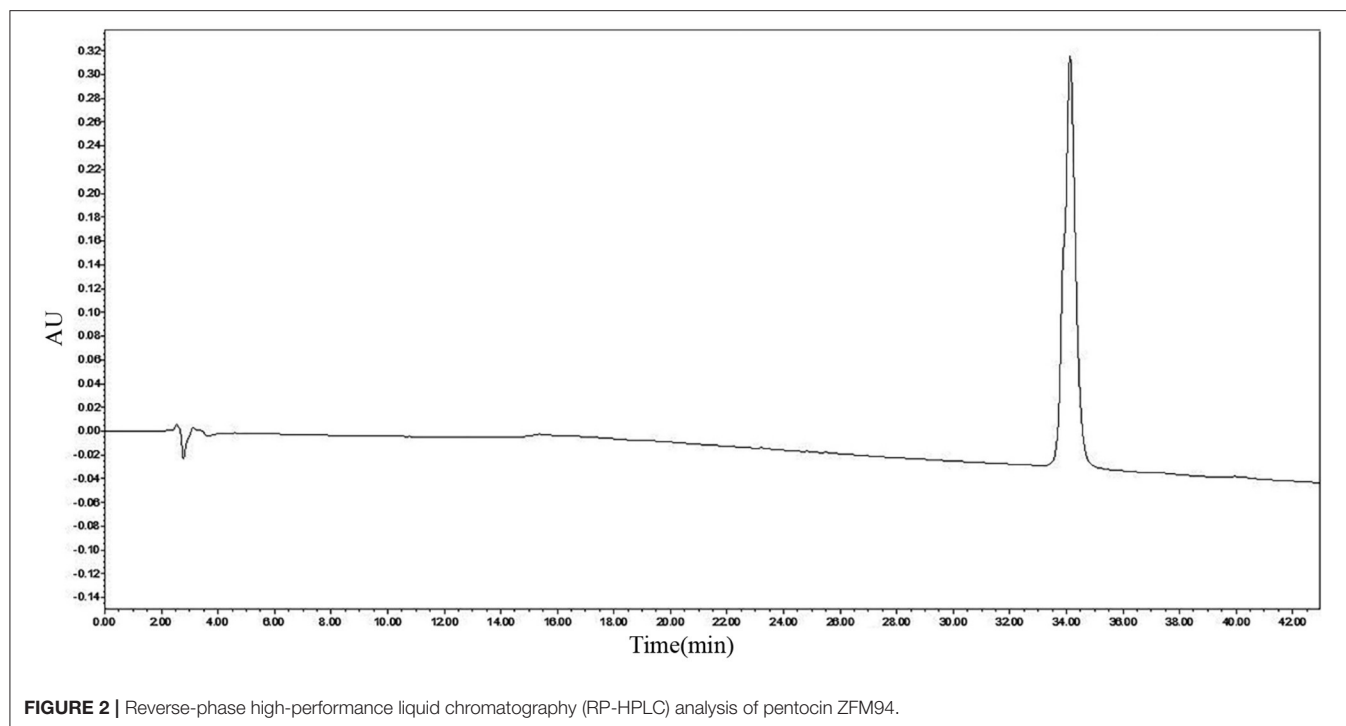
Antimicrobial Spectrum and MICs

Pentocin ZFM94 showed the inhibitory effects against most Gram-positive bacteria, some Gram-negative bacteria, and fungi, as shown in **Table 1**. Among the indicator species, pentocin ZFM94 showed high activities against *M. luteus* 10209, *S. aureus* D48, and *E. coli* DH5 α . In addition, it inhibited *L. monocytogenes* LM1, *Salmonella enterica* subsp. *enterica* ATCC14028, and *Saccharomyces cerevisiae* SM190. However, pentocin ZFM94 had no inhibitory activity against *Bacillus subtilis* BAS2, *Salmonella paratyphi-B* CMCC50094, and *Salmonella paratyphi-A* CMCC50093. Pentocin ZFM94 also inhibited Gram-positive bacteria *S. carnosus* pot20 and *L. monocytogenes* LM1, and *Saccharomyces cerevisiae* SM190. These results demonstrated that this bacteriocin had a broad antibacterial activity.

Minimal inhibitory concentrations were determined by the test tube method (23). Values of MICs for *M. luteus* 10209, *S. aureus* D48, and *E. coli* DH5 α were 1.75, 2.00, and 2.50 μ m, respectively, which exhibited obvious antibacterial activities.

The Effects of pH, Temperature, and Enzymes on Pentocin ZFM94

Pentocin ZFM94 had the best bacteriostatic effect at pH 3 and pH 6; when the pH increased from 8 to 10, the inhibition activity was significantly declined. Pentocin ZFM94 maintained complete activity after exposure from 50 to 80°C for 30 min (**Figure 4A**). When the temperature was higher than 80°C, the inhibition activity was significantly descended. The effects of enzymes were presented in **Figure 4B**. The activity of pentocin ZFM94 was significantly reduced by treatment with pepsin and trypsin. However, amylase, lysozyme, lipase, and ribonuclease A did not effect on the antimicrobial activity.



Antibacterial Action Mode of Pentocin ZFM94

The effect of pentocin ZFM94 on the membrane integrity of *M. luteus* 10209 was determined by the membrane potential sensitive dye DisC2(5). After the addition of DisC2(5), the fluorescence value decreased and reached stability in 3 min.

When 0.05% acetic acid was added, the fluorescence value did not change. As shown in **Figure 5**, with the addition of pentocin ZFM94 at a final concentration of $8.75 \mu\text{M}$ ($5 \times \text{MIC}$), the fluorescence value increased faster than the final concentration of 1.75 ($1 \times \text{MIC}$). It can be seen that the antibacterial action of pentocin ZFM94 was through the perforation of the bacterial

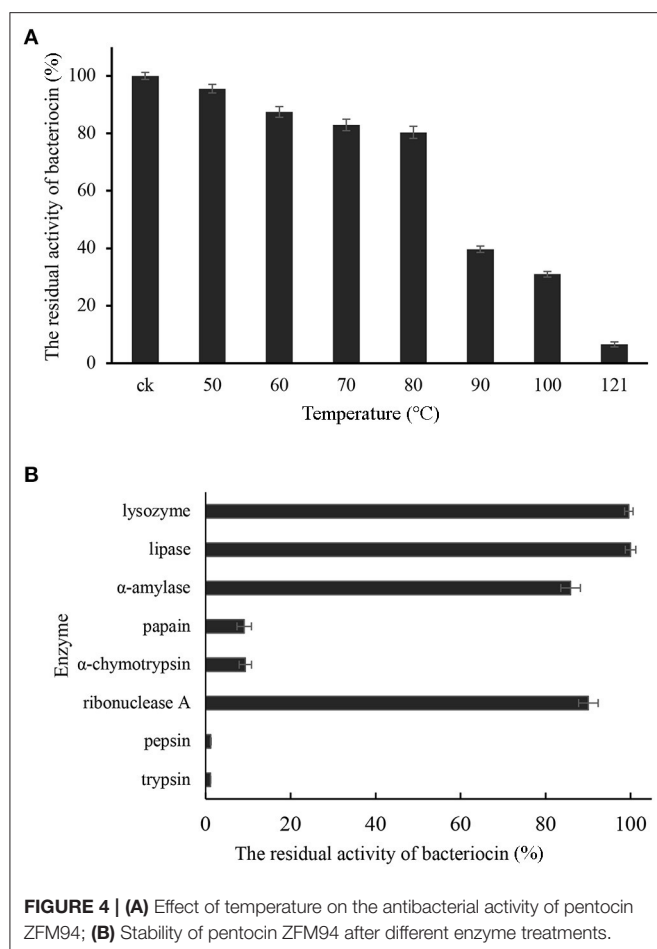


FIGURE 4 | (A) Effect of temperature on the antibacterial activity of pentocin ZFM94; **(B)** Stability of pentocin ZFM94 after different enzyme treatments.

membrane, and indicator bacteria were killed by causing leakage of intracellular electrolytes.

In order to further explore whether lipid II was the target of pentocin ZFM94, nisin was used as a control and *M. luteus* 10209 was used as an indicator. The lipid II (20 μ m) was mixed at a ratio of 2:1 with the pentocin ZFM94 (10 μ m). The bacteriostatic activity was detected by the agar well-diffusion method as shown in **Figure 6**. After pentocin ZFM94 was mixed with lipid II, the inhibitory action of pentocin ZFM94 did not change, but the antibacterial effect of nisin disappeared. The result showed that lipid II was not the target of pentocin ZFM94.

DISCUSSION

Bacteriocins are generally defined as a class of small molecular proteins or peptides synthesized by ribosomes in the metabolic process of some bacteria. *Lactobacillus Pentosus* has antibacterial activity, which is mainly related to its metabolites (26), and bacteriocin is one of them. *Lactobacillus Pentosus* can produce bacteriocin that has been reported, pentocin MQ1 produced by *L. pentosus* CS2 (19), and pentocin TV35b produced by *L. pentosus* TV35b (27). The appropriate separation and purification processes vary from different bacteriocins. Pentocin TV35b was purified by ammonium sulfate precipitation, followed

by sulfopropyl (SP)-sepharose cation exchange chromatography (27). Pentocin JL-1 was purified using macroporous resin, cation exchange, gel filtration, and semipreparative HPLC (17). Pentocin MQ1 was purified using the adsorption-desorption approach followed by RP-HPLC (19). In our study, pentocin ZFM94 was purified by a three-step process, including ammonium sulfate saturation at 40%, Sephadex G-25, and RP-HPLC from the supernatant of *L. pentosus* ZFM94. Then, we determined its molecular weight, determined its antibacterial spectrum, and explored its antibacterial mode.

Pentocin ZFM94 exhibited high thermal and pH stability. It retained 80.37% of its original antibacterial activity after heating at 80°C for 30 min. The antibacterial activity of pentocin ZFM94 was stable at pH 2–7. Pentocin MQ1 retained activity at 40–121°C, but unlike pentocin ZFM94, it was inactive at pH 6–7 (19). Nisin also exhibited a strong antibacterial activity at low pH, but it will be inactivated at pH close to 7 (28). Pentocin ZFM94 was sensitive to trypsin and pepsin, but not to amylase, lysozyme, lipase, and ribonuclease A. Studies have reported that leuconocin S and carnocin 54 are sensitive to amylase but are not sensitive to protease (29). Thus, pentocin ZFM94 has a proteinaceous nature like most other bacteriocins.

Pentocin ZFM94 performed activity against Gram-positive bacteria, Gram-negative bacteria, and fungi, especially for *S. aureus* D48, *M. luteus* 10209, and *E. coli* DH5 α . Many pentocins produced from *L. pentosus* also can inhibit a variety of Gram-positive bacteria, Gram-negative bacteria, and the fungi *Candida albicans* (27). Food spoilage caused by microbial contamination has been a huge challenge for production for the food industry. But so far, only nisin was allowed to be used as a food preservative. Nisin only can inhibit Gram-positive bacteria, and plantaricin 163 can inhibit Gram-positive and Gram-negative bacteria but cannot inhibit fungi (30). Most bacteriocins could not be widely and effectively used in the food industry due to their narrow spectrum and exhibit inhibitory activity against only genetically close bacteria. Therefore, pentocin ZFM94 has a wider application prospect. The MICs of pentocin ZFM94 against *S. aureus* D48, *M. luteus* 10209, and *E. coli* DH5 α were 2.00, 1.75, and 2.50 μ m. BMA has a molecular weight of 1.77 kDa produced by *L. crustorum* MN047, and MICs toward *S. aureus* ATCC 29213 and *E. coli* ATCC 25922 were 165 and 305 μ m, respectively (21). Pentocin ZFM94 performed a higher activity against *S. aureus* and *E. coli* than bacteriocin BMA.

The mode of action of many bacteriocins has been identified to inhibit microorganisms by disrupting the cell membrane integrity of microorganisms (31, 32). In our study, 1 \times and 5 \times MIC of pentocin ZFM94 were tested using a fluorescence leakage test. Both concentrations of pentocin ZFM94 were able to disrupt the integrity of *M. luteus* 10209 cell membrane. In addition, the disruption of cell membrane integrity was dose dependent. Similar dose-dependent inhibitory action has also been observed by aureocin A53 (32) and Plantaricin EF (Pln EF) (21). However, whether it is a specific membrane perforation still needs further study. Pediocin PA-1 (33) and Lactococcin G (34) all have specific membrane perforation mechanisms.

The mode of action of bacteriocin is not unique. Nisin not only has specific membrane perforation but also can mediate the formation of the hole by combining with lipid II. Studies also

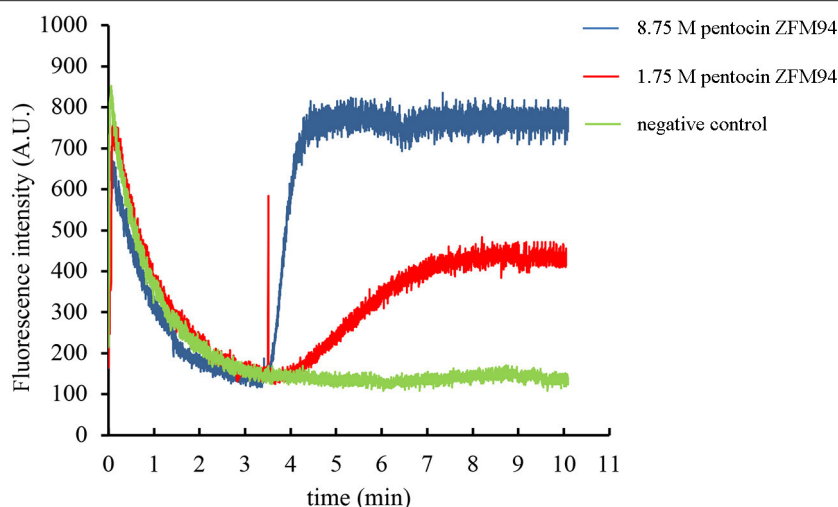


FIGURE 5 | Effect of different pentocin ZFM94 concentrations on the membrane of *Micrococcus luteus* (*M. luteus*).

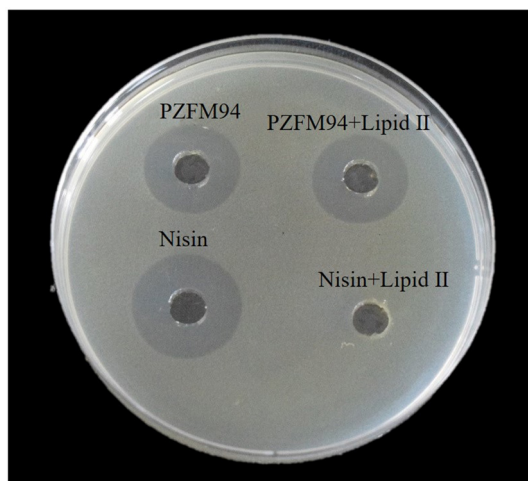


FIGURE 6 | Binding experiment of pentocin ZFM94 with lipid II.

found that lipid II was the target of many bacteriocins, such as nisin (12), mersacidin (35), and plantaricin C (36). The molar ratio 1:2 of pentocin ZFM94 and lipid II was studied using the agar well-diffusion test. After pentocin ZFM94 was mixed with lipid II, the inhibitory action did not change suggesting that lipid II is not the target of pentocin ZFM94.

In future studies, we will further optimize the purification method of pentocin ZFM94 and increase the recovery of it. The

target of the action, the amino acid sequence, and the structure of pentocin ZFM94 will be addressed in more detail.

DATA AVAILABILITY STATEMENT

The original contributions generated for the study are included in the article/supplementary material, further inquiries can be directed to the corresponding author/s.

AUTHOR CONTRIBUTIONS

QG, PL, and QZ conceived and designed the study. LX, MD, and YL completed the experiment. MD and DW conducted analysis the results and finished the paper. All authors contributed to the article and approved the submitted version.

FUNDING

This project was funded by the National Natural Science Foundation of China (No. U20A2066), the Key Research and Development Program of Zhejiang Province (No. 2020C04002), and the Natural Science Foundation of Zhejiang Province (No. LZ21C200001).

ACKNOWLEDGMENTS

We would like to thank Eefjan Breukink (Utrecht University, the Netherlands) for providing lipid II.

REFERENCES

1. Cotter PD, Ross RP, Hill C. Bacteriocins — a viable alternative to antibiotics? *Nat Rev Microbiol.* (2013) 11:95–105. doi: 10.1038/nrmicro2937
2. Reddy KVR, Yedery RD, Aranha C. Antimicrobial peptides: premises and promises. *Int J Antimicrob Agents.* (2004) 24:536–47. doi: 10.1016/j.ijantimicag.2004.09.005
3. Chatterjee S, Chatterjee S, Lad SJ, Phansalkar MS, Rupp RH, Ganguli BN, et al. Mersacidin, a new antibiotic from *Bacillus* fermentation, isolation, purification and chemical characterization. *J Antibiot.* (1992) 45:832–8. doi: 10.7164/antibiotics.45.832
4. Kumariya R, Garsa AK, Rajput YS, Sood SK, Akhtar N, Patel S. Bacteriocins: classification, synthesis, mechanism of action, and resistance development in food spoilage causing bacteria.

- Microb Pathogen.* (2019) 128:171–7. doi: 10.1016/j.micpath.2019.01.002
5. Eijssink VGH, Axelsson L, Diep DB, Håvarstein LS, Holo H, Nes IF. Production of class II bacteriocins by lactic acid bacteria; an example of biological warfare and communication. *Antonie van Leeuwenhoek.* (2002) 81:639–54. doi: 10.1023/A:1020582211262
 6. Garneau S, Martin NI, Vederas JC. Two-peptide bacteriocins produced by lactic acid bacteria. *Biochimie.* (2002) 84:577–592. doi: 10.1016/S0300-9084(02)01414-1
 7. Kleanhammer T. Genetics of bacteriocins produced by lactic acid bacteria. *FEMS Microbiol Rev.* (1993) 12:39–85. doi: 10.1016/0168-6445(93)90057-G
 8. Delves-Broughton J, Blackburn P, Evans RJ, Hugenholtz J. Applications of the bacteriocin, nisin. *Antonie van Leeuwenhoek.* (1996) 69:193–202. doi: 10.1007/BF00399424
 9. Garsa AK, Kumariya R, Sood SK, Kumar A, Kapila S. Bacteriocin production and different strategies for their recovery and purification. *Probiotics Antimicrob Prot.* (2014) 6:47–58. doi: 10.1007/s12602-013-9153-z
 10. Severina E, Severin A, Tomasz A. Antibacterial efficacy of nisin against multidrug-resistant Gram-positive pathogens. *J Antimicrob Chemother.* (1998) 41:341–7. doi: 10.1093/jac/41.3.341
 11. Kjos M, Borrero J, Opsata M, Birri DJ, Holo H, Cintas LM, et al. Target recognition, resistance, immunity and genome mining of class II bacteriocins from gram-positive bacteria. *Microbiology.* (2011) 157:3256–67. doi: 10.1099/mic.0.052571-0
 12. Breukink E. Use of the cell wall precursor lipid II by a pore-forming peptide antibiotic. *Science.* (1999) 286:2361–4. doi: 10.1126/science.286.5448.2361
 13. Aarti C, Khuroo A, Arasu MV, Agastian P, Al-Dhahi NA. Biological potency and characterization of antibacterial substances produced by *Lactobacillus pentosus* isolated from Hentak, a fermented fish product of North-East India. *Springerplus.* (2016) 5:1743. doi: 10.1186/s40064-016-3452-2
 14. Parks WM, Bottrill AR, Pierrat OA, Durrant MC, Maxwell A. The action of the bacterial toxin, microcin B17, on DNA gyrase. *Biochimie.* (2007) 89:500–7. doi: 10.1016/j.biochi.2006.12.005
 15. Delgado A, Brito D, Peres C, Noé-Arroyo F, Garrido-Fernández A. Bacteriocin production by *Lactobacillus pentosus* B96 can be expressed as a function of temperature and NaCl concentration. *Food Microbiol.* (2005) 22:521–8. doi: 10.1016/j.fm.2004.11.015
 16. Guerreiro J, Monteiro V, Ramos C, de Melo Franco BDG, Martinez RCR, Todorov SD, et al. *Lactobacillus pentosus* B231 isolated from a Portuguese PDO cheese: production and partial characterization of its bacteriocin. *Probiotics Antimicrob Prot.* (2014) 6:95–104. doi: 10.1007/s12602-014-9157-3
 17. Jiang H, Zou J, Cheng H, Fang J, Huang G. Purification, characterization, and mode of action of pentocin JL-1, a novel bacteriocin isolated from *Lactobacillus pentosus*, against drug-resistant *Staphylococcus aureus*. *BioMed Res Int.* (2017) 2017:1–11. doi: 10.1155/2017/7657190
 18. Todorov SD, Vaz-Velho M, Gibbs P. Comparison of two methods for purification of plantaricin ST31, a bacteriocin produced by *Lactobacillus plantarum* ST31. *Braz J Microbiol.* (2004) 35:157–60. doi: 10.1590/S1517-83822004000100026
 19. Wayah SB, Philip K. Pentocin MQ1: a novel, broad-spectrum, pore-forming bacteriocin from *Lactobacillus pentosus* CS2 with quorum sensing regulatory mechanism and biopreservative potential. *Front Microbiol.* (2018) 9:564. doi: 10.3389/fmicb.2018.00564
 20. Ye K, Li P, Gu Q. Complete genome sequence analysis of a strain *Lactobacillus pentosus* ZFM94 and its probiotic characteristics. *Genomics.* (2020) 112:3142–9. doi: 10.1016/j.ygeno.2020.05.015
 21. Yi L, Dang Y, Wu J, Zhang L, Liu X, Liu B, et al. Purification and characterization of a novel bacteriocin produced by *Lactobacillus crustorum* MN047 isolated from koumiss from Xinjiang, China. *J Dairy Sci.* (2016) 99:7002–15. doi: 10.3168/jds.2016-11166
 22. Tagg JR, McGiven AR. Assay system for bacteriocins. *Appl Microbiol.* (1971) 21:943. doi: 10.1128/am.21.5.943-943.1971
 23. Bédard F, Hammami R, Zirah S, Rebuffat S, Fliss I, Biron E. Synthesis, antimicrobial activity and conformational analysis of the class IIa bacteriocin pediocin PA-1 and analogs thereof. *Sci Rep.* (2018) 8:9029. doi: 10.1038/s41598-018-27225-3
 24. Ladokhin AS, Selsted ME, White SH. Sizing membrane pores in lipid vesicles by leakage of co-encapsulated markers: pore formation by melittin. *Biophys J.* (1997) 72:1762–6. doi: 10.1016/S0006-3495(97)78822-2
 25. Jiang H, Tang X, Zhou Q, Zou J, Li P, Breukink E, et al. Plantaricin NC8 from *Lactobacillus plantarum* causes cell membrane disruption to *Micrococcus luteus* without targeting lipid II. *Appl Microbiol Biotechnol.* (2018) 102:7465–73. doi: 10.1007/s00253-018-9182-3
 26. Lipińska L, Klewicki R, Sójka M, Bonikowski R, Zytelewicz D, Kołodziejczyk K, et al. Antifungal activity of *Lactobacillus pentosus* ŁOCK 0979 in the presence of polyols and galactosyl-polyols. *Probiotics Antimicrob Prot.* (2018) 10:186–200. doi: 10.1007/s12602-017-9344-0
 27. Okkers DJ, Dicks LMT, Silvester M, Joubert JJ, Odendaal HJ. Characterization of pentocin TV35b, a bacteriocin-like peptide isolated from *Lactobacillus pentosus* with a fungistatic effect on *Candida albicans*. *J Appl Microbiol.* (1999) 87:726–34. doi: 10.1046/j.1365-2672.1999.00918.x
 28. Garcera MJG, Elferink MGL, Driessen AJM, Konings WN. In vitro pore-forming activity of the lantibiotic nisin. Role of protonmotive force and lipid composition. *Eur J Biochem.* (1993) 212:417–22. doi: 10.1111/j.1432-1033.1993.tb17677.x
 29. Budde B. *Leuconostoc carnosum* 4010 has the potential for use as a protective culture for vacuum-packed meats: culture isolation, bacteriocin identification, and meat application experiments. *Int J Food Microbiol.* (2003) 83:171–84. doi: 10.1016/S0168-1605(02)00364-1
 30. Hu M, Zhao H, Zhang C, Yu J, Lu Z. Purification and characterization of plantaricin 163, a novel bacteriocin produced by *Lactobacillus plantarum* 163 isolated from traditional Chinese fermented vegetables. *J Agric Food Chem.* (2013) 61:11676–82. doi: 10.1021/jf403370y
 31. Huang HW, Chen F-Y, Lee M-T. Molecular mechanism of peptide-induced pores in membranes. *Phys Rev Lett.* (2004) 92:198304. doi: 10.1103/PhysRevLett.92.198304
 32. Netz DJA, Bastos Mdo C, Sahl H-G. Mode of action of the antimicrobial peptide aureocin a53 from *Staphylococcus aureus*. *AEM.* (2002) 68:5274–80. doi: 10.1128/AEM.68.11.5274-5280.2002
 33. Zhao H, Mattila J-P, Holopainen JM, Kinnunen PKJ. Comparison of the membrane association of two antimicrobial peptides, magainin 2 and indolicidin. *Biophys J.* (2001) 81:2979–91. doi: 10.1016/S0006-3495(01)75938-3
 34. Paiva AD, Breukink E, Mantovani HC. Role of lipid II and membrane thickness in the mechanism of action of the lantibiotic bovicin HC5. *Antimicrob Agents Chemother.* (2011) 55:5284–93. doi: 10.1128/AAC.00638-11
 35. Brötz H, Bierbaum G, Leopold K, Reynolds PE, Sahl H-G. The lantibiotic mersacidin inhibits peptidoglycan synthesis by targeting Lipid II. *Antimicrob Agents Chemother.* (1998) 42:154–60. doi: 10.1128/AAC.42.1.154
 36. Wiedemann I, Böttiger T, Bonelli RR, Schneider T, Sahl H-G, Martínez B. Lipid II-based antimicrobial activity of the lantibiotic plantaricin C. *AEM.* (2006) 72:2809–14. doi: 10.1128/AEM.72.4.2809-2814.2006

Conflict of Interest: The authors declare that the research was conducted in the absence of any commercial or financial relationships that could be construed as a potential conflict of interest.

Publisher's Note: All claims expressed in this article are solely those of the authors and do not necessarily represent those of their affiliated organizations, or those of the publisher, the editors and the reviewers. Any product that may be evaluated in this article, or claim that may be made by its manufacturer, is not guaranteed or endorsed by the publisher.

Copyright © 2021 Dai, Li, Xu, Wu, Zhou, Li and Gu. This is an open-access article distributed under the terms of the Creative Commons Attribution License (CC BY). The use, distribution or reproduction in other forums is permitted, provided the original author(s) and the copyright owner(s) are credited and that the original publication in this journal is cited, in accordance with accepted academic practice. No use, distribution or reproduction is permitted which does not comply with these terms.



The Protection of *Lactiplantibacillus plantarum* CCFM8661 Against Benzopyrene-Induced Toxicity via Regulation of the Gut Microbiota

Leilei Yu^{1,2,3}, Lingyu Zhang^{1,2}, Hui Duan^{1,2}, Ruohan Zhao^{1,2}, Yue Xiao^{1,2}, Min Guo^{1,2}, Jianxin Zhao^{1,2,3}, Hao Zhang^{1,2,3}, Wei Chen^{1,2,3} and Fengwei Tian^{1,2,3*}

¹ State Key Laboratory of Food Science and Technology, Jiangnan University, Wuxi, China, ² School of Food Science and Technology, Jiangnan University, Wuxi, China, ³ National Engineering Research Center for Functional Food, Jiangnan University, Wuxi, China

OPEN ACCESS

Edited by:

Huaxi Yi,
Ocean University of China, China

Reviewed by:

Fei Liu,
Northeast Agricultural University,
China
Jiachao Zhang,
Hainan University, China

*Correspondence:

Fengwei Tian
fwtian@jiangnan.edu.cn

Specialty section:

This article was submitted to
Nutritional Immunology,
a section of the journal
Frontiers in Immunology

Received: 04 July 2021

Accepted: 22 July 2021

Published: 10 August 2021

Citation:

Yu L, Zhang L, Duan H, Zhao R, Xiao Y, Guo M, Zhao J, Zhang H, Chen W and Tian F (2021) The Protection of *Lactiplantibacillus plantarum* CCFM8661 Against Benzopyrene-Induced Toxicity via Regulation of the Gut Microbiota. *Front. Immunol.* 12:736129. doi: 10.3389/fimmu.2021.736129

The present study evaluated the protection of *Lactiplantibacillus plantarum* CCFM8661, a candidate probiotic with excellent benzopyrene (B[a]P)-binding capacity *in vitro*, against B[a]P-induced toxicity in the colon and brain of mice. Mice that received B[a]P alone served as the model group. Each mouse in the *L. plantarum* treatment groups were administered 2×10^9 colony forming unit (CFU) of *L. plantarum* strains once daily, followed by an oral dose of B[a]P at 50 mg/kg body weight. Behavior, biochemical indicators in the colon and brain tissue, and the gut microbiota composition and short-chain fatty acid (SCFA) levels in the gut were investigated. Compared to the treatment in the model group, CCFM8661 treatment effectively reduced oxidative stress in the brain, improved behavioral performance, increased intestinal barrier integrity, and alleviated histopathological changes in mice. Moreover, CCFM8661 increased the gut microbiota diversity and abundance of *Ruminococcus* and *Lachnospiraceae* and reduced the abundance of pro-inflammatory *Turicibacter* spp. Additionally, the production of SCFAs was significantly increased by *L. plantarum* CCFM8661. Our results suggest that CCFM8661 is effective against acute B[a]P-induced toxicity in mice and that it can be considered as an effective and easy dietary intervention against B[a]P toxicity.

Keywords: probiotic, *Lactiplantibacillus plantarum*, benzopyrene, gut microbiota, SCFAs, gut barrier, behavioral performance

INTRODUCTION

Benzopyrene (B[a]P) is a kind of polycyclic aromatic hydrocarbon that is categorized as a group I carcinogen by the International Agency for Research on Cancer (1, 2). Contaminated food is an important source of human exposure to B[a]P, which is up to 125 ng per day for each person (2, 3). B[a]P would be produced during food processing, such as smoking, grilling, frying. B[a]P-contaminated foods include vegetables (13 ng/kg), cereals (262 ng/kg), smoked fish (800–13900 ng/kg), and dairy products (11–78 ng/kg) (4). After entering into the host's body, B[a]P would bind to the aryl-hydrocarbon receptor and be activated by cytochrome P-4501A1 (CYP1A1) to produce

immense size DNA adducts and ROS (2, 5), which would inactivate tumor suppressor genes or activate oncogenes, resulting in DNA damage, mutation, and cancer (6, 7).

B[a]P is neurotoxic and it affects the levels of 5-hydroxytryptamine, 5-hydroxyindoleacetic acid, and target protein kinase C (8), leading to neurotoxicity and behavioral disturbances (6, 9). More seriously, the neurotoxicity of B[a]P has a genetic effect (10). However, the effects of B[a]P on the gut have not been thoroughly studied so far. The intestinal tract is the first vital barrier against oral B[a]P exposure. Therefore, it is necessary to investigate the negative effects of B[a]P on the gut, especially the gut microbiota, gut barrier and intestinal histopathology. Previous researches have reported the harmful effects of B[a]P on the intestinal barrier, such as changes in the expression levels of tight junction (TJ) proteins (11, 12). Ribiere et al. demonstrated that B[a]P exposure dramatically changed the gut microbiota composition, thereby causing a pro-inflammatory intestinal environment and leading to moderate inflammation in ileum and colon of mice (13). Moreover, the important roles of intestine microbiota and SCFAs in regulating host health have aroused the increasing concern (14–16). For example, gut microbiota-generated SCFAs promote metabolism via gut-brain axis, thereby reducing body weight, adiposity, and blood glucose (15).

Lactic acid bacteria (LAB), a group of safe gram-positive microorganisms, are widely used in various fermented food (17). LAB are also the important components of the human gut microbiota with various physiological function, including balance of immune cell, regulation of metabolites and gut microbiota. *Lactiplantibacillus plantarum* is a super vital LAB that is capable of binding or sequestering various carcinogens *in vitro* and *in vivo* and is a safe and cost-effective intervention way (18–20). Apart from its capacity to bind carcinogens, *L. plantarum* regulates the gut microbiota and has antioxidative properties, which may be important for the alleviation of B[a]P toxicity. Therefore, the aim of this study was to select a novel probiotic strain with excellent B[a]P-binding ability from the 23 *L. plantarum* strains tested and evaluate its protective effects on the colons and brains of mice exposed to B[a]P, especially the impacts on the intestinal microbiota composition and intestinal barrier function. Moreover, possible protective mechanisms against B[a]P toxicity are proposed.

MATERIAL AND METHODS

Bacterial Strains and Culture

Twenty-three *Lactiplantibacillus plantarum* strains, including *L. plantarum* CCFM571, CCFM595, CCFM8610, CCFM438, CCFM726, CCFM408, CCFM8661, CCFM634, CCFM175, CCFM242, CCFM361, CCFM259, CCFM382, Lp45, FJSWX14-5, DYNDL58M4, PS3-9, FFJND7-L5, HY9-10, M2-05-R02, FJSZJ4-L5, 4L-4 and VNMWLT1M12, were obtained from Research Center of Food Biotechnology in Jiangnan University (Wuxi, China). The cultivation of all *L. plantarum* strains was in MRS broth (Hopebio, Qingdao, China) at 37°C for 18h.

Determination of the B[a]P-Binding Capacity of *L. plantarum* Strains *In Vitro*

The B[a]P-binding ability of the 23 *L. plantarum* strains was estimated as previously described (21). The cultured biomass was centrifuged at 5,000 × g for 15 min and washed twice with ultrapure water to acquire cell pellets. The cell pellets were re-suspended in the ultrapure water containing 10 µg/mL B[a]P (Sigma-Aldrich, St Louis, MO, USA). The suspension was centrifuged after incubation for 2h at 150 rpm and 37°C, and the residual B[a]P concentration in the supernatant was analyzed. B[a]P levels were measured using a high performance liquid chromatography (HPLC) equipped with a Waters Atlantis C18 reverse-phase column (4.6×250 mm×5 µm, 30°C; Waters Corporation, Milford, MA, USA). The mobile phase was acetonitrile:water (88:12). The injection volume was 20 µL, with a flow rate of 1 mL/min, and the fluorescence detection wavelength was 406 nm.

The B[a]P-binding abilities of the *Lactiplantibacillus* strains are expressed as the B[a]P removal rate, which was calculated as follows:

Removal rate (%) = $[(C_i - C_r) / C_i] \times 100\%$, C_i and C_r are the initial and residual B[a]P level, respectively.

Animal Experimental Procedure

Male adult BALB/c mice (8-week-old) were purchased from Slack limited company (Shanghai, China). Mice were kept in cages at a constant temperature (22°C ± 1°C) and humidity (55% ± 10%) under a 12-h/12-h light/dark cycle and had free access to food and water. All procedures and protocols of mice experiments were performed according to the guidelines of the Animal Care and Use Committee and the Ethics Committee of Jiangnan University (JN.No20190915b0481210).

The mice were divided into four groups and allowed to acclimatize to their environment for 1 week. The experimental schedule is shown in **Table 1**. Group 1 (control group) was administered skim milk and corn oil without B[a]P. Group 2 (model group) was administered B[a]P dissolved in corn oil at a dose of 50 mg/kg b.w. Groups 3 and 4 (CCFM8661 and CCFM382 groups, respectively) were administered 2×10^9 CFU of *L. plantarum* strains CCFM8661 and CCFM382, respectively, and 50 mg/kg b.w. of B[a]P. All treatments were administered *via* oral gavage for 5 weeks. Mice were fasted for 12h before sacrifice. Blood samples were collected and centrifuged at 3,000 × g for 15 min to obtain the serum, which was used for biochemical analysis. Colon and brain tissues were immediately washed with

TABLE 1 | Animal experimental protocol.

Group (n = 8)	Treatment (5 weeks)
Control	SM+CO
Model	SM+B[a]P
CCFM8661	<i>L. plantarum</i> CCFM8661+B[a]P
CCFM382	<i>L. plantarum</i> CCFM382+B[a]P

CO=0.2 mL corn oil; SM=0.2 mL skim milk; B[a]P=0.2 mL corn oil containing 50 mg/kg body weight of B[a]P; CCFM8661 = 0.2 mL skim milk containing 2×10^9 CFU of *L. plantarum* CCFM8661; CCFM382 = 0.2 mL skim milk containing 2×10^9 CFU of *L. plantarum* CCFM382. Animals received corn oil, skim milk, B[a]P, and *L. plantarum* strains *via* gavage.

0.9% saline and separated into two parts: one part was stored at -80°C for subsequent measurements, and the other part was fixed with 4% formalin for histopathological analysis.

Open-Field Test

The test was performed as previously described with minor modifications (22, 23). The size of apparatus used for the open-field test was 50cm×50cm square with four white walls. The edge region is a 15cm area near the walls and the rest of the field was the central area. Each mouse can move freely within the apparatus for 15min. A camera was used to record their movements, and the data were analyzed using EthoVision (Noldus, Wageningen, Netherlands). The apparatus was cleaned with 75% ethanol after each test to eliminate any possible odor cues. The total distance traveled and the times spent in the center and the edge regions were calculated to measure anxiety-like behavior.

Determination of 3-OH B[a]P Levels in Feces

The mouse feces were mixed with acetonitrile (1:2) by vortex oscillation. After centrifugation at 10000 rpm for 10 min, the 3-OH B[a]P levels in supernatant was analyzed by HPLC-fluorescence detection (24). The mobile phase was methanol: water (97:3, pH4.5). The injection volume was 20 µL, with a flow rate of 0.5 mL/min, and the fluorescence excitation and emission wavelength were 365 and 450 nm, respectively.

Determination of Oxidative Stress-Related Parameters in the Brain

The MDA level and SOD activity were measured using ELISA kit according to the operating instructions of the manufacturer (Jiancheng Bioengineering, Nanjing, China).

RT-qPCR Analysis

Colon and brain tissue (0.1g) samples were lysed in TRIzol reagent (Ambion, USA) for RNA extraction. cDNA was synthesized using the RevertAid (Thermo Fisher Scientific, Waltham, MA, USA). Gene expression levels were determined using validated primers for *Gapdh*, *Zo-1*, *Occludin*, *Claudin-1*, *CYP1A1*, *Bax*, *Bcl-2*, and *p53* (Table 2) and iTaq Universal (Bio-Rad, Hercules, CA, USA) on an RT-qPCR system (BioRad-CFX384) (25). The PCR program comprised initial denaturation at 95°C for 2 min, followed by 40 cycles of 95°C for 30 s, 60°C for 30 s, and 72°C for 30 s, and finally, 72°C for 5 min. Relative quantification of these target gene expression levels was performed after normalization to *Gapdh* gene expression levels using the $2^{-\Delta\Delta Ct}$ method.

Histopathological Analysis

Colon tissue was fixed in 10% formalin saline for 24 h and then embedded in paraffin. The paraffin was sliced into 5-µm-thick sections. After sectioning, the tissue samples were stained with H&E (26).

Analysis of the Gut Microbiota in Feces

Total DNA in feces was extracted using the FastDNA Spin Kit (MP Biomedicals, Santa Ana, CA, USA). The V3-V4 region of the 16S rRNA gene was amplified using 341F/806R primers.

TABLE 2 | Primer sequences used for RT-qPCR.

Primer		Sequence (5'-3')
GAPDH	Forward (F)	TGCACCACCAACTGCTTAG
	Reverse (R)	GATGCAGGGATGATGTTT
ZO-1	F	CTTCTCTTGCTGGCCCTAAAC
	R	TGGCTTCACTTGAGGTTTCTG
Occludin	F	CACACTTGCTTGGGACAGAG
	R	TAGCCATAGCCTCCATAGCC
Claudin-1	F	GATGTGGATGGCTGTCATTG
	R	CCTGGCCAAATTCATACCTG
CYP1A1	F	CCTCATGTACCTGGTAACCA
	R	AAGGATGAATGCCGAAGGT
Bax	F	CTACAGGGTTTCATCCAG
	R	CCAGTTCATCTCCAATTCTG
Bcl-2	F	GTGGATGACTGAGTACCT
	R	CCAGGAGAAATCAACAGAG
P53	F	GTATTTCAACCCTCAAGATCC
	R	TGGGCATCCTTTAACTCTA

The library was built and sequenced on an Illumina MiSeq PE300 platform.

Determination of SCFA Levels

Fecal samples (50mg) were dispersed in 50µL of saturated NaCl solution, acidified with 5% (v/v) H₂SO₄, and SCFAs were extracted with 1mL of diethyl ether. SCFA levels were tested by GC-MS (27).

Statistical Analysis

Statistical analyses were performed using Prism version 7 (GraphPad, San Diego, CA, USA). Significant differences were evaluated using a one-way analysis of variance. Microbiota-related analyses, including alpha diversity and biodiversity richness, were assessed with the QIIME (version 1.17) and R (version 3.5.0) software.

RESULTS

B[a]P-Binding Abilities

The B[a]P-binding abilities of the 23 *L. plantarum* strains are presented in Figure 1. The B[a]P-binding abilities were significantly different among the different *L. plantarum* strains. *L. plantarum* CCFM8661 had the highest B[a]P removal capacity, with a removal rate of 60.9%; thus, this strain was selected as the target strain for subsequent animal experiments. CCFM382 had the lowest removal rate of only 1.6%; thus, it was selected as the negative reference strain. The protection of these two *L. plantarum* strains against B[a]P-induced toxicity in the gut and the brain were compared.

Levels of 3-OH B[a]P in Feces

The levels of 3-OH B[a]P in the feces of mice significantly increased after B[a]P treatment, which was up to 0.27 µg/g (Figure 2; $P < 0.05$). The effects were significantly reversed by oral administration of *L. plantarum* CCFM8661 ($P < 0.05$), but not *L. plantarum* CCFM382 ($P > 0.05$). The 3-OH B[a]P level in the CCFM8661 and CCFM382 groups were 0.14µg/g, and 0.21µg/g, respectively.

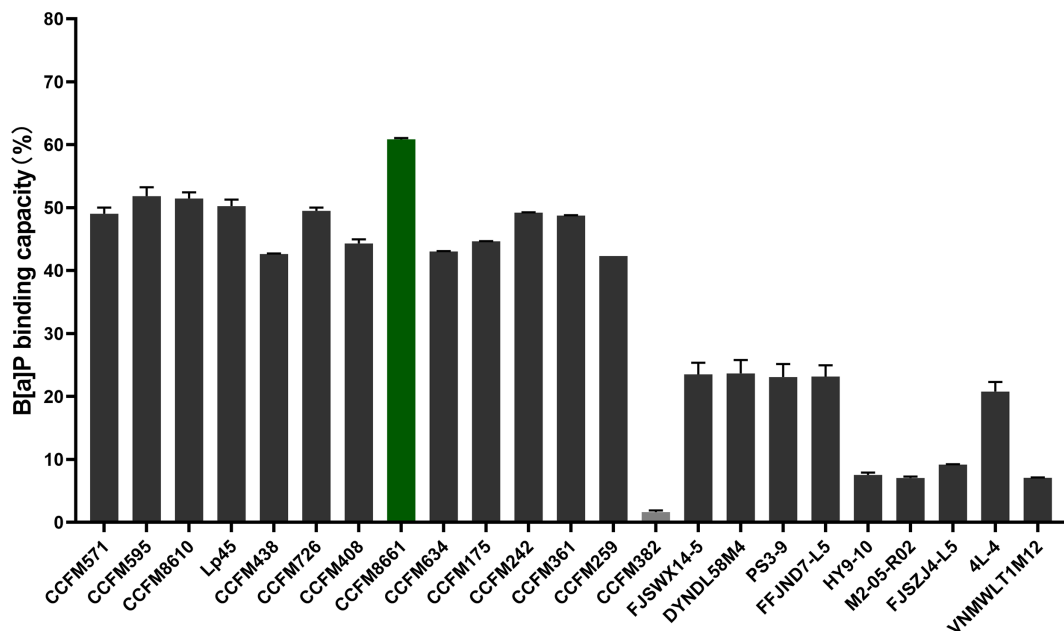


FIGURE 1 | B[a]P-binding capacity of *L. plantarum* strains.

Open-Field Test

The open-field test was used to evaluate the spatial cognitive ability of the experimental animals. The distance moved was used to represent autonomous activity ability, and the time spent in the central area was used to reflect their spatial cognition ability in a new environment. Mice with poor cognitive ability would quickly leave the central area and move along the periphery, thereby spending less exploration time in the central area. As shown in **Figure 3**, B[a]P-treated mice traveled a shorter total distance and spent less time in the center than mice in the control group ($P < 0.05$). However, mice in the CCFM8661 and CCFM382 group traveled a longer distance and spent more time in the central zone than those in the model group ($P < 0.05$). Importantly, *L. plantarum* CCFM8661 had a more significant increase on these two parameters than CCFM382. These results suggested that anxiety-like behavior caused by B[a]P can be better reversed by CCFM8661 supplementation.

Oxidative Stress- and Tumor-Related Parameters in the Brain

Malondialdehyde (MDA) levels were dramatically higher in the model group than those in the control group (**Figure 4B**, $P < 0.05$). Of the two *L. plantarum* intervention groups, only *L. plantarum* CCFM8661 sharply decreased the MDA levels ($P < 0.05$). Superoxide dismutase activity was not dramatically different between the groups (**Figure 4A**).

The expression levels of *Bcl-2* and *p53* in the brain increased dramatically in the model group, but *L. plantarum* CCFM8661 dramatically reduced the expression levels of these genes

(**Figures 4D, E**; $P < 0.05$). Although the decrease expression of *p53* in CCFM382 group was also observed, the difference was not significant ($P > 0.05$). In addition, the *Bax* expression level in the brain tissue of the control, model, and two *L. plantarum*-intervention groups were no significant differences (**Figure 4C**).

The mRNA Expression of TJ Proteins and CYP1A1 in the Colon

The mRNA expression levels of *Zo-1* and occludin in the colon were dramatically lower in B[a]P-exposed mice than in control mice (**Figure 5A**; $P < 0.05$). Oral administration of CCFM8661 and CCFM382 significantly increased occludin expression ($P < 0.05$). The mRNA expression levels of claudin-1 were increased in the model group ($P < 0.05$) but were not significantly affected by *L. plantarum* intervention ($P > 0.05$).

Levels of the B[a]P-metabolizing enzyme CYP1A1, a member of the P450 enzyme family, were increased about six-fold after B[a]P treatment (**Figure 5A**; $P < 0.05$), and *L. plantarum* CCFM8661, rather than *L. plantarum* CCFM382, significantly reduced its expression ($P < 0.05$), thus alleviating the damage to the colon caused by B[a]P.

Histopathological Changes in the Colon

Colonic histopathology was normal in mice in the control group (**Figure 5B**). However, B[a]P treatment led to serious injury to the colon, including crypt destruction, inflammatory cell infiltration, and severe ulceration. Colonic ulcers were reversed after *L. plantarum* CCFM382 administration, but there was still moderate inflammatory cell infiltration. Treatment with *L. plantarum* CCFM8661 significantly alleviated the colonic histopathological lesions to almost normal levels. Therefore,

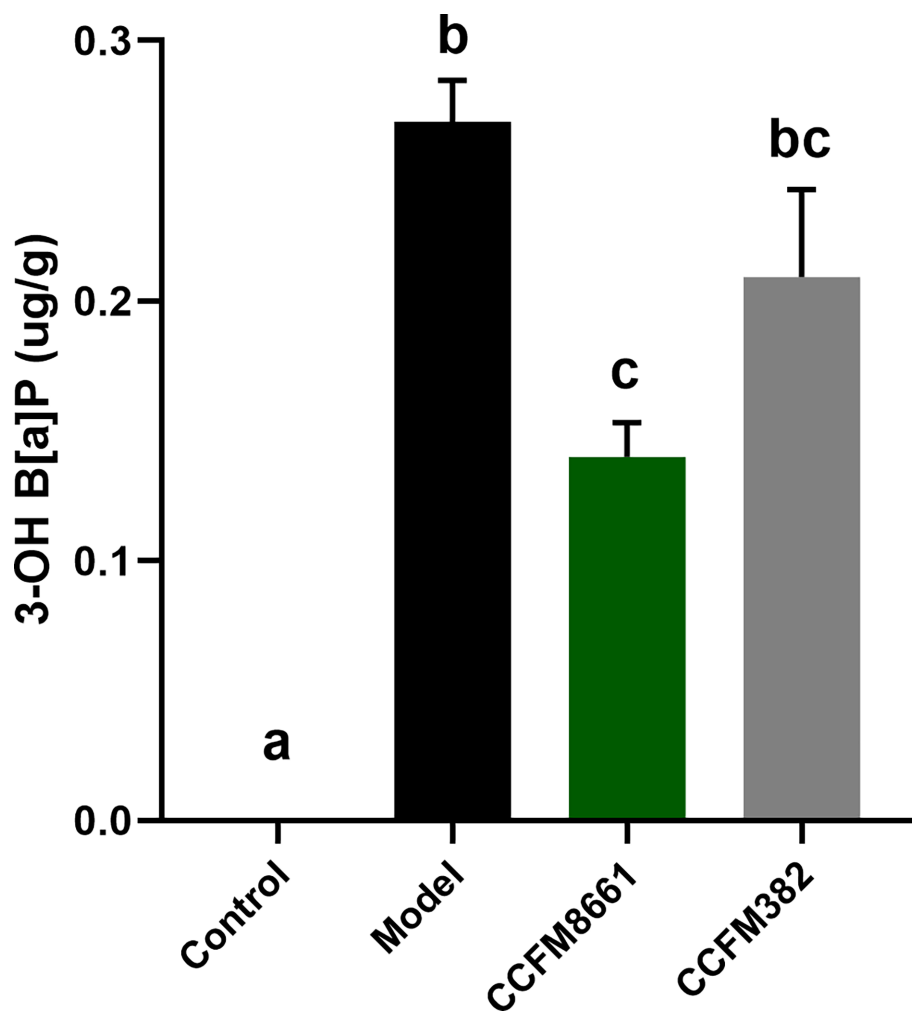


FIGURE 2 | Effect of *L. plantarum* CCFM8661 on 3-OH B[a]P levels in feces. The different letters indicate significant difference between groups ($P < 0.05$).

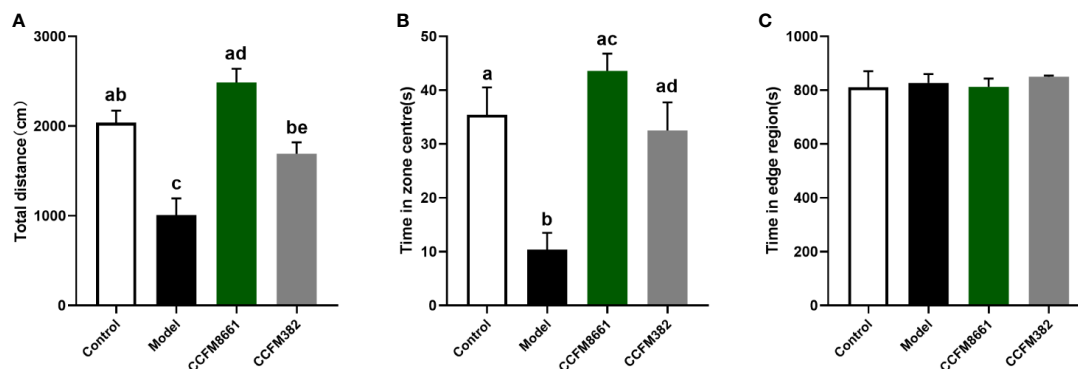


FIGURE 3 | Effects of *L. plantarum* CCFM8661 on B[a]P-induced behavioral changes. **(A)** The total distance, **(B)** The time spend in zone centres, **(C)** The time spend in edge region. The different letters indicate significant difference between groups ($P < 0.05$).

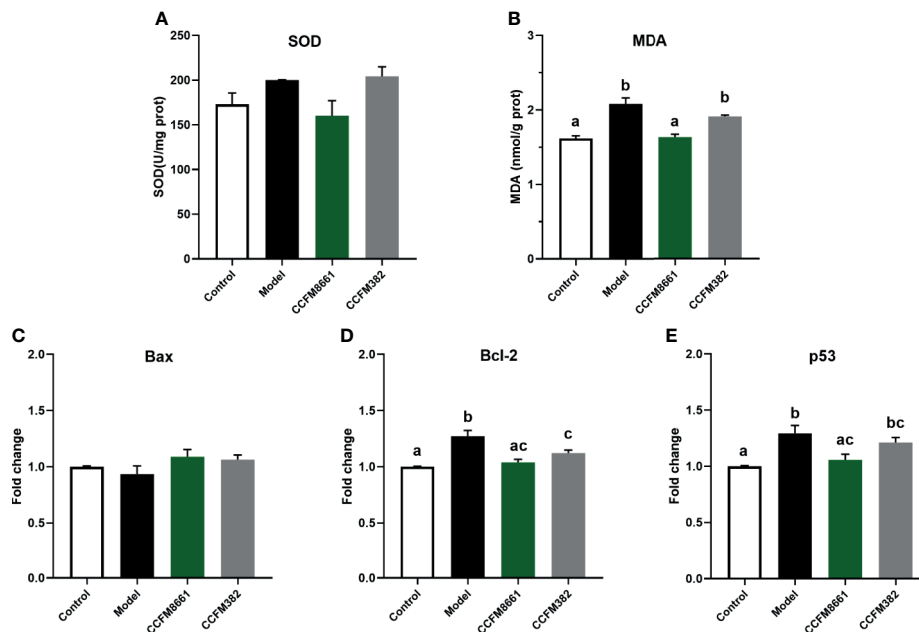


FIGURE 4 | Effect of *L. plantarum* CCFM8661 on oxidative stress- and tumor-related parameters in the brain. **(A)** SOD activity, **(B)** MDA level, **(C–E)** mRNA expression levels of apoptosis-related genes in brain. The different letters indicate significant difference between groups ($P < 0.05$).

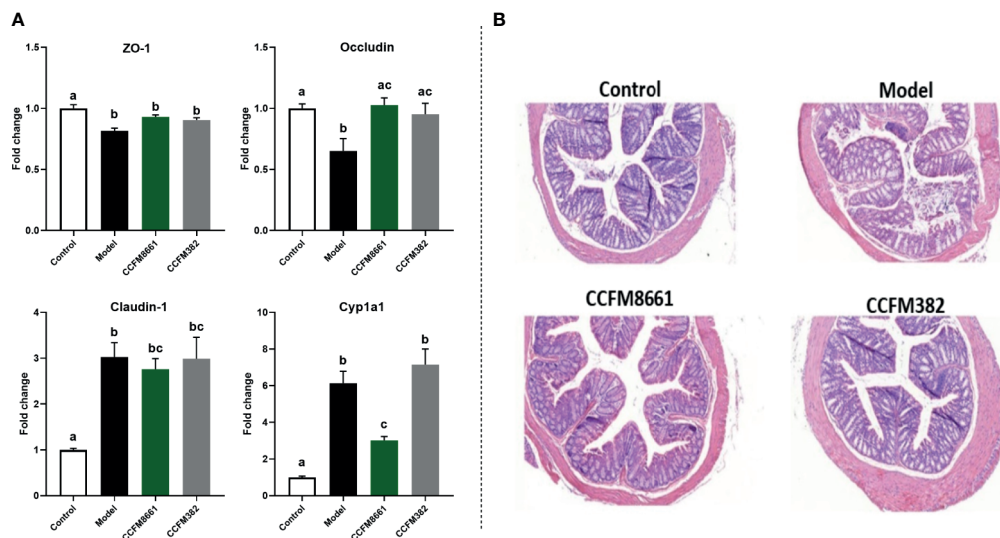


FIGURE 5 | Effect of *L. plantarum* CCFM8661 on the parameters related to the colon. **(A)** The mRNA expression of TJ proteins and CYP1A1. **(B)** Histopathological changes. The different letters indicate significant difference between groups ($P < 0.05$).

oral administration of *L. plantarum* CCFM8661 had a better alleviative effects on colonic damage induced by B[a]P.

Gut Microbiota Diversity

To determine whether the protective effects of *L. plantarum* CCFM8661 on B[a]P-induced colonic damage involved changes

in the gut microbiota, the α diversity and composition of gut microbiota were measured. The number of observed species and the Shannon index were used to represent the gut microbiota richness and diversity, respectively. The Faith_{pd} index represents phylogenetic diversity, which is a qualitative measure of community richness. As shown in **Figure 6A**, the observed

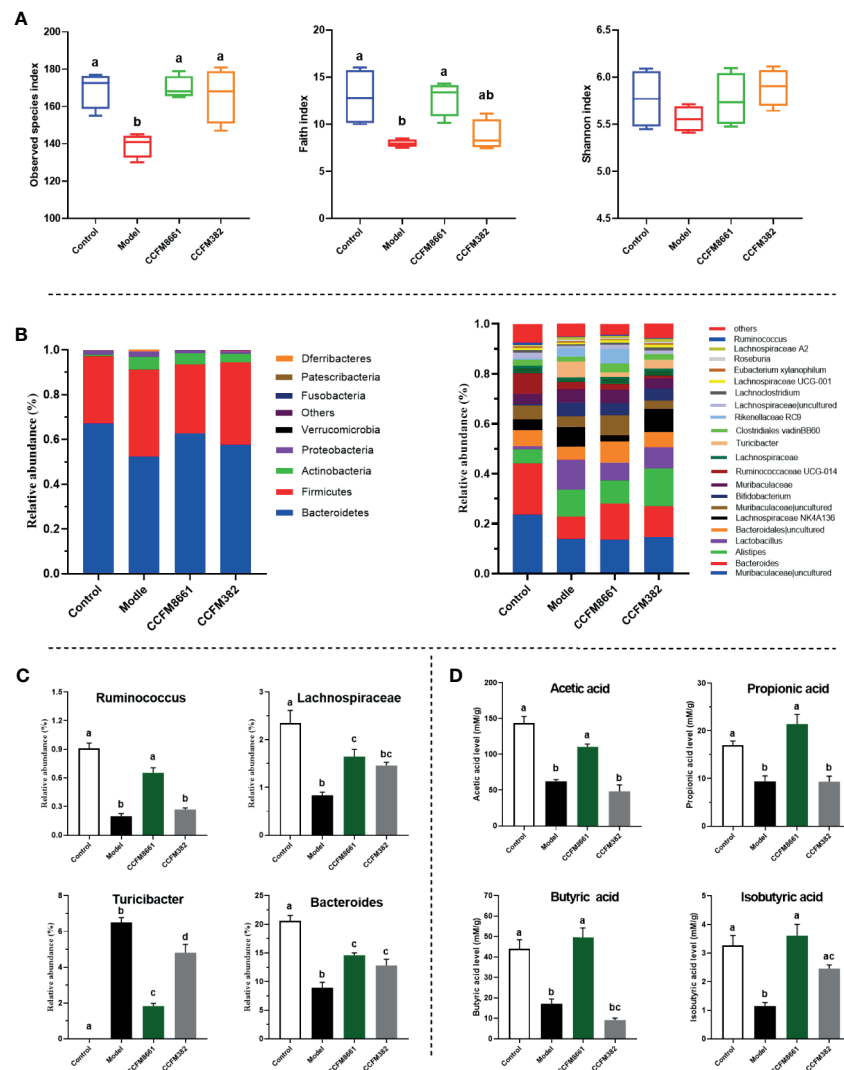


FIGURE 6 | Effect of *L. plantarum* CCFM8661 on the diversity and composition of the gut microbiota and SCFA levels. **(A)** α -diversity, **(B)** relative abundance of constituents of the gut microbiota at the phylum and genus levels, **(C)** relative abundance of significant bacterial communities, **(D)** SCFA levels. The different letters indicate significant difference between groups ($P < 0.05$).

species and Faith_{pd} indices decreased significantly in the model group, indicating that the richness and diversity of the gut microbiota were dramatically reduced ($P < 0.05$). Oral supplementation of *L. plantarum* CCFM8661 significantly increased these two indexes, but *L. plantarum* CCFM382 supplementation only elevated the observed species index ($P < 0.05$). The results showed that *L. plantarum* CCFM8661 had a stronger regulating ability than CCFM382 on gut microbiota diversity.

Composition of the Gut Microbiota

The α diversity results confirmed that B[a]P and *L. plantarum* CCFM8661 could, indeed, change the composition of the intestinal microbiota. Thus, changes in the gut microbiota

composition were further explored (Figure 6). At the phylum level, Bacteroidetes, Firmicutes, Actinobacteria, and Proteobacteria accounted for more than 95% of the gut microbiota (Figure 6B). In the control group, these four predominant bacterial phyla accounted for 67.1%, 30.1%, 0.7%, and 1.8% of the gut microbiota, respectively. The abundance of Bacteroidetes, Firmicutes, and Actinobacteria in the model group was 52.2%, 38.9%, and 5.8%, respectively, whereas the abundance of Proteobacteria (2.3%) remained almost unchanged. After supplement with *L. plantarum* CCFM8661, the abundance of Bacteroidetes (62.7%), Firmicutes (30.8%) and Proteobacteria (1.1%) gradually recovered to the levels of the control group, while the abundance of Actinobacteria (5.0%) was similar to their abundance in the model group, without significant changes. The abundances of these four bacterial phyla in CCFM382

group accounted for 57.6%, 36.8%, 3.9% and 1.1% respectively. The results showed that CCFM382 also affected the gut microbiota composition, but the effects were not as strong as that of CCFM8661. At the genus level, *Muribaculaceae*, *Bacteroides*, *Alistipes*, and *Lachnospiraceae* NK4A136 accounted for 23.6%, 20.6%, 5.6%, and 4.4%, respectively, in the control group (**Figure 6B**). The abundance of *Muribaculaceae* and *Bacteroides* in the model group decreased to 13.8% and 8.9%, respectively, and the abundance of *Alistipes* and *Lachnospiraceae* NK4A136 increased to 10.8% and 7.9%, respectively, compared with those in the control group. In the CCFM8661 group, the abundance of *Bacteroides* increased to 14.6% and the abundance of *Lachnospiraceae* NK4A136 decreased to 2.5%. Moreover, after B[a]P treatment, the abundance of *Ruminococcus*, *Lachnospiraceae*, and *Bacteroides* decreased significantly and the abundance of *Turicibacter* increased (**Figure 6C**, $P < 0.05$). *L. plantarum* CCFM8661 reversed the abundance of these four genera to their levels observed in the control group ($P < 0.05$), while *L. plantarum* CCFM382 only reversed the abundances of *Turicibacter* and *Bacteroides*.

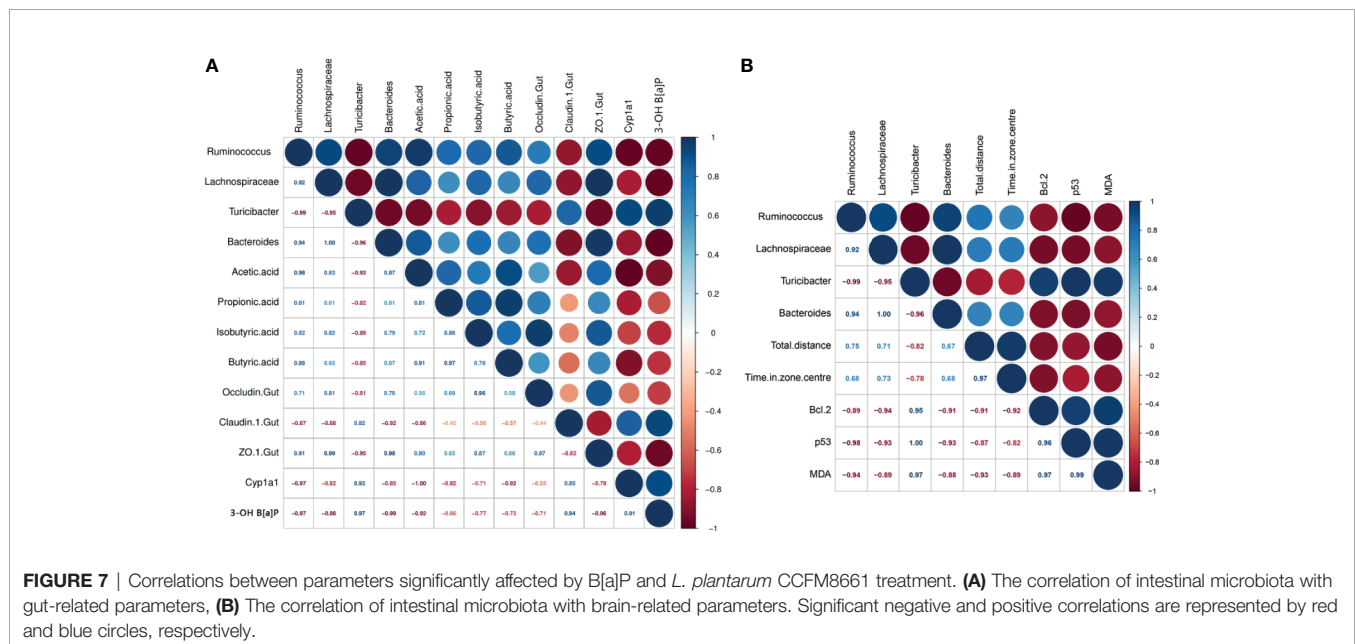
SCFA Levels

Compared to the levels in the control group, the levels of SCFAs, including acetic acid, butyric acid, isobutyric acid and propionic acid, were dramatically reduced in mice treated with B[a]P (**Figure 6D**). *L. plantarum* CCFM8661 sharply increased the levels of these SCFAs ($P < 0.05$) to levels almost the same as those in the control group. However, the administration of CCFM382 significantly increased only the levels of isobutyric acid among the SCFAs in B[a]P-treated mice ($P < 0.05$). The results showed that *L. plantarum* CCFM8661 had a better effect than CCFM382 on increase of SCFA levels.

Correlation and Heat Map Analyses

The parameters that were significantly affected by B[a]P and *L. plantarum* CCFM8661 were selected to assess their correlation using Pearson's correlation coefficients (**Figure 7**). The *Zo-1* expression levels were positive correlated with the abundance of *Ruminococcus* ($r = 0.91$), *Lachnospiraceae* ($r = 0.99$), and *Bacteroides* ($r = 0.98$), and negatively correlated with the *Turicibacter* abundance ($r = -0.95$), indicating that the gut microbiota was closely related to gut barrier function. The 3-OH B[a]P levels in feces had a strong positive correlation with *Turicibacter* abundance ($r = 0.97$) but a negative correlation with the abundance of *Ruminococcus* ($r = -0.97$), *Lachnospiraceae* ($r = -0.98$), and *Bacteroides* ($r = -0.99$) and *Zo-1* expression levels ($r = -0.96$). These results confirmed that the gut microbiota and the gut barrier affected 3-OH B[a]P excretion in the feces, and *vice versa*. Moreover, *Bcl-2* expression levels showed a strong positive correlation with the abundance of *Turicibacter* ($r = 0.95$) but a negative correlation with the abundance of *Lachnospiraceae* ($r = -0.94$) and *Bacteroides* ($r = -0.91$). *p53* levels were positively correlated with *Turicibacter* abundance ($r = 1.00$) and negatively correlated with the abundance *Ruminococcus* ($r = -0.98$), *Lachnospiraceae* ($r = -0.93$) and *Bacteroides* ($r = -0.93$). MDA levels were positively correlated with *Turicibacter* abundance ($r = 0.97$) and negatively correlated with the *Ruminococcus* abundance ($r = -0.94$), indicating that the gut microbiota was related to changes in tumor- and oxidative stress- related parameters in the brain.

Heatmap analysis was used to identify the similarities and differences among the four groups, as similar groups would cluster together in this analysis. As shown in **Figure 8**, the CCFM8661 treatment group was clustered with the control group, and the CCFM382 treatment group clustered with the model group, indicating that CCFM8661 had a strong protection



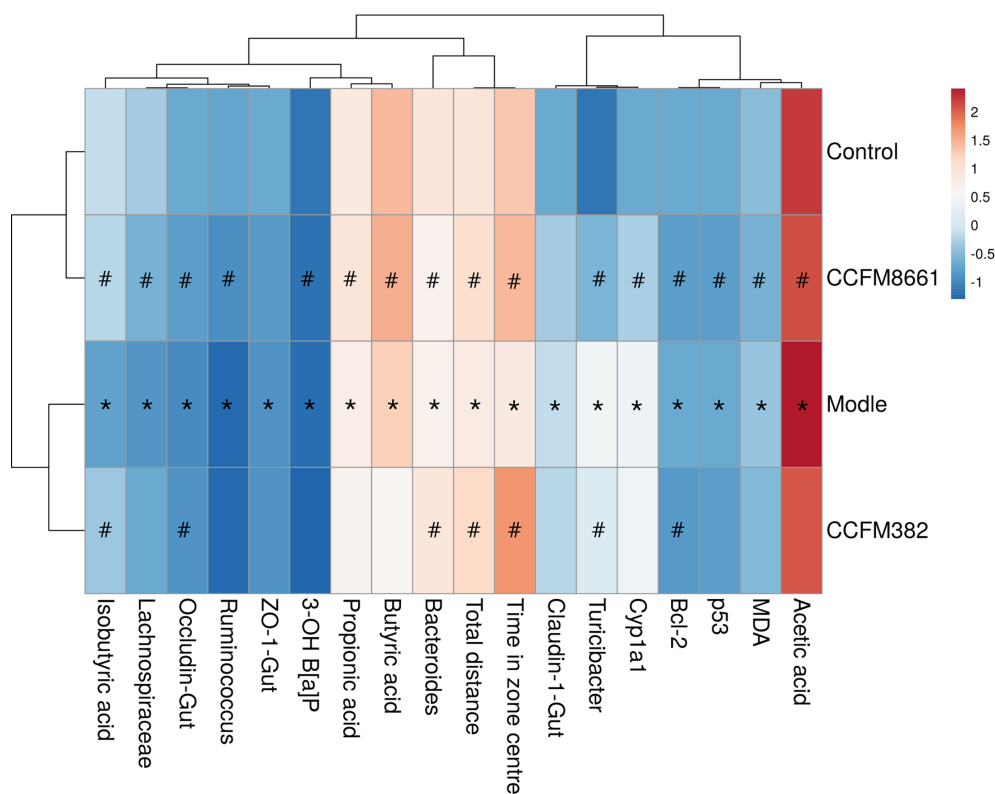


FIGURE 8 | Clustered heat map of the parameters significantly affected by B[a]P and *L. plantarum* CCFM8661 treatment. Red indicates an increase in the corresponding group and blue indicates a decrease in the corresponding group. The asterisks indicate significant difference between control and model groups ($P < 0.05$). The pound signs indicate significant difference between model and *L. plantarum* intervention groups ($P < 0.05$).

against B[a]P-induced damage, which may almost recover to the levels of the control group, while CCFM8661 only had a little protective effects.

DISCUSSION

When performing *in vitro* screening of strains of the probiotic *L. plantarum* for the potential to alleviate B[a]P toxicity, the B[a]P-binding ability should be considered. The selected strain should have superb B[a]P-binding ability, allowing it to bind B[a]P before it is absorbed by the host intestine, thereby resulting in excretion of B[a]P *via* the feces. In this study, the B[a]P-binding capacities varied among the 23 *L. plantarum* strains tested, and CCFM8661 was found to have the highest B[a]P-binding ability. The adsorption of B[a]P and other carcinogens by *Lactiplantibacillus* strains has previously been reported, and the mechanisms may involve the adsorption of polysaccharides and proteins on the cell surface (18, 19, 28). The main metabolic product of B[a]P *in vivo* is 3-OH B[a]P. The levels of 3-OH B[a]P in the feces of mice treated with B[a]P were decreased after *L. plantarum* CCFM8661 supplementation, indicating that this strain may bind to B[a]P *in vivo* and, thereby, reduce its metabolism. It has been reported that probiotic

Lactiplantibacillus spp. can bind to heavy metals, such as lead (29) and cadmium (30), and mycotoxins, such as aflatoxin (31), *in vivo*, thereby alleviating their toxic effects.

B[a]P treatment disturbed the balance of the gut microbiota. At the phylum level, B[a]P elevated the abundance of Proteobacteria and Firmicutes and reduced the abundance of Bacteroidetes. It has been reported that an increase in Proteobacteria and a decrease in Bacteroidetes are associated with polycyclic aromatic hydrocarbons (32, 33). At the genus level, the abundance of the beneficial bacteria Clostridiales, *Lachnospiraceae*, *Ruminococcus*, and *Bacteroides* decreased, and the abundance of the pro-inflammatory bacteria *Turicibacter* spp. increased significantly. However, *L. plantarum* CCFM8661 supplementation reversed these effects. A previous study also reported that *L. salivarius* Ls-33 can change the relative abundance of *Clostridium* spp. in the feces of obese juveniles (34). Some Clostridiales members produce butyrate, which may have an anti-inflammatory effect (13), and its levels usually decrease in an unhealthy state (35). Members of the family *Lachnospiraceae* are the most important butyrate-producing microorganisms in the intestine, as they regulate host energy metabolism and mucosal integrity and create a proinflammatory environment (36), while *Ruminococcus* has the ability to regulate mucin expression and mucosal glycosylation in the colonic mucosa (37). The significant changes observed in the abundance of these bacteria indicated that

B[a]P treatment can disrupt the gut microbiota composition, and *L. plantarum* CCFM8661 intervention can improve the homeostasis of the intestinal microbiota.

SCFAs are the metabolites of the gut microbiota, which can directly provide energy for intestinal epithelial cells and affect intestinal immunity and barrier function (38, 39). In this study, B[a]P exposure led to a decrease in the expression levels of the TJ-related genes *Zo-1* and occludin; this decrease may be attributed to the decrease in butyric and isobutyric acid production caused by B[a]P. *L. plantarum* CCFM8661 supplementation significantly increased the expression levels of occludin to almost normal levels. Previous studies have also reported that *Lactiplantibacillus* intervention can induce colonic TJ-related protein expression (40). In summary, B[a]P can significantly reduce the diversity of the intestinal microbiota, thus increasing the permeability of the intestinal barrier. Notably, *L. plantarum* CCFM8661 protected the integrity of the colonic mucosa and alleviated the pathological damage to the colon, which may have been related to changes in the intestinal microbiota. In addition, *L. plantarum* CCFM8661 significantly reduced the level of CYP1A1 induced by B[a]P and, thus, exerted a protective effect on the colon. Pithva et al. demonstrated similar results, showing that *L. rhamnosus* Vc alleviates colon injury caused by the carcinogen N-methyl-N'-nitroguanidine (41).

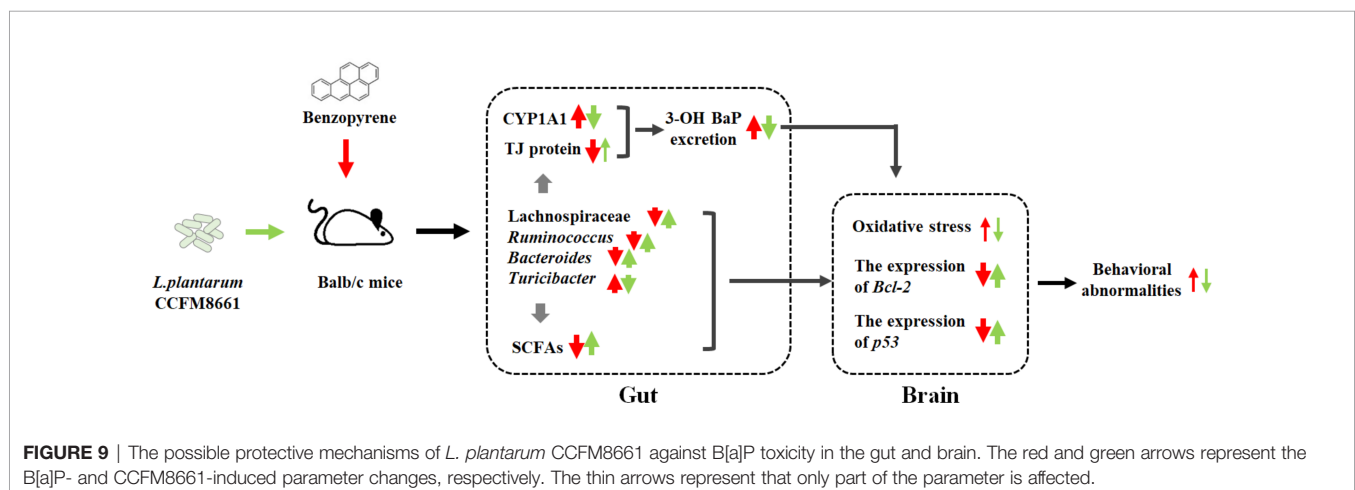
Mood and behavior are also closely related to changes in the intestine microbiota (42). B[a]P treatment resulted in disturbances of the gut microbiota, resulting in brain injuries and behavioral abnormalities. However, *L. plantarum* CCFM8661 reversed these effects. *Bcl-2* has anti-apoptotic roles, and its overexpression can reduce the production of oxygen free radicals and lipid peroxides and inhibit changes in mitochondrial permeability, thus inhibiting apoptosis. Exposure to B[a]P and the pesticide triazophos has been shown to significantly increase *Bcl-2* expression levels in the brain (43). The tumor suppressor gene *p53* is one of the most frequently mutated genes and is highly correlated with human cancers. Abnormal expression of this gene can be found in more than 50% of all malignant tumors. When DNA damage is minor, the *p53* gene helps the cell to repair itself; however, if the damage is

severe or the DNA repair mechanism fails, *p53* induces apoptosis. Intraperitoneal injection of B[a]P has been shown to increase the expression levels of *p53* in the cerebral cortex and hippocampus (44). *Lactiplantibacillus* administration has been shown to protect the brain from B[a]P-induced injury by reducing the expression levels of *Bcl-2* and *p53*. In addition, an increase in intestinal permeability induces systemic inflammation, causing an inflammatory response in the brain. The levels of MDA, an oxidative stress factor, reflect lipid peroxidation levels, which indicate the extent of injury to cells (45). A previous study also showed that B[a]P exposure increases MDA levels in the brain (46), indicating ROS generation and brain injury (47). Reportedly, *L. plantarum* strains have antioxidant abilities and induce a decrease in MDA levels (48).

In present study, the protection of two *L. plantarum* strains, with the highest and lowest B[a]P-binding ability respectively, against B[a]P-induced toxicity were compared. In terms of decreasing 3-OH B[a]P level in feces, improving colonic histopathology, oxidative stress- and tumor-related parameters in the brain and behavioral performance, regulating diversity and composition of gut microbiota and increasing SCFAs level, *L. plantarum* CCFM8661 performed better than *L. plantarum* CCFM382. The results of Heatmap analysis also proved this viewpoint. The underlying reasons for these different effects may main involve their significant difference in B[a]P-binding ability. However, in the aspect of colonic TJs expression and gut microbiota diversity, *L. plantarum* CCFM382 and *L. plantarum* CCFM8661 had the similar performance, which may attribute to the antioxidative ability or other probiotic properties of *L. plantarum* CCFM382.

CONCLUSION

Oral administration of *L. plantarum* CCFM8661 effectively alleviated colonic histopathological changes, reduced oxidative stress and tumor-related parameters in the brain, and improved behavioral performance. The underlying mechanism for these effects may involve the B[a]P-binding ability of CCFM8661 or



the regulation of the gut microbiota by CCFM8661, including an increase in the gut microbiota diversity and the abundance of *Ruminococcus* and Lachnospiraceae and a decrease in the abundance of the pro-inflammatory *Turicibacter* spp., thereby increasing the SCFA levels and improving the integrity of the gut barrier (Figure 9). Therefore, oral administration of *L. plantarum* CCFM8661 is an effective, easy, and safe intervention against B[a]P-induced toxicity.

DATA AVAILABILITY STATEMENT

The data presented in the study are deposited in the NCBI repository, accession number from SRR15244744 to SRR15244788.

ETHICS STATEMENT

All procedures and protocols of mice experiments were performed according to the guidelines of the Animal Care and Use Committee and the Ethics Committee of Jiangnan University (JN.No20190915b0481210).

REFERENCES

- Boström CE, Gerde P, Hanberg A, Jernström B, Johansson C, Kyrklund T, et al. Cancer Risk Assessment, Indicators, and Guidelines for Polycyclic Aromatic Hydrocarbons in the Ambient Air. *Environ Health Persp* (2002) 110:451–88. doi: 10.1289/ehp.110-1241197
- Jeong KH, Lee HJ, Park T, Shim SM. Catechins Controlled Bioavailability of Benzo (a) Pyrene (B Alpha P) From the Gastrointestinal Tract to the Brain Towards Reducing Brain Toxicity Using the *In Vitro* Bio-Mimic System Coupled With Sequential Co-Cultures. *Molecules* (2019) 24(11):2175–5. doi: 10.3390/molecules24112175
- Lee BM, Shim GA. Dietary Exposure Estimation of Benzo[a]Pyrene and Cancer Risk Assessment. *J Toxicol Env Heal A* (2007) 70(15-16):1391–4. doi: 10.1080/15287390701434182
- Stumpe-Viksna I, Morozovs A, Bartkevics V, Kukare A. Levels of Benzo(a) Pyrene (BaP) in Fish, Smoked According to Different Procedures. *Proc Latvia Univ Agric* (2008) 21(315):24–9.
- Omidian K, Rafiei H, Bandy B. Polyphenol Inhibition of Benzo[a]Pyrene-Induced Oxidative Stress and Neoplastic Transformation in an *In Vitro* Model of Carcinogenesis. *Food Chem Toxicol* (2017) 107:523–5. doi: 10.1016/j.fct.2017.07.028
- Chepelev NL, Moffat ID, Bowers WJ, Yauk CL. Neurotoxicity may be an Overlooked Consequence of Benzo[a]Pyrene Exposure That Is Relevant to Human Health Risk Assessment. *Mutat Res-Rev Mutat* (2015) 764:64–89. doi: 10.1016/j.mrrev.2015.03.001
- Irmawati A, Jasmin N, Sidarningsih. The Effect of Moderate Exercise on the Elevation of Bax/Bcl-2 Ratio in Oral Squamous Epithelial Cells Induced by Benzopyrene. *Vet World* (2018) 11(2):177–80. doi: 10.14202/vetworld.2018.177-180
- Yu D, Kazanietz MG, Harvey RG, Penning TM. Polycyclic Aromatic Hydrocarbon O-Quinones Inhibit the Activity of the Catalytic Fragment of Protein Kinase C. *Biochemistry* (2002) 41(39):11888–94. doi: 10.1021/bi020270p
- Grova N, Valley A, Turner JD, Morel A, Schroeder H. Modulation of Behavior and NMDA-R1 Gene mRNA Expression in Adult Female Mice After Sub-Acute Administration of Benzo(a)Pyrene. *Neurotoxicology* (2007) 28(3):630–6. doi: 10.1016/j.neuro.2007.01.010
- Perera FP, Rauh V, Tsai WY, Kinney P, Camann D, Barr D, et al. Effects of Transplacental Exposure to Environmental Pollutants on Birth Outcomes in a

AUTHOR CONTRIBUTIONS

LY: Methodology, Software, Formal analysis, Visualization, Funding acquisition, Writing—original draft. LZ: Investigation, Methodology, Software. HD: Writing—original draft, Methodology, Formal analysis. RZ: Investigation, Formal analysis. YX: Software, Software. MG: Investigation, Methodology. JZ: Supervision, Validation. HZ: Supervision, Validation. WC: Project administration, Funding acquisition. FT: Conceptualization, Writing—review and editing, Funding acquisition. All authors contributed to the article and approved the submitted version.

FUNDING

This work was supported by National Natural Science Foundation of China Key Program (31772090, 32001665, 31820103010, U1903205), Natural Science Foundation of Jiangsu Province (BK20180603), the Key Scientific and Technological Research Projects (2018AB010), BBSRC Newton Fund Joint Centre Award, the National first-class discipline program of Food Science and Technology (JUFSTR20180102).

- Multiethnic Population. *Environ Health Perspect* (2003) 111(2):201–5. doi: 10.1289/ehp.5742
- Laurent C, Feidt C, Grova N, Mpassi D, Rychen G. Portal Absorption of 14C After Ingestion of Spiked Milk With 14C-Phenanthrene, 14C-Benzo[a]Pyrene or 14C-TCDD in Growing Pigs. *Chemosphere* (2008) 48(8):843–8. doi: 10.1016/S0045-6535(02)00145-5
- Waxx AS, Regazzetti A, Dargère D, Auzeil N, Gil S, Brion DE. New *In Vitro* Biomarkers to Detect Toxicity in Human Placental Cells: The Example of Benzo[A]pyrene. *Toxicol Vitro* (2016) 32:76–85. doi: 10.1016/j.tiv.2015.11.022
- Ribière C, Peyret P, Parisot N, Darcha C, Déchelotte PJ, Barnich N, et al. Oral Exposure to Environmental Pollutant Benzo[a]Pyrene Impacts the Intestinal Epithelium and Induces Gut Microbial Shifts in Murine Model. *Sci Rep* (2016) 6(1):31027. doi: 10.1038/srep31027
- Li M, Esch BC, Wagenaar GT, Garssen J, Folkerts G, Henricks P. Pro-And Anti-Inflammatory Effects of Short Chain Fatty Acids on Immune and Endothelial Cells. *Eur J Pharmacol* (2018) 831:52–9. doi: 10.1016/j.ejphar.2018.05.003
- Vadder FD, Kovatcheva-Datchary P, Goncalves D, Vinera J, Mithieux G. Microbiota-Generated Metabolites Promote Metabolic Benefits via Gut-Brain Neural Circuits. *Cell* (2014) 156(1-2):84–96. doi: 10.1016/j.cell.2013.12.016
- Koh A, Vadder FD, Kovatcheva-Datchary P, Bäckhed F. From Dietary Fiber to Host Physiology: Short-Chain Fatty Acids as Key Bacterial Metabolites. *Cell* (2016) 165(6):1332–45. doi: 10.1016/j.cell.2016.05.041
- Kimoto-Nira H. New Lactic Acid Bacteria for Skin Health via Oral Intake of Heat-Killed or Live Cells. *Ani Sci J* (2018) 89(6):835–42. doi: 10.1111/asj.13017
- Suzuki T, Yamazaki K, Shinoda T, Shirai M, Yoshikawa H, Noguchi Y, et al. Excretion of 3,3',4,4', 5-Pentachlorobiphenyl (PCB126) From Rat Liver Following Oral Administration of Lactobacillus Reuteri and Lactobacillus Acidophilus[J]. *Food Sci Technol Res* (2014) 20(4):821–8. doi: 10.3136/fstr.20.821
- Apas AL, González SN, Arena ME. Potential of Goat Probiotic to Bind Mutagens[J]. *Anaerobe* (2014) 28:8–12. doi: 10.1016/j.anaerobe.2014.04.004
- Liu Y, Wu J, Xiao Y, Liu Q, Zhai Q. Relief of Cadmium-Induced Intestinal Motility Disorder in Mice by Lactobacillus Plantarum CCFM8610. *Front Immunol* (2020) 11:619574. doi: 10.3389/fimmu.2020.619574
- Zhao H, Zhou F, Qi Y, Dziugan P, Bai F, Walczak P, et al. Screening of Lactobacillus Strains for Their Ability to Bind Benzo (a) Pyrene and the

- Mechanism of the Process. *Food Chem Toxicol* (2013) 59:67–71. doi: 10.1016/j.fct.2013.05.040
22. Burokas A, Arboleya S, Moloney RD, Peterson VL, Murphy K, Clarke G, et al. Targeting the Microbiota-Gut-Brain Axis: Prebiotics Have Anxiolytic and Antidepressant-Like Effects and Reverse the Impact of Chronic Stress in Mice. *Biol Psychiatry* (2017) 82(7):472–87. doi: 10.1016/j.biopsych.2016.12.031
 23. Cryan JF, Markou A, Lucki I. Assessing Antidepressant Activity in Rodents: Recent Developments and Future Needs. *Trends Pharmacol Sci* (2002) 23(5):238–45. doi: 10.1016/S0165-6147(02)02017-5
 24. Liu X, Qi L, Yang B, Su D, Li F, Liu H. Determination of Benzo (a)Pyrene and 3-Hydroxy Benzo(a)Pyrene From Shellfish in Dalian. *Chin J Health Lab Technol* (2013) 23(5):1234–44.
 25. Xu Q, Li X, Wang E, He Y, Yin B, Fang D, et al. A Cellular Model for Screening of Lactobacilli That Can Enhance Tight Junctions. *RSC Adv* (2016) 6(113):111812–21. doi: 10.1039/C6RA24148D
 26. Yu L, Zhai Q, Zhu J, Zhang C, Li T, Liu X, et al. Dietary Lactobacillus Plantarum Supplementation Enhances Growth Performance and Alleviates Aluminum Toxicity in Tilapia. *Ecotoxicol Environ Saf* (2017) 143:307–14. doi: 10.1016/j.ecoenv.2017.05.023
 27. Wang G, Li X, Zhao J, Hao Z, Wei C. Lactobacillus Casei CCFM419 Attenuates Type 2 Diabetes via a Gut Microbiota Dependent Mechanism. *Food Funct* (2017) 8(9):3155–64. doi: 10.1039/C7FO00593H
 28. Lin D, Ji R, Wang D, Li Y, Qin T, Xing B, et al. The Research Progress in Mechanism and Influence of Biosorption Between Lactic Acid Bacteria and Pb (II): A Review. *Crit Rev Food Sci Nutr* (2019) 59(3):395–410. doi: 10.1080/10408398.2017.1374241
 29. Zafarullah M, Rabia R, Zhang S, Hu H, Ahsan H, Bakry AM, et al. Comparative Assessment of the Bioremedial Potentials of Potato Resistant Starch-Based Microencapsulated and Non-Encapsulated Lactobacillus Plantarum to Alleviate the Effects of Chronic Lead Toxicity. *Front Microbiol* (2018) 9:1306. doi: 10.3389/fmicb.2018.01306
 30. Zhai Q, Wang G, Zhao J, Liu X, Narbad A. Protective Effects of Lactobacillus Plantarum CCFM8610 Against Chronic Cadmium Toxicity in Mice Indicate Routes of Protection Besides Intestinal Sequestration. *Appl Environ Microb* (2014) 80(13):4063–71. doi: 10.1128/AEM.00762-14
 31. Zhang LY, Liu S, Zhao XJ, Wang N, Jiang X, Xin HS, et al. Lactobacillus Rhamnosus GG Modulates Gastrointestinal Absorption, Excretion Patterns, and Toxicity in Holstein Calves Fed a Single Dose of Aflatoxin B1. *J Dairy Sci* (2019) 102(2):1330–40. doi: 10.3168/jds.2018-15444
 32. Mukherjee S, Juottonen H, Siivonen P, Quesada CL, Tuomi P, Pulkkinen P, et al. Spatial Patterns of Microbial Diversity and Activity in an Aged Creosote-Contaminated Site. *Isme J* (2014) 8(10):2131–42. doi: 10.1038/ismej.2014.151
 33. Parajuli A, Gronroos M, Kauppi S, Plociniczak T, Roslund M, Galitskaya P, et al. The Abundance of Health-Associated Bacteria is Altered in PAH Polluted Soils-Implications for Health in Urban Areas? *PLoS One* (2017) 12(11):e0187852. doi: 10.1371/journal.pone.0187852
 34. Larsen N, Vogensen FK, Gobel RJ, Michaelsen KF, Jakobsen M, et al. Effect of Lactobacillus Salivarius Ls-33 on Fecal Microbiota in Obese Adolescents. *Clin Nutr* (2013) 32(6):935–40. doi: 10.1016/j.clnu.2013.02.007
 35. Gevers D, Kugathasan S, Denson LA, Baeza YV, Treuren WV, Ren B, et al. The Treatment-Naive Microbiome in New-Onset Crohn's Disease. *Cell Host Microbe* (2014) 15(3):382–92. doi: 10.1016/j.chom.2014.02.005
 36. Zhang J, Song L, Wang Y, Liu C, Zhang L, Zhu S, et al. Reduction in Butyrate-Producing Lachnospiraceae Contributes to Stress-Induced Visceral Hypersensitivity in Rats. *J Gastroen Hepatol* (2019) 34(8):1368–76. doi: 10.1111/jgh.14536
 37. Graziani F, Pujol A, Nicoletti C, Dou S, Maresca M, Giardina T, et al. Ruminococcus Gnavus E1 Modulates Mucin Expression and Intestinal Glycosylation. *J Appl Microbiol* (2016) 120(5):1403–17. doi: 10.1111/jam.13095
 38. Rooks MG, Garrett WS. Gut Microbiota, Metabolites and Host Immunity. *Nat Rev Immunol* (2016) 16(6):341–52. doi: 10.1038/nri.2016.42
 39. Ploeger S, Stumpff F, Penner GB, Schulzke JD, Gäbel G, Martens H, et al. Aschenbach: Microbial Butyrate and its Role for Barrier Function in the Gastrointestinal Tract. *Ann N Y Acad Sci* (2012) 1258:52–9. doi: 10.1111/j.1749-6632.2012.06553.x
 40. Jeong JJ, Kim KA, Hwang YJ, Han MJ, Kim DH. Anti-Inflammation Effects of Lactobacillus Brevis OW38 in Aged Mice. *Benef Microbe* (2016) 7(5):707–18. doi: 10.3920/BM2016.0016
 41. Pithva SP, Ambalam PS, Ramoliya JM, Dave JM, Vyas BRM. Antigenotoxic and Antimutagenic Activities of Probiotic Lactobacillus Rhamnosus Vc Against N-Methyl-N'-Nitro-N-Nitrosoguanidine. *Nutr Cancer* (2015) 67(7):1142–50. doi: 10.1080/01635581.2015.1073751
 42. Dinan TG, Cryan JF. Gut-brain Axis in 2016: Brain-Gut-Microbiota Axis — Mood, Metabolism and Behaviour. *Nat Rev Gastro Hepat* (2017) 14(2):69–70. doi: 10.1038/nrgastro.2016.200
 43. Wang G, Shao J, Wu M, Meng Y, Gul Y, Yang H, et al. Effect of Acute Exposure of Triazophos on Histological Structure and Apoptosis of the Brain and Liver of Zebrafish (Danio Rerio). *Ecotox Environ Safe* (2019) 180:646–55. doi: 10.1016/j.ecoenv.2019.05.053
 44. He J, Ji X, Li Y, Xue X, Feng G, Zhang H, et al. Subchronic Exposure of Benzo (a)Pyrene Interferes With the Expression of Bcl-2, Ki-67, C-Myc and P53, Bax, Caspase-3 in Sub-Regions of Cerebral Cortex and Hippocampus. *Exp Toxicol Pathol* (2016) 68(2-3):149–56. doi: 10.1016/j.etp.2015.11.007
 45. Apel K, Hirt H. Reactive Oxygen Species: Metabolism, Oxidative Stress, and Signal Transduction. *Annu Rev Plant Biol* (2004) 55:373–99. doi: 10.1146/annurev.arplant.55.031903.141701
 46. Saunders CR, Das SK, Ramesh A, Shockley DC, Mukherjee S. Benzo(a)pyrene-Induced Acute Neurotoxicity in the F-344 Rat: Role of Oxidative Stress. *J Appl Toxicol* (2006) 26(5):427–38. doi: 10.1002/jat.1157
 47. Dutta K, Ghosh D, Nazmi A, Kumawat KL, Basu A. A Common Carcinogen Benzo[a]pyrene Causes Neuronal Death in Mouse via Microglial Activation. *PLoS One* (2010) 5(4):e9984 50. doi: 10.1371/journal.pone.0009984
 48. Yu L, Zhai Q, Liu X, Wang G, Zhang Q, Zhao J, et al. Lactobacillus Plantarum CCFM639 Alleviates Aluminium Toxicity. *Appl Microbiol Biotechnol* (2016) 100(4):1891–900. doi: 10.1007/s00253-015-7135-7

Conflict of Interest: The authors declare that the research was conducted in the absence of any commercial or financial relationships that could be construed as a potential conflict of interest.

Publisher's Note: All claims expressed in this article are solely those of the authors and do not necessarily represent those of their affiliated organizations, or those of the publisher, the editors and the reviewers. Any product that may be evaluated in this article, or claim that may be made by its manufacturer, is not guaranteed or endorsed by the publisher.

Copyright © 2021 Yu, Zhang, Duan, Zhao, Xiao, Guo, Zhao, Zhang, Chen and Tian. This is an open-access article distributed under the terms of the Creative Commons Attribution License (CC BY). The use, distribution or reproduction in other forums is permitted, provided the original author(s) and the copyright owner(s) are credited and that the original publication in this journal is cited, in accordance with accepted academic practice. No use, distribution or reproduction is permitted which does not comply with these terms.



Consumption of Butylated Starch Alleviates the Chronic Restraint Stress-Induced Neurobehavioral and Gut Barrier Deficits Through Reshaping the Gut Microbiota

Peijun Tian^{1,2†}, Huiyue Zhu^{1,2†}, Xin Qian^{1,2}, Ying Chen^{1,2}, Zheng Wang^{1,2}, Jianxin Zhao^{1,2,3,4}, Hao Zhang^{1,2,3,4,5}, Gang Wang^{1,2,4*} and Wei Chen^{1,2,3}

¹ State Key Laboratory of Food Science and Technology, Jiangnan University, Wuxi, China, ² School of Food Science and Technology, Jiangnan University, Wuxi, China, ³ National Engineering Research Center for Functional Food, Jiangnan University, Wuxi, China, ⁴ (Yangzhou) Institute of Food Biotechnology, Jiangnan University, Yangzhou, China, ⁵ Wuxi Translational Medicine Research Center, Jiangsu Translational Medicine Research Institute, Wuxi, China

OPEN ACCESS

Edited by:

Huaxi Yi,
Ocean University of China, China

Reviewed by:

Zongxin Ling,
Zhejiang University, China
Zhen Feng,
Northeast Agricultural University,
China

*Correspondence:

Gang Wang
wanggang@jiangnan.edu.cn

[†]These authors have contributed
equally to this work

Specialty section:

This article was submitted to
Nutritional Immunology,
a section of the journal
Frontiers in Immunology

Received: 09 August 2021

Accepted: 02 September 2021

Published: 17 September 2021

Citation:

Tian P, Zhu H, Qian X, Chen Y,
Wang Z, Zhao J, Zhang H, Wang G
and Chen W (2021) Consumption
of Butylated Starch Alleviates the
Chronic Restraint Stress-Induced
Neurobehavioral and Gut Barrier Deficits
Through Reshaping the Gut Microbiota.
Front. Immunol. 12:755481.
doi: 10.3389/fimmu.2021.755481

The beneficial effect of short-chain fatty acids (SCFAs) on host health has been well recognized based on the booming knowledge from gut microbiome research. The role of SCFA in influencing psychological function is highlighted in recent years but has not been fully elucidated. In this study, the SCFA-acylated starches were used to accomplish a sizeable intestine-targeted release of the SCFAs, and the neurobehavioral, immunological, and microbial effects were further investigated. Acetylated-, butylated-, and isobutylated-starch could attenuate the depression-like behaviors and excessive corticosterone production in chronically stressed mice. Butylated- starch significantly reduced the colonic permeability *via* increasing the tight junction proteins (including ZO-1, Claudin, and Occludin) gene expression and reduced the level of the inflammatory cytokines (including IL-1 β and IL-6). The butylated starch's neurological and immunological benefits may be derived from the gut microbiome modifications, including normalizing the abundance of certain beneficial microbes (*Odoribacter* and *Oscillibacter*) and metabolomic pathways (*Tryptophan synthesis* and *Inositol degradation*). The present findings further validate the brain-beneficial effect of butyrate and offer novel guidance for developing novel food or dietary supplements for improving mental health.

Keywords: butyrate, starch, depression, gut barrier, inflammation

INTRODUCTION

Short-chain fatty acids (SCFAs) are the primary products of gut microbial fermentation from the undigested dietary fibers (1). Acetate, propionate, and butyrate (or isobutyrate) are the three major SCFAs (2). The regular communication between SCFAs and hosts participates in multiple physiological processes, including nutrients metabolism and immune system function (3). These SCFAs have been demonstrated to affect the host through multiple mechanisms: (a) SCFAs are

energy sources for gastrointestinal mucosal cells. In particular, butyrate is the primary energy source for colonocytes (4). (b) SCFAs are the ligands of G Protein-Coupled Receptors (GPCR). The activation of GPR43 and GPR41 *via* SCFAs promotes the secretion of various hormones involving blood glucose maintenance, such as glucagon-like peptide-1 (GLP-1) and peptide tyrosine (PYY) (5, 6). (c) SCFAs could act as the histone deacetylases (HDACs) and therefore normalize the gene expression involving cell proliferation and anti-inflammatory process (6).

In recent years, growing evidence suggested that SCFAs are also a class of signaling molecules regulating brain function through the gut-brain axis (7). For example, feeding the obese mice with butyrate could activate the vagus nerve, which suppresses the appetite-related hormones' release and then reduces the weight of mice (8). Besides, SCFAs secreted into the circulation could reach the brain and improve the blood-brain barrier's permeability by up-regulating the tight junction protein expression (9). Direct intake of SCFAs also showed noticeable neuromodulation effects. A prior oral supplementation of the SCFA mixture (acetate, propionate, and butyrate) could prevent the mice from the neurobehavioral deficits induced by the repeated psychosocial stress, including depression and anxiety-like behaviors and impaired gut barrier function (10). In addition, our previous studies also proved that the SCFAs facilitate the

biosynthesis of gut serotonin and the 5-hydroxytryptophan's circulation, and this mechanism may account for the antidepressant-like effect of some psychobiotic strains such as the *Bifidobacterium longum* CCFM687 and *Bifidobacterium breve* CCFM1025 (11–13).

Previous research from our group indicated that intaking of SCFA-acylated starch, which results in increased SCFAs levels in the large intestine, alleviates the constipation symptoms in mice (14). All the evidence indicates the SCFAs possess great psychotropic potential. Inspired by the reported findings, here we use the SCFA-acylated starches as the dietary supplement to investigate the role of each SCFA in managing stress-induced neurobehavioral, immunological, and gut microbial abnormalities.

MATERIAL AND METHODS

Animal Experiment

The animal procedures were approved by the Ethics Committee of Experimental Animals at Jiangnan University [JN.No20190930c0 501205(256)], following Directive 2010/63/EU guidelines. Animals were allowed to adapt to the environment (21°C~23°C, 50%~60% of humidity, 12:12h light-dark cycle) for seven days before the experiment. The group and experimental schedule are shown in **Figure 1A** (N=8–10 per group).

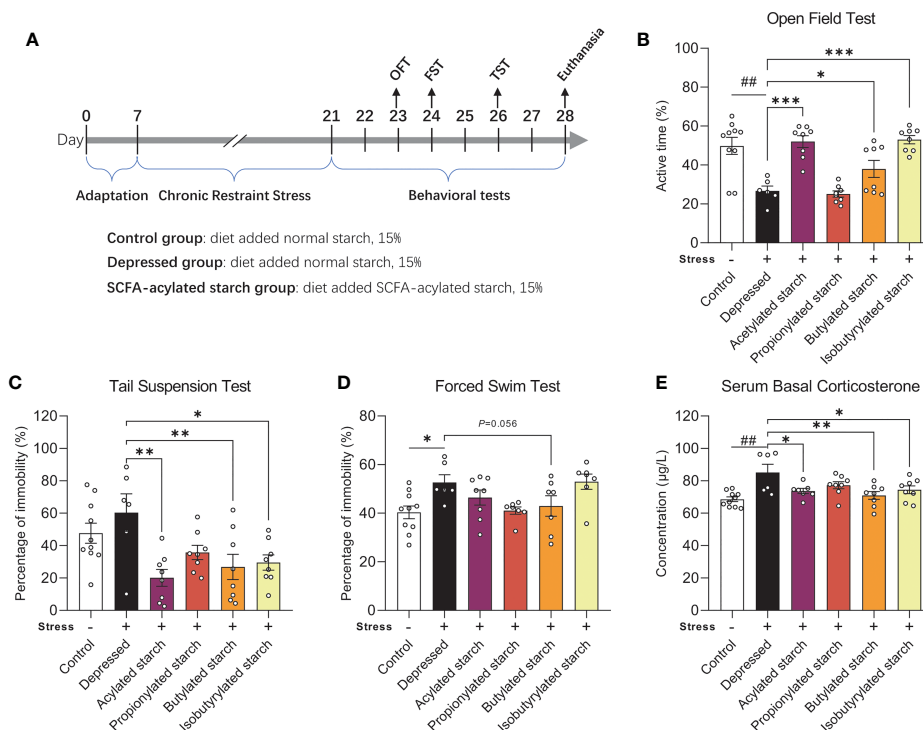


FIGURE 1 | The effect of the SCFA-acylated starches on the neurobehavioral phenotype. **(A)** The animal experiment schedule. **(B)** Open field test. **(C)** Tail suspension test. **(D)** Forced swim test. **(E)** Serum corticosterone levels. Except for the control, all groups are given two-week chronic restraint stress. Data are mean with SEM (n=6–10 per group for each test). $^{##}P<0.01$ in the unpaired t-tests. $^{*}P<0.05$, $^{**}P<0.01$, $^{***}P<0.001$ in the one-way ANOVA followed by Dunnett's multiple comparisons test against the *Depressed* group.

Chronic Restraint Stress

The chronic restraint stress (CRS) paradigm was used to establish the depression-like phenotype (15). Mice were exposed to the restraint stress three h per day (from 09:00 to 15:00 every day, 1 hour/each time, three times in total) for 14 consecutive days. Each mouse was put into a 50 mL plastic tube with a breathing hole and no food and water access. Mice in the control group fasted simultaneously during the CRS procedure. After the stress, all the mice were placed back in their home cages.

Behavioral Tests

The protocols of open field test (OFT), tail suspension test (TST), and forced swim test (FST) were described in detail in our previously published papers (13). For the OFT, mice were assessed for their locomotor activity in a square arena (50 cm×50 cm) enclosed by continuous opaque walls made of plexiglass. Animals were monitored for 10 minutes, and the time spent in the center zone and active time during the whole period were measured. For the TST, animals were hanged using adhesive tape to fix the tails to a suspension bar (30 cm high from the floor). Locomotor activity is monitored for six minutes, and the duration of immobility was measured. For the FST, mice were allowed to swim in the water with a temperature of 23–25°C, and the immobility time was recorded during the ten-minute swimming. All mice are trained to swim for 15 minutes the day before the test. Before all the behavioral tests, animals were habituated to the room for one hour. All tests were performed under dim light (60 lux) and monitored by the video tracking system (Ethovision version 13, Noldus, Netherland).

SCFA-Acylated Starches Preparation

SCFA-acylated starches were prepared as previously described (16, 17). Briefly, 40% (w/v) high amylose corn starch solution was continuously stirred in the water bath with a constant temperature of 40°. The pH was maintained at 8.00 by the addition of dilute NaOH (0.5 mol/L). Meanwhile, the acetic anhydride, propionic anhydride, butyric anhydride, and isobutyric anhydride were dripped into the starch solution, respectively, to reach a final amount of 20% (w/v). The solution was continued to be stirred for 2 hours, then adjusted to a pH of 5.70 using HCl (0.5 mol/L). The precipitation was collected by centrifuge (6000×g, 5min) and washed with water until the lotion was neutral. After a suction filtration at vacuum (-20 kPa, 10min), the precipitation was freeze-dried to get the SCFA-acylated starches. The starch solution without adding anhydride but processed as the same procedure above was used as control. The methods of measuring the degree of substitution of the SCFA-acylated starches and the results were described in **Supplemental 1.1**.

SCFAs Determination

SCFAs levels were measured as previously described with some modifications (12, 18). Fecal samples from the distal ileum and cecum are weighed (about 50 mg), homogenized, and

lyophilized. The samples were soaked in 500 µl of saturated NaCl solution for 30 min. The mixture was homogenized, and 40 µL 10% (w/v) sulfuric acid was added. 1 mL ether was added to the mixture and vortexed following centrifugation (18,000g, 15 min, 4°C). 500 µL supernatant was filtered (0.22 µm) before further analysis. SCFA concentrations were determined in the TSQ 9000 GC-MS system (Thermo Scientific) equipped with an Rtx-WAX capillary column, using helium as carrier gas (flow rate of 0.89 mL/min). A gradient profile of the oven temperature was used, starting at 100°C and increased to 140°C (7.5°C/min), then increased to 200°C (6.0°C/min) and maintained for 3 min. The ion source and interface temperature in the mass spectrometer were 220°C and 250°C, respectively.

Hormones and Cytokines Determination

Serum corticosterone and inflammatory cytokines (TNF-α, IL-β, and IL-6) were measured using enzyme-linked immunosorbent assay (ELISA) kits according to the manufacturer's protocol (SenBeiJia Biological Technology Co., Ltd., Nanjing, China).

Gene Transcription of the Tight Junction Proteins

Total RNA of the colon tissues was extracted using Trizol reagent (Invitrogen, USA). Complementary DNA was prepared using the HiFiScript gDNA Removal cDNA Synthesis Kit (ComWin Biotech Co., Ltd., China). Transcription levels of the zonula occludens-1 (ZO-1), Claudin, and Occludin were determined by quantitative PCR. The gene expression was normalized to *Gapdh* based on the cycle threshold (Ct) values and the $2^{-\Delta\Delta Ct}$ method. All samples are measured in triplicate. Primer sets information are shown in **Supplemental Table S1**.

16S rRNA-Amplicon Sequencing of the Fecal Microbiome

16S rRNA gene amplicon sequencing of the fecal microbiome was performed using universal primers (341F/806R, for V3-V4 region) as previously described. Raw data were processed using the QIIME2 software package, and the specialized bioinformatic analysis was performed using the online software of MicrobiomeAnalyst (<https://www.microbiomeanalyst.ca>), including alpha diversity, beta diversity, and network analysis (19, 20). Gut metabolic modules (GMMs) analysis was performed using the R version of the Gomixer tool as previously described (21, 22). Detailed bioinformatical methods are described in **Supplemental 1.2**.

Statistical Analysis

Data are presented as means with SEM. All data were checked for normality by the Shapiro-Wilk test. Unpaired Student's t-test was performed between the *Control* and *Depressed* groups. One-way ANOVA followed by Dunnett's multiple comparisons test against the *Depressed* group was performed to compare the effects of SCFA-acylated starches in the CRS-treated animals. A criterion for significance was set to $P < 0.05$ in all comparisons. The P -value of multiple comparisons was adjusted by family-wise significance and confidence levels of 0.05 (95% confidence interval).

RESULTS

Consumption of SCFA-Acylated Starches Changed the Depressive Symptoms of Stressed Mice

A two-week CRS induced significantly depressive behaviors, such as the significantly reduced active time in the OFT ($P=0.002$; **Figure 1B**) and increased immobility time in the FST ($P=0.011$; **Figure 1D**). The immobility time in the TST was increased but without any statistical difference ($P=0.308$; **Figure 1C**). Acetylated, butylated, and isobutylated starch reversed the animal's behavioral abnormality in the OFT (**Figure 1B**; $P<0.001$, $P=0.044$, $P<0.001$, respectively) and TST ($P=0.011$, $P=0.007$, $P=0.013$, respectively; **Figure 1C**). Butylated starch also reduced the animal's immobility time in the FST, with a trend statistical difference ($P=0.056$, **Figure 1D**). In addition, the stressed mice also showed a significantly reduced time spent in the center zone of the open field, but no SCFA-acylated starch reversed this abnormality (**Figure S1**). The hyperactivity of the hypothalamus-pituitary-adrenal axis was also observed in the stressed mice, as reflected by the significantly increased serum corticosterone level ($P=0.002$; **Figure 1E**). Acetylated, butylated, and isobutylated starch normalized the serum corticosterone level (**Figure 1E**; $P=0.031$, $P=0.005$, $P=0.040$, respectively).

SCFA-Acylated Starches Increased the SCFA Levels in the Large Intestine

In the distal ileum, the propionate ($P=0.001$), butyrate ($P=0.009$), and isobutyrate ($P<0.001$) levels were significantly increased

when compared with the depressed mice, while the acetate level was not changed by the acetylated starch (**Figures 2A–D**). In the cecum, the acetate ($P=0.044$) and butyrate ($P=0.024$) levels were significantly decreased in the depressed mice, and the abnormalities were reversed by the acetylated ($P=0.035$) and butylated ($P=0.001$) starch treatment (**Figures 2E, G**). The cecum propionate ($P=0.009$) and isobutyrate ($P<0.001$) levels were also significantly increased when compared to the depressed mice (**Figures 2F, H**). All above data indicated that the SCFA-acylated starches resulted in a release of SCFAs in the gut, especially in the large intestine.

Butylated Starch Improved the Gut Barrier Function of Depressed Mice

Gut barrier function was evaluated by the gene expression of tight junction protein levels. CRS induced a significant reduction of the transcriptional level of the ZO-1 gene ($P=0.049$), the Claudin gene ($P=0.038$), and the Occludin gene ($P=0.048$). Intriguingly, the butylated starch showed a superior effect to others to restore the gut barrier (**Figures 3A–C**). The deficit of gut barrier resulted in increased serum lipopolysaccharide (LPS; **Figure 3D**) and inflammatory cytokines, including serum IL-1 β ($P=0.001$), IL-6 ($P<0.001$), and TNF- α ($P=0.074$) (**Figures 3E–G**). Butylated starch significantly reduced the serum IL-1 β ($P=0.025$) and IL-6 ($P=0.002$) levels. The isobutyrate starch could also reduce the serum IL-6 level ($P=0.036$; **Figure 3F**). In addition, butylated starch reduced the serum TNF- α level, with a trend statistical difference ($P=0.054$, **Figure 3D**).

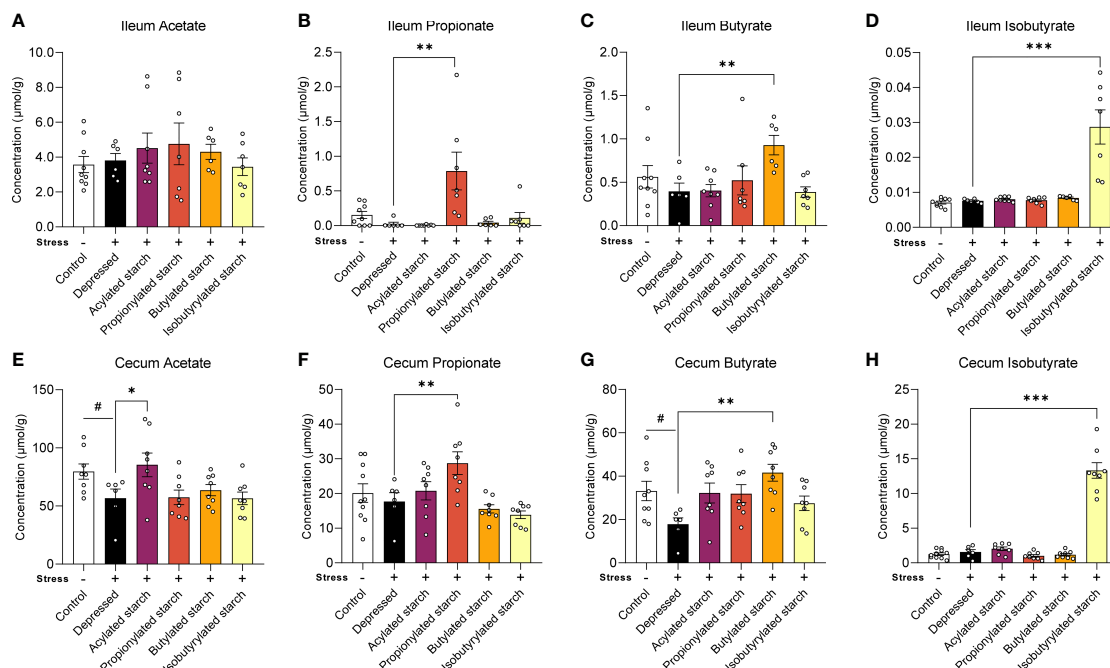


FIGURE 2 | The SCFAs levels in the ileum and cecum. (A–D) Acetate, propionate, butyrate, and isobutyrate levels in the ileum. (E–H) Acetate, propionate, butyrate, and isobutyrate levels in the cecum. Except for the control, all groups are given two-week chronic restraint stress. Data are mean with SEM ($n=6-10$ per group for each test). # $P<0.05$ in the unpaired t-tests. * $P<0.05$, ** $P<0.01$, *** $P<0.001$ in the unpaired t-tests.

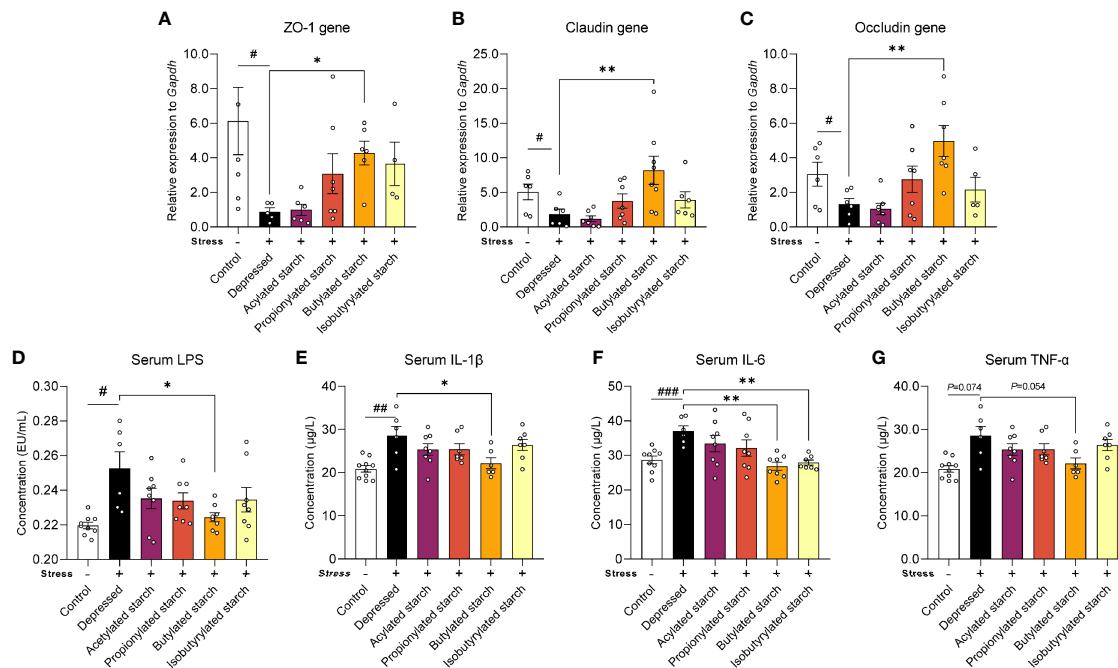


FIGURE 3 | The SCFAs levels in the ileum and cecum. **(A–C)** mRNA levels of the ZO-1, Claudin, and Occludin protein in the colon tissues. **(D–G)** Serum LPS and inflammatory cytokines (IL-1 β , IL-6, and TNF- α) levels. Except for the control, all groups are given two-week chronic restraint stress. Data are mean with SEM ($n=6-10$ per group for each test). $^{\#}P<0.05$, $^{\#\#}P<0.01$, $^{\#\#\#}P<0.001$ in the unpaired t-tests. $^*P<0.05$, $^{**}P<0.01$ in the unpaired t-tests.

Butylated Starch Changed the Gut Microbial Composition and Function of Depressed Mice

CRS induced a significantly increased gut microbial alpha-diversity, as reflected by the Shannon ($P<0.001$) and Chao1 ($P=0.001$) index (**Figures 4A, B**). The butylated starch treatment normalized the Chao1 changes ($P=0.003$; **Figure 4B**). Besides, the beta diversity estimated using Aitchison distance and principal component analysis (PCA) showed that every two groups are significantly different (PERMANOVA results in **Figure 4C**). The linear discriminant analysis (LDA) effect size algorithm (LEfSe) identified five genus-level biomarkers of the butylated starch treated gut microbiome, including *Bacteroides*, *Ruminiclostridium*, *Odoribacter*, and *Oscillibacter* (**Figure 4D**). The relative abundance of these four taxa was all significance decreased under stress, and the butylated starch treatment increased the *Odoribacter* ($P=0.072$) and *Oscillibacter* ($P=0.048$) abundances (**Figure 4E**). The microbial genomic functions were analyzed based on the gut-brain modules as previously described (22). A total of 17 pathways were identified, and four of them are significantly affected by the CRS and reversed by the butylated starch treatment, including *striatal dopamine (DA) and metabolite (DOPAC) synthesis*, *Dopamine degradation*, *Inositol degradation*, and *Tryptophan synthesis* (**Figure 4F**).

DISCUSSION

In the present study, oral intake of SCFA-acylated starches could significantly increase the SCFAs levels in the large intestine,

which improves the neurobiological conditions of the mice enduring chronic stress. In particular, the butylated starch could significantly enhance the gut barrier integrity and reduce inflammation. The butylated starch also improved the gut microbial composition and function, contributing to the recovery from the stress-induced disorder.

Although accumulated research have proved the beneficial role of SCFAs in regulating brain function, using dietary SCFAs to address psychological disorders did not make good progress (7). Since most SCFAs have a strong smell, the direct intake of SCFAs could cause olfactory discomfort and may affect neurobehavioral performance (23). Moreover, oral intake SCFAs are primarily absorbed by the upper intestine, which cannot mimic the natural production of SCFAs in the large intestine (24, 25). Since current evidence that supports the SCFAs' health effect is mainly generated from the research focused on the large intestine, direct oral intake of the SCFAs may not be the optimal choice (26). Intaking dietary fibers is another widely used way to enhance the SCFAs' production in the large intestine (27, 28). However, the production of each SCFA cannot be quantitatively controlled, and the role of each SCFA is hard to identify.

Accumulating studies demonstrated that acetylated starch has small enzyme resistance and could reach the large intestines (29, 30). Here, a catalytic reaction of corn starch with SCFA anhydrides was used to obtain the SCFA-acylated starches (31). These starches cannot be digested and absorbed when the degree of substitution was modified to the range of 0.2 to 0.3 (32). When reaching the large intestine, they are fermented by the gut

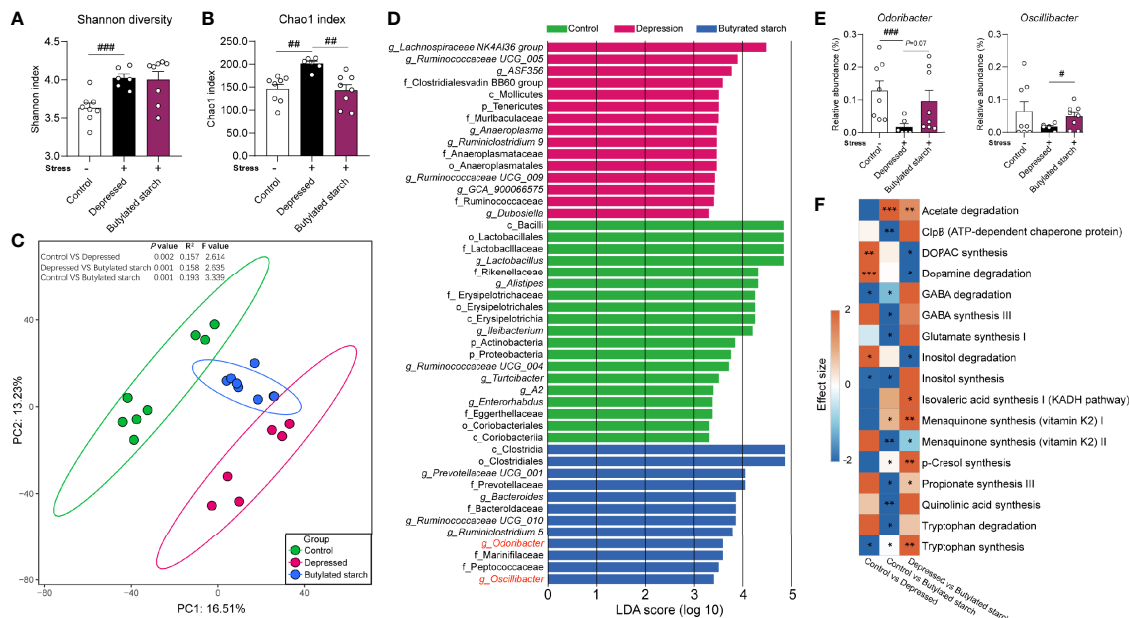


FIGURE 4 | The SCFAs levels in the ileum and cecum. **(A, B)** Alpha diversity of the gut microbiome, quantified using the Shannon and Chao 1 index. Except for the control, all groups are given two-week chronic restraint stress. Data are mean with SEM (n=6–10 per group). **P<0.01, ***P<0.001 in the unpaired t-tests. **(C)** Beta diversity of the gut microbiome. PCA based on the center-log ratio transferred Aitchison distance followed by the PERMANOVA. **(D)** Microbial biomarkers are identified by the linear discriminant analysis (LDA) effect size algorithm (LEfSe). $\alpha<0.05$ in the Wilcoxon rank-sum test and log LDA>2.0 were used as the threshold. **(E)** Relative abundance of selected microbes. Data are mean with SEM (n=6–10 per group). *P<0.05, ***P<0.001 in the unpaired t-tests. **(F)** Gut-brain module analysis. The colors of the boxes indicate the effect size between the two groups. Welch's t-test was performed between two groups. Asterisks in the heat map represent the Benjamini-Hochberg false discovery rate (FDR)-adjusted p-value: *P<0.05, **P<0.01, ***P<0.001.

microbiome and release the free SCFAs (16, 32). Our results reproduced the phenomenon, reflected as the higher SCFA levels in the cecum than in the ileum (Figure 2). Also, each starch only significantly increased the corresponding acid without affecting other acids' levels (Figure 2). Although not very precise, to some extent, the administration of SCFA-acylated starches realize a sizeable intestine-targeted release and elevation of each SCFA, which offers a great model for us to further investigate the SCFA's psychotropic effects.

A neurobehavioral change of stressed mice was observed in the acetylated-, butylated-, and isobutylated- starch treated mice, but only butylated starch significantly improved the gut barrier function and immune status. To investigate the underlying mechanisms, the gut microbiome was analyzed, and some interesting findings were observed. Butylated-starch treatment established a novel microbial structure that differs from healthy and depressed mice (Figure 4C). Specifically, the reduced *Odoribacter* and *Oscillibacter* abundance was largely recovered (Figure S2). *Odoribacter* is a common SCFA-producing microbe, and the deficit of *Odoribacter* has been correlated to many metabolic and immunological disorders, including chronic kidney disease (33), Crohn's disease (34), and inflammatory bowel disease (35). A recent study proved that *Odoribacter splanchnicus* has very low adherent and inflammatory capacity to the enterocytes or mucus and can secrete the outer membrane vesicles that exert anti-inflammatory action in the gut epithelium (36).

Oscillibacter is another microbial taxa that sensitively responded to stress (37, 38), and the abundance is found to be significantly decreased in significant depression disorder patients (39). In addition, the butylated-starch modified microbial function also facilitates the neurotransmission function through upregulating the *Tryptophan synthesis* and downregulating the *Inositol degradation* pathways. Tryptophan is the precursor of serotonin, which is a crucial neurotransmitter that regulating multiple brain functions. Inositol was widely verified to be efficacious in treating depression and obsessive-compulsive disorder, and the mechanism correlates to the enchantment of serotonin production *via* the 5-HT₂ receptors (40, 41). Collectively, normalizing the key microbes and metabolomic pathways seems beneficial to the host's immune and brain function.

CONCLUSIONS

In conclusion, the butylated starch could alleviate the chronic restraint stress-induced neurobehavioral and gut barrier deficits. The mechanisms may link to the modification of gut microbial composition and function. Butylated starch's anti-depressive and anti-inflammatory effects further validate the beneficial role of SCFAs in host health and offer novel guidance for developing novel food or dietary supplements for improving mental health.

DATA AVAILABILITY STATEMENT

The original contributions presented in the study are publicly available. This data can be found here: <https://www.ncbi.nlm.nih.gov/geo/query/acc.cgi?acc=GSE182262>.

ETHICS STATEMENT

The animal study was reviewed and approved by Ethics Committee of Experimental Animals at Jiangnan University (JN.No20190930c0501205[256]).

AUTHOR CONTRIBUTIONS

PT: conceptualization, investigation, writing-original draft, and funding acquisition. HuZ: investigation and formal analysis. YC, XQ, and ZW: formal analysis and visualization. HaZ and JZ: methodology, resources, and writing-review and editing. WC

and GW: supervision and funding acquisition. All authors contributed to the article and approved the submitted version.

FUNDING

This work was financially supported by the National Natural Science Foundation of China (No. 31972052, 32021005, 31820103010), the Fundamental Research Funds for the Central Universities (JUSRP22006, JUSRP51501), the China National Postdoctoral Program for Innovative Talents (BX2021114), China Postdoctoral Science Foundation (2021M691290), the Postdoctoral Science Foundation of Jiangsu Province (2021K127B), the Program of Collaborative Innovation Centre of Food Safety and Quality Control in Jiangsu Province.

SUPPLEMENTARY MATERIAL

The Supplementary Material for this article can be found online at: <https://www.frontiersin.org/articles/10.3389/fimmu.2021.755481/full#supplementary-material>

REFERENCES

- Morrison DJ, Preston T. Formation of Short Chain Fatty Acids by the Gut Microbiota and Their Impact on Human Metabolism. *Gut Microbes* (2016) 7(3):189–200. doi: 10.1080/19490976.2015.1134082
- Macfarlane S, Macfarlane GT. Regulation of Short-Chain Fatty Acid Production. *Proc Nutr Soc* (2003) 62(1):67–72. doi: 10.1079/PNS2002207
- Koh A, De Vadder F, Kovatcheva-Datchary P, Bäckhed F. From Dietary Fiber to Host Physiology: Short-Chain Fatty Acids as Key Bacterial Metabolites. *Cell* (2016) 165(6):1332–45. doi: 10.1016/j.cell.2016.05.041
- Pryde SE, Duncan SH, Hold GL, Stewart CS, Flint HJ. The Microbiology of Butyrate Formation in the Human Colon. *FEMS Microbiol Lett* (2002) 217(2):133–9. doi: 10.1016/S0378-1097(02)01106-0
- Tian P, Li B, He C, Song W, Hou A, Tian S, et al. Antidiabetic (Type 2) Effects of Lactobacillus G15 and Q14 in Rats Through Regulation of Intestinal Permeability and Microbiota. *Food Funct* (2016) 7(9):3789–97. doi: 10.1039/C6FO00831C
- Li K-K, Tian P-J, Wang S-D, Lei P, Qu L, Huang J-P, et al. Targeting Gut Microbiota: Lactobacillus Alleviated Type 2 Diabetes via Inhibiting LPS Secretion and Activating GPR43 Pathway. *J Funct Foods* (2017) 38:561–70. doi: 10.1016/j.jff.2017.09.049
- Dalile B, Van Oudenhove L, Vervliet B, Verbeke K. The Role of Short-Chain Fatty Acids in Microbiota–Gut–Brain Communication. *Nat Rev Gastroenterol Hepatol* (2019) 16(8):461–78. doi: 10.1038/s41575-019-0157-3
- Chambers ES, Morrison DJ, Frost G. Control of Appetite and Energy Intake by SCFA: What are the Potential Underlying Mechanisms? *Proc Nutr Soc* (2015) 74(3):328–36. doi: 10.1017/S0029665114001657
- Braniste V, Alasmakh M, Kowal C, Anuar F, Abbaspour A, Tóth M, et al. The Gut Microbiota Influences Blood-Brain Barrier Permeability in Mice. *Sci Transl Med* (2014) 6(263):263ra158. doi: 10.1126/scitranslmed.3009759
- van de Wouw M, Boehme M, Lyte JM, Wiley N, Strain C, O'Sullivan O, et al. Short-Chain Fatty Acids: Microbial Metabolites That Alleviate Stress-Induced Brain–Gut Axis Alterations. *J Physiol* (2018) 596(20):4923–44. doi: 10.1113/JP276431
- Tian P, Bastiaanssen TF, Song L, Jiang B, Zhang X, Zhao J, et al. Unravelling the Microbial Mechanisms Underlying the Psychobiotic Potential of a Bifidobacterium Breve Strain. *Mol Nutr Food Res* (2021) 2000704. doi: 10.1002/mnfr.202000704
- Tian P, Wang G, Zhao J, Zhang H, Chen W. Bifidobacterium With the Role of 5-Hydroxytryptophan Synthesis Regulation Alleviates the Symptom of Depression and Related Microbiota Dysbiosis. *J Nutr Biochem* (2019) 66:43–51. doi: 10.1016/j.jnubio.2019.01.007
- Tian P, O'Riordan KJ, Lee Y-K, Wang G, Zhao J, Zhang H, et al. Towards a Psychobiotic Therapy for Depression: Bifidobacterium Breve CCFM1025 Reverses Chronic Stress-Induced Depressive Symptoms and Gut Microbial Abnormalities in Mice. *Neurobiol Stress* (2020) 100216. doi: 10.1016/j.ynstr.2020.100216
- Wang L, Cen S, Wang G, Y-k L, Zhao J, Zhang H, et al. Acetic Acid and Butyric Acid Released in Large Intestine Play Different Roles in the Alleviation of Constipation. *J Funct Foods* (2020) 69:103953. doi: 10.1016/j.jff.2020.103953
- Zhu Y, Klomparsens EA, Guo S, Geng X. Neuroinflammation Caused by Mental Stress: The Effect of Chronic Restraint Stress and Acute Repeated Social Defeat Stress in Mice. *Neurol Res* (2019) 41(8):762–9. doi: 10.1080/01616412.2019.1615670
- Fukuda S, Toh H, Hase K, Oshima K, Nakanishi Y, Yoshimura K, et al. Bifidobacteria can Protect From Enteropathogenic Infection Through Production of Acetate. *Nature* (2011) 469(7331):543–7. doi: 10.1038/nature09646
- Han F, Liu M, Gong H, Lü S, Ni B, Zhang B. Synthesis, Characterization and Functional Properties of Low Substituted Acetylated Corn Starch. *Int J Biol Macromol* (2012) 50(4):1026–34. doi: 10.1016/j.jbiomac.2012.02.030
- Tian P, Zou R, Song L, Zhang X, Jiang B, Wang G, et al. Ingestion of Bifidobacterium Longum Subspecies Infantis Strain CCFM687 Regulated Emotional Behavior and the Central BDNF Pathway in Chronic Stress-Induced Depressive Mice Through Reshaping the Gut Microbiota. *Food Funct* (2019) 10(11):7588–98. doi: 10.1039/C9FO01630A
- Chong J, Liu P, Zhou G, Xia J. Using MicrobiomeAnalyst for Comprehensive Statistical, Functional, and Meta-Analysis of Microbiome Data. *Nat Protoc* (2020) 15(3):799–821. doi: 10.1038/s41596-019-0264-1
- Dhariwal A, Chong J, Habib S, King IL, Agellon LB, Xia J. MicrobiomeAnalyst: A Web-Based Tool for Comprehensive Statistical, Visual and Meta-Analysis of Microbiome Data. *Nucleic Acids Res* (2017) 45(W1):W180–8. doi: 10.1093/nar/gkx295
- Bastiaanssen T, Gururajan A, Wouw M, Moloney GM, Cryan JF. Volatility as a Concept to Understand the Impact of Stress on the Microbiome. *Psychoneuroendocrinology* (2021) 124:105047. doi: 10.1016/j.psyneuen.2020.105047
- Valles-Colomer M, Falony G, Darzi Y, Tigheelaar EF, Wang J, Tito RY, et al. The Neuroactive Potential of the Human Gut Microbiota in Quality of Life and Depression. *Nat Microbiol* (2019) 4(4):623–32. doi: 10.1038/s41564-018-0337-x

23. Breer H, Fleischer J, Strotmann J. The Sense of Smell: Multiple Olfactory Subsystems. *Cell Mol Life Sci* (2006) 63(13):1465–75. doi: 10.1007/s00018-006-6108-5
24. Ferreira TM, Leonel AJ, Melo MA, Santos RR, Cara DC, Cardoso VN, et al. Oral Supplementation of Butyrate Reduces Mucositis and Intestinal Permeability Associated With 5-Fluorouracil Administration. *Lipids* (2012) 47(7):669–78. doi: 10.1007/s11745-012-3680-3
25. Rupp H, Bar-Meir S, Soergel KH, Wood CM, Schmitt MG Jr. Absorption of Short-Chain Fatty Acids by the Colon. *Gastroenterology* (1980) 78(6):1500–7. doi: 10.1016/S0016-5085(19)30508-6
26. Bourassa MW, Alim I, Bultman SJ, Ratan RR. Butyrate, Neuroepigenetics and the Gut Microbiome: Can a High Fiber Diet Improve Brain Health? *Neurosci Lett* (2016) 625:56–63. doi: 10.1016/j.neulet.2016.02.009
27. Mandaliya D, Patel S, Seshadri S. Fiber in Our Diet and its Role in Health and Disease. *Funct Food Hum Health Springer* (2018) 247–55. doi: 10.1007/978-981-13-1123-9_12
28. Tan J, McKenzie C, Vuillermin PJ, Goverse G, Vinuesa CG, Mebius RE, et al. Dietary Fiber and Bacterial SCFA Enhance Oral Tolerance and Protect Against Food Allergy Through Diverse Cellular Pathways. *Cell Rep* (2016) 15(12):2809–24. doi: 10.1016/j.celrep.2016.05.047
29. Balamurugan R, Pugazhendhi S, Balachander GM, Dharmalingam T, Mortimer EK, Gopalsamy GL, et al. Effect of Native and Acetylated Dietary Resistant Starches on Intestinal Fermentative Capacity of Normal and Stunted Children in Southern India. *Int J Environ Res Public Health* (2019) 16(20):3922. doi: 10.3390/ijerph16203922
30. Englyst HN, Kingman SM, Cummings J. Classification and Measurement of Nutritionally Important Starch Fractions. *Eur J Clin Nutr* (1992) 46:S33–50.
31. Zhu J, Zhang S, Zhang B, Qiao D, Pu H, Liu S, et al. Structural Features and Thermal Property of Propionylated Starches With Different Amylose/Amylopectin Ratio. *Int J Biol Macromol* (2017) 97:123–30. doi: 10.1016/j.ijbiomac.2017.01.033
32. Annison G, Illman RJ, Topping DL. Acetylated, Propionylated or Butyrylated Starches Raise Large Bowel Short-Chain Fatty Acids Preferentially When Fed to Rats. *J Nutr* (2003) 133(11):3523–8. doi: 10.1093/jn/133.11.3523
33. Kim JE, Kim H-E, Park JI, Cho H, Kwak M-J, Kim B-Y, et al. The Association Between Gut Microbiota and Uremia of Chronic Kidney Disease. *Microorganisms* (2020) 8(6):907. doi: 10.3390/microorganisms8060907
34. Van Limbergen J, Dunn K, Wine E, Sigall Boneh R, Bielawski J, Levine A. OP22 Crohn's Disease Exclusion Diet Reduces Bacterial Dysbiosis Towards Healthy Controls in Paediatric Crohn's Disease. *J Crohn's Colitis* (2020) 14 (Supplement_1):S019–20. doi: 10.1093/ecco-jcc/jjz203.021
35. Morgan XC, Tickle TL, Sokol H, Gevers D, Devaney KL, Ward DV, et al. Dysfunction of the Intestinal Microbiome in Inflammatory Bowel Disease and Treatment. *Genome Biol* (2012) 13(9):1–18. doi: 10.1186/gb-2012-13-9-r79
36. Hiippala K, Barreto G, Burrello C, Diaz-Basabe A, Suutarinen M, Kainulainen V, et al. Novel *Odoribacter Splanchnicus* Strain and Its Outer Membrane Vesicles Exert Immunoregulatory Effects *In Vitro*. *Front Microbiol* (2020) 11:575455. doi: 10.3389/fmicb.2020.575455
37. Yang H-L, Li M-M, Zhou M-F, Xu H-S, Huan F, Liu N, et al. Links Between Gut Dysbiosis and Neurotransmitter Disturbance in Chronic Restraint Stress-Induced Depressive Behaviours: The Role of Inflammation. *Research Square* (2021). doi: 10.21203/rs.3.rs-469197/v1
38. Ma X, Zhang Y, Xu T, Qian M, Yang Z, Zhan X, et al. Early-Life Intervention Using Exogenous Fecal Microbiota Alleviates Gut Injury and Reduce Inflammation Caused by Weaning Stress in Piglets. *Front Microbiol* (2021) 12(671683). doi: 10.3389/fmicb.2021.671683
39. Jiang H, Ling Z, Zhang Y, Mao H, Ma Z, Yin Y, et al. Altered Fecal Microbiota Composition in Patients With Major Depressive Disorder. *Brain Behav Immun* (2015) 48:186–94. doi: 10.1016/j.bbi.2015.03.016
40. Fux M, Benjamin J, Belmaker R. Inositol Versus Placebo Augmentation of Serotonin Reuptake Inhibitors in the Treatment of Obsessive–Compulsive Disorder: A Double-Blind Cross-Over Study. *Int J Neuropsychopharmacol* (1999) 2(3):193–5. doi: 10.1017/S1461145799001546
41. Levine J, Mishori A, Susnosky M, Martin M, Belmaker RH. Combination of Inositol and Serotonin Reuptake Inhibitors in the Treatment of Depression. *Biol Psychiatry* (1999) 45(3):270–3. doi: 10.1016/S0006-3223(98)00145-0

Conflict of Interest: The authors declare that the research was conducted in the absence of any commercial or financial relationships that could be construed as a potential conflict of interest.

Publisher's Note: All claims expressed in this article are solely those of the authors and do not necessarily represent those of their affiliated organizations, or those of the publisher, the editors and the reviewers. Any product that may be evaluated in this article, or claim that may be made by its manufacturer, is not guaranteed or endorsed by the publisher.

Copyright © 2021 Tian, Zhu, Qian, Chen, Wang, Zhao, Zhang, Wang and Chen. This is an open-access article distributed under the terms of the Creative Commons Attribution License (CC BY). The use, distribution or reproduction in other forums is permitted, provided the original author(s) and the copyright owner(s) are credited and that the original publication in this journal is cited, in accordance with accepted academic practice. No use, distribution or reproduction is permitted which does not comply with these terms.



Synergistic Protective Effect of Konjac Mannan Oligosaccharides and *Bacillus subtilis* on Intestinal Epithelial Barrier Dysfunction in Caco-2 Cell Model and Mice Model of Lipopolysaccharide Stimulation

Lupeng Chen[†], Shuai Zhang[†], Shi Wu, Zhuqing Ren, Guoquan Liu and Jian Wu^{*}

College of Animal Sciences & Technology/College of Veterinary Medicine, Huazhong Agricultural University, Wuhan, China

OPEN ACCESS

Edited by:

Qixiao Zhai,
Jiangnan University, China

Reviewed by:

Xi Ma,
China Agricultural University, China
Jian Ge,
China Jiliang University, China

*Correspondence:

Jian Wu
wujian@mail.hzau.edu.cn

[†]These authors have contributed
equally to this work

Specialty section:

This article was submitted to
Nutritional Immunology,
a section of the journal
Frontiers in Immunology

Received: 16 April 2021

Accepted: 31 August 2021

Published: 17 September 2021

Citation:

Chen L, Zhang S, Wu S,
Ren Z, Liu G and Wu J (2021)
Synergistic Protective Effect of Konjac
Mannan Oligosaccharides and
Bacillus subtilis on Intestinal Epithelial
Barrier Dysfunction in Caco-2 Cell
Model and Mice Model of
Lipopolysaccharide Stimulation.
Front. Immunol. 12:696148.
doi: 10.3389/fimmu.2021.696148

As the first line of defense against intestinal bacteria and toxins, intestinal epithelial cells are always exposed to bacteria or lipopolysaccharide (LPS), whereas pathogenic bacteria or LPS can cause intestinal epithelial cell damage. Previous studies have shown that konjac mannan oligosaccharides (KMOS) have a positive effect on maintaining intestinal integrity, and *Bacillus subtilis* (BS) can promote the barrier effect of the intestine. However, it is still unknown whether KMOS and BS have a synergistic protective effect on the intestines. In this study, we used the LPS-induced Caco-2 cell injury model and mouse intestinal injury model to study the synergistic effects of KMOS and BS. Compared with KMOS or BS alone, co-treatment with KMOS and BS significantly enhanced the activity and antioxidant capacity of Caco-2 cell, protected mouse liver and ileum from LPS-induced oxidative damage, and repaired tight junction and mucus barrier damage by up-regulating the expression of Claudin-1, ZO-1 and MUC-2. Our results demonstrate that the combination of KMOS and BS has a synergistic repair effect on inflammatory and oxidative damage of Caco-2 cells and alleviates LPS-induced acute intestinal injury in mice.

Keywords: *Bacillus subtilis*, KMOS, Caco-2 cells, LPS, intestinal injury

INTRODUCTION

The intestinal tract, as the largest bacterial endotoxin reservoir in the body, has a complete intestinal epithelial barrier, which plays an important role in maintaining the permeability of epithelial cells and homeostasis of the internal environment of the body (1). Intestinal epithelial cells are an important part of the gut mucosal barrier, the first line of defense against intestinal toxins and bacteria (2, 3), and play an important regulatory role in the immune system of the host (4). Tight junctions (TJs) are the primary factors that determine paracellular permeability (5). The barrier and permeability properties of TJs are defined in a significant part by the ensemble of claudin proteins expressed (6). The cytoplasmic protein, zonula occludens-1 (ZO-1), is a key protein that maintains

TJ structure and intestinal epithelial barrier function (7). In the colonic mucosa, the main mucin gene is *MUC2*, a secretory mucin, and to a lesser extent *MUC1*, *MUC3*, and *MUC4*, which are both transmembrane mucins and secretory mucins from the splicing variants (8).

Oxidative stress is closely associated with inflammation and immunity. Intestinal epithelial cells are strongly involved in mucosal oxidative stress and inflammatory responses (9). Nuclear factor E2-related factor 2 (Nrf2) is a central regulator of cells against oxidative stress. High levels of lipopolysaccharide (LPS) are present in the colon. LPS not only causes inflammation damage, but also induces oxidative stress (10), causing damage to the intestinal structure and function (11). LPS is often used to induce intestinal epithelial barrier dysfunction in a Caco-2 cell model (12) and a pathological mouse model (13).

Konjac mannan oligosaccharides (KMOS) are important functional oligosaccharides, which are the hydrolytic products of konjac glucomannan, isolated from tubers of *Amorphophallus konjac* K. Koch (14). Konjac mannan oligosaccharide (KMOS) is a hydrolysis product of konjac glucomannan, consisting of β -D-mannose and β -D-glucose residues linked together by β -(1 \rightarrow 4) glycosidic bonds. Recently, the protective effects of KMOS on intestinal immunity and integrity have received much attention. KMOS supplementation has been reported to help improve trinitrobenzenesulfonic acid-induced colitis and improve the intestinal condition of patients with inflammatory bowel disease (IBD) (15). Furthermore, KMOS supplementation improved colonic epithelial integrity and blocked the production of pro-inflammatory cytokines including IL-1 β , IL-6 and TNF- α , indicating the inhibition of intestinal inflammation by KMOS (16). Recent studies suggest that KMOS amelioration of DSS-induced colitis requires activation of the SIGNR1 signaling pathway, and that activation of this signal is critical for KMOS-mediated macrophage phenotype switching (16). KMOS deliver various physiological functions, such as dietary fiber and prebiotics (17), regulation of immune system (18), antiobesity (19), and attenuation of glucose metabolism dysfunction (18). In particular, Liu et al. (15) indicated that konjac oligosaccharide is an anti-inflammatory agent and could be useful as a prebiotic to design functional foods for ulcerative colitis. Jian et al. (20) found a protective effect of Konjac oligo-glucomannan against H₂O₂-induced oxidative damage in a human hepatic cell line. The inclusion of Konjac flour in the gestation diet changes the gut microbiota, alleviates oxidative stress, and improves insulin sensitivity in sows (21). However, the exact molecular mechanisms involved in the anti-inflammatory and antioxidant effects of KMOS in intestinal epithelial cells remain poorly understood.

Probiotics can regulate intestinal flora and protect against intestinal injury. *Bacillus subtilis* is a biosafety bacterium used in many studies (22) and has extensive applications. In particular, there have been several studies on the protective effect of BS on intestinal barrier function. Musa et al. (23) indicated that *Bacillus subtilis* B21 improves the intestinal health and performance of broiler chickens with *Clostridium perfringens*-induced necrotic enteritis. Supplementation of the spores of BS and *Bacillus*

coagulans improved growth performance and was beneficial to the intestinal microbiota in rats (24). It was shown that oral administration of *Bacillus subtilis* fermented milk could reduce intestinal mucosal injury and inflammatory response and induce intestinal stem cell proliferation to promote the reconstruction of mucosal barrier. In addition, *Bacillus subtilis* can rebalance the intestinal flora, such as increasing the abundance of *Bacillus*, *Alistipes* and *Lactobacillus*, while decreasing the abundance of *Escherichia coli* (25) and *Bacillus mimicus* (26), as well as the relative number of *E. coli*. *Bacillus subtilis* increased ZO-1 protein expression, attenuated tight junction damage, and reduced apoptosis. Mechanistically, BS may have protected ZO-1 protein by activating toll-like receptor signaling pathways and reduced damage by downregulating death receptor genes and upregulating DNA repair genes (27).

However, there are still many bottleneck problems in the research and application of probiotics, especially the rapid colonization, growth, and maintenance of a rich concentration of bacteria in the body after addition. In practice, the application of probiotics alone cannot achieve a good and stable effect. However, whether KMOS and BS have synergistic protective effects on the intestinal tract, and the mechanism of their effects, are still unknown. In the present study, we detected the synergistic protective effect of KMOS and BS against LPS-induced intestinal epithelial cell injury in a Caco-2 cell model and a mouse model, respectively. Our study shows that the combined use of KMOS and BS has a synergistic repair effect on Caco-2 cells and intestinal injury in mice, can enhance the antioxidant function of cells, and has a good protective effect against LPS-induced acute injury in mice.

MATERIALS AND METHODS

Cell Culture and Treatment

When the Caco-2 cells covered the monolayer, the old medium was discarded and the cells were rinsed with sterile PBS three times. Next, 2 mL of 0.125% trypsin was added to digest the cells, the rounding of the cells was observed under the microscope, and discarded when the cell gap increased. The trypsin was then removed and a certain amount of high-sugar DMEM basal medium containing 10% FBS was added to terminate the digestion. The suspension was repeatedly pipetted until the cells were completely shed and dispersed into single cells, cultured in separate bottles, and placed in a 5% CO₂ incubator at 37°C. The fluid was changed every 2–3 days. After 70%–90% of the cells adhered to the wall, they were seeded on a 6-well plate and the cells were processed after 48 h.

In this study, Caco-2 cells were treated with different concentrations of LPS, and the optimal concentration and duration of LPS treatment were determined by detecting the expression of relevant inflammatory factors and changes of oxidation indexes at different time periods, so as to construct the inflammatory injury model and oxidative damage model of Caco-2 cells, respectively. In the LPS group, Caco-2 cells was diluted in ddH₂O with LPS (Sigma, USA). In the negative control

experiments, ddH₂O was added to untreated cells as a vehicle group. In the model experiment of inflammatory injury of Caco-2 cells, LPS with concentration of 1 µg/mL, KMOS and BS were added simultaneously for 6h. In the model experiment of oxidative injury, Caco-2 cells were treated with 2 µg/mL LPS, KMOS and BS at the same time for 8h. In all cell experiments, the supplemental concentrations of KMOS and BS were 2 g/L and 10⁷ CFU/mL, respectively. The culture conditions of *Bacillus subtilis* in the LPS+BS treatment group were normal LB liquid medium, while the LPS+KMOS+BS treatment group were LB liquid medium containing 2 g/L konjac mannan oligosaccharide. All the bacterial broths were incubated in a shaker at 200 rpm 37°C for 24h. The cells used in this study were human colon cancer epithelial cells (Caco-2 cells) from the Huazhong Agricultural University College of Fisheries. The KMOS used in the experiment was extracted from konjac refined powder and purchased from Enshi Tiantianjia Biotechnology Co., Ltd. BS was isolated from pig manure and has been deposited in China Center for Type Culture Collection (CCTCC) and the CCTCC NO: M2019185.

MTT Method to Detect Cell Viability

MTT colorimetry is an effective method for detecting cell survival and growth. The detection principle is that exogenous MTT can be reduced by succinate dehydrogenase in the mitochondria of living cells to water-insoluble blue-purple crystal formazan and deposited in the cells, but dead cells have no such function. Dimethyl sulfoxide (DMSO) can dissolve formazan in cells, and its absorbance was measured by enzyme-linked immunosorbent assay (ELISA) at 490 nm, which can indirectly reflect the number of living cells. In a certain range of cell numbers, the amount of MTT crystallization is proportional to the number of cells. The cell suspension was prepared and placed into a 96-well cell culture plate, 100 µL was added to each well (the control well and zero adjustment hole was set at the same time), 100 µL of the concentration gradient drug was added after the cells were covered at the bottom of the well, and then incubated for 24 h. Next, the cells were rinsed two times with PBS, 100 µL of 0.5% MTT medium was added to each well, and incubated for 4 h in the dark. After, 150 µL DMSO was added to each well, shaken at low speed for 10 min on a shaker, and left until the crystals are fully dissolved. The absorbance of each hole was measured at 490 nm wavelength.

Western Blotting

Tissues or cells were collected and homogenized in a lysis buffer with a handheld homogenizer to prepare a lysis solution. The total protein of the cells and tissues was extracted, and the protein concentration was determined using the Bradford method. The homologs were separated using sodium dodecyl sulfate-polyacrylamide gel electrophoresis (SDS-PAGE) and then transferred to polyvinylidene fluoride membranes. The membranes and antibodies were incubated overnight at 4°C. The samples were then washed twice with TBST (TBS containing 0.05% Tween - 20) and once with TBS (Tris-HCl Buffered Saline) for 10 min each time. The secondary antibody was incubated at room 37°C for 1 h, and chemiluminescence imaging was

performed. The following antibodies were used: anti-claudin-1, anti-ZO-1 (Cell Signaling Technologies), anti-SOD, anti-Nrf2 (Proteintech, Wuhan, China), horseradish peroxidase (HRP)-labeled goat anti-rabbit IgG (Proteintech, Wuhan, China), and HRP-labeled goat anti-mouse IgG (Proteintech, Wuhan, China).

Real-Time PCR

We used the QuantStudio6Flex real-time polymerase chain reaction system (ABI, Thermo Fisher, Shanghai, China) and Roche LightCycler[®] 480 (Roche, Switzerland), and the following PCR program for real-time polymerase chain reaction: denaturation at 95°C for 10 min, expansion at 95°C for 45 cycles for 15s, and annealing and extension at 60°C for 1 min. Next, 2×SYBR Green qPCR Master Mix (#B21203, Bimake, Shanghai, Shanghai, China) was used for RT-qPCR. The primer sequences are listed in **Table 1**. The specific amplification of certain PCR reactions was evaluated using the melting curves. To avoid potential contamination, a negative control reaction was performed in which water was replaced with the cDNA template. Sampling was repeated three times for each well, and the comparative Ct (2^{-ΔΔCt}) value method was used for relative quantification. GAPDH (NM_002046.6) was used as a reference gene.

Establishment of a Mouse LPS Injury Model

Thirty 6-week-old SPF-KM female mice (purchased from the Experimental Animal Center of Huazhong Agricultural University) were randomly divided into five groups: control group, LPS group, KMOS+LPS treatment group, BS+LPS treatment group, and KMOS+BS+LPS treatment group, with 6 mice in each group. All mice were kept in a normal environment with free access to food and water. KMOS was diluted with sterile water to 2 g/L, the gavage group was fed with BS at room temperature, and after washing twice with sterile PBS, the BS and BS + KMOS pre-feeding groups were treated with PBS and resuspended in 2 g/L KMOS and adjusted to a concentration of 1×10⁹ CFU/mL. The control group was gavaged with 200 µL sterile PBS by gavage needle, and the gavage treatment groups were gavaged with 200 µL bacterial solution and konjac mannan oligosaccharide, and the gavage was stopped at 9:00 a.m. every day for 7 days. 200 µL LPS (200 µg/each) was injected intraperitoneally to induce inflammation in mice, and samples were collected 24 hours later.

Tissue Collection

After 24 h of treatment, the blood was collected by enucleating and blood sampling, and then placed in a refrigerator at 4°C for 2 h. After centrifugation at 3000 g and 4°C for 10 min, the upper clear serum was carefully removed and quickly frozen at -80°C. After blood collection, the mice were euthanized by dislocating the cervical vertebrae, the liver was separated, the surface bloodstains were washed with normal saline pre-cooled to 4°C, and the filter paper was wiped dry. The other part was added with a double volume of pre-cooled normal saline, and the cut tissue was poured into a glass homogenization tube. Next, it was turned up and down dozens of times to fully grind and

TABLE 1 | Primer used for SYBR Green I qRT-PCR validation.

Gene Symbol	Primer Sequence 5'-3' (Forward)	Primer Sequence 5'-3' (Reverse)
homo-GAPDH	GGAAGCTTGTTCATCATCAATGG	CATCGCCCCACTTGATTTTG
homo-IL-1 β	GTACCTGAGCTCGCCAGTG	TGTTTAGGGCCATCAGCTT
homo-IL-6	GACAGCCACTCACCTCTTCA	TTCAACAGGCAAGTCTCTC
homo-TNF- α	CCGAGTCTGGGCAGGTCTA	CGTTTGGGAAGGTTGGATG
homo-ZO-1	CGGGACTGTTGGTATTGGCTAGA	GGCCAGGGCCATAGTAAAGTTTG
homo-Claudin-1	GCGCGATATTTCTTCTTGCAGG	TTCGTACCTGGCATTGACTGG
homo-Muc-2	AACGGCTGCAGAGCTATTG	ATCTTCTGCATGTTCCAAACTC
homo-NRF2	CGACGGAAGAGTATGAG	TGGAGTAGTTGGCAGAT
homo-SOD1	GACAGCCACTCACCTCTTCA	CTTCATTTCCACCTTTGCT
homo-GPx1	AAGGTACTACTTATCGAGA ATGTG	GTCAGGCTCGATGTCAATGGTCTG
homo-NOX2 homo-Keap1	AATCCCTGCTCCCACTAACAATGCAGCCAGATCCA	TTTCAAGATGCGTGGAACTACGCAGAAGTGTACCTGTTGA
homo-Keap1	ATGCAGCCAGATCCA	GCAGAAGTGTACCTGTTGA
mus-GAPDH	ACCCAGCAAGGACACTGAGCAAG	GGCCCTCCTGTTATTATGGGGT
mus-SOD1	TTCGAGCAGAAGGCAAGCGGTGAA	AATCCCAATCACACCACAAGCCAA
mus-SOD2	CAGACCTGCCTTACGACTATGG	CTCGGTGGCGTTGAGATTGTT
mus-IL-6	AGACAAAGCCAGAGTCTTCAGAGA	GCCACTCCTTCTGTGACTCCAGC
mus-TNF- α	AGCAGGCCATCACCAACAAGA	GTGCGTCACATCCTTGAAGTCAT
mus-NOX2	TGTTTTCATTTCTCATCAGAAG	CCAACCAACCAAGAATGACA
mus-Nrf2	CGAGATATACGCAGGAGAGGTAAGA	GCTCGACAATGTTCTCCAGCTT

Homo means *Homo sapiens* and mus means *Mus musculus*

homogenize the tissue. The prepared homogenate was centrifuged with a low-temperature centrifuge and the supernatant was collected for testing.

Five mice in each group were sacrificed by necking, subjected to aseptic dissection, and then 2 cm of the jejunum, ileum, and colon tissues of the two groups of mice were collected; a part was collected in a cryotube and transferred into liquid nitrogen quickly and stored at -80°C while the remaining 2 cm of the jejunum, ileum, and colon tissues were washed with sterile PBS, cleaned, and soaked in 4% paraformaldehyde for fixation.

Determination of Antioxidant Enzyme Content

Glutathione peroxidase (GSH-Px) activity can be expressed by the rate of the enzymatic reaction. The enzyme activity can be determined by measuring the consumption of glutathione (GSH) in this enzymatic reaction. GSH reacts with dithiodinitrobenzoic acid to produce the 5-thiodinitrobenzoic acid anion, which presents a relatively stable yellow color. The amount of GSH was calculated by measuring the absorbance at 412 nm. O_2^- , produced by the reaction of xanthine and xanthine oxidase, can oxidize hydroxylamine to form nitrite, which appears purple red under the action of a color developer. When the sample contains SOD, it has a specific inhibitory effect on O_2^- , reducing the formation of nitrite, and the absorbance decreases when the color is compared at 550 nm. The SOD in the sample was calculated using the vitality formula. The concentration of malondialdehyde in the plasma was determined using thiobarbituric acid colorimetry. Malondialdehyde is the final product of lipid peroxidation in the body. Malondialdehyde can react with thiobarbituric acid to form a red product. The substance has the strongest absorption at 532 nm, so the absorbance value of the reactant can be measured with an ultraviolet-visible spectrophotometer, and the concentration in the measured sample was calculated according to the formula in

the manual. The determination of GSH, SOD, T-AOC, and MDA content was performed in accordance with the kit instructions. The kits were purchased from the Nanjing Jiancheng Institute of Biological Engineering.

H&E Staining of Ileum Tissue

After being euthanized using the neck-inducing method, 2 cm of the ileum tissue was removed and washed with sterile PBS. After cleaning, the samples were immersed in 4% paraformaldehyde for fixation. Then, it was embedded in paraffin, and the sections were stained with alcohol-eosin staining solution.

Data Statistics

The statistical analysis software GraphPad Prism was used to calculate the means and standard errors of each group of data. Data of each group were expressed as means \pm SEM, and t test was used to analyze the significance of the mean difference of relevant groups of data. $P < 0.05$ was marked as significant difference and marked as *. $P < 0.01$ was marked as **; $P < 0.001$ is a very significant difference, marked as ***.

RESULTS

Co-Treatment With BS and KMOS Repairs Caco-2 Cell Viability Damage

To study the repair effects of probiotics and KMOS on Caco-2 cell injury, we constructed an LPS-induced intestinal epithelial cell injury model. Caco-2 cells were treated with different concentrations of LPS, and the expression of the related inflammatory factors IL-1 β and TNF- α was detected using qPCR. We found that after treatment with 1 μ g/mL LPS for 6 h, the expression of the two inflammatory factors was significantly upregulated (**Supplementary Figures S1A, B**),

indicating that the cells had an obvious inflammatory response. We also used different concentrations of BS to treat damaged cells and found that the optimal concentration of BS that could repair the damaged cells was 10^7 CFU/mL. In addition, different concentrations of KMOS promoted the growth of BS, and the growth effect was the best when using KMOS at a concentration of 2 g/L to treat BS for 24 h (**Supplementary Figures S1G–I**).

We used the best ratio of KMOS and BS in a culture mixture to achieve the best time of action, and then treated the damaged cells with the mixture. The MTT method was used to detect changes in the activity of Caco-2 cells. The results showed that compared with the LPS treatment group, the Caco-2 cell activity of the KMOS and probiotics co-treated group was significantly upregulated (**Figure 1A**), indicating that KMOS and probiotics worked together to repair the damaged Caco-2 cell activity, and is more conducive for the repair of intestinal epithelial cell activity damage than the konjac mannan oligosaccharide alone, and the effect was significant.

Co-Treatment With BS and KMOS Repairs Caco-2 Cell Tight Junction Damage

LPS treatment can also cause damage to the tight junctions of Caco-2 cells (28) (**Supplementary Figures S1C–F**), and probiotics can prevent damage to the tight junctions of cells (29, 30). Therefore, we wanted to know whether BS and KMOS have a synergistic repair effect on tight junction damage in Caco-2 cells. We used qPCR to detect changes in the expression of tight junctions ZO-1 and Claudin-1. The results showed that compared with the LPS treatment group, the expression of tight junction ZO-1 and Claudin-1 mRNA in the konjac mannan oligosaccharide and the probiotic co-treatment group was upregulated, and the expression of the tight junction was upregulated compared with the probiotic alone group (**Figures 1B, C**). This shows that the joint action of KMOS and probiotics can repair the damage of the tight junctions of Caco-2 cells, and it is more conducive for the repair of intestinal epithelial cell tight junctions than probiotics alone.

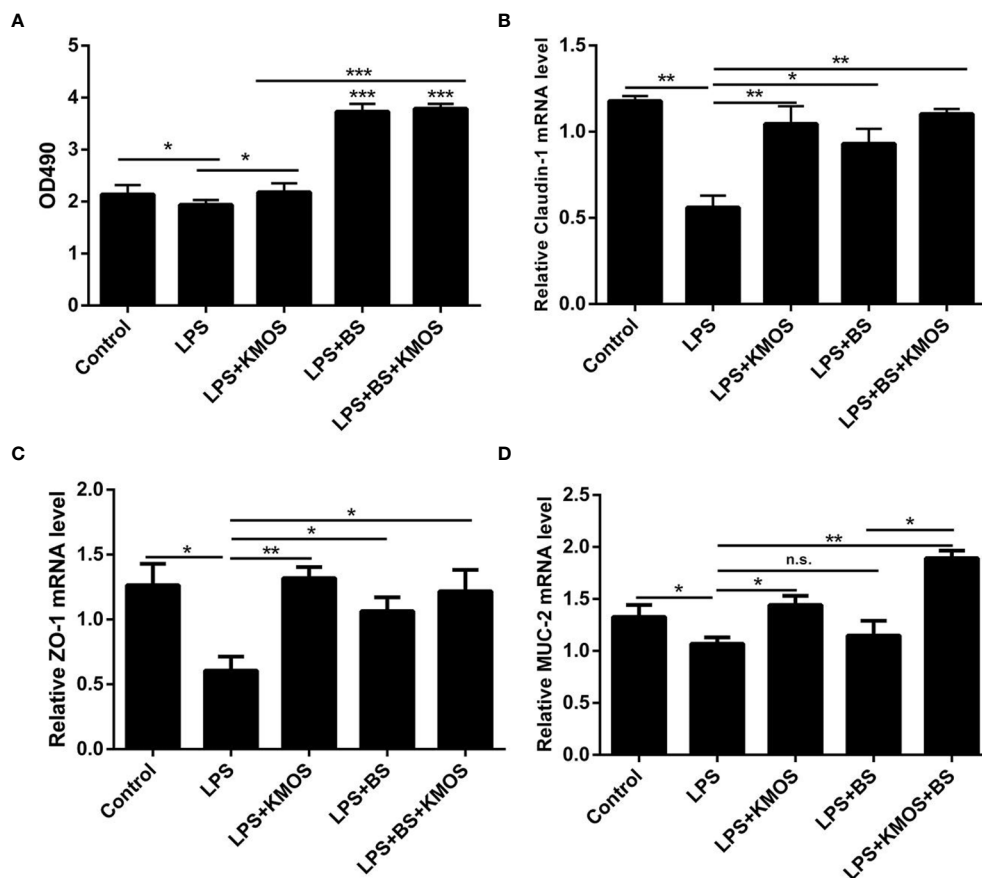


FIGURE 1 | The repair effect of KMOS and BS on cell damage. **(A)** KMOS and probiotics can repair cell activity damage. **(B)** Claudin-1 mRNA expression level. **(C)** ZO-1 mRNA expression level. **(D)** MUC-2 mRNA expression Level. These experiments were repeated three times. * $p < 0.05$, ** $p < 0.01$ and *** $p < 0.001$; ns, not significant.

Co-Treatment With BS and KMOS Repairs the Mucus Barrier Damage of Caco-2 Cells

After treating the cells with LPS, mucin expression in Caco-2 cells decreased, and the cell mucus layer was damaged. We used qPCR to detect MUC-2 mRNA expression. The results showed that compared with the LPS treatment group, the expression of MUC-2 mRNA in the co-treatment group of KMOS and probiotics was significantly upregulated, and the effect was better than that of KMOS and probiotics alone (Figure 1D).

Co-Treatment With BS and KMOS Repairs Oxidative Damage in Caco-2 Cells

LPS can also cause oxidative damage in cells (10). To test whether BS and KMOS can repair cell oxidative damage, we constructed a Caco-2 cell oxidative damage. We used different concentrations of LPS to treat Caco-2 cells to detect the expression level of GSH and found that when the stimulating concentration of LPS was 2 μ g/mL and the action time was 8 h, the GSH expression was the lowest (Supplementary Figure S2A), and NOX2 expression was significantly upregulated (Supplementary Figure S2B), SOD enzyme activity was significantly reduced (Supplementary Figure S2C), and MDA oxidation level increased significantly (Supplementary Figure S2D). Therefore, the above-mentioned concentration and treatment times are oxidative damage conditions for cells.

Then, we used the optimal ratio of KMOS and BS to mix the culture and then treated the damaged cells after reaching the optimal growth concentration. The results showed that the addition of BS and oligosaccharide mixtures significantly increased compared to the LPS treatment group. Down-regulation of the level of oxidation marker MDA (Figure 2A) and the expression of NADPH oxidase subtype NOX2 (Figure 2B), and the combination of the two has a better effect on cell repair. We also tested the SOD enzyme activity and GSH content in the cell culture supernatant and cell lysate and found that the SOD enzyme activity in the cell culture supernatant of the KMOS and probiotics co-treatment group was significantly upregulated (Figure 2C), and the GSH content was significantly increased (Figure 2D), and the SOD enzyme activity and GSH content in the cell lysate were similar to those in the supernatant (Figures 2E, F).

Next, we tested the expression levels of SOD1, Gpx1, and Nrf2 at the mRNA level, and found that the expression of SOD, Gpx1, and Nrf2 in the combined treatment group of probiotics and oligosaccharides was upregulated compared with the LPS-injured group (Figures 3A–C), but compared with the probiotics alone, there was no significant difference in the addition group. We also used western blotting to detect the expression of Nrf2 protein and found that the combined treatment of oligosaccharides and probiotics can significantly

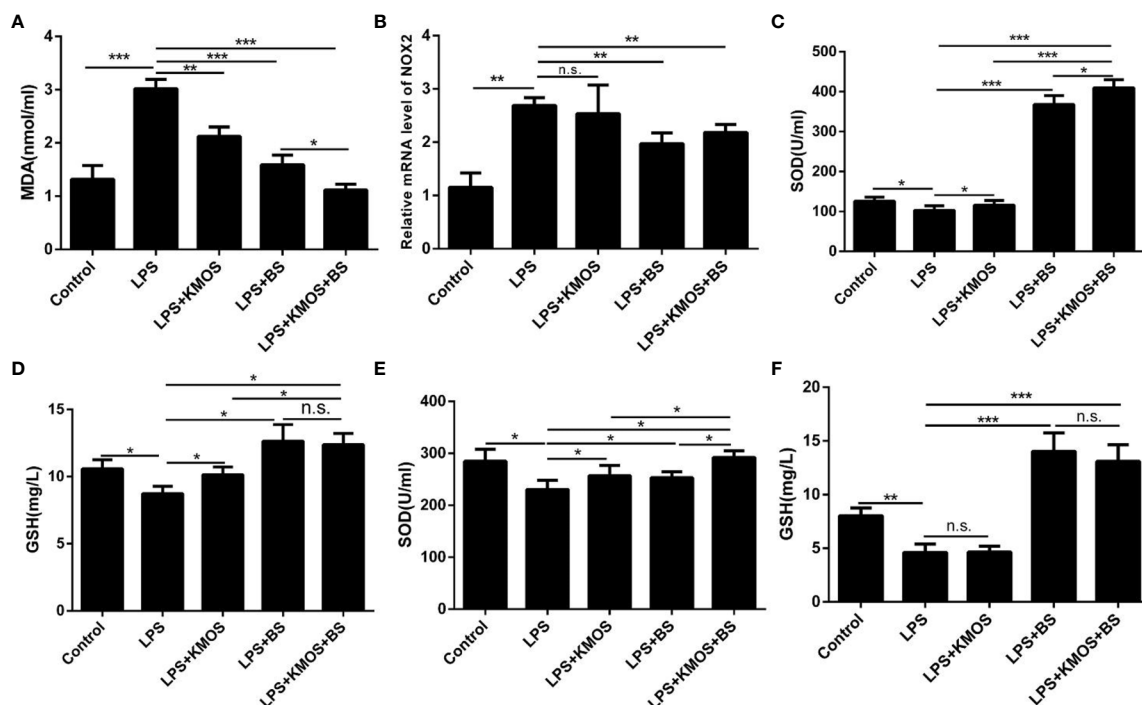


FIGURE 2 | Co-treatment with BS and KMOS on the repair of oxidative damage in Caco-2 cells. The level of cell (A) MDA in different treatment groups. (B) The expression level of NOX2. (C) SOD enzyme activity in cell culture supernatant. (D) The expression level of GSH. (E) SOD enzyme activity in cell lysate. (F) GSH content. These experiments were repeated three times. * $p < 0.05$, ** $p < 0.01$ and *** $p < 0.001$; ns, not significant.

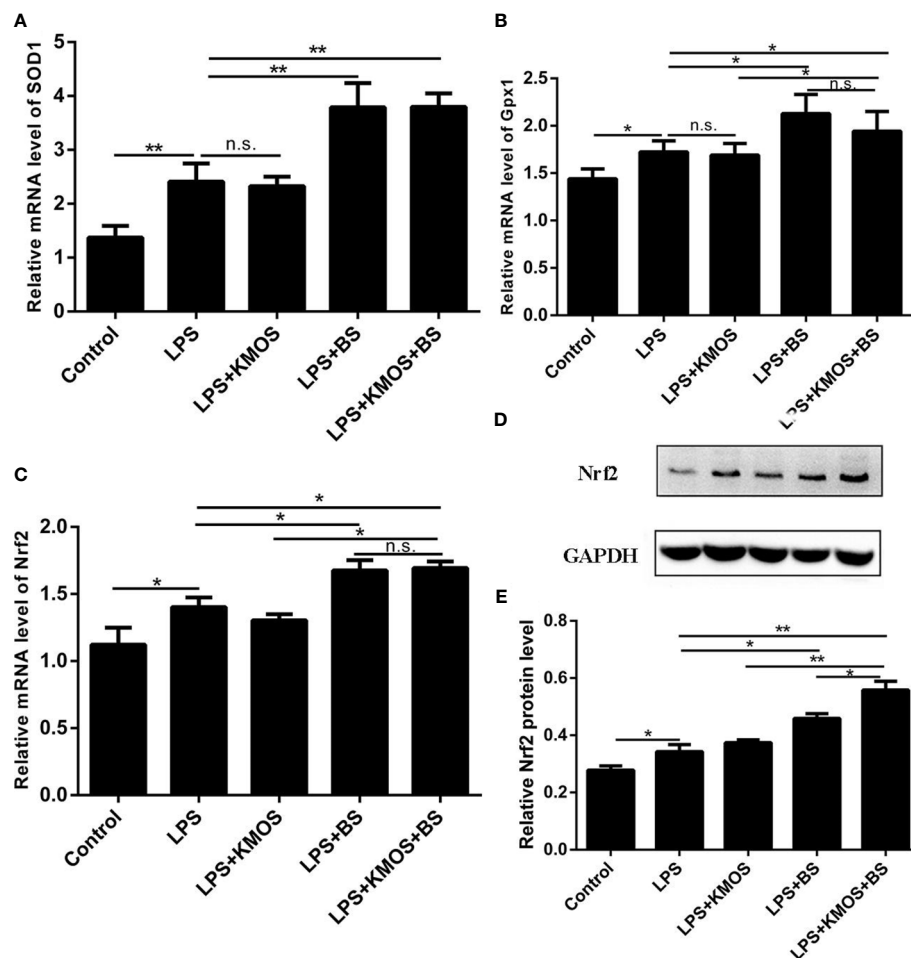


FIGURE 3 | The co-treatment of BS and KMOS can repair the oxidative damage of Caco-2 cells. Cell (A) SOD1 mRNA expression level in different treatment groups. (B) Gpx1 mRNA expression level. (C) The expression level of Nrf2 mRNA. (D) Western blot result of Nrf2 (E) Level of Nrf2 protein. These experiments were repeated three times. * $p < 0.05$ and ** $p < 0.01$; ns, not significant.

increase the expression of Nrf2 protein compared to the LPS alone injury group (Figures 3D, E).

Protective Effects of KMOS and BS on LPS-Induced Liver Injury in Mice

The above studies indicate that KMOS and BS have a synergistic repair effect on cell damage, but it is still unknown whether this synergistic repair functions *in vivo*. To study its synergistic repair effects *in vivo*, we administered BS, KMOS, and their mixtures to the stomach for 7 consecutive days, and then injected LPS into the intraperitoneal cavity to establish a mouse injury model. The mice were sacrificed 24 h later. In mice, the liver was collected to determine relevant antioxidant enzyme indices. The results showed that compared with the LPS treatment group, the pre-infused gastric oligosaccharide group significantly increased the activities of the three antioxidant enzymes (Figures 4A–C). The group of gastric probiotics only significantly improved the activities of superoxide dismutase and total antioxidant enzymes,

but had no significant effect on the content of GSH in the liver (Figures 4A–C). The combined treatment with KMOS and BS significantly improved the three antioxidant enzymes in the liver, and the effect was more significant than that of the group treated with probiotics alone (Figures 4A–C). We also tested the MDA levels in the serum of mice. The results showed that the serum MDA of mice in the LPS alone treatment group increased significantly, and both KMOS and BS gavage could significantly reduce the MDA content in the serum of LPS-treated mice. The effect of the combined gavage was more significant (Figure 4D).

Protective Effects of KMOS and BS on LPS-Induced Ileal Tissue Damage in Mice

Studies have shown that LPS treatment can damage the mouse ileum tissue (31). Therefore, we wanted to know whether KMOS and BS are beneficial for repairing damaged ileum tissue in mice. We performed H&E staining on the ileum tissue of each group of

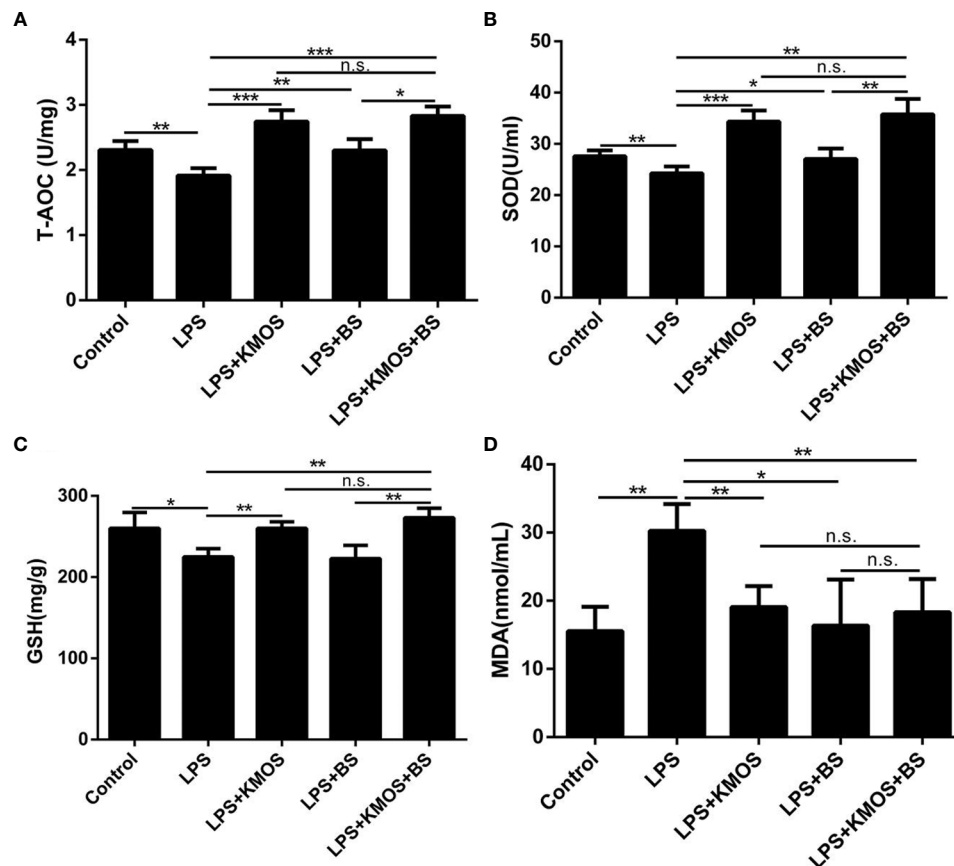


FIGURE 4 | The protective effects of KMOS and BS on LPS-induced liver injury in mice. Liver tissue (A) T-AOC enzyme activity of mice in different treatment groups. (B) SOD enzyme activity. (C) GSH enzyme activity. (D) MDA content. These experiments were repeated three times. * $p < 0.05$, ** $p < 0.01$ and *** $p < 0.001$; ns, not significant.

mice (Figures 5A–E). We found that LPS caused obvious damage to the ileum tissue of the mouse, with broken intestinal villi and tissue pyknosis (Figure 5B). The addition of KMOS and BS protected the mouse ileum tissue from the damage to varying degrees (Figures 5C–E).

To study the protective effects of oligosaccharides and probiotics on mouse intestinal inflammatory damage, we collected mouse ileum tissues and used RT-qPCR to detect changes in the expression of inflammation-related genes in mouse ileum tissues. The results showed that compared with the LPS treatment group, the expression of TNF- α was downregulated in the oligosaccharide and probiotic gavage groups, and the combined gavage group was more downregulated (Figure 5F). The IL-6 gene was significantly upregulated after LPS treatment. Pretreatment with BS and KMOS significantly inhibited LPS-induced upregulation of inflammatory factors in mouse ileum tissue caused by LPS (Figure 5G), indicating that oligosaccharides and probiotics are effective in mice, and inflammatory damage in the intestine has a synergistic repair effect.

Next, we studied the protective effects of oligosaccharides and probiotics on oxidative damage in the mouse intestine. We tested the effects of oligosaccharide and probiotic mouse gavage on mouse intestinal oxidase genes. The data showed that the expression of the oxidation gene NOX2 in the intestinal cells of mice in the LPS alone treatment group was significantly upregulated (Figure 5H), and the groups of gavage KMOS and BS could significantly inhibit the upregulation of the oxidation gene NOX2 caused by LPS. And the difference in downregulation of the two combined gavage groups was more significant than that of single gavage (Figure 5H). We then tested the changes in antioxidant enzymes and genes in the mouse intestines and found that the SOD enzyme activity and GSH content of mice in the LPS alone treatment group were significantly downregulated, and the groups of BS and KMOS were administered with the two antioxidants. Oxidase activity was significantly upregulated (Figures 5I, J). RT-qPCR was used to detect the expression of Nrf2, SOD1, and SOD2. The results showed that, compared with the blank control group, the acute oxidative damage induced by a high concentration of LPS destroyed the antioxidant enzyme

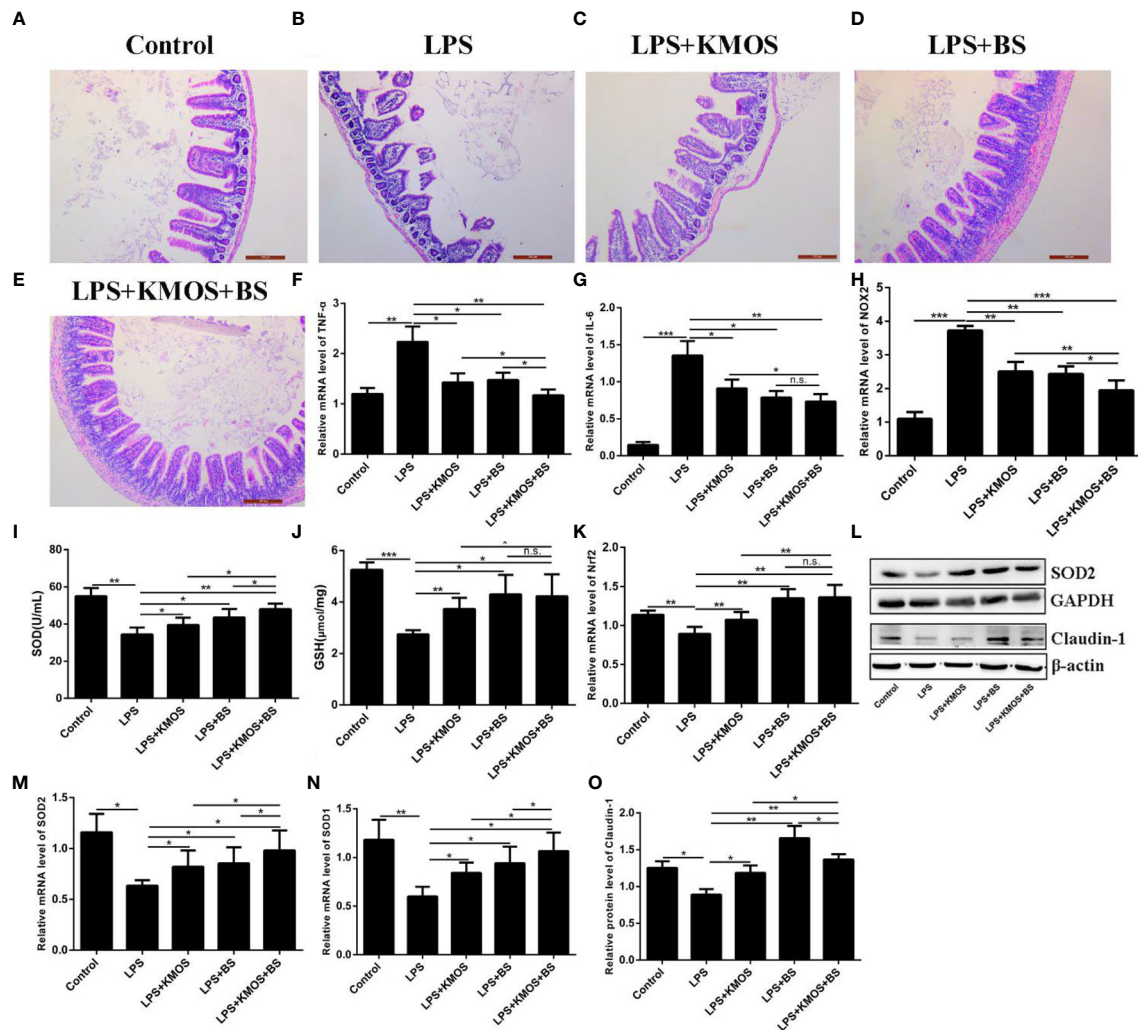


FIGURE 5 | The protective effects of KMOS and BS on LPS-induced ileal tissue damage in mice. Mouse ileum tissue (A–E) H&E staining in different treatment groups. (F) TNF- α mRNA expression level, (G) IL-6 mRNA expression level, (H) NOX2 mRNA expression level, (I) SOD enzyme activity, (J) GSH enzyme activity, (K) Nrf2 mRNA expression level, (L) Western blot result of SOD2 and Claudin-1, (M) SOD2 mRNA expression level, (N) SOD1 mRNA expression level, (O) Claudin-1 protein level. * $p < 0.05$, ** $p < 0.01$ and *** $p < 0.001$; ns, not significant.

system in the mouse intestine and inhibited the expression of mouse Nrf2, SOD1, and SOD2 genes (Figures 5K, M, N). Compared with the LPS treatment group, BS and Konjac mannan oligosaccharide pretreatment significantly increased the expression of the antioxidant genes. Western blot analysis revealed that the expression of SOD2 protein was consistent with the transcription level (Figure 5L). This shows that both BS and KMOS can significantly upregulate the expression of antioxidant genes in the mouse intestine, improve the antioxidant capacity of mice, and have a good protective effect against oxidative damage in mice.

Finally, we studied the protective effects of oligosaccharides and probiotics on LPS-induced intestinal tight junction protein damage in mice. Our data showed that the expression of Claudin-1 protein was significantly downregulated in the LPS treatment group, while

the expression of Claudin-1 protein in the group supplemented with BS and KMOS was significantly upregulated (Figures 5L, O), indicating that it has a good protective effect on the intestinal tight junction damage caused by LPS.

DISCUSSION

The intestine is the largest reservoir of bacteria and endotoxins in the human body. Intestinal epithelial cells provide a physical barrier for the body, which can protect the body from microbial invasion (32). Previous studies have shown that KMOS is effective in keeping the intestinal mucosa tight and intact, improving immunity (8), regulating the balance of intestinal flora, and

improving intestinal function (33). By interacting with microorganisms, BS can promote intestinal barrier function and maintain the integrity of the intestinal epithelial barrier (34). However, whether KMOS and BS have a synergistic repair effect on intestinal injury remains unknown. In this study, we used the LPS-induced Caco-2 cell and mouse intestinal injury model to study the synergistic effects of KMOS and BS on Caco-2 cells and intestinal injury. Our research results show that the combined use of KMOS and BS has a synergistic repair effect on Caco-2 cells and mouse intestinal injury, and can enhance the antioxidant function of cells, which is beneficial for LPS-induced acute injury in mouse models.

LPS is a biologically active bacterial structural component released after the death and disintegration of bacteria and is the main pathogenic factor of bacteria (35). LPS acts on intestinal epithelial cells and can increase the permeability of intestinal epithelial cells (35, 36), increases the expression of related inflammatory cytokines, causes inflammation (36–38), and inhibits the expression of tight junction proteins in intestinal epithelial cells (38), resulting in damage to the intestinal barrier. Intestinal homeostasis is precisely regulated by a variety of cytokines (39). The tightly linked proteins ZO-1 and ZO-2 can bind directly to cytoskeletal proteins, thereby regulating cellular tissue and epithelial morphogenesis (7, 40). Deletion of ZO-1 can increase intestinal epithelial permeability and promote the development of intestinal inflammation (41, 42). It has been reported that the probiotic *B. subtilis* CW14 repairs the epithelial barrier and reduces the toxicity of ochratoxin A to Caco-2 cells by promoting the expression of ZO-1 protein (27). Claudin-1 is also an important tight junction protein and helps regulate intestinal epithelial homeostasis by regulating Notch signaling (43). Intake of BS in mice upregulated the expression of TJ proteins (claudin-1, and ZO-1), thereby repairing intestinal barrier function (44), which is consistent with our findings. Mucins are major components of mucus and form a protective barrier between the resident microbiota and the underlying immune cells in the intestine. Oral administration of *Bacillus subtilis* fermented milk promotes the expression of MUC-2 in inflammatory epithelial cells and may play a role in the treatment of dextran sulfate sodium salt (DSS)-induced IBD (27). This repair effect may be due to some bioactive peptides produced by bovine β -casein of *Bacillus subtilis* acting through the protective function of Mucin2 (27). The enhanced expression of MUC-2 by combined treatment of KMOS and BS to repair LPS-induced adhesive damage may be due to the role of bioactive substances in this repair process. Metabolites of BS, such as surfactant A and poly- γ -glutamic acid, have been reported to alleviate symptoms in animal models of IBD (45). In addition, nattokinase of BS inhibits inflammation and oxidative stress in mice (46).

Bacillus subtilis fermented milk inhibits the expression of the pro-inflammatory cytokine TNF and promotes the expression of anti-inflammatory cytokines, thereby reducing local inflammatory damage to the intestinal mucosa (25). Overexpression of TNF leads to apoptosis of intestinal epithelial cells (IECs). In contrast, the anti-inflammatory factor IL-6 is usually associated with inflammation and promotes proliferation and repair of the intestinal epithelium

(39). The expression of TNF- α in epithelial cells could be inhibited by the synergistic effect of KMOS and BS, which might inhibit apoptosis of intestinal epithelial cells and thus alleviate the injury. In contrast, the expression of IL-6 was lower in the KMOS and BS co-treatment group, indicating the inhibition of intestinal inflammation (16).

Intestinal cells sense LPS and other pathogenic receptors of intestinal flora through pattern recognition receptors, promote the expression of NADPH oxidase and the activity of reactive oxygen species, and produce a large number of reactive oxygen species (47, 48). Although the generated active oxygen can kill pathogenic bacteria, the attack of a large amount of active oxygen on the intestinal epithelium also causes oxidative damage to the intestinal epithelium (49) and causes damage to the structure and function of the intestine (50–52). The precondition for cells to exert their antioxidative stress effect is to activate Nrf2. When the body is oxidatively damaged, the expression of Nrf2 increases, and the expression of downstream antioxidants such as SOD1, HO-1, and GPX1 is upregulated to combat free radical damage. In addition, the KMOS treatment group had no significant effect on antioxidant factors at the transcriptional level. We speculate that the antioxidant action mechanism of KMOS may be clearing active oxygen free radicals through its own physical and chemical properties because some plant polysaccharides, such as APS and garlic polysaccharides, scavenge free radicals and improve the activity of antioxidant enzymes (39, 40). The antioxidant system of the human body is inextricably linked to the immune system. Oxidative stress is often accompanied by inflammation (53). Overexpression of TNF leads to apoptosis of intestinal epithelial cells (IECs) (39). *Bacillus subtilis* fermented milk can inhibit the expression of pro-inflammatory cytokines TNF and promote the expression of anti-inflammatory cytokines, thus reducing local inflammatory damage in the intestinal mucosa (25). The expression of TNF- α in epithelial cells can be inhibited by the synergistic effect of KMOS and BS, which may inhibit apoptosis of intestinal epithelial cells thereby alleviating the injury. The anti-inflammatory factor IL-6 is usually associated with inflammation and may promote proliferation and repair of intestinal epithelium (39). In contrast, the expression of IL-6 was lower in the KMOS and BS co-treatment groups, indicating the inhibition of intestinal inflammation (25).

Inflammatory damage in the intestine has been reported to be associated with a decrease in the abundance and diversity of the intestinal microbiota (54). Whether oral administration of KMOS and BS altered the composition of the intestinal flora in mice in this study remains to be further investigated, and we hypothesize that KMOS and BS administration may alter the intestinal flora diversity in mice. Because it has been shown in other studies that oral administration of *Bacillus subtilis* fermented milk can significantly increase the variety and diversity of intestinal microbiota (25). As for the mechanism of how KMOS affects intestinal microbial diversity, more in-depth studies are needed. In animal experiments, KMOS could affect the antioxidant enzyme system in the intestine of mice, and there was a significant effect of oxidative enzymes, which may be related to the utilization of KMOS by microorganisms in the intestine (55). In conclusion, our study suggests that the combined use of KMOS and BS can help

improve LPS-induced intestinal damage in mice and is expected to be a potential novel combination functional food.

DATA AVAILABILITY STATEMENT

The original contributions presented in the study are included in the article/**Supplementary Material**, further inquiries can be directed to the corresponding author/s.

ETHICS STATEMENT

The animal study was reviewed and approved by the Institutional Animal Care and Use Committee of Huazhong Agricultural University.

AUTHOR CONTRIBUTIONS

JW conceived and designed the research. SZ and SW conducted the experiments. LC analyzed data. LC and JW wrote the

manuscript. All authors contributed to the article and approved the submitted version.

FUNDING

This work was supported by the Fundamental Research Funds for the Central Universities (Program No. 2662019FW012), the National Key R&D Program of China (Program No. 2018YFD0500204) and the Science and Technology Program of Wuhan, China (Program No. 2016020101010091).

SUPPLEMENTARY MATERIAL

The Supplementary Material for this article can be found online at: <https://www.frontiersin.org/articles/10.3389/fimmu.2021.696148/full#supplementary-material>

REFERENCES

- Macara IG, Guyer R, Richardson G, Huo Y, Ahmed SM. Epithelial Homeostasis. *Curr Biol* (2014) 24(17):R815–25. doi: 10.1016/j.cub.2014.06.068
- Haller D, Jobin C. Interaction Between Resident Luminal Bacteria and the Host: Can a Healthy Relationship Turn Sour? *J Pediatr Gastroenterol Nutr* (2004) 38(2):123–36. doi: 10.1097/00005176-200402000-00004
- Lavelle EC, Murphy C, O'Neill LA, Creagh EM. The Role of TLRs, NLRs, and RLRs in Mucosal Innate Immunity and Homeostasis. *Mucosal Immunol* (2010) 3(1):17–28. doi: 10.1038/mi.2009.124
- Zhu L, Mou C, Yang X, Lin J, Yang Q. Mitophagy in TGEV Infection Counteracts Oxidative Stress and Apoptosis. *Oncotarget* (2016) 7(19):27122–41. doi: 10.18632/oncotarget.8345
- Zhu H, Xiao X, Shi Y, Wu Y, Huang Y, Li D, et al. Inhibition of miRNA-29a Regulates Intestinal Barrier Function in Diarrhea-Predominant Irritable Bowel Syndrome by Upregulating ZO-1 and CLDN1. *Exp Ther Med* (2020) 20(6):155–5. doi: 10.3892/etm.2020.9284
- Piontek J, Winkler L, Wolburg H, Müller SL, Zuleger N, Piehl C, et al. Formation of Tight Junction: Determinants of Homophilic Interaction Between Classic Claudins. *FASEB J* (2008) 22(1):146–58. doi: 10.1096/fj.07-8319com
- Buckley A, Turner JR. Cell Biology of Tight Junction Barrier Regulation and Mucosal Disease. *Cold Spring Harb Perspect Biol* (2018) 10(1):a029314. doi: 10.1101/cshperspect.a029314
- Jung TH, Park JH, Jeon WM, Han KS. Butyrate Modulates Bacterial Adherence on LS174T Human Colorectal Cells by Stimulating Mucin Secretion and MAPK Signaling Pathway. *Nutr Res Pract* (2015) 9(4):343–9. doi: 10.4162/nrp.2015.9.4.343
- Zhang Y, Shen L, Zhang K, Guo T, Zhao J, Li N, et al. Enhanced Antioxidation via Encapsulation of Isooctyl P-Methoxycinnamate With Sodium Deoxycholate-Mediated Liposome Endocytosis. *Int J Pharm* (2015) 496(2):392–400. doi: 10.1016/j.jpharm.2015.10.010
- Xiong W, Ma H, Zhang Z, Jin M, Wang J, Xu Y, et al. The Protective Effect of Icaritin and Phosphorylated Icaritin Against LPS-Induced Intestinal Epithelial Cells Injury. *BioMed Pharmacother* (2019) 118:109246. doi: 10.1016/j.biopha.2019.109246
- Bein A, Zilbershtein A, Golosovsky M, Davidov D, Schwartz B. LPS Induces Hyper-Permeability of Intestinal Epithelial Cells. *J Cell Physiol* (2017) 232(2):381–90. doi: 10.1002/jcp.25435
- He S, Guo Y, Zhao J, Xu X, Wang N, Liu Q. Ferulic Acid Ameliorates Lipopolysaccharide-Induced Barrier Dysfunction via MicroRNA-200c-3p-Mediated Activation of PI3K/AKT Pathway in Caco-2 Cells. *Front Pharmacol* (2020) 11:376. doi: 10.3389/fphar.2020.00376
- Hughes KR, Schofield Z, Dalby MJ, Caim S, Chalklen L, Bernuzzi F, et al. The Early Life Microbiota Protects Neonatal Mice From Pathological Small Intestinal Epithelial Cell Shedding. *FASEB J* (2020) 34(5):7075–88. doi: 10.1096/fj.202000042R
- Behera SS, Ray RC. Konjac Glucomannan, a Promising Polysaccharide of Amorphophallus Konjac K. Koch in Health Care. *Int J Biol Macromol* (2016) 92:942–56. doi: 10.1016/j.ijbiomac.2016.07.098
- Liu R, Li Y, Zhang B. The Effects of Konjac Oligosaccharide on TNBS-Induced Colitis in Rats. *Int Immunopharmacol* (2016) 40:385–91. doi: 10.1016/j.intimp.2016.08.040
- Tang J, Liu J, Yan Q, Gu Z, August A, Huang W, et al. Konjac Glucomannan Oligosaccharides Prevent Intestinal Inflammation Through SIGNR1-Mediated Regulation of Alternatively Activated Macrophages. *Mol Nutr Food Res* (2021), e2001010. doi: 10.1002/mnfr.202001010
- Zeng Y, Zhang J, Zhang Y, Men Y, Zhang B, Sun Y. Prebiotic, Immunomodulating, and Antifatigue Effects of Konjac Oligosaccharide. *J Food Sci* (2018) 83(12):3110–7. doi: 10.1111/1750-3841.14376
- Zhu D, Yan Q, Li Y, Liu J, Liu H, Jiang Z. Effect of Konjac Mannan Oligosaccharides on Glucose Homeostasis via the Improvement of Insulin and Leptin Resistance In Vitro and In Vivo. *Nutrients* (2019) 11(8):1705. doi: 10.3390/nu11081705
- Wang H, Zhang X, Wang S, Li H, Lu Z, Shi J, et al. Mannan-Oligosaccharide Modulates the Obesity and Gut Microbiota in High-Fat Diet-Fed Mice. *Food Funct* (2018) 9(7):3916–29. doi: 10.1039/c8fo00209f
- Jian W, Chen YH, Wang L, Tu L, Xiong H, Sun YM. Preparation and Cellular Protection Against Oxidation of Konjac Oligosaccharides Obtained by Combination of γ -Irradiation and Enzymatic Hydrolysis. *Food Res Int* (2018) 107:93–101. doi: 10.1016/j.foodres.2018.02.014
- Tan C, Wei H, Ao J, Long G, Peng J. Inclusion of Konjac Flour in the Gestation Diet Changes the Gut Microbiota, Alleviates Oxidative Stress, and Improves Insulin Sensitivity in Sows. *Appl Environ Microbiol* (2016) 82(19):5899–909. doi: 10.1128/AEM.01374-16
- Zhang K, Su L, Duan X, Liu L, Wu J. High-Level Extracellular Protein Production in *Bacillus Subtilis* Using an Optimized Dual-Promoter Expression System. *Microb Cell Fact* (2017) 16(1):32–2. doi: 10.1186/s12934-017-0649-1
- Musa BB, Duan Y, Khawar H, Sun Q, Ren Z, Elsidid Mohamed MA, et al. *Bacillus Subtilis* B21 and *Bacillus Licheniformis* B26 Improve Intestinal Health and Performance of Broiler Chickens With *Clostridium Perfringens*-

- Induced Necrotic Enteritis. *J Anim Physiol Anim Nutr (Berl)* (2019) 103 (4):1039–49. doi: 10.1111/jpn.13082
24. Mazkour S, Shekarforoush SS, Basiri S. The Effects of Supplementation of *Bacillus Subtilis* and *Bacillus Coagulans* Spores on the Intestinal Microflora and Growth Performance in Rat. *Iran J Microbiol* (2019) 11(3):260–6. doi: 10.18502/ijm.v11i3.1336
 25. Zhang X, Tong Y, Lyu X, Wang J, Wang Y, Yang R. Prevention and Alleviation of Dextran Sulfate Sodium Salt-Induced Inflammatory Bowel Disease in Mice With *Bacillus Subtilis*-Fermented Milk via Inhibition of the Inflammatory Responses and Regulation of the Intestinal Flora. *Front Microbiol* (2020) 11:622354. doi: 10.3389/fmicb.2020.622354
 26. Jia R, Sadiq FA, Liu W, Cao L, Shen Z. Protective Effects of *Bacillus Subtilis* ASAG 216 on Growth Performance, Antioxidant Capacity, Gut Microbiota and Tissues Residues of Weaned Piglets Fed Deoxynivalenol Contaminated Diets. *Food Chem Toxicol* (2021) 148:111–962. doi: 10.1016/j.fct.2020.111962
 27. Peng M, Liu J, Liang Z. Probiotic *Bacillus Subtilis* CW14 Reduces Disruption of the Epithelial Barrier and Toxicity of Ochratoxin A to Caco-2 Cells. *Food Chem Toxicol* (2019) 126:25–33. doi: 10.1016/j.fct.2019.02.009
 28. Chen M, Liu Y, Xiong S, Wu M, Li B, Ruan Z, et al. Dietary L-Tryptophan Alleviated LPS-Induced Intestinal Barrier Injury by Regulating Tight Junctions in a Caco-2 Cell Monolayer Model. *Food Funct* (2019) 10 (5):2390–8. doi: 10.1039/c9fo00123a
 29. Blackwood BP, Yuan CY, Wood DR, Nicolas JD, Grothaus JS, Hunter CJ. Probiotic *Lactobacillus* Species Strengthen Intestinal Barrier Function and Tight Junction Integrity in Experimental Necrotizing Enterocolitis. *J Probiotics Health* (2017) 5(1):159. doi: 10.4172/2329-8901.1000159
 30. Montalto M, Maggiano N, Ricci R, Curigliano V, Santoro L, Di Nicuolo F, et al. *Lactobacillus Acidophilus* Protects Tight Junctions From Aspirin Damage in HT-29 Cells. *Digestion* (2004) 69(4):225–8. doi: 10.1159/000079152
 31. Li C, Ma D, Zhou H, Zhang M, An L, Wang Y, et al. Effects of Different Doses Lipopolysaccharides on the Mucosal Barrier in Mouse Intestine. *Res Vet Sci* (2020) 133:75–84. doi: 10.1016/j.rvsc.2020.09.005
 32. Ivanov AI, Nusrat A, Parkos CA. The Epithelium in Inflammatory Bowel Disease: Potential Role of Endocytosis of Junctional Proteins in Barrier Disruption. *Novartis Found Symp* (2004) 263:115–124; discussion 124–132, 211–118. doi: 10.1002/0470090480.ch9
 33. Brüssow H, Parkinson SJ. You Are What You Eat. *Nat Biotechnol* (2014) 32 (3):243–5. doi: 10.1038/nbt.2845
 34. Yang GY, Zhu YH, Zhang W, Zhou D, Zhai CC, Wang JF. Influence of Orally Fed a Select Mixture of *Bacillus* Probiotics on Intestinal T-Cell Migration in Weaned MUC4 Resistant Pigs Following *Escherichia Coli* Challenge. *Vet Res* (2016) 47(1):71. doi: 10.1186/s13567-016-0355-8
 35. Guo S, Al-Sadi R, Said HM, Ma TY. Lipopolysaccharide Causes an Increase in Intestinal Tight Junction Permeability In Vitro and In Vivo by Inducing Enterocyte Membrane Expression and Localization of TLR-4 and CD14. *Am J Pathol* (2013) 182(2):375–87. doi: 10.1016/j.ajpath.2012.10.014
 36. Guo S, Nighot M, Al-Sadi R, Alhmodt T, Nighot P, Ma TY. Lipopolysaccharide Regulation of Intestinal Tight Junction Permeability Is Mediated by TLR4 Signal Transduction Pathway Activation of FAK and Myd88. *J Immunol* (2015) 195(10):4999–5010. doi: 10.4049/jimmunol.1402598
 37. Liu Y, Fatheree NY, Mangalat N, Rhoads JM. Human-Derived Probiotic *Lactobacillus Reuteri* Strains Differentially Reduce Intestinal Inflammation. *Am J Physiol Gastrointest Liver Physiol* (2010) 299(5):G1087–96. doi: 10.1152/ajpgi.00124.2010
 38. Ling X, Linglong P, Weixia D, Hong W. Protective Effects of *Bifidobacterium* on Intestinal Barrier Function in LPS-Induced Enterocyte Barrier Injury of Caco-2 Monolayers and in a Rat NEC Model. *PloS One* (2016) 11(8):e0161635. doi: 10.1371/journal.pone.0161635
 39. Jeffery V, Goldson AJ, Dainty JR, Chieppa M, Sobolewski A. IL-6 Signaling Regulates Small Intestinal Crypt Homeostasis. *J Immunol* (2017) 199:304–11. doi: 10.4049/jimmunol.1600960
 40. Roy S, Esmailniakooshkghazi A, Patnaik S, Wang Y, George SP, Ahrorov A, et al. Villin-1 and Gelsolin Regulate Changes in Actin Dynamics That Affect Cell Survival Signaling Pathways and Intestinal Inflammation. *Gastroenterology* (2018) 154:1405–20.e2. doi: 10.1053/j.gastro.2017.12.016
 41. Poritz LS, Garver KI, Green C, Fitzpatrick L, Ruggiero F, Koltun WA. Loss of the Tight Junction Protein ZO-1 in Dextran Sulfate Sodium Induced Colitis. *J Surg Res* (2007) 140:12–9. doi: 10.1016/j.jss.2006.07.050
 42. Fanning AS, Van Itallie CM, Anderson JM. Zonula Occludens-1 and -2 Regulate Apical Cell Structure and the Zonula Adherens Cytoskeleton in Polarized Epithelia. *Mol Biol Cell* (2012) 23:577–90. doi: 10.1091/mbc.E11-09-0791
 43. Pope JL, Bhat AA, Sharma A, Ahmad R, Krishnan M, Washington MK, et al. Claudin-1 Regulates Intestinal Epithelial Homeostasis Through the Modulation of Notch-Signalling. *Gut* (2014) 63:622–34. doi: 10.1136/gutjnl-2012-304241
 44. Gong Y, Li H, Li Y. Effects of *Bacillus Subtilis* on Epithelial Tight Junctions of Mice With Inflammatory Bowel Disease. *J Interferon Cytokine Res* (2016) 36:75–85. doi: 10.1089/jir.2015.0030
 45. Yan L, Liu G, Zhao B, Pang B, Wu W, Ai C, et al. Novel Biomedical Functions of Surfactin A From *Bacillus Subtilis* in Wound Healing Promotion and Scar Inhibition. *J Agric Food Chem* (2020) 68:6987–97. doi: 10.1021/acs.jafc.0c01658
 46. Wu H, Wang Y, Zhang Y, Xu F, Chen J, Duan L, et al. Breaking the Vicious Loop Between Inflammation, Oxidative Stress and Coagulation, A Novel Anti-Thrombus Insight of Nattokinase by Inhibiting LPS-Induced Inflammation and Oxidative Stress. *Redox Biol* (2020) 32:101500. doi: 10.1016/j.redox.2020.101500
 47. Schmelzer C, Lorenz G, Rimbach G, Döring F. In Vitro Effects of the Reduced Form of Coenzyme Q(10) on Secretion Levels of TNF-Alpha and Chemokines in Response to LPS in the Human Monocytic Cell Line THP-1. *J Clin Biochem Nutr* (2009) 44(1):62–6. doi: 10.3164/jcbs.08-182
 48. Yu X, Lan P, Hou X, Han Q, Lu N, Li T, et al. HBV Inhibits LPS-Induced NLRP3 Inflammasome Activation and IL-1 β Production via Suppressing the NF-k β Pathway and ROS Production. *J Hepatol* (2017) 66(4):693–702. doi: 10.1016/j.jhep.2016.12.018
 49. Sudip B, Krishnendu S, Parames CS. Cytochrome P450s: Mechanisms and Biological Implications in Drug Metabolism and its Interaction With Oxidative Stress. *Curr Drug Metab* (2014) 15:719–42. doi: 10.2174/1389200215666141125121659
 50. Zhu RL, Zhi YK, Yi L, Luo JF, Li J, Bai SS, et al. Sinomenine Regulates CD14/TLR4, JAK2/STAT3 Pathway and Calcium Signal via $\alpha 7$ nachr to Inhibit Inflammation in LPS-Stimulated Macrophages. *Immunopharmacol Immunotoxicol* (2019) 41(1):172–7. doi: 10.1080/08923973.2019.1568451
 51. Ranneh Y, Akim AM, Hamid HA, Khazaai H, Fadel A, Mahmoud AM. Stingless Bee Honey Protects Against Lipopolysaccharide Induced-Chronic Subclinical Systemic Inflammation and Oxidative Stress by Modulating Nrf2, NF-k β and P38 MAPK. *Nutr Metab (Lond)* (2019) 16:15. doi: 10.1186/s12986-019-0341-z
 52. Yu GM, Tan W. Melatonin Inhibits Lipopolysaccharide-Induced Inflammation and Oxidative Stress in Cultured Mouse Mammary Tissue. *Mediators Inflamm* (2019) 2019:8597159. doi: 10.1155/2019/8597159
 53. Liu W, Wang Z, Hou JG, Zhou YD, He YF, Jiang S, et al. The Liver Protection Effects of Maltol, A Flavoring Agent, on Carbon Tetrachloride-Induced Acute Liver Injury in Mice via Inhibiting Apoptosis and Inflammatory Response. *Molecules* (2018) 23(9):2120. doi: 10.3390/molecules23092120
 54. Hernández-Chirilaque C, Aranda CJ, Ocón B, Capitán-Cañadas F, Ortega-González M, Carrero JJ, et al. Germ-Free and Antibiotic-Treated Mice Are Highly Susceptible to Epithelial Injury in DSS Colitis. *J Crohns Colitis* (2016) 10:1324–35. doi: 10.1093/ecco-jcc/jjw096
 55. Pourabedin M, Guan L, Zhao X. Xylo-Oligosaccharides and Virginiamycin Differentially Modulate Gut Microbial Composition in Chickens. *Microbiome* (2015) 3:15–5. doi: 10.1186/s40168-015-0079-4

Conflict of Interest: The authors declare that the research was conducted in the absence of any commercial or financial relationships that could be construed as a potential conflict of interest.

Publisher's Note: All claims expressed in this article are solely those of the authors and do not necessarily represent those of their affiliated organizations, or those of the publisher, the editors and the reviewers. Any product that may be evaluated in this article, or claim that may be made by its manufacturer, is not guaranteed or endorsed by the publisher.

Copyright © 2021 Chen, Zhang, Wu, Ren, Liu and Wu. This is an open-access article distributed under the terms of the Creative Commons Attribution License (CC BY). The use, distribution or reproduction in other forums is permitted, provided the

original author(s) and the copyright owner(s) are credited and that the original publication in this journal is cited, in accordance with accepted academic practice. No use, distribution or reproduction is permitted which does not comply with these terms.



Sodium Acetate Inhibit TGF- β 1-Induced Activation of Hepatic Stellate Cells by Restoring AMPK or c-Jun Signaling

Weiwei Li¹, Mingjuan Deng², Jiahui Gong¹, Xiaoying Zhang³, Shaoyang Ge⁴ and Liang Zhao^{1,2*}

¹ Key Laboratory of Functional Dairy, College of Food Science and Nutritional Engineering, China Agricultural University, Beijing, China, ² Department of Nutrition and Health, Beijing Advanced Innovation Center for Food Nutrition and Human Health, China Agricultural University, Beijing, China, ³ Inner Mongolia Dairy Technology Research Institute Co., Ltd., Hohhot, China, ⁴ Hebei Engineering Research Center of Animal Product, Sanhe, China

OPEN ACCESS

Edited by:

Jiong-Wei Wang,
National University of
Singapore, Singapore

Reviewed by:

Xiongwen Lv,
Anhui Medical University, China
Chun-Feng Guo,
Northwest A&F University, China
Wenwei Lu,
Jiangnan University, China
Chaodong Wu,
Texas A&M University, United States

*Correspondence:

Liang Zhao
lzhao@cau.edu.cn

Specialty section:

This article was submitted to
Nutritional Immunology,
a section of the journal
Frontiers in Nutrition

Received: 23 June 2021

Accepted: 02 September 2021

Published: 30 September 2021

Citation:

Li W, Deng M, Gong J, Zhang X, Ge S
and Zhao L (2021) Sodium Acetate
Inhibit TGF- β 1-Induced Activation of
Hepatic Stellate Cells by Restoring
AMPK or c-Jun Signaling.
Front. Nutr. 8:729583.
doi: 10.3389/fnut.2021.729583

Short-chain fatty acids (SCFAs) are crucial gut microbial metabolites that play a major role in the occurrence and development of hepatic fibrosis (HF). However, the effect of SCFAs on hepatic stellate cells (HSCs), the major pro-fibrogenic cells, is yet undefined. In this study, the effects of three major SCFAs (acetate, propionate, and butyrate) were assessed on the activation of HSCs. LX2 cells were activated with TGF- β 1 and treated with sodium acetate (NaA), sodium propionate (NaP), or sodium butyrate (NaB). SCFA treatment significantly reduced the protein levels of α -SMA and the phosphorylation of Smad2 and decreased the mRNA expression of *Acta2/Col1a1/Fn* in cells compared to the TGF- β 1 treatment. Among the three SCFAs, NaA revealed the best efficacy at alleviating TGF- β 1-induced LX2 cell activation. Additionally, acetate accumulated in the cells, and G protein-coupled receptor (GPR) 43 silencing did not have any impact on the inhibition of LX2 cell activation by NaA. These findings indicated that NaA enters into the cells to inhibit LX2 cell activation independent of GPR43. The results of phosphokinase array kit and Western blot indicated that NaA increased the AMP-activated protein kinase (AMPK) activation and reduced the phosphorylation of c-Jun in cultured LX2 cells, and siRNA-peroxisome proliferator-activated receptor (PPAR) γ abolished the inhibitory effects of NaA against TGF- β 1-induced LX2 cell activation. In conclusion, this study showed that NaA inhibited LX2 cell activation by activating the AMPK/PPAR γ and blocking the c-Jun signaling pathways. Thus, SCFAs might represent a novel and viable approach for alleviating HF.

Keywords: short chain fatty acid, fibrosis, hepatic stellate cells, AMPK, PPAR γ

INTRODUCTION

Hepatic fibrosis (HF) is a wound-healing response of the liver to the continuous action of various injury factors, characterized by the net accumulation of extracellular matrix (ECM) or scar (1). A variety of chronic stimuli, including chronic viral infection (hepatitis B or C virus), toxic damage, alcohol abuse (long-standing excessive alcohol consumption), non-alcoholic fatty liver

disease (NAFLD)/non-alcoholic steatohepatitis (NASH), autoimmune liver diseases, and metabolic and genetic diseases, could cause HF (2). Subsequently, HF may progress to cirrhosis associated with several complications, such as functional liver failure, hepatic encephalopathy, renal and cardiac disturbances, and hepatocellular carcinoma (HCC) (3). During HF, the ongoing liver injury results in excessive ECM deposition, and abundant Col1a1 and 3 lead to scarring and fibrosis (4). HSCs are the primary source of activated myofibroblasts and portal fibroblasts that drive the fibrogenic process. In response to liver injury, the quiescent, vitamin-A storing HSCs transdifferentiate to contractile, proliferative, and fibrogenic myofibroblasts (5). Then, the cells produce collagen as well as other types of ECM tissue inhibitors of metalloproteinases and matrix metalloproteinases (MMPs) that elicit liver architecture remodeling, thus propagating fibrosis (6). This process is known as HSC activation, and activated HSCs are responsible for about 80% of total fibrillar Col1a1 in the fibrotic liver (7). Therefore, inhibiting HSCs activation is emerging as a promising target for fibrosis alleviation.

Currently, the literature is focused on the correlation between gut and liver. The liver receives most of its blood flow (70%) from intestinal vascularization, and hence, is constantly exposed to nutrients, toxins, and products of the gut microbiota (8). Moreover, the gastrointestinal tract receives a liver product in the form of bile acid (9). This functional bidirectional correlation between the liver and gastrointestinal tract is known as the gut-liver axis (GLA) (8). The dysregulation of the microbiota has been confirmed in patients with HF (10). Several studies reported that the ratio of *Firmicutes/Bacteroidetes* in microbiota was correlated with lipid accumulation and HF in both human and animal models (11, 12). In a group of biopsy-proven NAFLD patients, a higher abundance of *Bacteroides* were observed in fibrosis subjects compared to those without fibrosis, suggesting a correlation between *Bacteroides* and HF severity (13). Previous studies also showed that patients with cirrhosis had a decrease in commensal SCFA-producing bacteria, especially butyrate-producing bacteria, including Lachnospiraceae and Ruminococcaceae (14). Accumulating evidence indicated a balance in the microbial community by supplementing probiotics or prebiotics, which alleviated HF. Gadallah et al. (15) demonstrated that treatment with the probiotic mixture and prebiotic insulin suppressed the expression of inflammatory IL-6 and reduced the level of fibrotic TGF- β 1 and α -SMA markers in the experimental rats. In humanized mice, dietary fiber altered the intestinal microbiota composition produced abundant SCFAs and exerted a protective effect on mouse HF (16). These studies suggested that gut microbiota had a tight correlation with HF, and SCFAs could be major regulators of these processes.

SCFAs are the main microbial metabolites of dietary fibers of gut microbiota. Acetate, propionate, and butyrate are the most abundant SCFAs in the human gut (17). Importantly SCFAs are not only metabolic substrates but also signaling molecules that regulate liver metabolism (18). A previous study indicated that fructo-oligosaccharide treatment increased intestinal SCFAs and improved hepatic steatosis, inflammatory cell infiltration, and hepatocyte ballooning of NASH mice (19).

Takayama et al. (20) showed that feeding partially hydrolyzed guar gum increases butyrate, acetate, and propionate in the gut and attenuates liver inflammatory markers (TNF- α and MCP-1) and fibrogenic markers (Col1a1 and α -SMA) in mice. These results indicated that regulating the level of gut SCFAs alleviates NASH-related fibrosis via complicated processes. In addition, direct oral supplementation of butyrate remarkably alleviates the liver fibrosis stage by decreasing the expression of inflammatory marker protein (MyD88) and alleviating liver steatosis and lipid degeneration of NASH mice, interestingly, the inhibition of iNOS may be involved in the potential mechanism for butyrate alleviating NASH (21). However, only a few studies have focused on the protective effects of specific SCFAs on the development of HF, especially in HSC activation; nonetheless, the related mechanisms are not yet elucidated.

In this study, TGF- β 1-activated HSCs were employed to evaluate the effects of three dominant SCFAs, NaA, NaP, and NaB, on fibrotic markers. The mechanisms related to the NaA-induced inhibition of HSC activation were assessed using protein antibody chip and RNA interference (RNAi) in HSCs.

MATERIALS AND METHODS

Cell Culture

HSC-LX2 cells were purchased from Stem Cell Bank, Chinese Academy of Sciences (Shanghai, China) and cultured in Dulbecco's modified Eagle's medium (DMEM; Gibco, Grand Island, NY, USA) containing 2% fetal bovine serum (FBS, Gibco) and 100 U/mL penicillin and streptomycin (Beyotime, Beijing, China) in a 5% CO₂ incubator at 37°C (22). To study the effects of SCFAs on TGF- β 1-induced fibrogenesis, LX2 cells were seeded in six-well plates (Corning, Corning, NY, USA) in 2 mL of DMEM medium at a density of 1×10^6 cells/mL. After achieving 70–80% confluency, the cells were subjected to 12 h of serum starvation, while the control group was incubated with fresh DMEM and the cells in the other groups were incubated with DMEM containing 2.5 ng/mL TGF- β 1 (PeproTech, Rocky Hill, NJ, USA) and varying concentrations of NaA (0.1 or 1 mM) for an additional 48 h. Next, we selected the concentration based on previous toxicological studies in LX2 cells, especially those related to fibrogenesis. Subsequently, the cells were used for Western blot analysis and/or harvested for total RNA isolation.

Cell Cytotoxicity Assays

An Enhanced Cell Counting Kit 8 Assay (Beyotime, Shanghai, China) was used to determine cell cytotoxicity of SCFAs (23). LX2 cells were seeded at a density of 5×10^3 per well onto flat-bottom 96-well culture plates (Corning). Cells were treated by NaA, NaP or NaB (0 to 1 mM) as mentioned earlier. The absorbance values of viable cells were finally determined at 450 nm using a microplate spectrophotometer (BioTek, Winooski, VT, USA). The cell inhibitory rates were calculated using the following formula: Cell inhibition rate (%) = $(1 - A_{450}(\text{sample}) / A_{450}(\text{control})) \times 100$.

Western Blot Analysis

Total protein was isolated from cultured cells using lysis buffer supplemented with protease and phosphatase inhibitors. The protein concentration was measured using a protein assay kit (Bio-Rad, Hercules, CA, USA). An equivalent of 30 μ g (24) protein extract was separated by sodium dodecyl sulfate-polyacrylamide gel electrophoresis (SDS-PAGE) and transferred to polyvinylidene difluoride membranes (PVDF). The membranes were incubated with primary antibodies: phosphorylated AMPK α (p-AMPK α), AMPK α , glyceraldehyde-3-phosphate dehydrogenase (GAPDH), phosphorylated c-Jun (Ser63) (p-c-Jun), c-Jun, phosphorylated Smad2 (p-Smad2), Smad2, β -Actin (CST, Danvers, MA, USA), PPAR α , and PPAR γ (Abcam). After incubation with a goat anti-rabbit horseradish peroxidase-conjugated secondary antibody (Beyotime, Shanghai, China) at a dilution of 1:10,000 for 1 h, the proteins were visualized using a Luminata Forte Enhanced Chemiluminescence Kit (Millipore, Billerica, MA, USA). The band intensities were analyzed using Quantity One analysis software.

Quantitative Real-Time Polymerase Chain Reaction

Total RNA was extracted using TRIzol Reagents (Ambion, Austin, TX, USA) and subjected to reverse transcription using a Prime Script RT-PCR kit (TaKaRa). qRT-PCR was carried out using SYBR Premix Ex Taq (TaKaRa) on the Light-Cycler 480 (Roche Diagnostics GmbH) and analyzed by the software (25). The primers were synthesized by Sangon Biotech, China (Supplementary Table 1). The fluorescence data of the target genes were analyzed by the $2^{-\Delta\Delta C_t}$ method for relative quantification using *Actin* or *GAPDH* as an internal control.

Measurement of Intracellular Sodium Acetate Concentration

SCFA extraction: 10^8 cells were mixed with 2 mL extraction reagent (water:phosphoric acid = 1:3) and homogenized for 20 s at $6,500 \times g$ using a Precellys 24 homogenizer (Bertin Technologies, Montigny Bretonnexus, France). The cell extract was prepared by adding 2 mL ether on ice for 10 min, followed by centrifugation at $4,000 \times g$ for 20 min (26). The remaining aqueous layer was further extracted with ether. Subsequently, the ether layers were pooled and diluted to 2 mL. Then, samples were subjected to gas chromatography-mass spectrometer (GC-MS) analysis using a 7890B gas chromatograph/5977 mass selective detector (Agilent Technologies, Santa Clara, CA, USA) with an HB-5 ms capillary column (30 m \times 0.25 mm \times 0.25 μ m film thickness) (Agilent Technologies), with helium as carrier gas at a constant flow rate of 1 mL/min. Samples (0.5 μ L) were injected using a pressure pulsed split mode (10 psi) with a split ratio of 10:1. The initial column oven temperature was 100°C for 1 min, and then increased to 120°C at a rate of 10°C/min and held for 5 min, then increased to a final temperature of 220°C at a rate of 30°C/min and held for 3 min. The total run time was 14.3 min and all the data was collected in full scan mode with a mass range of 40–300 m/z (27). Pure water was used as a blank sample to

correct the background. A blank sample was processed similar to that of cells samples. The corrected peak area of acetic acid was calculated by the peak areas of samples minus that of the blank sample detected under the same conditions.

Small Interfering RNA Transfection

siRNA targeting GPR43, PPAR γ , or control siRNA was synthesized by Biolino Biotech (Tianjin, China) (Supplementary Tables 2, 3). Transfections were performed using the Lipofectamine[®] 2000 RNAiMax reagent (Invitrogen, Karlsruhe, Germany) following the manufacturer's instructions. As described previously, cells were treated with three concentrations of SCFAs and TGF- β 1 for 48 h after 24 h post-transfection (28). The downregulation of the GPR43 or PPAR γ targeted by siRNA was confirmed by RT-PCR.

Phosphokinase Array

Relative protein phosphorylation levels were obtained by profiling 43 specific phosphorylation sites (Supplementary Table 4) using the Proteome Profiler Human Phosphokinase Array Kit (ARY003B, R&D Systems), according to the manufacturer's instructions. Briefly, the cells were rinsed with phosphate-buffered saline (PBS), resuspended in lysis buffer (1×10^7 cells/mL), and agitated at 4°C for 30 min (29). The array membranes were blocked with 1.0 mL of Array Buffer one and incubated with 500 μ g cell lysates at room temperature for 1 h. Next, cocktails of biotinylated detection antibodies were added and samples were incubated at room temperature for 2 h. Phosphorylated proteins were revealed using streptavidin-HRP/chemiluminescence substrate (sc-201696, Santa Cruz Biotechnology, Santa Cruz, CA, USA) and autoradiography films. The resulting spots were scanned, and images were quantified using the Image Lab software (Bio-Rad).

Measurement of Intracellular AMP:ATP Ratio

Following exposure to acetate, LX2 cells were removed the supernatant and washed three times with ice-cold PBS, and then added 3 mL of ice-cold aqueous acetonitrile (50%, v/v) (VWR) to break cells to extract intracellular nucleotides. The resulting extract was maintained on ice for 10 min, followed by centrifugation at $14,000 \times g$ for 1 min at 0°C. The extract of cell contents was collected and dried using a refrigerated SpeedVac (Savant). The dried extract was resuspended in 240 μ L of deionized water and filtered using a 0.22- μ m syringe filter unit for high-performance liquid chromatography (HPLC) analysis (30). The chromatographic separation and analysis were performed on an Agilent system (1,200 series), equipped with a diode-array detector and a C18 reverse-phase column (Kromasil, 5 μ m, 100 \AA ; 4.6×150 mm) at a flow rate of 1 mL/min and a linear gradient of acetonitrile (0–7%) in 10 mM triethylammonium acetate buffer (Glen Research) over 20 min. AMP and ATP were identified based on their retention times.

Statistical Analyses

Numeric data were presented as mean \pm SD. Statistical significance was determined using the one-way ANOVA followed by LSD post-tests with SPSS 22.0. Differences were considered significant at a two-tailed p -value < 0.05 .

RESULTS

NaA-H Ameliorates TGF- β 1-induced LX2 Cell Activation

A CCK-8 assay was performed to evaluate the potential cytotoxic effect of SCFA on HSCs. The results showed that after treatment with the maximum concentration of SCFAs (1 mM) for 48 h, $>80\%$ of the LX2 cells survived (**Figure 1A**), indicating that SCFAs did not affect cell viability. Regarding the antifibrotic effects of the three different SCFAs on TGF- β 1-induced HSCs activation, the protein expression level of α -SMA, the marker of fibrogenesis, was analyzed by Western blot. Compared to the control group, TGF- β 1 treatment significantly elevated α -SMA in the MOD group, which indicated LX2 cell activation by TGF- β 1. SCFA treatment significantly inhibited the overexpression of α -SMA in activated LX2 cells except high-dose of NaP compared to the MOD group. Specifically, high-dose of NaA (NaA-H) or NaB (NaB-H) reduced 72.2 or 53.7% α -SMA levels in cells compared to the MCD group (**Figures 1B,D**). NaA-H generated maximum efficacy at reducing α -SMA among the SCFA treatment groups. Similar results were also observed in gene expression levels of *Acta2*, the α -SMA-coding gene. TGF- β 1 treatment increased the levels of *Acta2* compared to the control group, while treatment with high-dose of SCFAs inhibited *Acta2* levels, which were 57.7% (NaA-H), 26.4% (NaB-H), and 19.8% (NaP-H) lower than those in the MOD group, respectively (**Figure 1C**). These results confirmed that NaA-H had the best inhibitory effect on LX2 cell activation. Moreover, SCFAs also suppressed the overexpression of fibrosis marker genes *Col1a1* and *Fn* in TGF- β 1-activated LX2 cells. For *Col1a1* gene expression, a high dose of NaA or NaB showed significant inhibition compared to the MOD group (**Figure 1D**). For *Fn* gene, all high-dose groups of three SCFAs represented significant inhibition to the MOD group (**Figure 1E**). The results indicated that SCFA treatment ameliorated TGF- β 1-induced LX2 cell activation. NaA-H revealed the best efficacy at alleviating TGF- β 1-induced LX2 cell activation relative to propionate and butyrate. Therefore, NaA-H was selected for further experiments.

NaA Treatment Inhibited TGF- β 1/Smad2 Signaling in LX2 Cells

As the downstream cascade, Smad2 signaling plays a key role in TGF- β 1-induced HSC activation. Compared to the control group, TGF- β 1 markedly enhanced the phosphorylation level of Smad2 protein, while NaA treatment significantly ameliorated the phosphorylation of Smad2 (**Figure 2**). These phenomena were consistent with previous results, indicating that NaA inhibits the phenotype and key signaling pathways.

NaA Entered Into Cells to Inhibit LX2 Cell Activation Independent of GPR43

Next, we examined whether GPR43, a promising receptor of acetate, participated in the LX2 cell inhibition by acetate. GPR43 siRNA was used to silence its target mRNA, specifically in LX2 cells. Herein, we designed three siGPR43 sequences; the silencing efficiency of the siGPR43-2 sequence was 90.6%, and hence, it was selected for downstream experiments in LX2 cells (**Figure 3A**). The results showed that GPR43 silencing did not have an impact on the decreased expression of α -SMA protein and *Col1a1* mRNA by NaA (**Figures 3B,C**), indicating that NaA inhibited the activation of LX2 cells via pathways independent of GPR43. In addition to G proteins, histone deacetylase (HDAC) enzymes may also act as target sites of SCFA. SCFAs exert their effects by binding to metabolite-sensing GPR41, GPR43, and GPR109A or epigenetically via HDAC modulation. Since the GPR43 receptor does not influence the function of acetate, the impact of acetate on HDAC was further investigated and speculated to be involved in the beneficial effects of SCFAs. Compared to the control group, TGF- β 1 or NaA treatment did not significantly alter the expression of HDAC2, HDAC4, HDAC5, HDAC6, HDAC7, HDAC8, HDAC9, and HDAC11. Although NaA treatment had a significant effect on the expression of HDAC1, HDAC3 and HDAC10, TGF- β 1 treatment had no influence on the expression of these genes indicating they were not involved in activation of LX2 cells. Therefore, the results showed that HDAC did not participate in NaA inhibiting the activation of LX2 cells (**Supplementary Figure 1**). These results indicated that GPR43 or HDAC might not participate in the inhibition of NaA-activated HSCs.

On the other hand, NaA may enter into the cells and have some effects. To verify this hypothesis, we used a GC-MS to detect the intracellular acetate content. Compared to the control and model groups, treatment with NaA (1 mM) caused a significant increase in the content of acetate, while the other two groups were lower than the detection limit ($0.42 \mu\text{g/mL}$) (**Figure 3D**). The present results showed that inhibiting HSC activation by acetate might be achieved by NaA entering into the cell.

NaA Attenuated LX2 Cells Activation in an AMPK α - and c-Jun-Dependent Manner

To analyze the potential mechanism of NaA on the activation of LX2 cells induced by TGF- β 1, a phosphokinase array kit containing 43 kinase phosphorylation targets was used (**Supplementary Table 2**). TGF- β 1 induced significant changes in the phosphorylation level of 18 proteins compared to the control group. NaA treatment altered the phosphorylation level of 22 proteins compared to the MOD group. Herein, the significant changes in the phosphorylation of the protein effectuated by both TGF- β 1 and NaA treatment were investigated (**Figure 4A**). We found that the phosphorylation of AMPK α was decreased when LX2 cells were exposed to a medium containing TGF- β 1, while NaA supplementation enhanced the phosphorylation of AMPK α significantly (**Figures 4B,C**). On the other hand, phosphorylation of c-Jun was significantly upregulated in TGF- β 1-activated HSCs, and NaA treatment

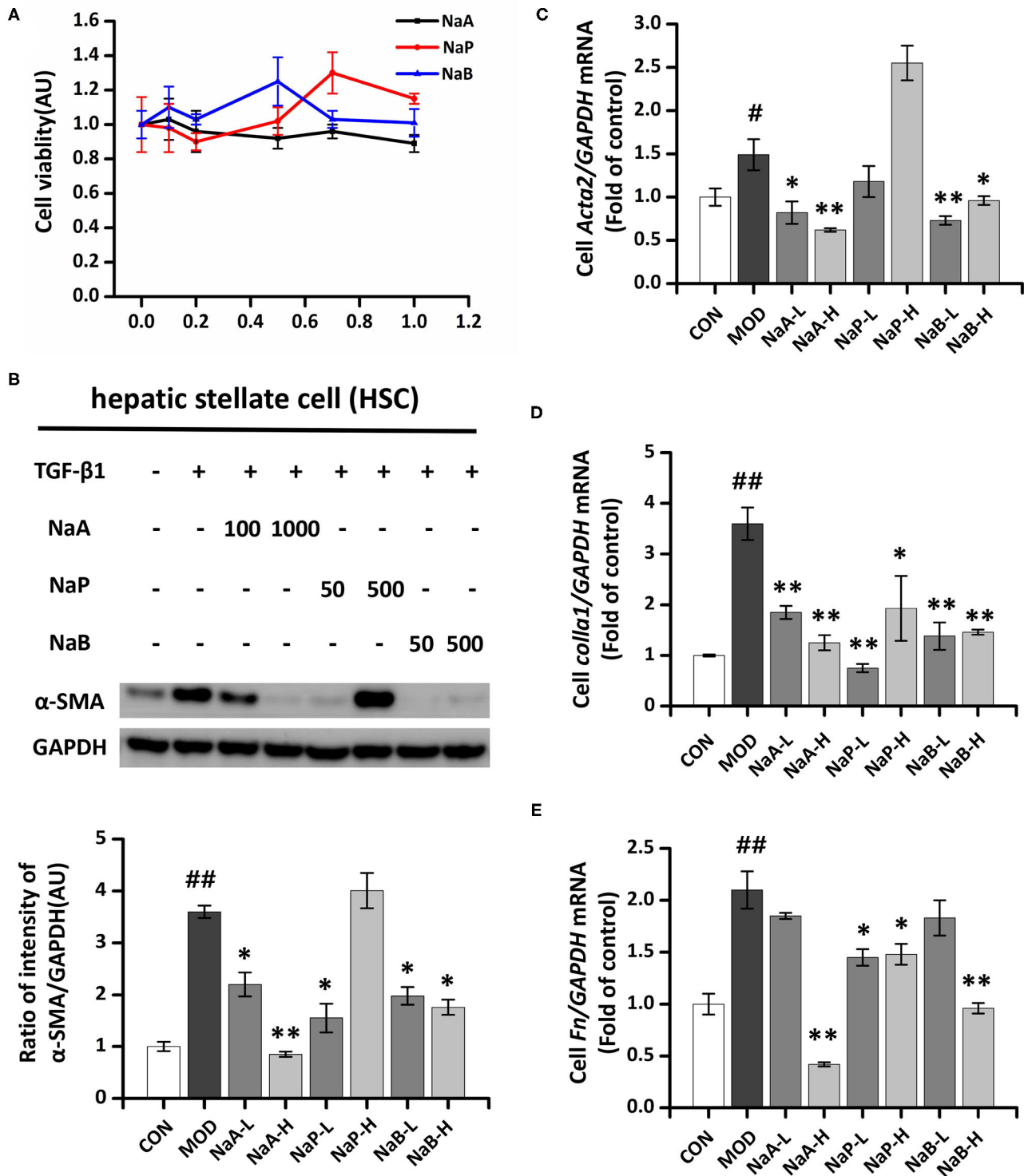


FIGURE 1 | Effects of SCFAs on TGF- β 1 induced LX2 cells activation. **(A)** SCFAs cytotoxic effects. After serum starvation for 12 h, a CCK8 assay was performed for LX2 cells treated with SCFAs at doses of 0–1 mM for 48 h. **(B)** The protein expression of α -SMA was assessed by the Western blot. LX2 cells were treated with or without 2.5 ng/ml TGF- β 1 and 1 mM of SCFAs for 48 h. **(C–E)** Real-time PCR was used to evaluate the mRNA expressions of *Acta2*, *Col1a1*, and *Fn*. LX2 cells were treated with or without 2.5 ng/ml TGF- β 1 and 1 mM of SCFAs for 48 h. LX2 cells were treated as detailed in the section Materials and Methods. For all bar graphs, data are the mean \pm SD, $\#p < 0.05$, $\#\#p < 0.01$, as compared with CON, and $*p < 0.05$, $**p < 0.01$, as compared with MOD. The significant difference was assessed using the one-way ANOVA followed by LSD post-tests. Control group (CON), group model cell treated with a TGF- β 1 (MOD), low dose of sodium acetate (NaA-L), high dose of sodium acetate (NaA-H), low dose of sodium propionate (NaP-L), high dose of sodium propionate (NaP-H), low dose of sodium butyrate (NaB-L), high dose of sodium butyrate (NaB-H), arbitrary unit (AU).

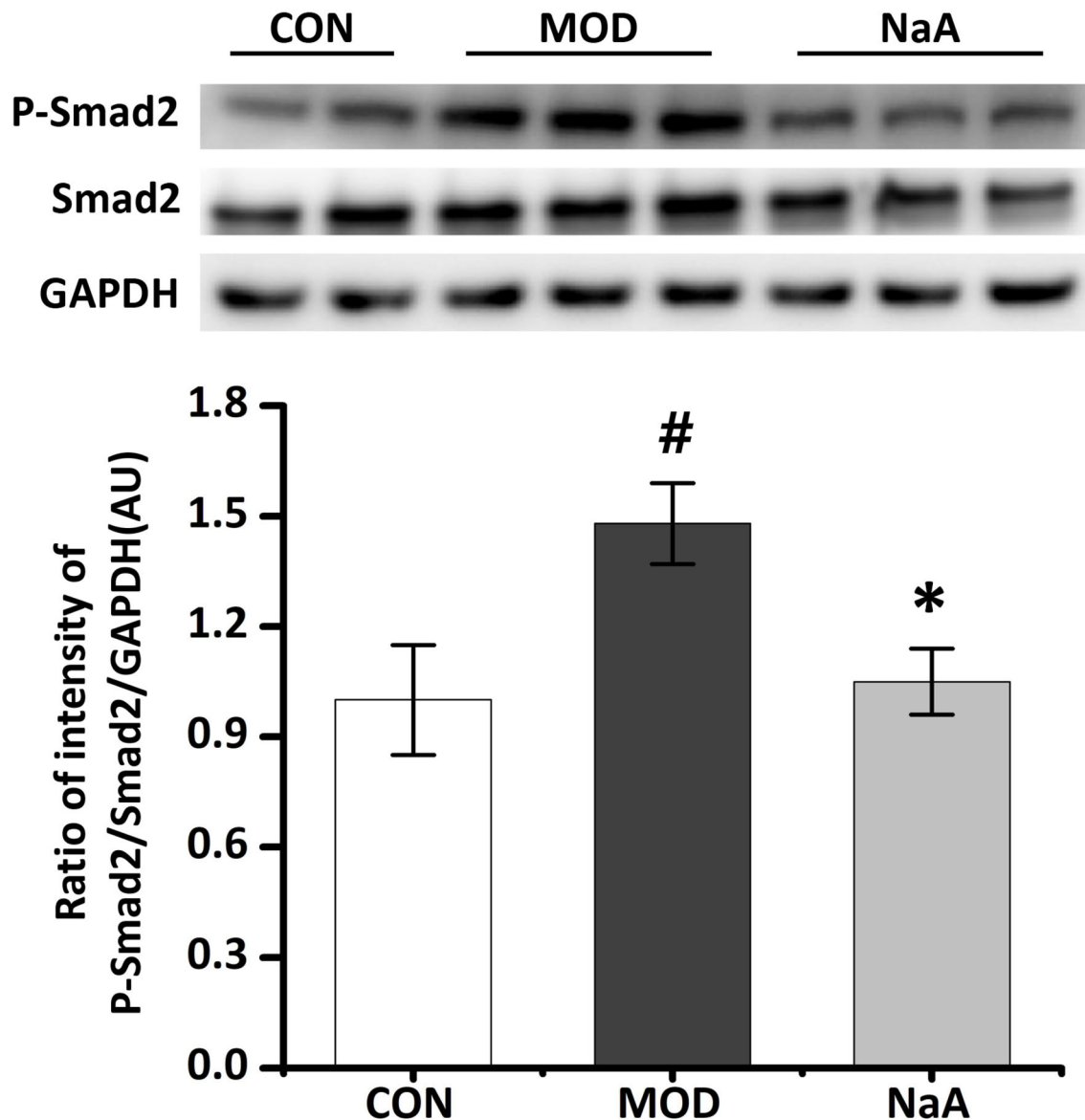


FIGURE 2 | NaA inhibited TGF- β 1 induced HSCs activation in LX2 cells. LX2 cells were treated with or without 2.5 ng/ml TGF- β 1 and 1 mM of NaA for 48 h. Western blot was used to evaluate the phosphorylation of Smad2. LX2 cells were treated as detailed in the section Materials and Methods. For all bar graphs, data are the mean \pm SD, # $p < 0.05$, as compared with CON, and * $p < 0.05$, as compared with MOD. The significant difference was assessed using the one-way ANOVA followed by LSD post-tests. Control group (CON), group model cell treated with a TGF- β 1 (MOD), sodium acetate (NaA), arbitrary unit (AU).

restored the increasing trend (Figures 4B,D). These findings indicated that AMPK α and c-Jun pathways were highly related to the inhibition of NaA-activated LX2 cells.

Next, we employed Western blot to verify the ChIP data and confirmed that the phosphorylation of AMPK α was significantly decreased in LX2 cells after short-term exposure to 2.5 ng/mL TGF- β 1, which was increased after NaA addition (Figure 5A). Also, NaA treatment significantly reduced TGF- β 1-induced phosphorylation of c-Jun (Figure 5B), which was consistent with the ChIP results. Furthermore, we used HPLC to measure the intracellular AMP/ATP content and found that the AMP/ATP

ratio decreased in the MOD group but was restored in the NaA treatment group, which might contribute to the changes in the AMPK α phosphorylation level (Figure 5C). These results indicated that a high dose of NaA was capable of inhibiting TGF- β 1-induced cell activation via AMPK α and c-Jun pathways.

NaA-Alleviated LX2 Cell Activation Is Related to PPAR γ Pathway

We also explored whether PPAR γ , the potential target of SCFA for HE, is involved in the protective effect of SCFAs in HSC activation. The roles of PPAR γ in the inhibition of

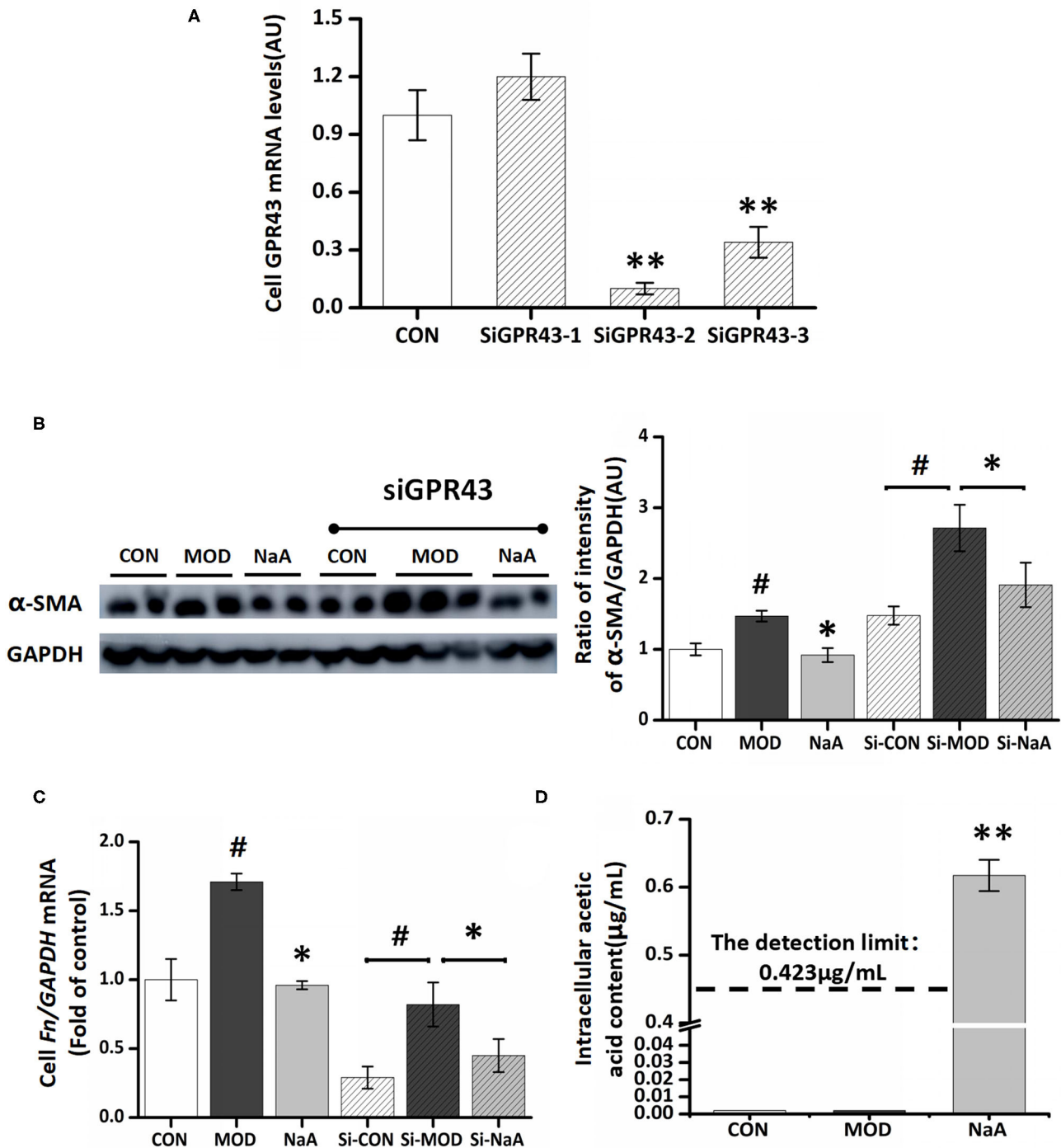
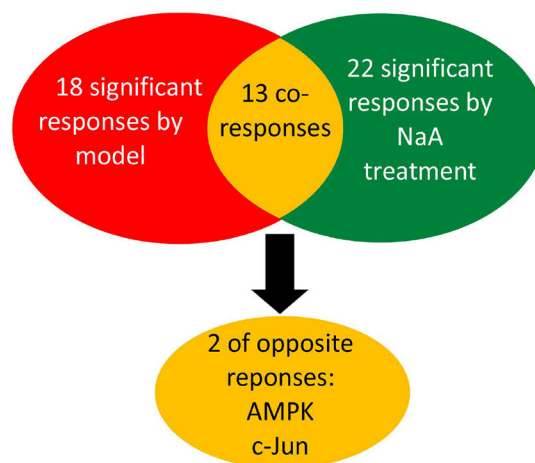


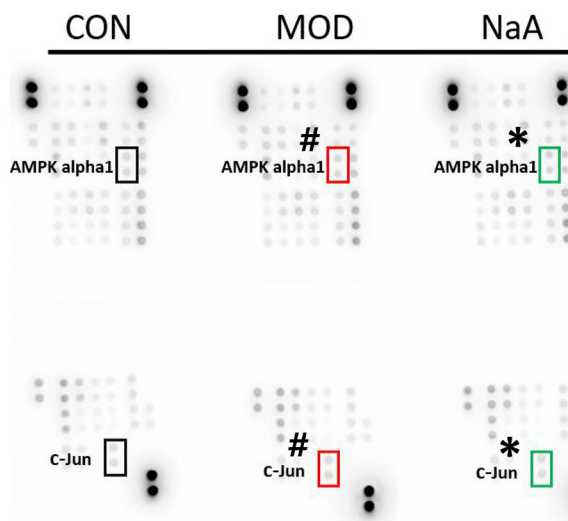
FIGURE 3 | GPR43 possessed limiting ability in the process of NaA inhibited TGF- β 1 induced HSCs activation. **(A)** LX2 cells were cultured and transfected with 50 nM Lipofectamine[®] 2000 RNAiMax reagent and GPR43 siRNA, selected the sequences with the best silence efficiency. **(B)** Western blot was used to evaluate the protein of α -SMA. LX2 cells were treated with or without 2.5 ng/ml TGF- β 1 and 0–1 mM of NaA for 48 h at 24 h post-transfection. **(C,D)** Real-time PCR was used to evaluate the mRNA expression of *Col1a1*. LX2 cells were treated with or without 2.5 ng/ml TGF- β 1 and 0–1 mM of NaA for 48 h at 24 h post-transfection. LX2 cells were treated as detailed in the section Materials and Methods. For all bar graphs, data are the mean \pm SD, # p < 0.05, as compared with CON, and * p < 0.05, ** p < 0.01, as compared with MOD. The significant difference was assessed using the one-way ANOVA followed by LSD post-tests. Control group (CON), group model cell treated with a TGF- β 1 (MOD), sodium acetate (NaA), arbitrary unit (AU).

- A**
- Significant differences of phosphorylation level between control group and model group ($P < 0.05$)
 - Significant differences of phosphorylation level between model group and sodium acetate treatment group ($P < 0.05$)
 - Significant differences of phosphorylation level in control group compared with model group and the sodium acetate treatment group

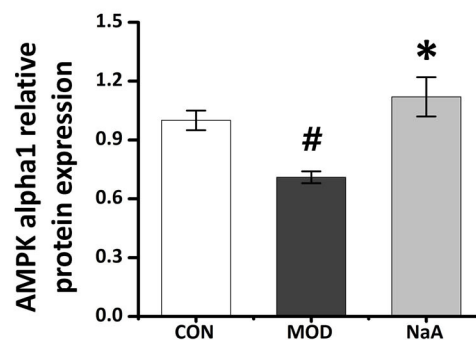
p38alpha	-	-	STAT6	■	-	AMPKalpha2	■	■	RSK1/2/3	-	■
ERK1/2	■	■	STAT5b	-	-	beta-Catenin	-	-	eNOS	■	■
JNK 1/2/3	■	■	Hck	-	-	Src	-	■	STAT3	-	■
GSK-3alpha/beta	-	■	Chk-2	-	-	Lyn	■	-	p27	-	-
EGF R	-	-	FAK	-	-	Lck	-	-	PLC-gamma1	■	■
MSK1/2	-	■	PDGF Rbeta	■	■	STAT2	■	■	STAT3	■	-
AMPKalpha1	■	■	STAT5a/b	■	-	STAT5a	-	-	WNK1	-	■
Akt 1/2/3	-	-	PRAS40	-	-	Fyn	■	■	PYK2	■	■
TOR	■	■	p53	-	■	Yes	-	-			
CREB	■	■	p70 S6 Kinase	-	■	Fgr	-	-			
HSP27	■	■	c-Jun	■	■	HSP60	-	■			



B



C



D

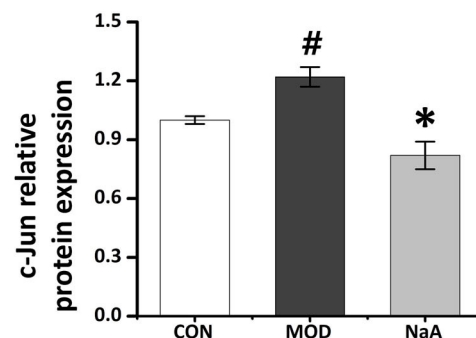
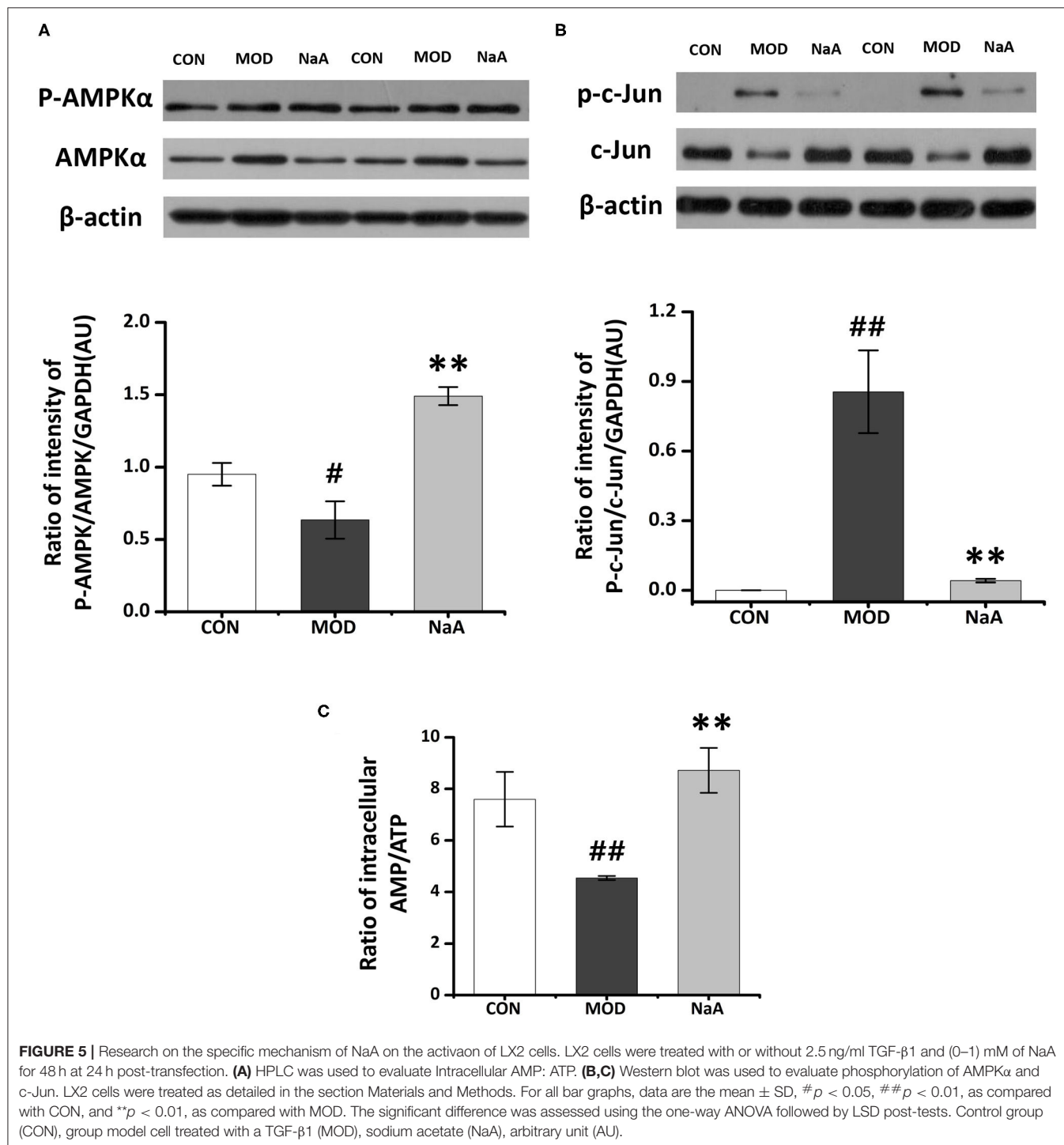


FIGURE 4 | Potential targets of NaA. LX2 cells were treated with or without 2.5 ng/ml TGF- β 1 and 0–1 mM of NaA for 48 h. After quantitative analysis of the results using gray analysis software. **(A)** The component-target network. Phosphorylation analysis of 43 potential targets. 43 protein contains a protein called p53, protein p53 has three phosphate sites (s15, s392, and s46), we will uniform them as p53. The red represents to compare with the CON, the model is significantly different, (Continued)

FIGURE 4 | the green represent to the NaA treatment group is significantly different from MOD, the yellow part means that both MOD and NaA treatment group are significant. **(B–D)** Phospho-kinase array screening. Differentially expressed phosphor-proteins are labeled by frames, two types with opposite trends, namely AMPK α and c-Jun amino-terminal kinase. LX2 cells were treated as detailed in the section Materials and Methods. For all bar graphs, data are the mean \pm SD, # $p < 0.05$, as compared with CON, and * $p < 0.05$, as compared with MOD. The significant difference was assessed using the one-way ANOVA followed by LSD post-tests. Control group (CON), group model cell treated with a TGF- β 1 (MOD), sodium acetate (NaA), arbitrary unit (AU).



acetate-activated LX2 cells were verified using PPAR γ silencing. The expression of PPAR γ in the silenced cells was decreased (Figure 6A), and siPPAR γ -2 represented the best silencing efficiency. Western blot showed that the inhibition of α -SMA (Figure 6B) and phosphorylation of Smad2 (Figure 6C) by SCFAs were significantly disrupted by siRNA-PPAR γ . Moreover, siRNA-PPAR γ abolished the inhibitory effects of SCFAs against TGF- β 1 induced increase in the gene expression of *Colla1* and *Fn* (Figures 6D,E). Taken together, these data indicated that the inhibition of HF by SCFAs was dependent on PPAR γ .

DISCUSSION

This study evaluated the potential antifibrotic effects of three dominant SCFAs, acetate, propionate, and butyrate, based on TGF- β 1-activated LX2 cells. NaA represented the best efficacy at inhibiting fibrotic markers, indicating the ability to alleviate HSCs activation. Furthermore, the underlying mechanisms were elucidated. We found that NaA could enter into cells to inhibit HSC activation rather than through GPR43 receptor or act as an inhibitor of HDAC. Finally, we demonstrated NaA regulates AMPK α /PPAR γ and c-Jun signaling pathways, which further block TGF- β 1/Smad2 to suppress the activation of LX2 cells. To the best of our knowledge, this is the first study to investigate the direct effects of different SCFAs on activating HSCs and revealing the underlying mechanisms.

As major gut microbial metabolites, SCFAs showed their direct or indirect influence on the gut-liver communications and played a role in liver functions (22). However, inconsistent effects of different SCFAs on liver functions were observed previously. Previous studies demonstrated that SCFAs contributed to obesity and liver steatosis as they provide \sim 10% of daily caloric consumption and might enhance nutrient absorption by promoting the expression of glucagon-like peptide 2 (GLP-2), obesity, and liver steatosis that could trigger liver inflammation and NAFLD, as well as HF (31). Moreover, another study showed that acetate activated the parasympathetic nervous system resulting in increased ghrelin secretion and glucose-stimulated insulin secretion (GSIS), which in turn generated ectopic lipid deposition and insulin resistance in the liver (32). Conversely, accumulating evidence showed that SCFAs act through GPR41 and GPR43 in L cells to promote peptide YY (PYY) and GLP-1 and alter satiety and energy intake, which further alleviates obesity or NAFLD indirectly (33). SCFAs also regulate hepatic metabolism by altering hepatic AMPK phosphorylation and expression of PPAR α target genes involved in free fatty acids (FFAs) oxidation. Thus, SCFAs might act both directly and indirectly to alleviate hepatic metabolism disorder via complicated processes (17). HF was closely associated with various types of chronic inflammatory damage in the liver as a compensatory pathophysiological process, especially for steatosis or steatohepatitis. The activation of HSCs had been confirmed to play a critical role in HF (6). Currently, there is no evidence to show how exogenous SCFAs directly affect HF. To address whether SCFAs improved HF symptoms and which SCFAs

were the most effective, we provided primary data concerning the direct effects of acetate, propionate, and/or butyrate on alleviating TGF- β 1-induced LX2 cell activation. Among these, high-dose sodium acetate (1 mM) was considered efficacious in alleviating LX2 cell activation. Similarly, in our previous study, NaA displayed maximum efficacy at decreasing liver steatosis (18), i.e., supplementation of SCFA is beneficial for managing HSC activation. We also observed that high dose of propionate increased level of α -SMA and related gene (*Acta2*), but have no influence on *Colla1* and *Fn*. These results suggested high dose of propionate might induce the fibrosis. However, few studies provided similar evidence, except Lee et al. (34) showed propionate level in stool samples increased with worsening fibrosis severity (level of fibrogenic genes and proteins, such as α -SMA) of non-obese NAFLD patients. We noticed that high dose propionate (500–1,000 μ mol/L) stimulated viability of LX2 cells (Figure 1A). Since we speculated that induced expression of α -SMA by high dose propionate may related high cell viability by the treatment of propionate. The clear mechanism need to be elucidated in future studies.

The mechanisms of acetate inhibiting HSCs activation were further investigated in LX2 cells. The biological responses of acetate on host cells result from the inhibition of HDAC or the activation of GPRs, such as GPR41 and GPR43 (32). GPR43 has been identified in the colon, as well as in adipocytes, hepatocytes, enteroendocrine cells, and immune cells (polymorphonuclear cells and macrophages) (35). Next, we assessed whether acetate activates GPR43, the membrane FA receptor for which acetate had the highest affinity, during the HSC suppression (36). In contrast to expectations, the decrease in GPR43 by RNA silencing could not attenuate acetate-altered expression of α -SMA protein and *Colla1* mRNA. Then, we investigated whether acetate altered HSC activation by inhibiting HDAC in LX2 cells, while acetate and/or TGF- β 1 treatment did not have an impact on the expression of HDAC mRNA, indicating that NaA inhibited the activation of HSCs via pathways independent of GPR43 or HDAC. On the other hand, the concentration of intracellular acetate was significantly increased in LX2 cells treated by NaA, indicating that acetate entered the cells and affected the intracellular signals. This phenomenon was consistent with the previous report, wherein SCFAs attenuate intestinal inflammation by entering Caco-2 cells (37) through monocarboxylate transporter 1 (MCT1) or sodium monocarboxylate transporter 1 (SMCT1) transport protein and act independently of GPR43 or HDAC (26). Similarly, another study indicated that acetate was absorbed mainly by passive diffusion, accumulated inside m-ICcl2 cells, and stimulated lipid consumption in enterocytes (30). The increasing intracellular concentration of NaA demonstrated that NaA partially inhibits LX2 cell activation by entering the cells.

Acetate might directly interact with intracellular signaling molecules to regulate HSCs activation. However, the molecular mechanisms underlying this effect are yet to be elucidated. Herein, we used antibody-based array kits to analyze the mechanism by which acetate inhibited LX2 cell activation.

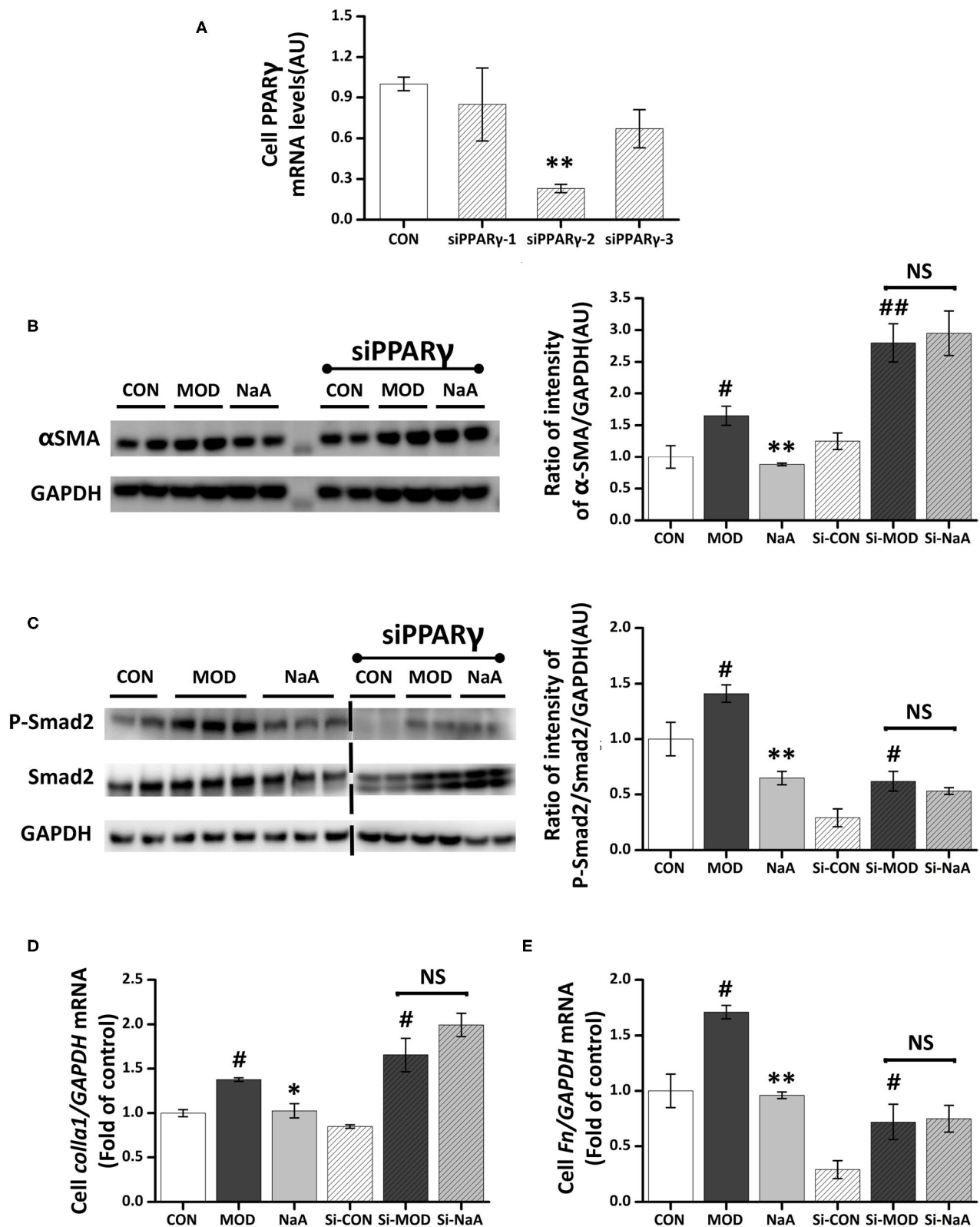


FIGURE 6 | NaA-mediated anti-fibrosis effects were partially reversed by siRNA-PPAR γ . LX2 cells were cultured and transfected with 50 nM Lipofectamine[®] 2000 RNAiMax reagent and PPAR γ siRNA. **(A)** Real-time PCR was used to evaluate the mRNA expression of PPAR γ , selected the sequences with the best

(Continued)

FIGURE 6 | silence efficiency. **(B,C)** Western blot was used to evaluate the protein of α -SMA and phosphorylation of Smad2. LX2 cells were treated with or without 2.5 ng/ml TGF- β 1 and 0, 1 mM of NaA for 48 h at 24 h post-transfection. **(D,E)** Real-time PCR was used to evaluate the mRNA expressions of *Col1a1* and *Fn*. LX2 cells were treated with or without 2.5 ng/ml TGF- β 1 and 0–1 mM of NaA for 48 h at 24 h post-transfection. LX2 cells were treated as detailed in the section Materials and Methods. For all bar graphs, data are the mean \pm SD, # p < 0.05, ## p < 0.01, as compared with CON, and * p < 0.05, ** p < 0.01, as compared with MOD. The significant difference was assessed using the one-way ANOVA followed by LSD post-tests. Control group (CON), group model cell treated with a TGF- β 1 (MOD), sodium acetate (NaA), arbitrary unit (AU).

We found that acetate might inhibit HSC activation through AMPK α and c-Jun pathways. AMPK acted as the primary sensor of cellular energy status and was closely related to HF (38). A previous study showed that the loss of AMPK exaggerates the pathology of NASH caused by diet, including increased liver damage and fibrosis (38), while AMPK activation reduced NASH and HF by suppressing the production of fat, promoting the mitochondrial function in the liver, and inhibiting the proliferation of HSCs (39). AMPK is also considered the target of SCFAs involved in the alleviation of metabolic disease. Some studies reported that enterocytes exposed to acetate induced a marked increase in phosphorylated AMPK α and ameliorated lipid metabolism (30). These observations suggested that AMPK might play a role in HSC suppression by acetate. The antibody-based array kits and Western blot revealed that the phosphorylation of AMPK α was reduced after TGF- β 1 treatment, indicating that the low phosphorylation level of AMPK α is closely related to HSC activation. We observed that acetate restored the decreased phosphorylation level of AMPK α induced by TGF- β 1 and regulated the intracellular ratio of AMP and ATP, which might be critical to induce AMPK α phosphorylation. Reportedly, acetate was converted to acetyl CoA with the formation of AMP by the catalytic action of cytosolic acetyl CoA synthetase (AceCS1), and it might lead to increased AMP/ATP ratio in the cytosol. An increase in AMP/ATP ratio in the cytosol activated AMPK (40), which was considered as the primary mechanism related to activation of AMPK by acetate. Based on the results of the phosphokinase array and Western blot, we observed that c-Jun was involved in acetate-alleviated LX2 cell activation. Also, acetate reduced the phosphorylation of c-Jun and thus reduced the expression of the protein. Moreover, the reduced expression of c-Jun could inhibit its binding with Smad2, which in turn affects the TGF- β 1-induced transcription of α -SMA (41). Fu et al. (42) demonstrated that acetate reduces the phosphorylation of c-Jun in adipocytes. Although c-Jun signaling was found to participate in the process of acetate-inhibited HSCs activation, future studies should explore the detailed mechanisms underlying the roles of c-Jun in HF, especially in HSC activation.

PPAR γ is a nuclear receptor expressed in vascular smooth muscle cells and HSCs. It plays a role in the transcriptional control of cell growth, differentiation, and liver fibrosis. Cross-regulation by PPAR γ of key fibrogenic factor TGF- β 1 signaling have been identified as a main mechanisms by which PPAR γ inhibits liver fibrosis (43, 44). PPAR γ has been shown to disrupt TGF- β 1-activated stress-activated protein kinase/c-Jun N-terminal kinase signaling, leading to decreased Smad2/3

activity and myofibroblast activation (34, 43). Similarly, Choi et al. showed that Capsaicin can ameliorate hepatic fibrosis by inhibiting the TGF- β 1/Smad pathway via PPAR γ activation (45). Our study indicated that NaA can activate PPAR γ by increasing the phosphorylation of AMPK or reducing the phosphorylation of c-Jun. Considering the credible relation between PPAR γ and TGF- β 1/Smad2 pathway, we concluded that NaA inhibited TGF- β 1/Smad2 pathway via PPAR γ activation. PPAR γ was highly expressed in quiescent HSCs of the normal liver but stimulated the inhibited HSC proliferation during hepatic fibrogenesis by reducing the expression of α -SMA protein and *Col1a1* mRNA (46). Intriguingly, PPAR γ agonists/ligands inhibit both HSCs activation and HF (47). Therefore, PPAR γ status is a pivotal marker for the success of antifibrotic therapy. AMPK is a known upstream agonist of PPAR γ , and the activation of AMPK upregulates PPAR γ expression (48). Some studies showed that the activation of AMPK/PPAR γ pathway was related to the alleviation of NAFLD in mice (49). Na et al. (50) reported that acetate activated AMPK by increasing the AMP/ATP ratio, thereby increasing the PPAR γ expression for blood pressure control. In this study, we found that NaA inhibited TGF- β 1-induced increase in α -SMA expression and Smad2 phosphorylation, and silenced PPAR γ disrupted the effects of NaA. These results at least partially confirmed the involvement of PPAR γ in the inhibition of LX2 cells activated by NaA. We also observed that the phosphorylation level of AMPK α was related to HSC activation and thus, speculated that NaA inhibited HSC activation via AMPK/PPAR γ pathway. The detailed interactions between AMPK and PPAR γ and the role of acetate in this process need to be elucidated further.

CONCLUSION

The TGF- β 1-activated LX2 cells were alleviated by the effects of three dominant SCFAs, acetate, propionate, and butyrate. Acetate showed the best efficacy in suppressing fibrogenic markers and key signaling pathways in LX2 cells. We also found that NaA enters the cells and inhibits LX2 cell activation independent of GPR43, the canonical receptor of acetate. NaA also restores the phosphorylation levels of AMPK that are reduced in activated HSCs, while c-Jun and PPAR γ are involved in the progress of inhibiting the activation of HSCs. Next, we suggested that the AMPK/PPAR γ /Smad2 pathway is a novel mechanism associated with NaA-mediated anti-fibrosis against the activation of HSCs. This study provides evidence with respect to the correlation between gut microbial metabolites and the

occurrence and development of HF and the connection of gut-liver axis and proposed sodium acetate as a putative candidate for the regulation of HF.

DATA AVAILABILITY STATEMENT

The datasets presented in this study can be found in online repositories. The names of the repository/repositories and accession number(s) can be found in the article/**Supplementary Material**.

AUTHOR CONTRIBUTIONS

XZ, SG, and LZ: conceptualization and supervision. WL: data curation and writing—original draft preparation. WL, MD, and JG: investigation, methodology, and validation. WL and LZ: writing—reviewing and editing. All authors contributed to the article and approved the submitted version.

FUNDING

The authors declare that this study received funding from National Natural Science Foundation of China (32072196)

REFERENCES

- Friedman SL. Hepatic stellate cells: protean, multifunctional, and enigmatic cells of the liver. *Physiol Rev.* (2008) 88:125–72. doi: 10.1152/physrev.00013.2007
- Elpek GO. Cellular and molecular mechanisms in the pathogenesis of liver fibrosis: an update. *World J Gastroenterol.* (2014) 20:7260–76. doi: 10.3748/wjg.v20.i23.7260
- Han X, Wu Y, Yang Q, Cao G. Peroxisome proliferator-activated receptors in the pathogenesis and therapies of liver fibrosis. *Pharmacol Ther.* (2021) 222:107791. doi: 10.1016/j.pharmthera.2020.107791
- Tripathi A, Debelius J, Brenner DA, Karin M, Loomba R, Schnabl B, et al. The gut-liver axis and the intersection with the microbiome. *Nat Rev Gastroenterol Hepatol.* (2018) 15:397–411. doi: 10.1038/s41575-018-0011-z
- Josan S, Billingsley K, Orduna J, Park JM, Luong R, Yu L, et al. Assessing inflammatory liver injury in an acute CCl₄ model using dynamic 3D metabolic imaging of hyperpolarized 1-C-13 pyruvate. *NMR Biomed.* (2015) 28:1671–77. doi: 10.1002/nbm.3431
- Puche JE, Saiman Y, Friedman SL. Hepatic stellate cells and liver fibrosis. *Compr.* (2013) 3:1473–92. doi: 10.1002/cphy.c120035
- Rao HY, Wei L, Li J, Zhang LF, Chen HY, Zhu LM, et al. Liver fibrosis and hepatic stellate cells improvement of chronic hepatitis C patients by interferon- β -1 α with or without sustained viral response. *Hepato Gastroenterol.* (2009) 56:328–34.
- Mazzotti A, Caletti MT, Sasdelli AS, Brodosi L, Marchesini G. Pathophysiology of non-alcoholic fatty liver disease: lifestyle-gut-gene interaction. *Dig Dis.* (2016) 34:3–10. doi: 10.1159/000447275
- Poeta M, Pierri L, Vajro P. Gut-liver axis derangement in non-alcoholic fatty liver disease. *Children.* (2017) 4:66. doi: 10.3390/children4080066
- Le Roy T, Llopis M, Lepage P, Bruneau A, Rabot S, Bevilacqua C, et al. Intestinal microbiota determines development of non-alcoholic fatty liver disease in mice. *Gut.* (2013) 62:1787–94. doi: 10.1136/gutjnl-2012-303816
- Cani PD. Human gut microbiome: hopes, threats and promises. *Gut.* (2018) 67:1716–25. doi: 10.1136/gutjnl-2018-316723
- Parekh PJ, Balart LA, Johnson DA. The influence of the gut microbiome on obesity, metabolic syndrome and gastrointestinal disease. *Clin Transl Gastroenterol.* (2015) 6:e91. doi: 10.1038/ctg.2015.16

and the 111 Project from the Education Ministry of China (No. B18053).

SUPPLEMENTARY MATERIAL

The Supplementary Material for this article can be found online at: <https://www.frontiersin.org/articles/10.3389/fnut.2021.729583/full#supplementary-material>

Supplementary Figure 1 | HDAC had a restrictive ability in the process of NaA inhibited TGF- β 1 induced HSCs activation. LX2 cells were treated with or without 2.5 ng/ml TGF- β 1 and 1 mM of NaA for 48 h. Real-time PCR was used to evaluate the mRNA expression of *HDAC*. LX2 cells were treated as detailed in the section Materials and Methods. For all bar graphs, data are the mean \pm SD, # p < 0.05, as compared with CON, and * p < 0.05, as compared with MOD. The significant difference was assessed using the one-way ANOVA followed by LSD post-tests. Control group (CON), group model cell treated with a TGF- β 1 (MOD), sodium acetate (NaA), arbitrary unit (AU).

Supplementary Table 1 | Primers used in real-time qPCR.

Supplementary Table 2 | Design of GPR43 siRNA targeting sequences.

Supplementary Table 3 | Design of PPAR γ siRNA targeting sequences.

Supplementary Table 4 | Comparison of level of protein phosphorylation among groups.

- Boursier J, Mueller O, Barret M, Machado M, Fizanne L, Araujo PF, et al. The severity of non-alcoholic fatty liver disease is associated with gut dysbiosis and shift in the metabolic function of the gut microbiota. *Hepatology.* (2016) 63:764–75. doi: 10.1002/hep.28356
- Kakiyama G, Pandak WM, Gillevet PM, Hylemon PB, Heuman DM, Daita K, et al. Modulation of the fecal bile acid profile by gut microbiota in cirrhosis. *J Hepatol.* (2013) 58:949–55. doi: 10.1016/j.jhep.2013.01.003
- Gadallah SH, Eissa S, Ghanem HM, Ahmed EK, Hasanin AH, Mahdy MM, et al. Probiotic-prebiotic-synbiotic modulation of (*YAP1*, *LATS1* and *NF2* mRNAs/*miR-1205/lnc RNA SRD5A3-AS1*) panel in NASH animal model. *Biomed Pharmacother.* (2021) 140:111781. doi: 10.1016/j.biopha.2021.111781
- Li M, Zhou Y, Zuo L, Nie D, Li X. Dietary fiber regulates intestinal flora and suppresses liver and systemic inflammation to alleviate liver fibrosis in mice. *Nutrition.* (2021) 81:110959. doi: 10.1016/j.nut.2020.110959
- Besten G, Bleeker A, Gerding A, Eunen K, Havinga R, Dijk TH, et al. Short-chain fatty acids protect against high-fat diet-induced obesity via a PPAR-dependent switch from lipogenesis to fat oxidation. *Diabetes.* (2015) 64:2398–408. doi: 10.2337/db14-1213
- Deng M, Qu F, Chen L, Liu C, Zhang M, Ren F, et al. SCFAs alleviated steatosis and inflammation in mice with NASH induced by MCD. *J Endocrinol.* (2020) 245:425–37. doi: 10.1530/JOE-20-0018
- Takai A, Kikuchi K, Ichimura M, Tsuneyama K, Moritoki Y, Matsumoto K, et al. Fructo-oligosaccharides ameliorate steatohepatitis, visceral adiposity, and associated chronic inflammation via increased production of short-chain fatty acids in a mouse model of non-alcoholic steatohepatitis. *BMC Gastroenterol.* (2020) 20:46. doi: 10.1186/s12876-020-01194-2
- Takayama S, Katada K, Takagi T, Iida T, Ueda T, Mizushima K, et al. Partially hydrolyzed guar gum attenuates non-alcoholic fatty liver disease in mice through the gut-liver axis. *World J Gastroenterol.* (2021) 27:2160–76. doi: 10.3748/wjg.v27.i18.2160
- Jin Y, Lu L, Tu W, Luo T, Fu Z. Impacts of polystyrene microplastic on the gut barrier, microbiota and metabolism of mice. *Sci Total Environ.* (2019) 649:08–17. doi: 10.1016/j.scitotenv.2018.08.353
- Wu JL, Zou JY, Hu ED, Chen DZ, Chen L, Lu FB, et al. Sodium butyrate ameliorates S100/FCA-induced autoimmune hepatitis through regulation of

- intestinal tight junction and toll-like receptor 4 signaling pathway. *Immunol Lett.* (2017) 190:169–76. doi: 10.1016/j.imlet.2017.08.005
23. Shi H, Bi H, Sun X, Dong H, Jiang Y, Mu H, et al. Antitumor effects of tubemimoside-1 in NCI-H1299 cells are mediated by microRNA-126-5p-induced inactivation of VEGF-A/VEGFR-2/ERK signaling pathway. *Mol Med Rep.* (2018) 17:4327–36. doi: 10.3892/mmr.2018.8459
 24. Luo X, Li H, Ma L, Zhou J, Guo X, Woo SL, et al. Expression of STING is increased in liver tissues from patients with NAFLD and promotes macrophage-mediated hepatic inflammation and fibrosis in mice. *Gastroenterology.* (2018) 155:1971. doi: 10.1053/j.gastro.2018.09.010
 25. Guo X, Li H, Xu H, Halim V, Thomas LN, Woo SL, et al. Disruption of inducible 6-phosphofructo-2-kinase impairs the suppressive effect of PPAR γ activation on diet-induced intestine inflammatory response. *J Nutr Biochem.* (2013) 24:770–75. doi: 10.1016/j.jnutbio.2012.04.007
 26. Coady MJ, Wallendorff B, Bourgeois F, Charron F, Lapointe JY. Establishing a definitive stoichiometry for the Na⁺/monocarboxylate cotransporter SMCT1. *Biophys J.* (2007) 93:2325–31. doi: 10.1529/biophysj.107.108555
 27. Cai JW, Zhang JT, Tian Y, Zhang LM, Hatzakis E, Krausz KW, et al. Orthogonal comparison of GC MS and H-1 NMR spectroscopy for short chain fatty acid quantitation. *Anal Chem.* (2017) 89:7900–06. doi: 10.1021/acs.analchem.7b00848
 28. Huang W, Man Y, Gao C, Zhou L, Gu J, Xu H, et al. Short-chain fatty acids ameliorate diabetic nephropathy via GPR43-mediated inhibition of oxidative stress and NF- κ B signaling. *Oxid Med Cell Longevity.* (2020) 2020:4074832. doi: 10.1155/2020/4074832
 29. Serrano HG, Dolores CM, Carlos MJ, Corrales SV, Carlos MJ, Nunez LE, et al. Phospho-kinase profile of colorectal tumors guides in the selection of multi-kinase inhibitors. *Oncotarget.* (2015) 6:31272–83. doi: 10.18632/oncotarget.5211
 30. Araujo JR, Tazi A, Burlen DO, Vichier GS, Nigro G, Licandro H, et al. Fermentation products of commensal bacteria alter enterocyte lipid metabolism. *Cell Host Microbe.* (2020) 27:358. doi: 10.1016/j.chom.2020.01.028
 31. Tan YQ, Chen HW, Li J, Wu QJ. Efficacy, chemical constituents, and pharmacological actions of radix paeoniae rubra and radix paeoniae alba. *Front Pharmacol.* (2020) 11:1054. doi: 10.3389/fphar.2020.01054
 32. Liu H, Wang J, He T, Becker S, Zhang G, Li D, et al. Butyrate: a double-edged sword for health? *Adv Nutr.* (2018) 9:21–29. doi: 10.1093/advances/nmx009
 33. Tolhurst G, Heffron H, Lam YS, Parker HE, Habib AM, Diakogiannaki E, et al. Short-chain fatty acids stimulate glucagon-like peptide-1 secretion via the G-protein-coupled receptor FFAR2. *Diabetes.* (2012) 61:364–71. doi: 10.2337/db11-1019
 34. Lee G, You HJ, Bajaj JS, Joo SK, Yu J, Park S, et al. Distinct signatures of gut microbiome and metabolites associated with significant fibrosis in non-obese NAFLD. *Nat Commun.* (2020) 11:4982. doi: 10.1038/s41467-020-18754-5
 35. Maslowski KM, Vieira AT, Ng A, Kranich J, Sierro F, Yu D, et al. Regulation of inflammatory responses by gut microbiota and chemoattractant receptor GPR43. *Nature.* (2009) 461:1282–U119. doi: 10.1038/nature08530
 36. Koh A, De Vadder F, Kovatcheva-Datchary P, Backhed F. From dietary fiber to host physiology: short-chain fatty acids as key bacterial metabolites. *Cell.* (2016) 165:1332–45. doi: 10.1016/j.cell.2016.05.041
 37. Kumar A, Alrefai WA, Borthakur A, Dudeja PK. *Lactobacillus acidophilus* counteracts enteropathogenic *E. coli*-induced inhibition of butyrate uptake in intestinal epithelial cells. *Am J Physiol Gastrointest Liver Physiol.* (2015) 309:G602–G07. doi: 10.1152/ajpgi.00186.2015
 38. Zhao P, Sun X, Chaggaan C, Liao Z, Wong KI, He F, et al. An AMPK-caspase-6 axis controls liver damage in non-alcoholic steatohepatitis. *Science.* (2020) 367:652. doi: 10.1126/science.aay0542
 39. Jiang S, Li T, Yang Z, Yi W, Di S, Sun Y, et al. AMPK orchestrates an elaborate cascade protecting tissue from fibrosis and aging. *Ageing Res Rev.* (2017) 38:18–27. doi: 10.1016/j.arr.2017.07.001
 40. Yamashita H. Biological function of acetic acid-improvement in obesity and glucose tolerance by acetic acid in type 2 diabetic rats. *Crit Rev Food Sci Nutr.* (2016) 56:S171–S75. doi: 10.1080/10408398.2015.1045966
 41. Liu F, Shang YX. Sirtuin 6 attenuates epithelial-mesenchymal transition by suppressing the TGF- β 1/Smad3 pathway and c-Jun in asthma models. *Int Immunopharmacol.* (2020) 82:106333. doi: 10.1016/j.intimp.2020.106333
 42. Fu C, Liu L, Li F. Acetate alters the process of lipid metabolism in rabbits. *Animal.* (2018) 12:1895–902. doi: 10.1017/S1751731117003275
 43. Zhao C, Chen W, Yang L, Chen L, Stimpson SA, Diehl AM. PPAR γ agonists prevent TGF β 1/Smad3-signaling in human hepatic stellate cells. *Biochem Biophys Res Commun.* (2006) 350:385–91. doi: 10.1016/j.bbrc.2006.09.069
 44. Zhang F, Lu Y, Zheng S. Peroxisome proliferator-activated receptor- γ cross-regulation of signaling events implicated in liver fibrogenesis. *Cell Signalling.* (2012) 24:596–605. doi: 10.1016/j.cellsig.2011.11.008
 45. Choi JH, Jin SW, Choi CY, Kim HG, Lee GH, Kim YA, et al. Capsaicin inhibits dimethylnitrosamine-induced hepatic fibrosis by inhibiting the TGF- β 1/Smad pathway via peroxisome proliferator-activated receptor γ activation. *J Agric Food Chem.* (2017) 65:317–26. doi: 10.1021/acs.jafc.6b04805
 46. Wang CY, Liu Q, Huang QX, Liu JT, He YH, Lu JJ, et al. Activation of PPAR γ is required for hydroxysafflor yellow A of *Carthamus tinctorius* to attenuate hepatic fibrosis induced by oxidative stress. *Phytomedicine.* (2013) 20:592–99. doi: 10.1016/j.phymed.2013.02.001
 47. Lee MF, Liu ML, Cheng AC, Tsai ML, Ho CT, Liou WS, et al. Pterostilbene inhibits dimethylnitrosamine-induced liver fibrosis in rats. *Food Chem.* (2013) 138:802–07. doi: 10.1016/j.foodchem.2012.11.094
 48. Burns KA, Vanden Heuvel JP. Modulation of PPAR activity via phosphorylation. *Biochimica et Biophysica Acta.* (2007) 1771:952–60. doi: 10.1016/j.bbali.2007.04.018
 49. Liu E, Wang X, Li X, Tian P, Xu H, Li Z, et al. Co-exposure to multi-walled carbon nanotube and lead ions aggravates hepatotoxicity of non-alcoholic fatty liver by inhibiting AMPK/PPAR γ pathway. *Ageing Us.* (2020) 12:14189–204. doi: 10.18632/aging.103430
 50. Na L, Chu X, Jiang S, Li C, Li G, He Y, et al. Vinegar decreases blood pressure by down-regulating AT1R expression via the AMPK/PGC-1 α /PPAR γ pathway in spontaneously hypertensive rats. *Eur J Nutr.* (2016) 55:1245–53. doi: 10.1007/s00394-015-0937-7

Conflict of Interest: XZ was employed by Inner Mongolia Dairy Technology Research Institute Co., Ltd.

The remaining authors declare that the research was conducted in the absence of any commercial or financial relationships that could be construed as a potential conflict of interest.

Publisher's Note: All claims expressed in this article are solely those of the authors and do not necessarily represent those of their affiliated organizations, or those of the publisher, the editors and the reviewers. Any product that may be evaluated in this article, or claim that may be made by its manufacturer, is not guaranteed or endorsed by the publisher.

Copyright © 2021 Li, Deng, Gong, Zhang, Ge and Zhao. This is an open-access article distributed under the terms of the Creative Commons Attribution License (CC BY). The use, distribution or reproduction in other forums is permitted, provided the original author(s) and the copyright owner(s) are credited and that the original publication in this journal is cited, in accordance with accepted academic practice. No use, distribution or reproduction is permitted which does not comply with these terms.



Short-Chain Fatty Acids Alleviate Hepatocyte Apoptosis Induced by Gut-Derived Protein-Bound Uremic Toxins

Mingjuan Deng¹, Xingqi Li¹, Weiwei Li¹, Jiahui Gong¹, Xiaoying Zhang², Shaoyang Ge³ and Liang Zhao^{1,4*}

¹ Key Laboratory of Functional Dairy, College of Food Science and Nutritional Engineering, China Agricultural University, Beijing, China, ² Inner Mongolia Dairy Technology Research Institute Co., Ltd., Hohhot, China, ³ Hebei Engineering Research Center of Animal Product, Sanhe, China, ⁴ Department of Nutrition and Health, Beijing Advanced Innovation Center for Food Nutrition and Human Health, China Agricultural University, Beijing, China

OPEN ACCESS

Edited by:

Huaxi Yi,
Ocean University of China, China

Reviewed by:

Xue Han,
Harbin Institute of Technology, China
Weitao Geng,
Tianjin University of Science and
Technology, China

*Correspondence:

Liang Zhao
lzhao@cau.edu.cn

Specialty section:

This article was submitted to
Nutritional Immunology,
a section of the journal
Frontiers in Nutrition

Received: 11 August 2021

Accepted: 07 September 2021

Published: 12 October 2021

Citation:

Deng M, Li X, Li W, Gong J, Zhang X,
Ge S and Zhao L (2021) Short-Chain
Fatty Acids Alleviate Hepatocyte
Apoptosis Induced by Gut-Derived
Protein-Bound Uremic Toxins.
Front. Nutr. 8:756730.
doi: 10.3389/fnut.2021.756730

Chronic kidney disease (CKD) is characterized with the influx of uremic toxins, which impairs the gut microbiome by decreasing beneficial bacteria that produce short-chain fatty acids (SCFAs) and increasing harmful bacteria that produce gut-derived protein-bound uremic toxins (PBUTs). This study aimed to assess the proapoptotic effects of three major gut-derived PBUTs in hepatocytes, and the effects of SCFAs on apoptosis phenotype *in vitro*. HepG2 (human liver carcinoma cells) and THLE-2 (immortalized human normal liver cells) cell line were incubated with 0, 2, 20, 200, 2000 μ M p-cresol sulfate (PCS), indoxyl sulfate (IS), and hippuric acid (HA), respectively, for 24 h. Flow cytometry analysis indicated that three uremic toxins induced varying degrees of apoptosis in hepatocytes and HA represented the highest efficacy. These phenotypes were further confirmed by western blot of apoptosis protein expression [Caspase-3, Caspase-9, B-cell lymphoma 2 (Bcl-2), and Bcl-2-associated X protein (Bax)]. Human normal hepatocytes (THLE-2) are more sensitive to PBUTs-induced apoptosis compared with human hepatoma cells (HepG2). Mechanistically, extracellular HA could enter hepatocytes, increase reactive oxygen species (ROS) generation, and decrease mitochondrial membrane potential dose-dependently in THLE-2 cells. Notably, coculture with SCFAs (acetate, propionate, butyrate) for 24 h significantly improved HA-induced apoptosis in THLE-2 cells, and propionate (500 μ M) represented the highest efficacy. Propionate reduction of apoptosis was associated with improving mitochondria dysfunction and oxidative stress in a manner involving reducing Caspase-3 expression, ROS production, and increasing the Bcl-2/Bax level. As such, our studies validated PBUTs accumulation might be an important cause of liver dysfunction in patients with CKD, and supplementation of SCFAs might be a viable way to protect the liver for patients with CKD.

Keywords: uremic toxins, hepatocytes, apoptosis, hippuric acid, short chain fatty acid

INTRODUCTION

Chronic kidney disease (CKD) has become a serious health issue affecting 10–15% of the global population (1). The pathogenesis of CKD is characterized by kidney filtration dysfunction, leading to blood retention of uremic toxins (2). More than 130 uremic toxins have now been identified and categorized as small water-soluble molecules, middle-sized molecules, and protein-bound uremic toxins (PBUTs) (2, 3). Several of the most harmful PBUTs, including indoxyl sulfate (IS), p-cresol sulfate (PCS), and hippuric acid (HA), are produced by gut bacteria and are hard to be removed by current conventional dialysis (2, 4). Intestinal flora metabolizes tryptophan and tyrosine, leading to the production of indole and p-cresol, which are subsequently metabolized as PBUTs by hepatic cytosolic enzymes and finally secreted to the blood circulation (5–7). The accumulation of PBUTs could exert harmful biological activity on other tissues or organs, mainly on the kidney and the cardiovascular system (8, 9). Notably, patients with primary renal disease often have coexisting liver disease, which presents diagnostic and treatment challenges (10). Zhu et al. found that PCS induced oxidative stress, glutathione depletion, and cellular necrosis in human hepatocytes (11). IS and PCS could affect hepatic bile acid transport and mitochondrial functions (6, 8). In this respect, Weigand et al. revealed that HA mediated liver injury primarily *via* mitochondrial toxicity (12). These studies evidenced that PBUTs also induced liver injury, although the mechanism is still unclear. Apoptosis is critically involved in PBUTs-induced harmful biological activities. PCS induced adipocyte and cardiomyocyte apoptosis *via* mitochondria-related pathways (13, 14). Lin et al. found IS caused apoptosis *via* oxidative stress and mitogen-activated protein kinase (MAPK) signaling inhibition in human astrocytes (15). IS also triggered apoptosis in the myoblast resulting in uremic sarcopenia (16). However, scarce research has been conducted to explore the proapoptotic effects of PBUTs on the liver, an extremely important organ to the metabolism, which attracted our scientific interest.

Biochemical disorders in CKD have been confirmed to some degree as a consequence of insufficient short-chain fatty acids (SCFAs) production due to gut dysbiosis (17). SCFAs are the main intestinal bacterial metabolites of dietary fiber (18). The most abundant SCFAs in the human gut are acetate, propionate, and butyrate, which constitute over 95% of the total SCFAs content (18, 19). Previous evidence showed that SCFAs regulated metabolic processes as substrates and signaling molecules by entering the systematic circulation (20). Additionally, Hu et al. found that acetate and butyrate improved β -cell apoptosis-involved mitochondrial-dependent pathways (21). Furthermore, propionate was established to inhibit the apoptosis of human islet and hippocampus cells *via* mitochondrial dysfunction attenuation (22–24). Dietary supplementation with sodium butyrate alleviated dairy goat hepatocyte apoptosis (25). These findings implied the potential of SCFAs apoptosis pathway regulation. However, insufficient investigations have been performed so far to assess the effects of SCFAs on human hepatocyte apoptosis.

In this study, we explored the proapoptotic effect of three important gut-derived uremic toxins (HA, IS, and PCS) and their potential mechanisms of action on human hepatoma and hepatocyte cells. Furthermore, we also evaluated the impact of three major SCFAs (acetate, propionate, and butyrate) on hepatocyte apoptosis-related phenotypes.

MATERIALS AND METHODS

Cell Culture

HepG2 cells, a human hepatoma cell line, were purchased from the Stem Cell Bank, Chinese Academy of Sciences (Shanghai, China), and cultured in Dulbecco's Modified Eagles Medium (DMEM, Gibco, USA) containing 10% fetal bovine serum (Gibco, USA) and 100 U/ml penicillin and streptomycin (Beyotime, China) in a 5% CO₂ incubator at 37°C. THLE-2 cells, a human hepatocyte cell line, were purchased from the Stem Cell Bank, Chinese Academy of Sciences (Shanghai, China), and cultured in RPMI 1640 medium (Gibco, USA) containing 10% fetal bovine serum (Gibco, USA) and 100 U/ml penicillin and streptomycin (Beyotime, China) in a 5% CO₂ incubator at 37°C.

Cell Cytotoxicity Assays

An enhanced Cell Counting Kit-8 assay (Beyotime, China) was used to determine cell viability. HepG2 and THLE-2 cells were seeded at a density of 5×10^3 per well onto flat-bottom 96-well culture plates (Corning, USA) and treated for 24 h with 0–5 mM PCS, IS, HA, potassium chloride (KCL) (Sigma, USA), or uremic toxin mixtures, respectively. The doses applied were set based on clinical uremic concentration data in patients with CKD. The following mean concentrations were used: 1,000 μ M HA, 200 μ M IS, and 100 μ M PCS. The highest concentrations utilized were as follows: 2,000 μ M HA, 1,000 μ M IS, and 200 μ M PCS (26, 27). KCL was used as a control treatment to exclude osmotic pressure interference since IS and PCS exist in the form of potassium salt in the circulation (4). Uremic toxins mixtures were admixed with the mean (Mixtoxins-L) and highest dose (Mixtoxins-H) of the three uremic toxins, respectively. The absorbance values of viable cells were finally determined at 450 nm using a microplate spectrophotometer (BioTek Winooski, VT, USA). The cell inhibitory rates were measured according to the product protocol.

Hepatocyte Apoptosis Assessment

Annexin V-Fluorescein isothiocyanate/propidium iodide (FITC/PI) detection kit (Beyotime, China) was used for apoptosis assessment. To explore the proapoptotic effects of gut-derived PBUTs on hepatocytes, HepG2 and THLE-2 cells were seeded into six-well plates at a density of 1×10^6 cells. The cells were treated for 24 h with 2, 20, 200, and 2,000 μ M IS, PCS, and HA, correspondingly. To explore the effects of SCFAs on HA-induced apoptosis in hepatocytes, THLE-2 cells grown in a six-well plate were treated with 2,000 μ M HA in the presence/absence of SCFAs (500 or 5,000 μ M sodium acetate, 50 or 500 μ M sodium propionate, and 50 or 500 μ M sodium butyrate) (28) when the confluency reached 70–80%. After the treatment, the cells were washed with PBS, trypsinized,

and resuspended in $1 \times$ binding buffer. Then, the cells were stained with 5 μ l of annexin V-FITC and 10 μ l of PI in the dark for 20 min at room temperature. The samples were analyzed by flow cytometry (Beckman Coulter Inc., Brea, CA, USA) after staining. Annexin V-/PI- indicated viable cells, Annexin V+/PI- early-stage apoptotic cells, Annexin V+/PI+ end-stage apoptotic cells, and Annexin V-/PI+ cell debris.

Mitochondrial Membrane Potential Measurement

A mitochondrial membrane potential (MMP) assay kit with 5,5',6,6'-tetrachloro-1,1',3,3'-tetraethylbenzimidazolylcarbocyanine iodide (JC-1) (Beyotime, China) was used according to the product instruction. THLE-2 cells were seeded into a six-well plate and treated with various concentrations of HA for 24 h. The cells were next washed with PBS and incubated in JC-1 working solution for 20 min at 37°C in the dark. After the incubation, we discarded the supernatant and washed the cells with JC-1 dying buffer. A volume of 2 ml of complete DMEM medium further was added in each well of the six-well plate. JC-1 monomer (green fluorescence distribution with an excitation wavelength of 490 nm and emission wavelength of 530 nm) and j-aggregates (red fluorescence distribution with an excitation wavelength of 525 nm and emission wavelength of 590 nm) were measured by a fluorescent microscope (Olympus, Tokyo, Japan). Mitochondrial depolarization was indicated by the decrease in the red/green fluorescence intensity ratio.

Intracellular Reactive Oxygen Species Production Measurement

A reactive oxygen species (ROS) assay kit (Beyotime, China) was used for intracellular ROS detection following the product guidelines. THLE-2 cells were seeded into a six-well plate and treated for 24 h with various concentrations of HA, PCS, and IS in the presence/absence of 500 μ M sodium propionate. Cells were incubated with 2', 7'-dichlorofluorescein diacetate (DCFH-DA) dissolved in serum-free DMEM (1:1,000) in the dark for 20 min. Fluorescence intensity was measured by flow cytometry and/or fluorescent microscope (Olympus, Japan) quantified by Image J software.

Intracellular and Extracellular HA Determination

Ultra-high-performance liquid chromatography (HPLC, Waters, USA) coupled with a TripleTOF[®] 5600 plus (Applied Biosystems, Foster City, CA, USA) mass spectrometer was used to measure the intracellular and extracellular HA content in THLE-2 cells as previously described (29) with a modification in the sample preparation, which is detailed below. Cells were seeded into six-well plates at a density of 1×10^6 cells. The cells were then treated with various doses of HA for 24 h or 15 min after confluency had reached 80%. After the treatment, the medium was collected and centrifuged at 350 g for 5 min. The pellet was discarded, and the supernatant was collected for extracellular HA measurement. The cells in the plates after the treatment were washed with PBS two times, scraped, and

homogenized, and then centrifuged for 10 min at 4,000 g and 4°C. Finally, the supernatant was collected for intracellular HA determination.

Western Blot Analysis

HepG2 and THLE-2 cells were cultured in a six-well plate and treated as described above. Cultured cells were prepared for Western blot analysis as reported previously (28). The membranes were incubated with primary antibodies: glyceraldehyde-3-phosphate dehydrogenase (GAPDH), B-cell lymphoma 2 (Bcl-2), Bcl-2-associated X protein (Bax), cleaved caspase-3, and cleaved caspase-9 (CST, USA). After the incubation with a goat anti-rabbit horseradish peroxidase-conjugated secondary antibody (Beyotime, China) at a dilution of 1:10,000 for 1 h, the proteins were visualized using a Luminata Forte Enhanced Chemiluminescence Kit (Millipore, Bedford, MA, USA), and the band intensities were analyzed using the QuantityOne analysis software (Bio-Rad, Hercules, CA, USA).

Statistical Analysis

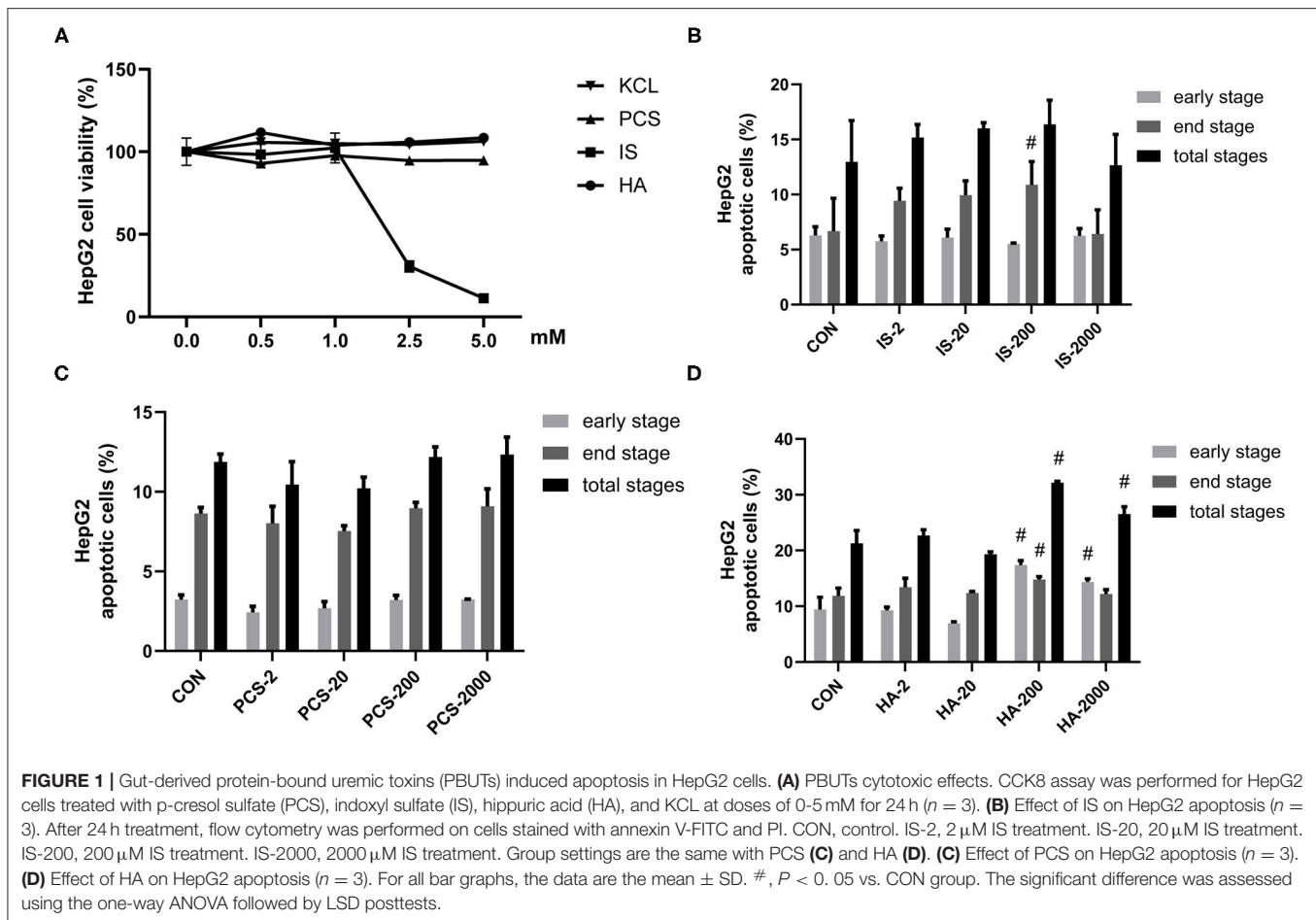
Numeric data were expressed as mean \pm SD. Statistical significance was determined using the one-way ANOVA followed by least significant difference (LSD) posttests with statistical package for the social sciences (SPSS) 25.0. Differences were considered statistically significant at a two-tailed p -value < 0.05 .

RESULTS

Gut-Derived PBUTs Induced Apoptosis in HepG2 Cells

Uremic syndrome coupled with kidney dysfunction is characterized by retention of uremic toxins, and several of the most harmful uremic toxins are produced by gut bacteria, including HA, IS, and PCS (5). These toxins are protein-bound and are, therefore, hard to remove, which leads to their abnormal blood circulating concentrations, exert harmful biological activity on other organs (27). Although PCS was found to induce oxidative stress, glutathione depletion, and cellular necrosis in a human liver cell line, more evidence is needed to clarify the effects of gut-derived PBUTs on hepatocytes (11). In this study, we determined the effects of 0–5 mM HA, IS, PCS, and KCL on HepG2 cell viability (**Figure 1A**). Cell viability was not significantly reduced by the incubation with 0–5 mM PCS or HA for 24 h. The KCL treatment failed to influence HepG2 cell viability, which excluded the potential interference of the potassium salt form of IS and PCS on the osmotic pressure. The treatment with 0–1 mM IS for 24 h did not alter HepG2 cell viability, whereas doses beyond 1 mM caused a significant reduction in cell viability (**Figure 1A**).

Next, we sought to examine the proapoptotic effects of three PBUTs in HepG2 cells. Notably, the treatment with 200 μ M IS for 24 h markedly elevated the end-stage apoptosis with no significant alterations achieved in the other treatments (**Figure 1B**; **Supplementary Figure S1A**). As for PCS, various doses incubation for 24 h failed to induce apoptosis in HepG2 cells (**Figure 1C**; **Supplementary Figure S1B**). Notably, we found that the HA treatment with 200 and 2,000 μ M in of



the HepG2 cells led to a significantly higher total apoptosis cell percentage than that of the control group, by 10.86% and 5.26% (Figure 1D; Supplementary Figure S1C).

Gut-Derived PBUTs Induced Apoptosis in the THLE-2 Cells

We also examined the metabolic effects of IS, PCS, and HA on the human hepatocyte cell line THLE-2. The treatment and concentrations were set as detailed in section Materials and Methods. Similarly, to the results we obtained in the HepG2 cells, the THLE-2 cell viability was not significantly reduced by incubation with 0–5 mM PCS, HA and 0–1 mM IS for 24 h, whereas IS beyond 1 mM markedly decreased THLE-2 cell viability (Figure 2A). PBUTs are always present together in the system circulation of patients with CKD (30), which raised our research interest in the effects of PBUTs mixture on hepatocytes. We found that neither the low (HA: 1,000 μ M, IS: 200 μ M, PCS: 100 μ M), nor the high doses (HA: 2,000 μ M, IS: 1,000 μ M, PCS: 200 μ M) of PBUTs mixture altered the THLE-2 cell viability as compared with that of the control group (Figure 2B).

The treatments with 2, 20, and 200 μ M IS for 24 h failed to induce apoptosis in THLE-2 cells, whereas the treatment with 2,000 μ M IS induced 0.36-, 1.02-, and 0.55-fold increases in the early, late, and total apoptosis percentages as compared

with the control group (Figure 2C; Supplementary Figure S2A). The incubation of 2,000 μ M PCS with THLE-2 cells for 24 h induced significantly higher apoptosis, 0.96, 1.57, and 1.13-fold in the early, late, and total apoptosis, as compared with the control group (Figure 2D; Supplementary Figure S2B). The treatments with 200 and 2,000 μ M HA induced significantly higher THLE-2 cell apoptosis in a dose-dependent manner. The incubation with 2,000 μ M HA for 24 h resulted in increased early, late, and total apoptosis levels to 33.89, 12.17, and 46.07%, correspondingly, which was 1.92-, 0.69-, and 1.45-fold higher than the respective values in the control group (Figure 2E; Supplementary Figure S2C). The high doses of the three PBUT mixtures significantly increased the apoptosis level in the THLE-2 cells. The total apoptosis percentage was 17.69% higher followed by that of the late apoptosis (13.23%) and the early apoptosis (4.45%), as compared with the control group respective values (Figure 2F; Supplementary Figure S2D).

Effects of PBUTs on the Apoptotic Protein Expression in Hepatocytes

We sought to examine the effects of the three PBUTs studied on the apoptosis signaling in hepatocytes by Western blot analysis, and determination of the levels of crucial apoptotic proteins, including cleaved caspase-3, cleaved caspase-9, Bcl-2,

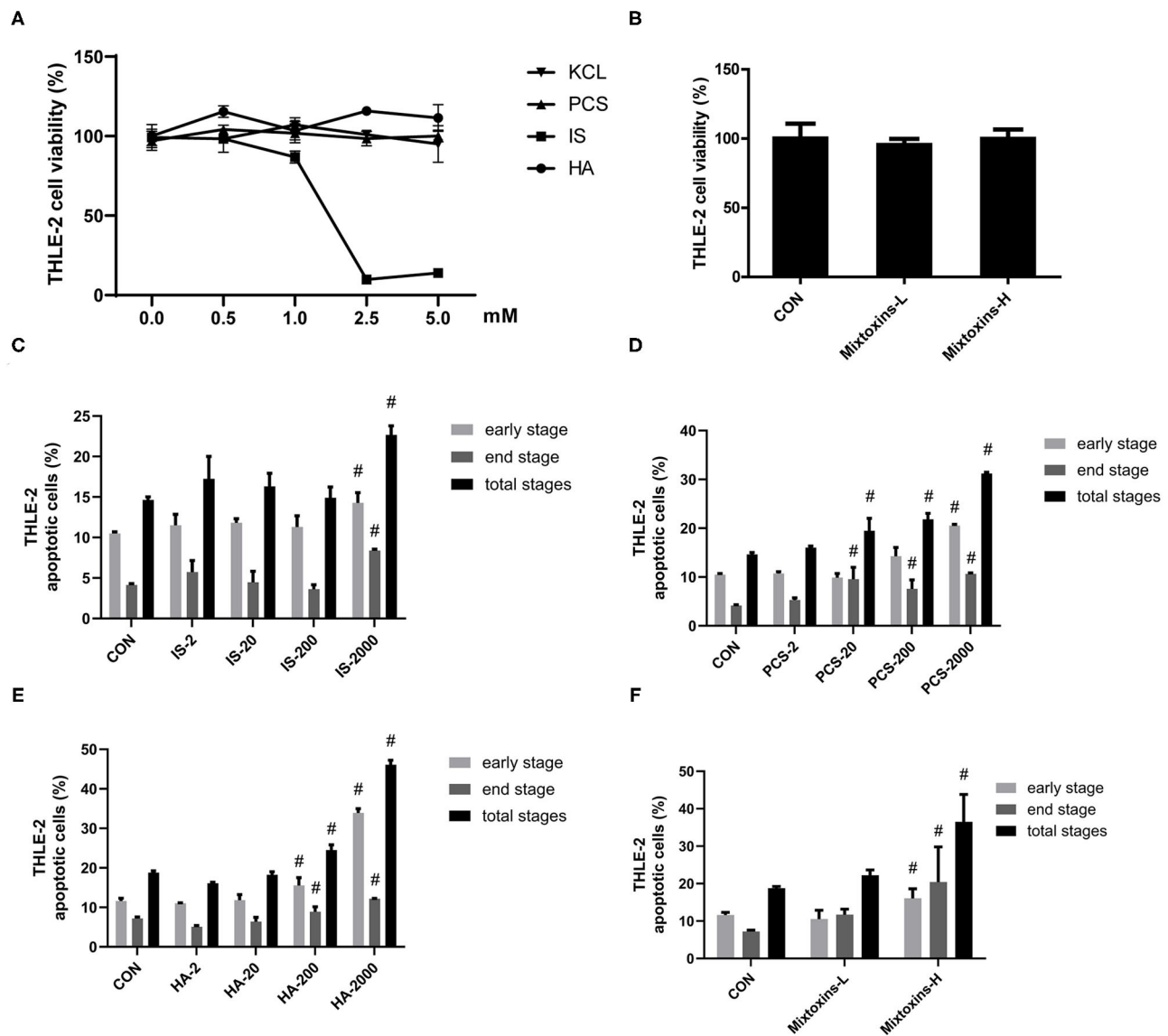


FIGURE 2 | Gut-derived PBUTs induced apoptosis in THLE-2 cells. **(A)** PBUTs cytotoxic effects. CCK8 assay was performed for THLE-2 cells treated with PCS, IS, HA, and KCL at doses of 0–5 mM for 24 h ($n = 3$). **(B)** Effects of three PBUTs mixture on THLE-2 cell viability ($n = 5$). **(C)** Effect of IS on THLE-2 apoptosis ($n = 2-3$). After 24 h treatment, flow cytometry was performed on cells stained with annexin V-FITC and PI. CON, control. IS-2, 2 μ M IS treatment. IS-20, 20 μ M IS treatment. IS-200, 200 μ M IS treatment. IS-2000, 2000 μ M IS treatment. Group settings are the same with PCS **(D)** and HA **(E)**. **(D)** Effect of PCS on THLE-2 apoptosis ($n = 2-3$). **(E)** Effect of HA on THLE-2 apoptosis ($n = 3$). **(F)** Effects of three gut-derived PBUTs mixture on THLE-2 apoptosis ($n = 3$). For all bar graphs, the data are the mean \pm SD. #, $P < 0.05$ vs. CON group. The significant difference was assessed using the one-way ANOVA followed by LSD posttests.

and Bax. The treatment of cultured HepG2 cells with 2, 200 μ M IS for 24 h did not cause significant changes in the apoptotic protein expression (**Figure 3A**). In the THLE-2 cells, various doses of IS significantly decreased the Bcl-2/Bax expression level, which functions as an important apoptosis regulator (31) (**Figure 3B**). The treatments with 2 and 200 μ M PCS did not alter significantly the apoptotic protein expression in HepG2 cells (**Figure 3C**). However, the treatment with 200 μ M PCS increased the cleaved caspase-3 expression, but 2,000 μ M PCS

significantly decreased the Bcl-2/Bax expression level in the THLE-2 cells (**Figure 3D**). The treatment with 200 μ M HA significantly elevated the cleaved caspase-9 expression in the HepG2 cells (**Figure 3E**); the incubation with both 2 and 200 μ M HA for 24 h significantly decreased the Bcl-2/Bax expression level in the THLE-2 cells (**Figure 3F**). These results, together with the findings displayed in **Figures 1, 2**, strongly indicate that the three PBUTs induced partial apoptosis in the hepatocytes.

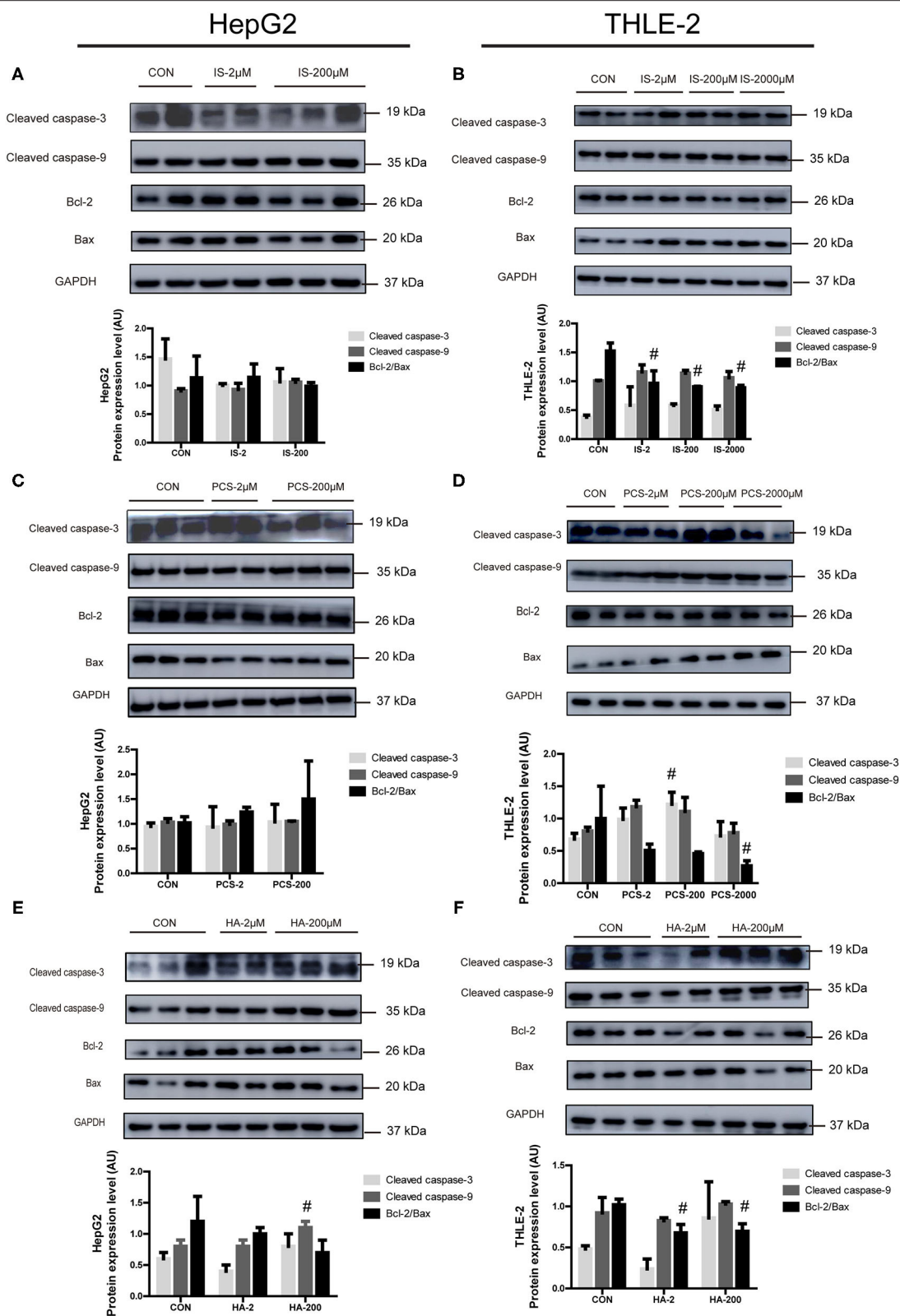


FIGURE 3 | Effects of PBUTs on the apoptotic apoptosis protein expression in hepatocytes. HepG2 and THLE-2 cells were treated as detailed in section “Materials and Methods.” (A,B) Effects of IS on apoptosis protein expression. (C,D) Effects of PCS on apoptosis protein expression. (E,F) Effects of HA on apoptosis protein expression. HepG2 and THLE-2 cells were examined for apoptosis protein using Western blot. Bar graphs display quantification of blots. For all bar graphs, the data are the mean \pm SD ($n = 2-3$). #, $P < 0.05$ vs. CON group. The significant difference was assessed using the one-way ANOVA followed by LSD posttests.

PBUTs Induced ROS Generation and Mitochondrial Damage in the Hepatocytes

Reactive oxygen species have been tightly linked to the activation of the mitochondria-related apoptosis pathway (32). We measured the effects of gradient doses of PBUTs on the ROS production in THLE-2 cells. The IS or HA treatments with 200 and 2,000 μM for 24 h induced significantly higher ROS generation in the THLE-2 cells, whereas the PCS treatment exerted no significant alteration (Figures 4A–C). We chose HA for further investigation since HA had the highest proapoptotic efficacy among the three PBUTs based on our aforementioned results. Previously, HA had been proven to induce mitochondrial dysfunction in human endothelial cells (33), but the underlying mechanism is yet unknown. We aimed to elucidate whether HA could enter into the cells and act directly on their biological activity. Our results showed that 24 h of incubation with 200 or 2,000 μM HA dose-dependently increased the intracellular HA concentration in the THLE-2 cells (Figure 4D). Notably, we established that the incubation with 2,000 μM HA for 24 h or 15 min caused no significant difference in the intracellular HA concentration, which indicated that extracellular HA entered the hepatocytes and reached a dynamic balance within 15 min (Figure 4D). The incubation with 200 or 2,000 μM HA for 24 h considerably increased the ROS production in a dose-dependent manner (Supplementary Figure S3). MMP decline is an important marker during cell apoptosis (34), and thus we also measured the alteration in MMP level induced in THLE-2 cells by the HA treatment. The diverse doses of HA induced obvious dose-dependent increases in the green fluorescence intensity and decreases in the red fluorescence as compared with the control (Figure 4E), which indicated that HA reduced the MMP level. These results revealed that HA might induce apoptosis involving ROS generation increase and mitochondrial damage.

Propionate Alleviated HA-Induced Apoptosis in THLE-2 Cells

Short-chain fatty acids are the main microbial metabolites of dietary fibers in the gut that participate in metabolic processes as substrates or signaling molecules (19, 28). Recent studies showed that SCFAs improved β -cell apoptosis involved mitochondrial-related ROS suppression (21). In this study, we explored the effects of three major SCFAs (acetate, propionate, and butyrate) on HA-induced apoptosis in a human liver cell line (THLE-2). Surprisingly, we found that the coculture with various doses of acetate, propionate, and butyrate, respectively, for 24 h improved the apoptosis induced by the treatment with 2,000 μM HA (Figure 5A). Of the three SCFAs investigated, sodium propionate had the highest efficacy. The treatment with 500 μM (NaP-H) and 50 μM (NaP-L) propionate markedly reduced the apoptosis, which was 1.48-fold and 1.00-fold lower than that in the HA-2000 group. Then, we examined the effects of propionate on the apoptotic protein expression in the THLE-2 cells. Notably, 500 μM propionate cocultured with THLE-2 cell for 24 h reversed the increase in the cleaved caspase-3 and the decrease in the Bcl-2/Bax expression levels induced by the HA treatment (Figure 5B). Besides, the treatment with 500 μM

propionate significantly reduced the ROS production induced by HA as well (Figure 5C). These results revealed that propionate improved the HA-induced hepatocyte apoptosis by decreasing ROS generation and caspase-3 protein expression, but increasing the Bcl-2/Bax protein expression level.

DISCUSSIONS

The accumulation of uremic toxins is the most prominent feature of CKD and end-stage renal disease. Uremic toxins are conventionally classified based on the physicochemical characteristics affecting their clearance during dialysis, of which PBUT is an important category. Several PBUTs originate from the gut and are metabolized in the liver (6), which have been confirmed to impair insulin resistance, kidney fibrosis, granulocyte function, and cardiovascular health (9, 35). Several recent studies evidenced that PBUTs induced oxidative stress, glutathione depletion, cellular necrosis, and bile acid transport disorders in the liver (6, 8, 11, 12). However, more evidence is needed to clarify the impact of PBUTs on the liver. The present study provides the primary data concerning the direct effects of three gut-derived PBUTs (HA, PCS, and IS) on human hepatocytes (THLE-2) and hepatoma cells (HepG2), focusing on the involvement of apoptotic pathways in which mitochondria are tightly involved.

Gut-derived PBUTs are bioactive microbiota metabolites originating exclusively from protein fermentation realized by the gut flora; they enter the blood circulation, where they are sulfated in the liver (36). Current clinical data indicated that the plasma level of PBUTs is rather low in the healthy population (HA: 16 μM , IS: 2 μM , PCS: 10 μM), but their average concentrations increase sharply in patients with CKD (HA: 398 μM , IS: 108 μM , PCS: 111 μM), as well as their highest concentrations (HA: 2,631 μM , IS: 940 μM , PCS: 219 μM) (27, 37). Existing evidence indicated that PBUTs induced cellular apoptosis in the kidneys, brain, muscles, bones, and the heart (14–16, 38, 39), whereas no such evidence for the liver. In the present study, IS and PCS exerted limited proapoptotic effects on HepG2 cells, whereas 2,000 μM IS and PCS induced marked apoptosis in the THLE-2 cells. HA (200 and 2,000 μM) induced apoptosis in both THLE-2 and HepG2 with the highest efficacy among the three PBUTs. The different apoptotic effects of the three PBUTs might be partly due to their involvement in diverse metabolic pathways in the liver. PCS and IS are sulfated in the hepatic Golgi apparatus and the endoplasmic reticulum (2, 40). HA is synthesized by the combination of benzyl-CoA and glycine in the mitochondrial matrix, which is more likely to induce apoptosis by damaging the mitochondria in toxic concentrations (26, 41). However, further investigation is needed to confirm this hypothesis. Our results also indicated that the THLE-2 cells were more sensitive to PBUTs-induced apoptosis than the HepG2 cells; all three PBUTs induced apoptosis in the THLE-2 cells, whereas only the high dose of HA exerted this effect in the HepG2 cells. This might be explained by the programmed cell death escape of the cancer cells by disordering apoptosis pathways (42, 43). The apoptotic effects of the three PBUTs mixtures on THLE-2 cells were also measured

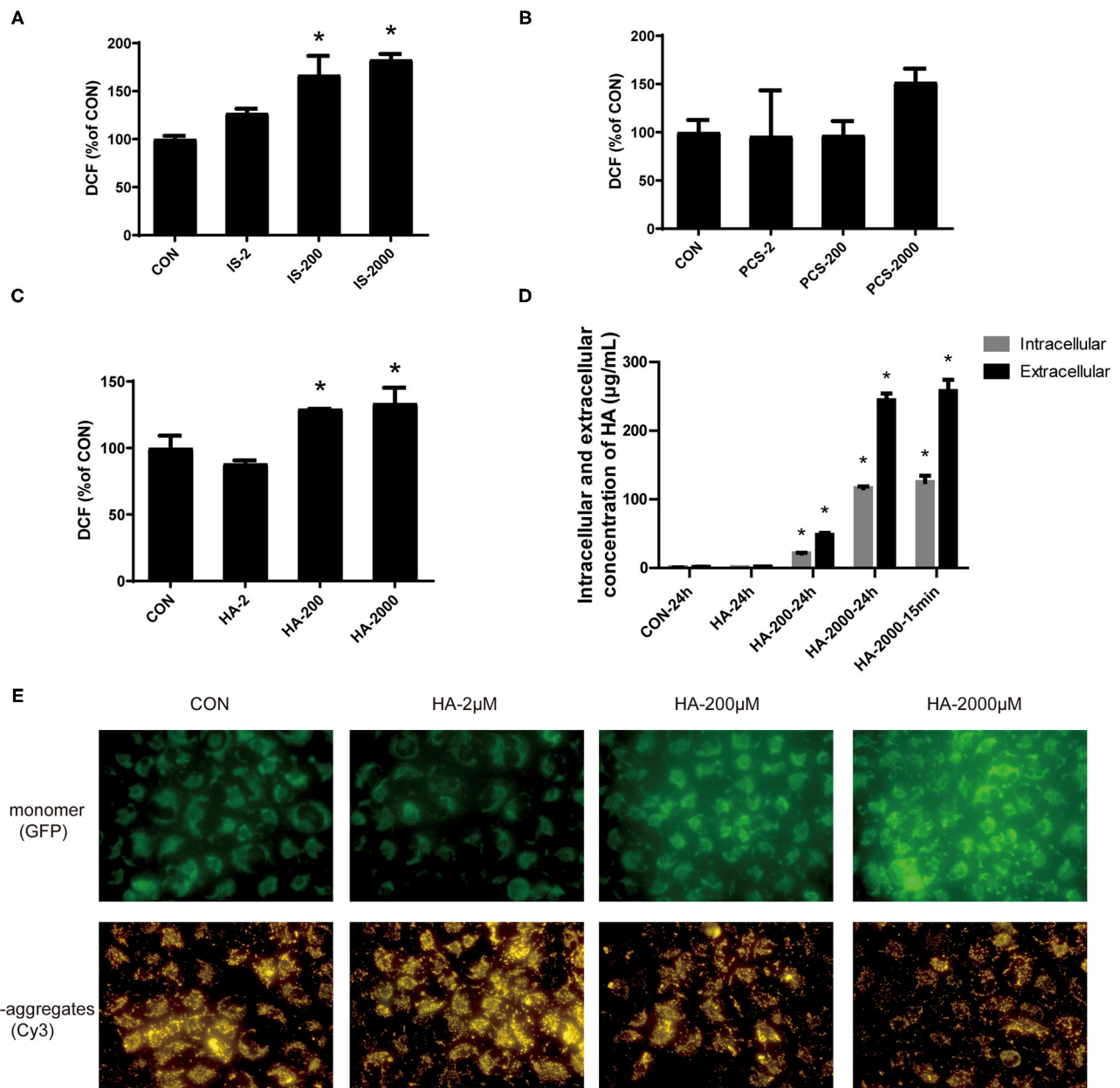


FIGURE 4 | PBUTs induced reactive oxygen species (ROS) generation and mitochondria mitochondrial damage in the hepatocytes. **(A)** Effects of IS on ROS production in THLE-2 cells. **(B)** Effects of PCS on ROS production in THLE-2 cells. **(C)** Effects of HA on ROS production in THLE-2 cells. After treatment, cells were stained with DCFH-DA and measured by flow cytometry ($n = 3$). **(D)** Intracellular and extracellular HA concentration in THLE-2 cells cultured with different doses of HA after 24 h or 15 min ($n = 3$). **(E)** Effects of HA on mitochondrial membrane potential (MMP) in THLE-2 cells. After 24 h HA treatment, cells were stained with JC-1 solution to measure MMP level. For all bar graphs, data are the mean \pm SD. *, $P < 0.05$ vs. CON group. The significant difference was assessed using the one-way ANOVA followed by LSD posttests.

by the dose simulation of the average and highest plasma level in patients with CKD, whereas markedly induced apoptosis was observed only in the high-dose groups (HA: 2,000 μ M, IS: 1,000 μ M, and PCS: 200 μ M). This finding provides further evidence for the positive feedback between PBUTs accumulation and liver injury in patients with CKD (44, 45).

Moreover, PBUTs treatment markedly increased ROS production, caspase-3 protein expression, but decreased the

Bcl-2/Bax protein level in the THLE-2 cells. These proteins are considered to be mitochondria-mediated apoptosis regulators (46). Oxidative stress plays a crucial role in the potential apoptotic mechanism of PBUTs action. Supporting evidence exist that 500 μ M PCS induced cardiac apoptosis partly *via* triggering NADPH oxidase activity and ROS production (14). Additionally, 10 μ M IS induced apoptosis in human astrocytes through oxidative stress induction and MAPK pathway inhibition (15).

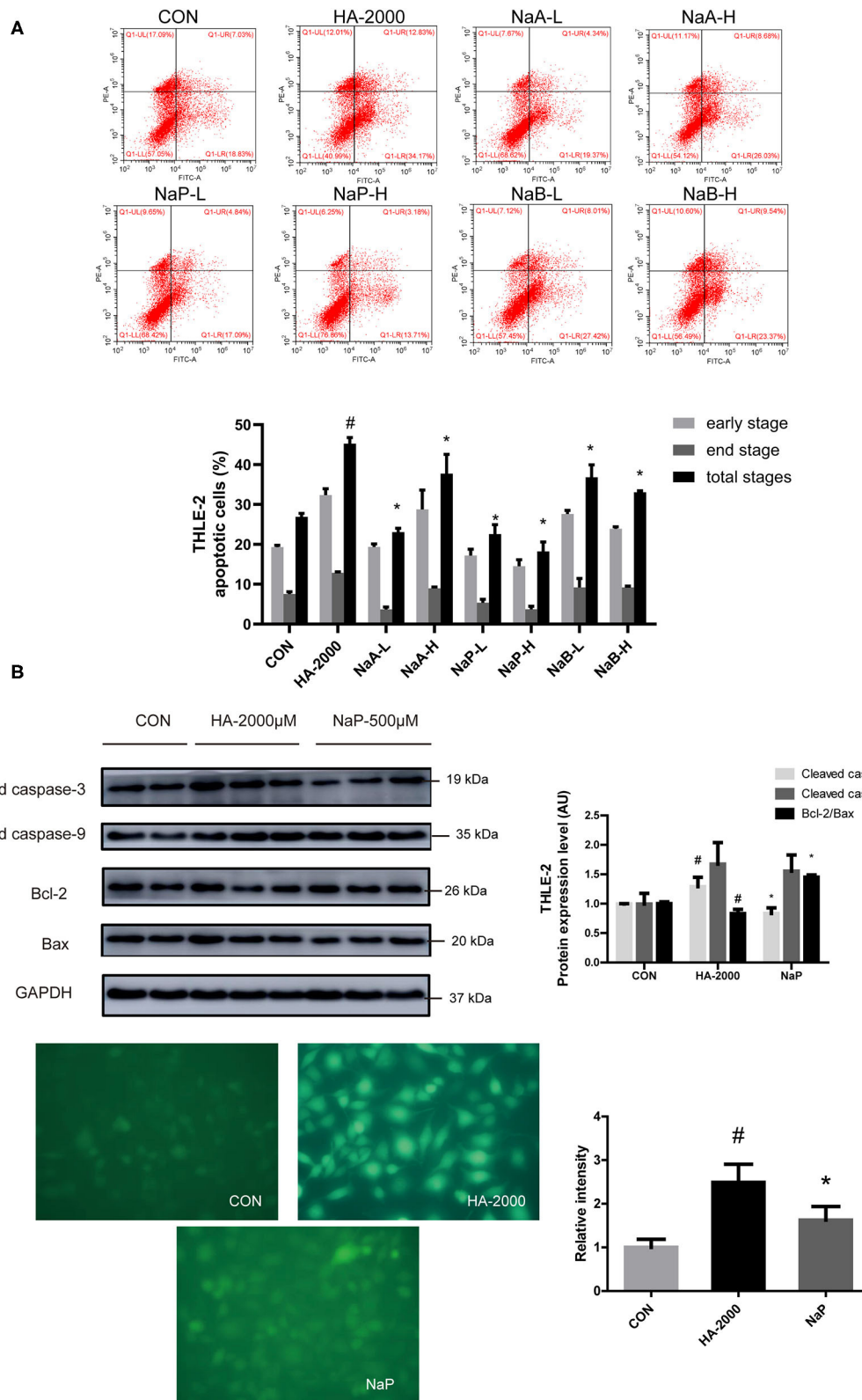


FIGURE 5 | SCFA improved PBUT-induced apoptosis in THLE-2 cells. **(A)** Effects of SCFAs on HA-induced apoptosis in THLE-2 cells ($n = 3$). CON, control group. HA-2000, 2000 μM . NaA-L, 500 μM sodium acetate. NaA-H, 5000 μM sodium acetate. NaP-L, 50 μM sodium propionate. NaP-H, 500 μM sodium propionate. NaB-L, 50 μM sodium butyrate. NaB-H, 500 μM sodium butyrate. **(B)** Propionate improved HA-induced apoptosis protein expression in THLE-2 cells ($n = 2-3$). **(C)** Propionate improved HA-induced ROS production in THLE-2 cells ($n = 3$). For all bar graphs, the data are the mean \pm SD. #, $P < 0.05$ vs. CON group. *, $P < 0.05$ vs. HA-2000 group. The significant difference was assessed using the one-way ANOVA followed by LSD posttests.

Moreover, 40 mM HA triggered apoptosis mediated partly by p53 and endoplasmic reticulum stress in pig renal tubular cells (47). Notably, we found that extracellular HA entered hepatocytes reaching dynamic balance within 15 min, increasing the ROS production and reducing the MMP level, which provided the potential for HA to directly damage the mitochondria by entering the hepatocytes (12). HA is not eliminated by the liver, and avid influx and efflux occur across the basolateral membrane, mediated by the hepatic monocarboxylate transporter 2 (48, 49). Mitochondria could be the target of uremic toxins, and thus consequent mitochondrial damage might directly affect the production of uremic toxins; hence, a positive feedback circle emerges leading to the accumulation of uremic solutes, exerting harmful influence on the liver (3). Our present findings indicate that a toxic concentration of HA may enter the hepatocytes, causing mitochondrial damage and ROS production, and thus inducing hepatocyte apoptosis.

Short-chain fatty acids, predominantly acetate, propionate, and butyrate, are the main microbial metabolites of dietary fibers in the gut. Our previous studies confirmed that SCFAs improved hepatic dysfunction by modulating lipid metabolism and inflammation (28). The present study revealed that three major SCFAs improved HA-induced apoptosis in human hepatocytes, of which propionate had the highest antiapoptotic efficacy and was selected for research to obtain mechanistic insights. The mechanisms of the antiapoptotic effects of each SCFA might be different and network-like. Supporting evidence exist that at concentrations lower than 1 mM, acetate and butyrate inhibit apoptosis *via* improving mitochondrial dysfunction and ROS production, whereas higher concentrations have adverse effects on human islet cells (50). A concentration of 4 mM butyrate and propionate induced apoptosis not only in cancer cells but also in normal neutrophils by histone deacetylase (HDAC) inhibitor activity without the involvement of the G-protein-coupled receptor (GPR)-41/GPR-43 pathway (50). Acetate and propionate are confirmed to protect the islets from apoptosis in a GPR43-dependent manner through reduced caspase-3/7 activities (21, 22). Butyrate attenuated neuronal apoptosis *via* GPR41/Gβγ/PI3K/Akt pathway in rats (51). Recent studies showed that the mitochondrial function, GPRs, caspase-3 pathways, and HDAC activity might play a role in the antiapoptosis effects of SCFA. Furthermore, SCFA might exert positive impacts by enhancing the apoptosis of tumor cells and alleviating that of normal cells in various organs or tissues. Recently, reduced oxidative stress was found to account, at least partially, for propionate actions, because its effects, such as reduced caspase-3 expression, ROS production, but increased Bcl-2/Bax level, are tightly associated with mitochondrial-dependent apoptosis pathways (46). Although propionate was confirmed to inhibit apoptosis *via* increasing mitochondrial antioxidant enzyme levels and inducing autophagy to initiate mitochondria biogenesis (24, 52), further research is needed to elucidate the mechanism of action of propionate on the mitochondria.

In conclusion, the present study is the first to reveal that PBUTs (HA, PCS, and IS) induce apoptosis in human hepatocytes, of which HA has the highest efficacy. Normal liver cells (THLE-2) are more sensitive to PBUTs-induced

apoptosis than liver cancer cells (HepG2). SCFAs (acetate, propionate, and butyrate) alleviate HA-induced apoptosis in THLE-2 cells, of which the treatment with propionate has the highest efficacy. Mechanistically, HA may induce liver apoptosis by entering hepatocytes, causing mitochondrial damage and ROS production. Propionate reduction of apoptosis is associated with mitochondrial dysfunction and oxidative stress improvement by reducing caspase-3 expression, ROS production, but by increasing the Bcl-2/Bax level. Therefore, our study confirms that PBUTs accumulation might be an important cause of liver dysfunction in patients with CKD. Notably, the supplementation of SCFAs might be a viable strategy for liver protection in patients with CKD.

DATA AVAILABILITY STATEMENT

The original contributions presented in the study are included in the article/**Supplementary Material**, further inquiries can be directed to the corresponding author/s.

AUTHOR CONTRIBUTIONS

MD, XL, WL, and JG carried out most experiments involving cells. MD and XL acquired data and analyzed data. XZ, SG, and LZ contributed to the scientific discussion. MD wrote the manuscript. LZ came up with the study concept and revised the manuscript. All authors contributed to the article and approved the submitted version.

FUNDING

This study was supported by the National Natural Science Foundation of China (32072196) and the 111 Project from the Education Ministry of China (No. B18053).

SUPPLEMENTARY MATERIAL

The Supplementary Material for this article can be found online at: <https://www.frontiersin.org/articles/10.3389/fnut.2021.756730/full#supplementary-material>

Supplementary Figure S1 | (A) Effect of IS on HepG2 apoptosis ($n = 3$). After 24 h treatment, flow cytometry was performed on cells stained with annexin V-FITC and PI. CON, control. IS-2, 2 μ M IS treatment. IS-20, 20 μ M IS treatment. IS-200, 200 μ M IS treatment. IS-2000, 2000 μ M IS treatment. Group settings are the same with PCS **(B)** and HA **(C)**. **(B)** Effect of PCS on HepG2 apoptosis ($n = 3$). **(C)** Effect of HA on HepG2 apoptosis ($n = 3$).

Supplementary Figure S2 | (A) Effect of IS on THLE-2 apoptosis ($n = 2-3$). After 24 h treatment, flow cytometry was performed on cells stained with annexin V-FITC and PI. CON, control. IS-2, 2 μ M IS treatment. IS-20, 20 μ M IS treatment. IS-200, 200 μ M IS treatment. IS-2000, 2000 μ M IS treatment. Group settings are the same with PCS **(B)** and HA **(C)**. **(B)** Effect of PCS on THLE-2 apoptosis ($n = 2-3$). **(C)** Effect of HA on THLE-2 apoptosis ($n = 3$). **(D)** Effects of three gut-derived PBUTs mixture on THLE-2 apoptosis ($n = 3$).

Supplementary Figure S3 | Effects of HA-induced oxidative stress in THLE-2 cells. ROS level showed by fluorescent pictures after being treated with doses of HA, quantified by Image J software ($n = 5$). Data are the mean \pm SD. *, $P < 0.05$ vs. CON group. The significant difference was assessed using the one-way ANOVA followed by LSD posttests.

REFERENCES

- Sun B, Wang X, Liu X, Wang L, Ren F, Wang X, et al. Hippuric acid promotes renal fibrosis by disrupting redox homeostasis via facilitation of NRF2-KEAP1-CUL3 interactions in chronic kidney disease. *Antioxidants*. (2020) 9:9. doi: 10.3390/antiox9090783
- Graboski AL, Redinbo MR. Gut-derived protein-bound uremic toxins. *Toxins*. (2020) 12:9. doi: 10.3390/toxins12090590
- Popkov VA, Silachev DN, Zalevsky AO, Zorov DB, Plotnikov EY. Mitochondria as a source and a target for uremic toxins. *Int J Mol Sci*. (2019) 20:12. doi: 10.3390/ijms20123094
- Lekawanvijit S. Role of gut-derived protein-bound uremic toxins in cardiorenal syndrome and potential treatment modalities. *Circ J*. (2015) 79:10:2088-97. doi: 10.1253/circj.CJ-15-0749
- Prokopenko AJ, West RE, 3rd, Stubbs JR, Nolin TD. Development and validation of a UHPLC-MS/MS method for measurement of a gut-derived uremic toxin panel in human serum: an application in patients with kidney disease. *J Pharm Biomed Anal*. (2019) 174:618-24. doi: 10.1016/j.jpba.2019.06.033
- Lin CJ, Liou TC, Pan CF, Wu PC, Sun FJ, Liu HL, et al. The role of liver in determining serum colon-derived uremic solutes. *PLoS ONE*. (2015) 10:e0134590. doi: 10.1371/journal.pone.0134590
- Koppe L, Pillon NJ, Vella RE, Croze ML, Pelletier CC, Chambert S, et al. p-Cresyl sulfate promotes insulin resistance associated with CKD. *J Am Soc Nephrol*. (2013) 24:88-99. doi: 10.1681/ASN.2012050503
- Jourde-Chiche N, Burtsey S. Accumulation of protein-bound uremic toxins: the kidney remains the leading culprit in the gut-liver-kidney axis. *Kidney Int*. (2020) 97:1102-4. doi: 10.1016/j.kint.2020.02.026
- Lau WL, Savoj J, Nakata MB, Vaziri ND. Altered microbiome in chronic kidney disease: systemic effects of gut-derived uremic toxins. *Clin Sci*. (2018) 132:509-22. doi: 10.1042/CS20171107
- Wong F. Renal diseases and the liver. *Clin Liver Dis*. (2011) 15:39-53. doi: 10.1016/j.cld.2010.09.011
- Zhu S, Rong Y, Kiang TKL. Effects of p-Cresol on oxidative stress, glutathione depletion, and necrosis in heparg cells: comparisons to other uremic toxins and the role of p-cresol glucuronide formation. *Pharmaceutics*. (2021) 13:6. doi: 10.3390/pharmaceutics13060857
- Weigand KM, Schirris TJ, Houweling M, van den Heuvel J, Koenderink JB, Dankers ACA, et al. Uremic solutes modulate hepatic bile acid handling and induce mitochondrial toxicity. *Toxicol In Vitro*. (2019) 56:52-61. doi: 10.1016/j.tiv.2019.01.003
- Tanaka S, Yano S, Sheikh AM, Nagai A, Sugimoto T. Effects of uremic toxin p-cresol on proliferation, apoptosis, differentiation, and glucose uptake in 3T3-L1 cells. *Artif Organs*. (2014) 38:566-71. doi: 10.1111/aor.12252
- Han H, Zhu J, Zhu Z, Ni J, Du R, Dai Y, et al. p-Cresyl sulfate aggravates cardiac dysfunction associated with chronic kidney disease by enhancing apoptosis of cardiomyocytes. *J Am Heart Assoc*. (2015) 4:e001852. doi: 10.1161/JAHA.115.001852
- Lin YT, Wu PH, Tsai YC, Hsu YL, Wang HY, Kuo MC, et al. Indoxyl sulfate induces apoptosis through oxidative stress and mitogen-activated protein kinase signaling pathway inhibition in human astrocytes. *J Clin Med*. (2019) 8:2. doi: 10.3390/jcm8020191
- Rodrigues GGC, Delle H, Brito RBO, Cardoso VO, Fernandes KPS, Mesquita-Ferrari RA, et al. Indoxyl sulfate contributes to uremic sarcopenia by inducing apoptosis in myoblasts. *Arch Med Res*. (2020) 51:21-9. doi: 10.1016/j.arcmed.2019.12.020
- Marzocco S, Fazeli G, Di Micco L, Autore G, Adesso S, Dal Piaz F, et al. Supplementation of short-chain fatty acid, sodium propionate, in patients on maintenance hemodialysis: beneficial effects on inflammatory parameters and gut-derived uremic toxins: a pilot study (PLAN Study). *J Clin Med*. (2018) 7:10. doi: 10.3390/jcm7100315
- Canfora EE, Jocken JW, Blaak EE. Short-chain fatty acids in control of body weight and insulin sensitivity. *Nat Rev Endocrinol*. (2015) 11:577-91. doi: 10.1038/nrendo.2015.128
- den Besten G, van Eunen K, Groen AK, Venema K, Reijngoud DJ, Bakker BM. The role of short-chain fatty acids in the interplay between diet, gut microbiota, and host energy metabolism. *J Lipid Res*. (2013) 54:2325-40. doi: 10.1194/jlr.R036012
- Koh A, De Vadder F, Kovatcheva-Datchary P, Backhed F. From dietary fiber to host physiology: short-chain fatty acids as key bacterial metabolites. *Cell*. (2016) 165:1332-45. doi: 10.1016/j.cell.2016.05.041
- Hu S, Kuwabara R, de Haan BJ, Smink AM, de Vos P. Acetate and butyrate improve beta-cell metabolism and mitochondrial respiration under oxidative stress. *Int J Mol Sci*. (2020) 21:4. doi: 10.3390/ijms21041542
- Pingitore A, Gonzalez-Abuin N, Ruz-Maldonado I, Huang GC, Frost G, Persaud SJ. Short chain fatty acids stimulate insulin secretion and reduce apoptosis in mouse and human islets *in vitro*: role of free fatty acid receptor 2. *Diabetes Obes Metab*. (2019) 21:330-9. doi: 10.1111/dom.13529
- Pingitore A, Chambers ES, Hill T, Maldonado IR, Liu B, Bewick G, et al. The diet-derived short chain fatty acid propionate improves beta-cell function in humans and stimulates insulin secretion from human islets *in vitro*. *Diabetes Obes Metab*. (2017) 19:257-65. doi: 10.1111/dom.12811
- Cheng Y, Mai Q, Zeng X, Wang H, Xiao Y, Tang L, et al. Propionate relieves pentylenetetrazol-induced seizures, consequent mitochondrial disruption, neuron necrosis and neurological deficits in mice. *Biochem Pharmacol*. (2019) 169:113607. doi: 10.1016/j.bcp.2019.08.009
- Chang G, Liu X, Ma N, Yan J, Dai H, Roy AC, et al. Dietary addition of sodium butyrate contributes to attenuated feeding-induced hepatocyte apoptosis in dairy goats. *J Agric Food Chem*. (2018) 66:9995-10002. doi: 10.1021/acs.jafc.8b03526
- Vanholder R, De Smet R, Glorieux G, Argilés A, Baurmeister U, Brunet P, et al. Review on uremic toxins: classification, concentration, and interindividual variability. *Kidney Int*. (2003) 63:1934-43. doi: 10.1046/j.1523-1755.2003.00924.x
- Mutsaers HA, van den Heuvel LP, Ringens LH, Dankers AC, Russel FG, Wetzels JF, et al. Uremic toxins inhibit transport by breast cancer resistance protein and multidrug resistance protein 4 at clinically relevant concentrations. *PLoS ONE*. (2011) 6:e18438. doi: 10.1371/journal.pone.0018438
- Deng M, Qu F, Chen L, Liu C, Zhang M, Ren F, et al. SCFAs alleviated steatosis and inflammation in mice with NASH induced by MCD. *J Endocrinol*. (2020) 245:425-37. doi: 10.1530/JOE-20-0018
- Wang X, Yang S, Li S, Zhao L, Hao Y, Qin J, et al. Aberrant gut microbiota alters host metabolome and impacts renal failure in humans and rodents. *Gut*. (2020) 69:2131-42. doi: 10.1136/gutjnl-2019-319766
- Deltombe O, Van Biesen W, Glorieux G, Massy Z, Dhondt A, Elout S. Exploring protein binding of uremic toxins in patients with different stages of chronic kidney disease and during hemodialysis. *Toxins*. (2015) 7:3933-46. doi: 10.3390/toxins7103933
- Takahashi S, Yoshimura Y, Yamamoto T, Wakita M. Cellular expression of Bcl-2 and Bax in atrophic submandibular glands of rats. *Int J Exp Pathol*. (2008) 89:303-8. doi: 10.1111/j.1365-2613.2008.00613.x
- Redza-Dutordoir M, Averill-Bates DA. Activation of apoptosis signalling pathways by reactive oxygen species. *Biochim Biophys Acta*. (2016) 1863(12):2977-92. doi: 10.1016/j.bbamcr.2016.09.012
- Huang M, Wei R, Wang Y, Su T, Li P, Chen X. The uremic toxin hippurate promotes endothelial dysfunction via the activation of Drp1-mediated mitochondrial fission. *Redox Biol*. (2018) 16:303-13. doi: 10.1016/j.redox.2018.03.010
- Ma ZJ, Lu L, Yang JJ, Wang XX, Su G, Wang ZL, et al. Laricresinol induces apoptosis in HepG2 cells via mitochondrial-mediated apoptosis pathway. *Eur J Pharmacol*. (2018) 821:1-10. doi: 10.1016/j.ejphar.2017.12.027
- Addi T, Dou L, Burtsey S. Tryptophan-derived uremic toxins and thrombosis in chronic kidney disease. *Toxins*. (2018) 10:10. doi: 10.3390/toxins10100412
- Rocchetti MT, Cosola C, Ranieri E, Gesualdo L. Protein-bound uremic toxins and immunity. *Methods Mol Biol*. (2021) 2325:215-27. doi: 10.1007/978-1-0716-1507-2_15
- Duranton F, Cohen G, De Smet R, Rodriguez M, Jankowski J, Vanholder R, et al. Normal and pathologic concentrations of uremic toxins. *J Am Soc Nephrol*. (2012) 23:1258-70. doi: 10.1681/ASN.2011121175
- Kim YH, Kwak KA, Gil HW, Song HY, Hong SY. Indoxyl sulfate promotes apoptosis in cultured osteoblast cells. *BMC Pharmacol Toxicol*. (2013) 14:60. doi: 10.1186/2050-6511-14-60
- Ellis RJ, Small DM, Ng KL, Vesey DA, Vitetta L, Francis RS, et al. Indoxyl sulfate induces apoptosis and hypertrophy in human

- kidney proximal tubular cells. *Toxicologic Pathology*. (2018) 46:449-59. doi: 10.1177/0192623318768171
40. Gamage N, Barnett A, Hempel N, Duggleby RG, Windmill KF, Martin JL, et al. Human sulfotransferases and their role in chemical metabolism. *Toxicol Sci*. (2006) 90:5-22. doi: 10.1093/toxsci/kfj061
 41. Mair RD, Sirich TL, Meyer TW. Uremic toxin clearance and cardiovascular toxicities. *Toxins*. (2018) 10:6. doi: 10.3390/toxins10060226
 42. Mohammad RM, Muqbil I, Lowe L, Yedjou C, Hsu HY, Lin LT, et al. Broad targeting of resistance to apoptosis in cancer. *Semin Cancer Biol*. (2015) 35(Suppl):S78-103. doi: 10.1016/j.semcancer.2015.03.001
 43. Pistrutto G, Trisciuglio D, Ceci C, Garufi A, D'Orazi G. Apoptosis as anticancer mechanism: function and dysfunction of its modulators and targeted therapeutic strategies. *Aging*. (2016) 8:603-19. doi: 10.18632/aging.100934
 44. Marcuccilli M, Chonchol M. NAFLD and chronic kidney disease. *Int J Mol Sci*. (2016) 17:562. doi: 10.3390/ijms17040562
 45. Musso G, Gambino R, Tabibian JH, Ekstedt M, Kechagias S, Hamaguchi M, et al. Association of non-alcoholic fatty liver disease with chronic kidney disease: a systematic review and meta-analysis. *PLoS Med*. (2014) 11:e1001680. doi: 10.1371/journal.pmed.1001680
 46. Sinha K, Das J, Pal PB, Sil PC. Oxidative stress: the mitochondria-dependent and mitochondria-independent pathways of apoptosis. *Arch Toxicol*. (2013) 87:1157-80. doi: 10.1007/s00204-013-1034-4
 47. Edamatsu T, Fujieda A, Ezawa A, Itoh Y. Classification of five uremic solutes according to their effects on renal tubular cells. *Int J Nephrol*. (2014) 2014:512178. doi: 10.1155/2014/512178
 48. Schwab AJ, Tao L, Yoshimura T, Simard A, Barker F, Pang KS. Hepatic uptake and metabolism of benzoate: a multiple indicator dilution, perfused rat liver study. *Am J Physiol Gastrointest Liver Physiol*. (2001) 280:G1124-36. doi: 10.1152/ajpgi.2001.280.6.G1124
 49. Yoshimura T, Schwab AJ, Tao L, Barker F, Pang KS. Hepatic uptake of hippurate: a multiple-indicator dilution, perfused rat liver study. *Am J Physiol*. (1998) 274:G10-20. doi: 10.1152/ajpgi.1998.274.1.G10
 50. Aoyama M, Kotani J, Usami M. Butyrate and propionate induced activated or non-activated neutrophil apoptosis via HDAC inhibitor activity but without activating GPR-41/GPR-43 pathways. *Nutrition*. (2010) 26:653-61. doi: 10.1016/j.nut.2009.07.006
 51. Zhou Z, Xu N, Matei N, McBride DW, Ding Y, Liang H, et al. Sodium butyrate attenuated neuronal apoptosis via GPR41/Gβγ/PI3K/Akt pathway after MCAO in rats. *J Cereb Blood Flow Metab*. (2021) 41:267-81. doi: 10.1177/0271678X20910533
 52. Tang Y, Chen Y, Jiang H, Nie D. Short-chain fatty acids induced autophagy serves as an adaptive strategy for retarding mitochondria-mediated apoptotic cell death. *Cell Death Differ*. (2011) 18:602-18. doi: 10.1038/cdd.2010.117

Conflict of Interest: XZ is employed by Inner Mongolia Dairy Technology Research Institute Co., Ltd.

The remaining authors declare that the research was conducted in the absence of any commercial or financial relationships that could be construed as a potential conflict of interest.

Publisher's Note: All claims expressed in this article are solely those of the authors and do not necessarily represent those of their affiliated organizations, or those of the publisher, the editors and the reviewers. Any product that may be evaluated in this article, or claim that may be made by its manufacturer, is not guaranteed or endorsed by the publisher.

Copyright © 2021 Deng, Li, Li, Gong, Zhang, Ge and Zhao. This is an open-access article distributed under the terms of the Creative Commons Attribution License (CC BY). The use, distribution or reproduction in other forums is permitted, provided the original author(s) and the copyright owner(s) are credited and that the original publication in this journal is cited, in accordance with accepted academic practice. No use, distribution or reproduction is permitted which does not comply with these terms.



***Lactobacillus plantarum* CCFM1143 Alleviates Chronic Diarrhea via Inflammation Regulation and Gut Microbiota Modulation: A Double-Blind, Randomized, Placebo-Controlled Study**

OPEN ACCESS

Edited by:

Huaxi Yi,
Ocean University of China, China

Reviewed by:

Zhihong Sun,
Inner Mongolia Agricultural University,
China
Huaixiang Tian,
Shanghai Institute of Technology,
China

*Correspondence:

R. Paul Ross
p.ross@ucc.ie
Wei Chen
chenwei66@jiangnan.edu.cn

Specialty section:

This article was submitted to
Nutritional Immunology,
a section of the journal
Frontiers in Immunology

Received: 24 July 2021

Accepted: 10 September 2021

Published: 15 October 2021

Citation:

Yang B, Yue Y, Chen Y, Ding M, Li B,
Wang L, Wang Q, Stanton C,
Ross RP, Zhao J, Zhang H and
Chen W (2021) *Lactobacillus plantarum*
CCFM1143 Alleviates Chronic Diarrhea
via Inflammation Regulation and Gut
Microbiota Modulation: A Double-Blind,
Randomized, Placebo-Controlled Study.
Front. Immunol. 12:746585.
doi: 10.3389/fimmu.2021.746585

Bo Yang^{1,2,3}, Yue Yue^{1,2}, Yang Chen^{1,2}, Mengfan Ding^{1,2}, Bowen Li^{1,2}, Linlin Wang^{1,2},
Qun Wang⁴, Catherine Stanton^{3,5,6}, R. Paul Ross^{3,5*}, Jianxin Zhao^{1,2}, Hao Zhang^{1,2,7,8}
and Wei Chen^{1,2,7*}

¹ State Key Laboratory of Food Science and Technology, Jiangnan University, Wuxi, China, ² School of Food Science and Technology, Jiangnan University, Wuxi, China, ³ International Joint Research Laboratory for Pharmabiotics & Antibiotic Resistance, Jiangnan University, Wuxi, China, ⁴ Yancheng Tinghu District People's Hospital, Yancheng, Jiangsu, China, ⁵ APC Microbiome Ireland, University College Cork, Cork, Ireland, ⁶ Teagasc Food Research Centre, Moorepark, Fermoy, Ireland, ⁷ National Engineering Research Center for Functional Food, Jiangnan University, Wuxi, China, ⁸ Wuxi Translational Medicine Research Center, Jiangsu Translational Medicine Research Institute Wuxi Branch, Wuxi, China

Irritable bowel syndrome with diarrhea and functional diarrhea are both functional bowel disorders that cause chronic diarrhea. Chronic diarrhea is closely related to daily life and the psychological condition of diarrhea in patients, and probiotics can play a significant role in alleviating chronic diarrhea in some research. *Lactobacillus plantarum* CCFM1143 can relieve diarrhea in mice caused by enterotoxigenic *Escherichia coli* (ETEC); however, its clinical effects remain unclear. This study aimed to assess the effects of CCFM1143 as a therapy for chronic diarrhea patients. Fifty-five patients with chronic diarrhea were randomly assigned into the probiotic group (n = 28) and the placebo group (n = 27), receiving the routine regimen with or without probiotics for 4 weeks, respectively. CCFM1143 can mitigate the apparent clinical symptoms and improve the health status and quality of life of patients. In addition, it could inhibit the increase in interleukin 6 (IL-6) and the decrease in motilin; modulate the short-chain fatty acids, especially acetic and propionic acids; and regulate the gut microbiota, particularly reducing the abundance of *Bacteroides* and *Eggerthella* and enriching the abundance of *Akkermansia*, *Anaerostipes*, and *Terrisporobacter*. In addition, treatment with probiotics showed clinical effectiveness in managing chronic diarrhea when compared with the placebo group. The findings could help to develop and further the application of probiotics for chronic diarrhea.

Keywords: probiotics, *Lactobacillus plantarum*, chronic diarrhea, gut microbiota, clinical trial

INTRODUCTION

Chronic diarrhea is a complex and common problem faced by primary care clinicians. Its prevalence worldwide is estimated to be 3%–20% (1). It also has a significant negative impact on the health-related quality of life, causes high healthcare utilization, and increases the economic burden (2). Generally, chronic diarrhea lasts longer than 28 days, and in addition to the duration of symptoms, it tends to occur without a clear onset (1). Stool frequency (more than two bowel movements per day) and/or stool consistency (loose or watery stools) are the common criteria to define diarrhea (3). Recent literature has recommended using abnormal stool consistency rather than stool frequency, as it correlates best with the objective measures of whole gut transit time (4).

Irritable bowel syndrome with diarrhea (IBS-D) and functional diarrhea (FD) are the most common causes of chronic diarrhea in western populations (5) and are attributed to functional bowel disorder. Previous studies have combined the incidences of IBS-D and functional diarrhea to report the prevalence of chronic diarrhea in the general population (6), but the underlying pathophysiology remains poorly understood. According to Roman standards, the main difference in the symptoms between FD and IBS-D is the presence of abdominal pain (4). It is particularly challenging when diarrhea becomes chronic and therefore less likely to resolve spontaneously.

IBS-D and FD are common diseases accompanied by disturbances in the intestinal function. Some studies have reported that probiotics could improve IBS symptoms in IBS-D patients, which include *Lactobacillus brevis* KB290 and β -carotene (7) and a combination of *Lactobacillus acidophilus* CL1285, *Lactobacillus casei* LBC80R, and *Lactobacillus rhamnosus* CLR2 (8). In addition, *Bifidobacterium infantis* Y1 and *Bifidobacterium breve* Y8 ameliorated the clinical symptoms and changed the diversity and composition of the gut microbiota in chronic diarrhea patients (9). Probiotics, including *Lactobacillus* and *Bifidobacterium*, were favored over placebo for their effects on the overall symptoms of IBS (10, 11). However, some studies have reported contrasting effects, which may be related to strain-specific properties and a change in the host itself (12). Since the prevalence and clinical picture of IBS show great variations between race and ethnicity, differences in the gut microbiota between individuals might also exert a role in IBS (13). Although imbalance in the gut microbiota is a possible mechanism driving the development of IBS, a lot of previous research focused on the clinical outcomes. Thus, extensive clinical studies are still required to elucidate the role the gut microbiota play in the development of chronic diarrhea and to design specialized therapy for patients. Previous studies have shown that *Lactobacillus plantarum* CCFM1143 can relieve diarrhea caused by enterotoxigenic *Escherichia coli* (ETEC) (14). In this study, chronic diarrhea patients were assigned into a probiotic group and a placebo group to evaluate the efficacy of *L. plantarum* CCFM1143 in relieving chronic diarrhea, which will provide not only new evidence for probiotics as an alternative therapy to alleviate chronic diarrhea but also a

foundation of knowledge for exploring the mechanism of probiotic treatment in alleviating chronic diarrhea.

MATERIALS AND METHODS

Subjects

Ninety patients were randomly assigned to the probiotic and placebo groups (**Figure 1**). The inclusion criteria for patients with diarrhea were as follows: 1) males and females 18–65 years old; 2) Rome IV standard was used as the diagnostic criterion. The frequency of defecation is greater than or equal to three times/day. According to the Bristol Stool Scale, normal stool of types 3 and 4 are used as a reference. Types 5, 6, and 7 can be regarded as diarrhea, as shown in **Table 1**. 3) Not using any drugs that can affect gastrointestinal motility in the past weeks; 4) the subjects or their guardians have signed an informed consent and have good compliance; and 5) routine blood, urine, and stool tests before treatment and liver and kidney function tests are all within the normal range. The exclusion criteria were pregnancy, drug abuse, alcohol addiction, and any immunodeficiency or organic disease. Participants who had taken medications within 4 weeks prior to this trial were excluded.

Clinical Trial Design

During the study period, volunteers need to record the consumption of probiotic preparations and emergency medicines, as well as information related to defecation, and record the frequency of diarrhea, stool consistency (Bristol Stool Form Scale, BSFS), pain, and abdominal distension. Patients with diarrhea were divided into two large groups, namely, the *L. plantarum* CCFM1143 intervention group [3.52×10^9 colony forming units (CFU)/day] and the placebo (maltodextrin) group. Probiotics can be taken directly, mixed with warm water (not exceeding 37°C) or mixed with fresh milk (yogurt or lactic acid bacteria products are not recommended), and taken 30 min after meals, once a day, for a period of 30 days. Stool collection was carried out in the fifth week and related indicators were tested. The experimental preparation period was 1 week and the experimental process was 4 weeks, with a total duration of 5 weeks. The patients were recruited through the Yancheng Tinghu District People's Hospital (Yancheng, Jiangsu Province, China). The trial was approved by the Ethnic Committee of the hospital (no. ET2020088).

Assessment of Clinical Outcomes

Patients with diarrhea underwent routine physical examinations at the first visit and in the fourth week of follow-up visits. The characteristics examined included height, weight, blood pressure, blood glucose, blood lipids, four blood routines, urine routine, stool routine, and liver function. The defecation frequency and stool status were also recorded to evaluate the relieving effect. At the same time, abdominal symptoms [we refer to the Irritable Bowel Syndrome Severity Scoring System (IBS-SSS) for the evaluation of IBS severity] and daily life points [we refer to the diarrhea section of the Irritable Bowel Syndrome Quality of Life

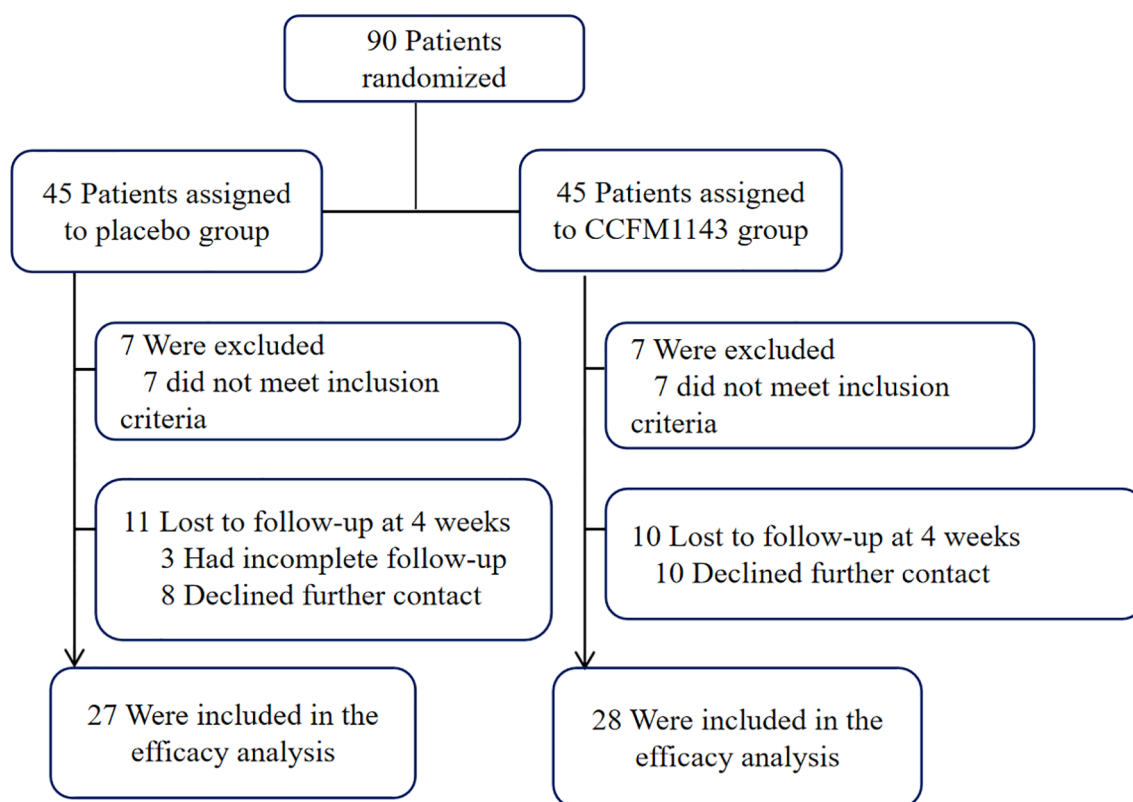









FIGURE 1 | Clinical course of *Lactobacillus plantarum* CCFM1143 relieving chronic diarrhea.

TABLE 1 | Bristol stool scale.

Bristol typing	Form	Description
1. Nut-like stool		Hard, small pieces, like rabbit dung
2. Dry hard stool		The texture is hard, with multiple small pieces stuck together, in the shape of a sausage.
3. Wrinkled stool		The surface is covered with cracks and is sausage-like.
4. Banana-shaped stool		Soft texture, smooth surface, sausage-like
5. Soft stool		Soft semi-solid with uneven edges
6. Slightly shaped stool		Soft flakes, porridge with rough edges or no fixed shape
7. Watery stool		Watery, completely liquid without solids

(IBS-QOL) table) were scored (15, 16). Stool satisfaction, the 36-Item Short Form Health Survey (SF-36) diarrhea mood score, and the SF-36 overall health score were calculated (17). A lower score means an improvement in the quality of life of patients with diarrhea.

Neurobiological Factors, Cytokines, and MTL Evaluation

Serum was provided by The Tinghu People's Hospital, Yancheng, and the commercialized kits purchased from Wuhan Elabscience Biotechnology Co., Ltd (Wuhan, China) were used to determine

tumor necrosis factor- α (TNF- α), interleukin-6 (IL-6), motilin (MTL), and vasoactive intestine peptide (VIP) and 5-hydroxytryptamine (5-HT) following the manufacturer's instructions.

Determination of SCFAs

Briefly, short-chain fatty acids (SCFAs) were extracted using a previous method, with some modifications (18). A known mass of feces (50–100 mg) was weighed directly into sterile tubes, followed by soaking in 500 μ l of saturated NaCl solution for 30 min. The soaked matter was homogenized and acidified with 40 μ l of 10% sulfuric acid. One milliliter of ether was added to the acidified homogenates and vortexed before centrifugation at $18,000 \times g$ at 4°C for 15 min. Of the supernatants, 500 μ l was carefully filtered through a 0.22- μ m pore filter and transferred into a gas phase vial for gas chromatography–mass spectrometry analysis.

High-Throughput Sequencing of the Gut Microbiota

Metagenomic DNA from the fecal samples was obtained using a FastDNA Spin Kit for Feces (cat. no. 6570200, MP Biomedicals, Irvine, CA, USA) according to the manufacturer's instructions. The V3–V4 region of the 16S rRNA gene was PCR amplified from microbial genomic DNA (forward primer, 5'-AYT GGG YDT AAA GNG-3'; reverse primer, 5'-TAC NVG GGT ATC TAA TCC-3') as described previously (19). The sequencing data obtained from the Illumina MiSeq PE300 platform was processed using QIIME 2 (20). Then, Marker Data Profiling (<https://www.microbiomeanalyst.ca/>) was used for alpha diversity (Chao1 and Shannon indexes) and beta diversity analyses, in which analysis of the beta diversity was based on non-metric multidimensional scaling (NMDS) analysis. Linear discriminant analysis effect size (LEfSe) was performed online (<http://huttenhower.sph.harvard.edu/galaxy>).

Statistical Analysis

Data were processed with GraphPad Prism and SPSS and displayed as the mean \pm SEM of each group. The Mann–Whitney *U* test was used to analyze statistical significance. A $p < 0.05$ indicates a statistically significant difference.

RESULTS

L. plantarum CCFM1143 Improved the Apparent Symptoms in Chronic Diarrhea Patients

The basic characteristics of patients with chronic diarrhea are shown in **Table 2**. The body mass index (BMI) values of the two

groups were mostly concentrated in the range of normal (18.5–22.9 kg/m²) and overweight (23.0–27.9 kg/m²), which were roughly the same.

There was no significant difference in the blood pressure, blood routine, serum biochemistry, and urine routine (baseline) of the enrolled diarrhea patients in the placebo and *L. plantarum* CCFM1143 groups (before intervention, Placebo-B, CCFM1143-B; after intervention, placebo-A, CCFM1143-A). The routine occult blood test of stool was negative and the microscopic examination was normal, indicating that there was no serious inflammatory disease. After the 4-week intervention, there was no significant difference between the placebo and *L. plantarum* CCFM1143 groups in those indicators. *L. plantarum* CCFM1143 showed no effects on the blood pressure, blood routine, serum biochemistry, and urine routine of patients with diarrhea (**Table 3**).

Analysis of the visual indicators in patients with diarrhea showed that there was no significant difference between the placebo group and the *L. plantarum* CCFM1143 group at baseline (0 week) in bowel frequency and stool consistency (Bristol score) (**Table 4**). After the 4-week intervention, the placebo group had no improvement in defecation frequency and stool consistency, while the defecation frequency and Bristol score of patients in the *L. plantarum* CCFM1143 group have been significantly reduced, indicating that the chronic diarrhea symptoms had been partially relieved. The abdominal symptom score, daily life score, SF-36 diarrhea mood score, and SF-36 diarrhea overall health score of the placebo group and the CCFM1143-treated group showed no significant difference before and after intervention. Moreover, reductions of the abdominal symptom score, daily life score, and SF-36 diarrhea overall health score were higher in the *L. plantarum* CCFM1143 group than those of the placebo group, but were not significant.

Effect of *L. plantarum* CCFM1143 on Neurobiological Factors, Cytokines, and MTL in Chronic Diarrhea Patients

To further explore the effect of *L. plantarum* CCFM1143 on the immune response, intestinal motility, and nerve-related indicators of patients with diarrhea, human serum TNF- α , IL-6, MTL, 5-HT, and VIP were measured. The results showed that, at baseline (before intervention), there was no significant difference in TNF- α , IL-6, MTL, 5-HT, and VIP between the placebo and *L. plantarum* CCFM1143 groups (**Figure 2**). After 4 weeks of intervention, in the placebo group, IL-6 was significantly increased ($p < 0.05$), the MTL level was

TABLE 2 | Basic characteristics of patients with diarrhea.

Group	Male-to-female ratio	Age (years)	Height (cm)	Weight (kg)	BMI (kg/m ²)		
					Normal	Overweight	Obese
Placebo	10:17	47.37 \pm 12.77	165.15 \pm 6.53	64.48 \pm 9.86	12	14	1
<i>L. plantarum</i> CCFM1143	8:20	52.68 \pm 9.1	163.58 \pm 6.74	64.23 \pm 10.8	14	12	2

TABLE 3 | Information on the routine physical examination for patients with diarrhea.

Item		Placebo-B	Placebo-A	CCFM1143-B	CCFM1143-A
Blood pressure	Systolic	118.75 ± 12.03	115.46 ± 10.57	120.46 ± 11.89	120.2 ± 8.82
	Diastolic	75.74 ± 9.69	75.35 ± 9.17	76.75 ± 8.71	76.2 ± 7.89
Blood routine	Red blood cell	4.68 ± 0.5	4.52 ± 0.47	4.51 ± 0.35	4.52 ± 0.29
	Mean corpuscular hemoglobin concentration	136.93 ± 23.89	135.31 ± 15.79	137.96 ± 11.88	139.54 ± 12.17
	Platelet	190.48 ± 47.32	202.04 ± 40.89	236.29 ± 51.48	224.46 ± 59.28
	White blood cell	5.88 ± 1.35	5.71 ± 1.16	5.84 ± 1.34	5.39 ± 1.12
Serum biochemistry	Alkaline phosphate (Alp)	67.38 ± 19.88	68.42 ± 21.55	62.54 ± 13.48	71.82 ± 14.95
	Alanine aminotransferase (Alt)	32.62 ± 20.62	23.54 ± 12.9	22.64 ± 9.73	29.88 ± 17.86
	Aspartate aminotransferase (Ast)	24.52 ± 6.42	22.38 ± 6.12	25.15 ± 14.29	25.79 ± 13.14
	Total bilirubin (Tbil)	17.31 ± 6.68	14.47 ± 4.52	15.84 ± 5.32	15.83 ± 5.83
	Urea (Bun)	5.05 ± 1.37	4.86 ± 1.01	5.75 ± 1.18	5.38 ± 1.23
	Creatinine (Cr)	68.59 ± 12.72	68.79 ± 16.38	60.05 ± 11.64	59.28 ± 12.4
	Uric acid (Ua)	352.78 ± 108.91	321.04 ± 79.59	299.42 ± 60.55	291.57 ± 65.11
	Glucose (Glu)	5.82 ± 1.55	5.84 ± 1.59	5.28 ± 1	5.54 ± 1.62
	Total cholesterol (Cho)	4.43 ± 0.73	4.54 ± 1.09	5.2 ± 0.99	5.2 ± 1.09
	Triglyceride (Tg)	1.7 ± 0.89	1.89 ± 1.19	1.33 ± 0.45	1.63 ± 0.73
	High-density lipoprotein cholesterol (hdl)	1.16 ± 0.24	1.13 ± 0.19	1.44 ± 0.19	1.42 ± 0.29
	Low-density lipoprotein (ldl)	2.59 ± 0.71	2.72 ± 0.79	3.15 ± 0.85	3.03 ± 0.71
	High-sensitivity C-reactive protein	3.47 ± 2.93	3.91 ± 2.71	2.8 ± 1.87	3.33 ± 3.69
Urine routine	Urine sugar	Negative	Negative	Negative	Negative
	Urine bilirubin (bil)	Negative	Negative	Negative	Negative
	Ketones (ket)	Negative	Negative	Negative	Negative
	Proportion (sg)	1.02 ± 0.003	1.02 ± 0.002	1.02 ± 0.01	1.02 ± 0.01
	pH value (pH)	6.08 ± 0.41	6.1 ± 0.57	5.76 ± 0.69	6.08 ± 0.91
	Urine protein (pro)	Negative	Negative	Negative	Negative
	Urobilinogen (ubg)	Negative	Negative	Negative	Negative
	Nitrite (nit)	Negative	Negative	Negative	Negative
	Leukocyte esterase (leu)	Negative	Negative	Negative	Negative
	Urine color	Yellow	Yellow	Light yellow	Yellow
	Clarity	Transparent	Transparent	Transparent	Transparent
	Occult blood	Negative	Negative	Negative	Negative
	Microscopic examination of white blood cells	No abnormality	No abnormality	No abnormality	No abnormality
	Microscopic examination of red blood cells	No abnormality	No abnormality	No abnormality	No abnormality

significantly decreased, VIP had a rising trend but was not significant, and TNF- α and 5-HT were not modified. However, after the intervention with *L. plantarum* CCFM1143, TNF- α , IL-6, MTL, and 5-HT all showed a tendency to decrease and had a certain inhibitory effect, although there was no significant difference, and VIP was affected at a certain extent before and after the intervention (**Figure 2**). Although *L. plantarum* CCFM1143 had no significant effect on MTL regulation, placebo treatment significantly reduced the MTL level, which also reflected the effectiveness of *L. plantarum* CCFM1143 on MTL regulation (**Figure 2**).

Effect of *L. plantarum* CCFM1143 on Fecal SCFAs in Chronic Diarrhea Patients

In order to explore the effect of *L. plantarum* CCFM1143 on SCFAs in chronic diarrhea patients, GC-MS analysis was performed on human stool samples. After 4 weeks of intervention, there were no significant changes in acetic acid, propionic acid, isobutyric acid, and butyric acid in the placebo group. It is worth noting that *L. plantarum* CCFM1143 had a significant increase in the contents of acetic acid and propionic acid, but had no significant effect on isobutyric acid and butyric acid (**Figure 3**).

TABLE 4 | Relief scores of *L. plantarum* CCFM1143.

Index	Placebo				<i>L. plantarum</i> CCFM1143			
	0 week	4 weeks	Effect	<i>p</i>	0 week	4 weeks	Effect	<i>p</i>
Bowel frequency	3.48 ± 0.51	3.22 ± 0.51	-0.26	0.073	3.25 ± 0.57	2.93 ± 0.53	-0.32	0.044
Stool consistency	5.60 ± 0.89	5.26 ± 1.19	-0.34	0.758	5.68 ± 0.66	5.28 ± 0.84	-0.40	0.041
Abdominal symptom score	4.15 ± 1.66	4.29 ± 1.59	0.14	0.953	5.18 ± 2.22	4.54 ± 2.15	-0.64	0.350
Daily life score	31.93 ± 10.76	33.00 ± 12.73	1.07	0.946	37.14 ± 14.97	32.93 ± 15.18	-4.21	0.266
Stool satisfaction	2.41 ± 0.79	2.29 ± 0.67	-0.12	0.664	2.96 ± 0.94	2.50 ± 1.02	-0.46	0.113
SF-36 diarrhea mood score	13.70 ± 2.83	16.23 ± 4.92	2.53	0.384	14.64 ± 2.78	14.04 ± 2.92	-0.60	0.764
SF-36 diarrhea overall health score	10.33 ± 2.86	10.70 ± 2.45	0.37	0.927	12.14 ± 1.73	11.29 ± 2.52	-0.85	0.601

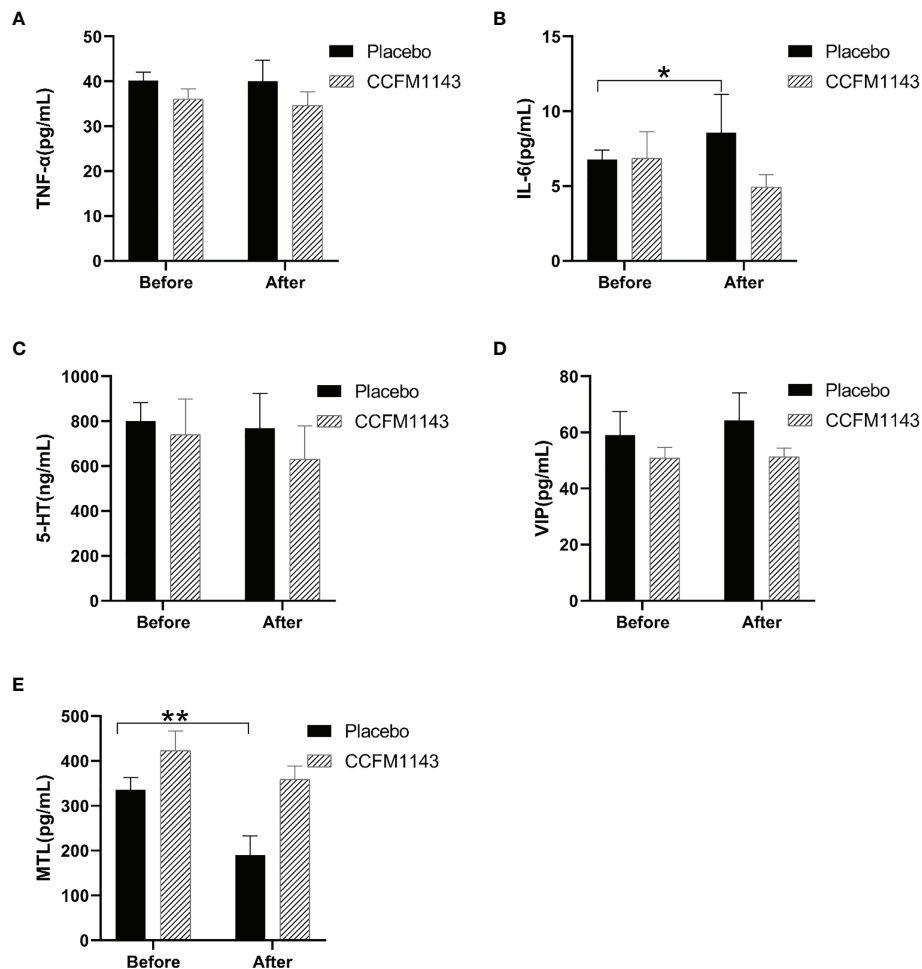


FIGURE 2 | Effect of *Lactobacillus plantarum* CCFM1143 on serum neurobiological factors, cytokines, and motilin (MTL) in patients with diarrhea. (A–E) Concentrations of tumor necrosis factor alpha (TNF-α) (A), interleukin-6 (IL-6) (B), 5-hydroxytryptamine (5-HT) (C), vasoactive intestine peptide (VIP) (D), and MTL (E). * $p < 0.05$, ** $p < 0.01$.

Modulation of *L. plantarum* CCFM1143 on Gut Microbiota in Chronic Diarrhea Patients

In order to evaluate the influence of *L. plantarum* CCFM1143 on the diversity of the gut microbiota in chronic diarrhea patients, the Chao1 and Shannon indexes were used to evaluate the alpha diversity and NMDS analysis was used to analyze the beta diversity of the gut microbiota. Chronic diarrhea patients in the placebo and *L. plantarum* CCFM1143 groups did not show a significant change in the diversity of the gut microbiota before and after the intervention (Figure 4A). There was no significant change in the beta diversity of the gut microbiota in the placebo group before and after the intervention, while the beta diversity of the gut microbiota in the *L. plantarum* CCFM1143-treated patients before and after the intervention was changed significantly, indicating that after 4 weeks of continuous intervention, *L. plantarum* CCFM1143 changed the diversity of gut microbiota in chronic diarrhea patients (Figures 4B, C).

In order to further analyze the influence of *L. plantarum* CCFM1143 on the profiles of the gut microbiota in patients with chronic diarrhea, we examined the phylum abundance. The results showed that the four main phyla in the gut microbiota of patients with chronic diarrhea were Firmicutes, Bacteroidetes, Proteobacteria, and Actinomycota, among which Firmicutes had the highest proportion, while Proteobacteria had a higher relative abundance in chronic diarrhea patients than in healthy subjects (Figure 5A). The placebo group had no significant effect on these four phyla after the intervention, which was consistent with the placebo group having no change in the gut microbiota diversity after the intervention. Moreover, *L. plantarum* CCFM1143 treatment significantly reduced the abundance of Bacteroidetes. In addition, *L. plantarum* CCFM1143 had no significant effect on Proteobacteria and Actinomycetes. Moreover, the Firmicutes and Bacteroidetes (F/B) ratio in the CCFM1143 treatment showed an upward trend, while that in the placebo group showed no significant difference (Figure 5B).

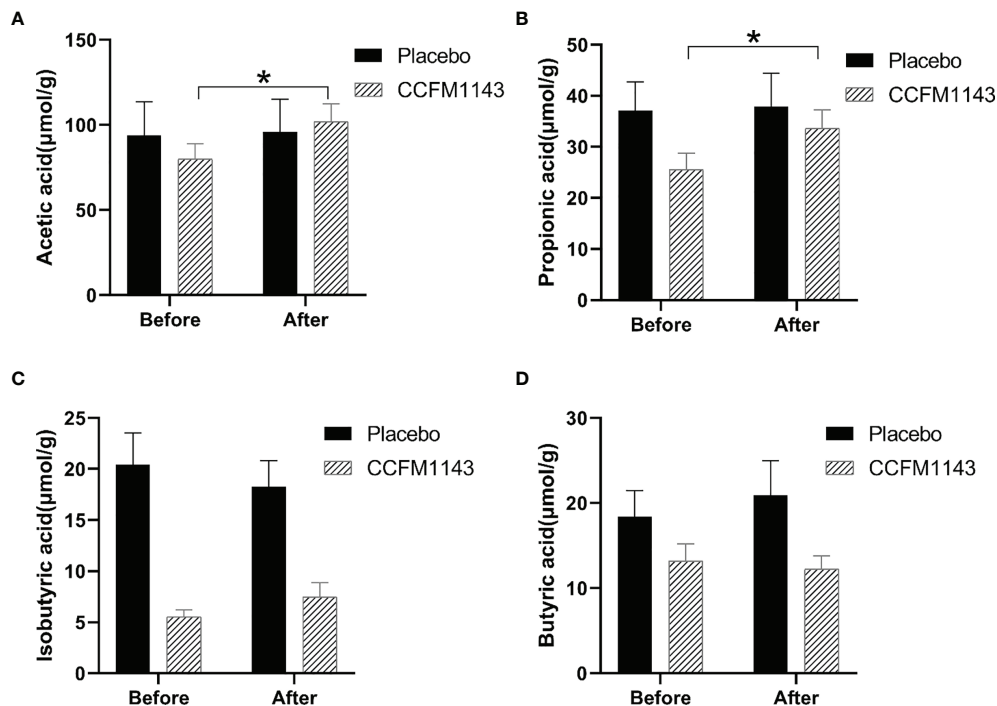


FIGURE 3 | Effect of *Lactobacillus plantarum* CCFM1143 on short-chain fatty acids (SCFAs) in patients with diarrhea. (A–D) Concentrations of acetic acid (A), propionic acid (B), isobutyric acid (C), and butyric acid (D) in feces. * $p < 0.05$.

In order to further explore the influence of *L. plantarum* CCFM1143 on the changes of the intestinal genera in patients with chronic diarrhea, LEfSe was used to analyze the abundance of genera in order to determine the statistically significant biomarkers. The results showed that the different genera in the placebo group before intervention were *Fusicatenibacter* and *Lactococcus*, while those of the *L. plantarum* CCFM1143 group were the *Ruminococcus torques* group, *Bacteroides*, *Anaerostipes*, *Lachnospiraceae* UCG-004, and *Intestinibacter*. After intervention, the different genera of the placebo group were *Coprobaecillus*, *Eisenbergiella*, and *Escherichia-Shigella*, while the different genera in the *L. plantarum* CCFM1143-treated group were *Eggerthella*, *Odoribacter*, *Terrisporobacter*, *Akkermansia*, and *Escherichia-Shigella* (Figures 6A, B). Further analysis of the relative abundance of the different genera between the placebo and *L. plantarum* CCFM1143 groups showed that placebo treatment insignificantly decreased *Escherichia-Shigella*, and the adjustment changes to the other genera were small. However, *L. plantarum* CCFM1143 administration caused relatively rich variations of the different microbes, in which it significantly reduced the relative abundance of *Bacteroides*, *Eggerthella*, *Lachnospiraceae*, and *Lachnospira* and increased the relative abundance of *Akkermansia*, *Anaerostipes*, *Terrisporobacter*, and *Escherichia-Shigella*. Before and after the intervention, the relative abundance of *Escherichia-Shigella* in the placebo group increased by 7.24%, while that in the

L. plantarum CCFM1143-treated group increased by 1.47%, which was a significant reduction compared with that in placebo treatment (Figures 6C, D).

DISCUSSION

IBS-D and FD are common chronic diarrhea diseases, and variations in the gut microbiota among individuals have been considered a possible cause (21). Probiotics have shown the potential to alleviate the clinical symptoms of chronic diarrhea (22, 23). The purpose of this study was to explore the relieving effect of *L. plantarum* CCFM1143 on the symptoms of chronic diarrhea. Thus, a randomized, placebo-controlled clinical trial was designed and performed, which showed effects of improvement in the quality of life and mental state, regulation of the immune responses, modulation of SCFAs, and alleviation of gut microbiota dysbiosis.

A BMI between 18.5 and 22.9 kg/m² is considered normal, between 23.0 and 27.9 kg/m² is the overweight range, and a BMI ≥ 28 kg/m² denotes obesity (6). Before and after the intervention, the routine physical examination indicators were not changed significantly in chronic diarrhea patients. However, *L. plantarum* CCFM1143 treatment significantly decreased the defecation frequency and Bristol stool score. It was shown that the abdominal distension, defecation frequency, and stool abnormality rate of IBS-D patients treated with a multi-strain

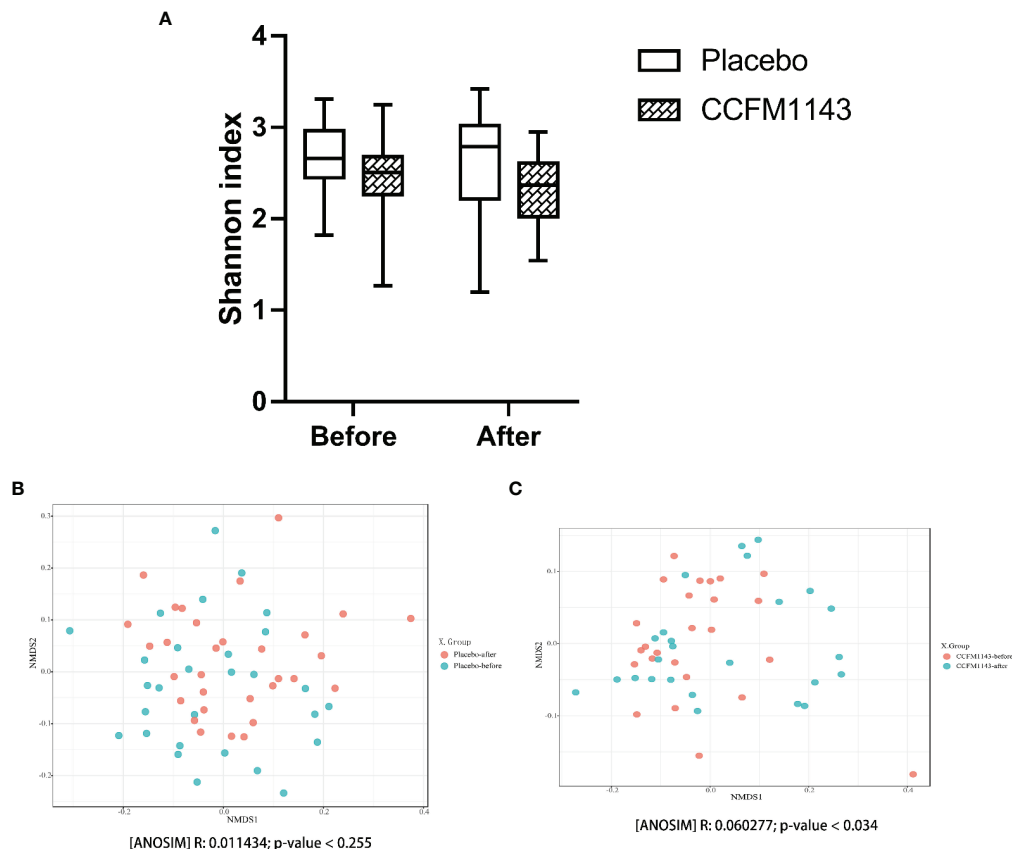


FIGURE 4 | Effect of *Lactobacillus plantarum* CCFM1143 on the diversity of the gut microbiota in patients with diarrhea. **(A)** Alpha diversity indicated by the Shannon index. **(B)** Beta diversity of the placebo group indicated by non-metric multidimensional scaling (NMDS). **(C)** Beta diversity of the *L. plantarum* CCFM1143 group indicated by NMDS.

probiotic formulation were significantly lower than those before treatment (8), which was consistent with our current results. The mixture of *Lactobacillus* and *Bifidobacterium* could improve the quality of life of IBS-D patients (24). *Lactobacillus gasseri* significantly improved the diarrhea symptoms in patients with IBS-D, such as abdominal pain, bloating, daily routine, and average bowel frequency (25). Meanwhile, *B. infantis* M-63 effectively improved the symptoms, quality of life, and the SF-36 score in patients with IBS after 3 months of intervention. However, *L. plantarum* CCFM1143 treatment showed no significant effect on the quality of life and stool satisfaction. *L. plantarum* CCFM1143 played a certain role in improving the symptoms of diarrhea, and no adverse events occurred during the trial period and after the follow-up; hence, the use of *L. plantarum* CCFM1143 as a dietary intervention may be a safe and effective alternative strategy to relieve chronic diarrhea.

It is well known that inflammation in patients with diarrhea is high. Intervention with *Bifidobacterium* and *Lactobacillus* for 4 weeks in patients with atopic dermatitis did not significantly relieve the level of pro-inflammatory cytokines in the serum (26), and the results were similar to those of the current study, which may be related to the short probiotic intervention time and to

uncontrollable factors such as patients. The significant increase in the level of IL-6 in the current placebo group indicated that *L. plantarum* CCFM1143 intervention had a better regulation on IL-6. A previous report showed that the serum IL-6 and TNF- α levels in patients with IBS-D were significantly lower after taking *Bifidobacterium longum* ES1 compared with those before treatment (27), but it should be noted that these patients took *B. longum* ES1 for 8 or 12 weeks. Therefore, the reduction of IL-6 in patients with chronic diarrhea by *L. plantarum* CCFM1143 treatment was not significant, which may be related to the number of viable *Lactobacillus* taken and the duration of treatment. MTL is an excitatory gastrointestinal hormone with a main physiological function of affecting gastrointestinal motility (28). In the study, administration of *L. plantarum* CCFM1143 inhibited the decrease of MTL compared with the placebo group. *Bifidobacterium trifecta* viable capsules could significantly improve the gastrointestinal hormones in patients with IBS-constipation (IBS-C) and alleviate their clinical symptoms (29). 5-HT is an important neurotransmitter in the brain-gut axis and is one of the key mediators of intestinal motility, secretion, and sensation and can also induce high sensitivity of the visceral afferent nerve and the intestinal

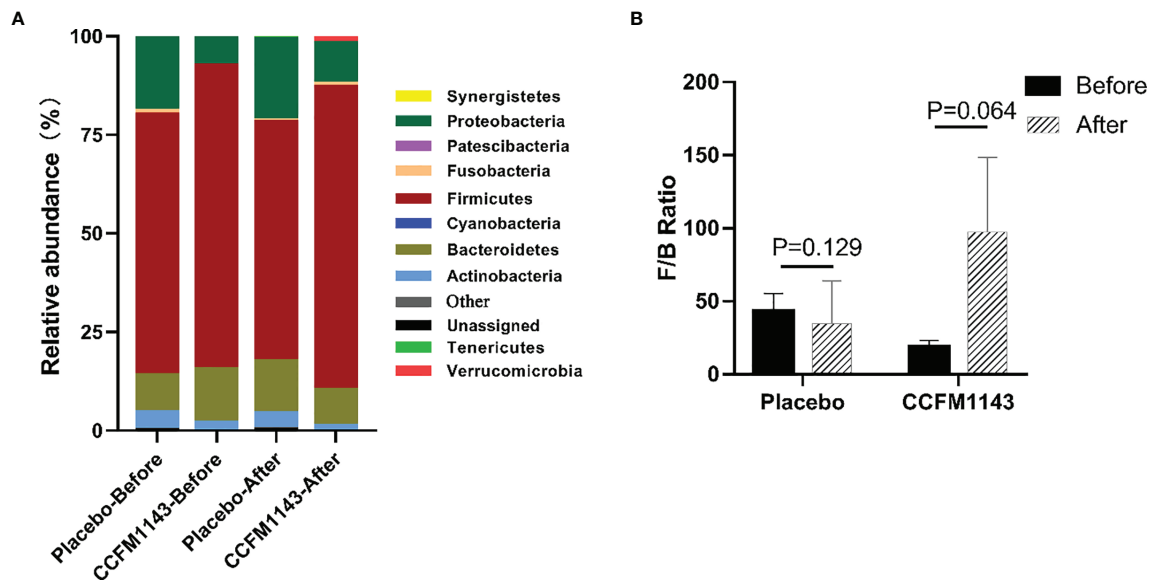


FIGURE 5 | Effect of *Lactobacillus plantarum* CCFM1143 on the phylum level of the gut microbiota in patients with diarrhea. **(A)** Microbial distribution at the phylum level. **(B)** The Firmicutes and Bacteroidetes (F/B) ratio.

nervous system, resulting in abdominal pain, abdominal distension, and other symptoms. 5-HT has always been the subject of interest in the evaluation of the pathophysiological mechanism of IBS (30). The level of 5-HT in patients with IBS-C was significantly lower than that before probiotics intervention (29). However, *L. plantarum* CCFM1143-treated patients showed insignificant decreases in the levels of 5-HT. VIP is distributed in the nervous system and the gastrointestinal tract and is involved in the regulation process of neurosecretion and relaxation of the gastrointestinal smooth muscle. In addition, VIP is an inhibitory gastrointestinal hormone that can directly cause lower esophageal sphincter (LES) relaxation, which is the main cause of gastroesophageal reflux disease (31). It has been reported that VIP is associated with watery diarrhea syndrome (32). Although *L. plantarum* CCFM1143 treatment showed no significant effect on MTL regulation, the MTL level in the placebo group was significantly reduced, which also reflected the effectiveness of *L. plantarum* CCFM1143 on MTL regulation. In general, *L. plantarum* CCFM1143 can help regulate the immune response and inhibit the increase of IL-6 and the decrease of MTL in patients with diarrhea, which has a certain correlation with the decrease of the diarrhea-related scores.

An earlier report showed that *L. casei* increased the contents of SCFAs when alleviating antibiotic-related diarrhea, and the intake of probiotics and dietary fiber would affect the composition of the gut microbiota, thereby promoting the utilization of SCFAs (33). *L. plantarum* CCFM1143 intervention significantly increased the contents of acetic acid and propionic acid. The increase of SCFAs such as propionic acid can contribute to the host immune response (34). SCFAs (particularly acetate, propionate, and butyrate) could alleviate

TNF- α - or lipopolysaccharide-induced endothelial activation by inhibiting the production of pro-inflammatory cytokines (e.g., IL-6) (35). In summary, *L. plantarum* CCFM1143 can alleviate diarrhea symptoms and modulate inflammation mainly related to the production of SCFAs. This was similar to a previous result showing that *L. plantarum* CCFM1143 increased the contents of acetic acid and propionic acid in ETEC-infected diarrhea mice (14).

Probiotics could change the composition of the gut microbiota in patients with IBS-D or FD clinically. It has been found that changes of the gut microbiota may be related to the improvement of the clinical characteristics (9), which is somewhat similar to the current results. In general, the gut microbiota of healthy people is composed of four main bacterial phyla, namely, Firmicutes, Bacteroidetes, Actinomycetes, and Proteobacteria, of which Proteobacteria are usually less than 1%. In addition, it has been proven that Bacteroidetes is closely related to the occurrence of human diarrhea (36); the F/B ratio was often related to the occurrence of diseases. With a lower F/B ratio, the risk of disease occurrence was greater (37). In general, *L. plantarum* CCFM1143 treatment can significantly reduce the abundance of Bacteroidetes and increase the abundance of Firmicutes to restore the gut microbiota. A previous study that performed phylogenetic analysis showed that 16 butyric acid producers isolated from the cecum of chickens were associated with four different lineages in Firmicutes (38). It is known that exogenous harmful substances activated the NLRP3 inflammasomes through *Escherichia-Shigella*, thereby inducing lung tissue damage in broilers (39). Among them, *Escherichia* was known to increase the risk of pathogenic invasion and has the potential

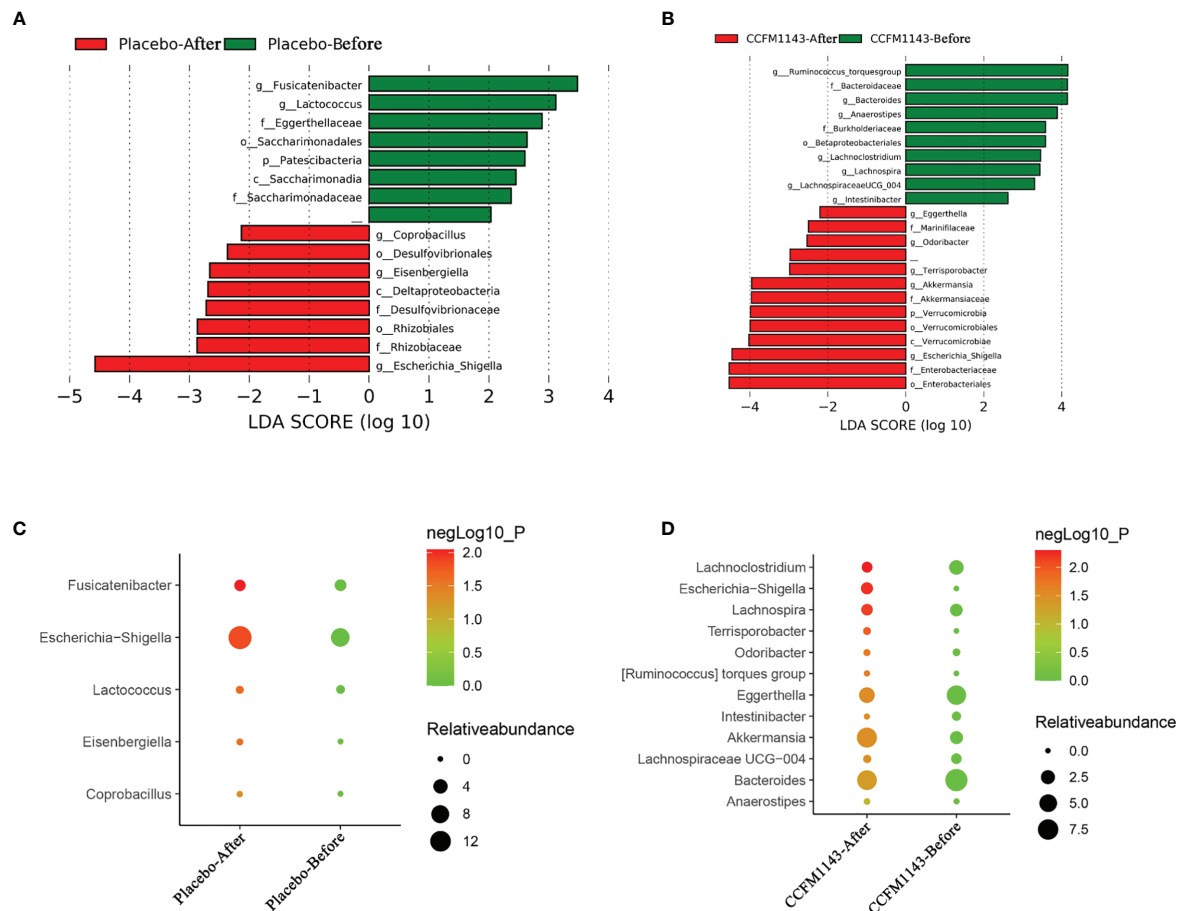


FIGURE 6 | Effect of *Lactobacillus plantarum* CCFM1143 on the different genera of the gut microbiota in patients with diarrhea. **(A)** Distribution histogram of the placebo group based on linear discriminant analysis (LDA), with a log LDA score above 2.0. Significant taxa were labeled and annotated with tags in the right panel. **(B)** Distribution histogram of the *L. plantarum* CCFM1143 group based on LDA, with a log LDA score above 2.0. Significant taxa were labeled and annotated with tags in the right panel. **(C)** Relative abundance of the different microorganisms in the placebo group. **(D)** Relative abundance of the different microorganisms in the *L. plantarum* CCFM1143 group.

to result in severe invasive infections (40). *Bacteroides* has been proven to be the cause of diarrheal diseases (41); however, *Akkermansia* can reduce inflammation (42). For instance, *L. plantarum* CCFM8610 could increase the relative abundance of *Anaerostipes* when alleviating IBS-D, which has a strong butyric acid production capacity (43). *Terrisporobacter* played a probiotic role as a beneficial intestinal bacterium (44). These results suggested that the relief of diarrhea by *L. plantarum* CCFM1143 may be related to its regulation of the gut microbiota composition. The mixed bacterial powder of *L. casei* Zhang, *Bifidobacterium animalis* spp. *lactis* V9, and *L. plantarum* P-8 was reported to reduce the relative abundance of *Bacteroides*, *E. coli*, and *Citrobacter* in the intestine of patients with IBS and to increase the relative abundance of *Bifidobacterium* and *Butyrivibrio*. These gut microbiota changes had a relation with the improvement of the clinical symptoms of IBS (45). Patients with IBS-D consuming IgA-coated bacteria had a more significant increase in the relative abundance of *Escherichia*–

Shigella (46). Therefore, it is worth noting that, similar to previous reports, *L. plantarum* CCFM1143 treatment increased the abundance of *Escherichia*–*Shigella*, which had a close relation with the complicated diet of patients.

CONCLUDING REMARKS

Generally, the use of probiotics showed clinical effectiveness compared to placebo in managing chronic diarrhea. *L. plantarum* CCFM1143 can significantly alleviate the bowel frequency and Bristol stool score, inhibit the increase in IL-6 and the decrease in MTL, regulate the gut microbiota by reducing the abundance of harmful bacteria and increasing the abundance of beneficial bacteria, and modulate SCFAs. The current results could help further the development and application of functional probiotic products for chronic diarrhea.

DATA AVAILABILITY STATEMENT

The datasets presented in this study can be found in online repositories. The names of the repository/repositories and accession number(s) can be found below: <https://www.ncbi.nlm.nih.gov/>, PRJNA765509.

ETHICS STATEMENT

The studies involving human participants were reviewed and approved by Ethics Committee of Tinghu District People's Hospital, Yancheng, China. The patients/participants provided written informed consent to participate in this study.

AUTHOR CONTRIBUTIONS

BY, RR, and WC conceptualized the study. BY and YY helped with the methodology. MD and BL contributed to software development. BY and YY did the validation. LW performed formal analysis. BY, YY, and QW performed the investigation. HZ and WC helped with the resources. BY, YY, and HZ curated

the data. BY, YC, and YY wrote the original draft. CS, RR, and WC reviewed and edited the manuscript. JZ helped with the visualization. RR, HZ, and WC supervised the study. JZ administered the project. WC acquired funding. All authors contributed to the article and approved the submitted version.

FUNDING

This research was supported by the National Natural Science Foundation of China (32021005), National First-Class Discipline Program of Food Science and Technology (JUFSTR20180102), the Fundamental Research Funds for the Central Universities (JUSRP52003B), 111 Project (BP0719028), and Collaborative Innovation Center of Food Safety and Quality Control in Jiangsu Province.

ACKNOWLEDGMENTS

We thank the Collaborative Innovation Center of Food Safety and Quality Control in Jiangsu Province.

REFERENCES

- Schiller LR, Pardi DS, Sellin JH. Chronic Diarrhea: Diagnosis and Management. *Clin Gastroenterol Hepatol* (2017) 15:182–93. doi: 10.1016/j.cgh.2016.07.028
- Schiller LR. Evaluation of Chronic Diarrhea and Irritable Bowel Syndrome With Diarrhea in Adults in the Era of Precision Medicine. *Am J Gastroenterol* (2018) 113:660–9. doi: 10.1038/s41395-018-0032-9
- Mearin F, Lacy BE, Chang L, Chey WD, Lembo AJ, Simren M, et al. Bowel Disorders. *Gastroenterology* (2016) 150:1393–407. doi: 10.1053/j.gastro.2016.02.031
- Singh P, Mitsuhashi S, Ballou S, Rangan V, Sommers T, Cheng V, et al. Demographic and Dietary Associations of Chronic Diarrhea in a Representative Sample of Adults in the United States. *Am J Gastroenterol* (2018) 113:593–600. doi: 10.1038/ajg.2018.24
- Longstreth GF, Thompson WG, Chey WD, Houghton LA, Mearin F, Spiller RC. Functional Bowel Disorders. *Gastroenterology* (2006) 130:1480–91. doi: 10.1053/j.gastro.2005.11.061
- Zhao YF, Guo XJ, Zhang ZS, Ma XQ, Wang R, Yan XY, et al. Epidemiology of Functional Diarrhea and Comparison With Diarrhea-Predominant Irritable Bowel Syndrome: A Population-Based Survey in China. *PloS One* (2012) 7: e43749. doi: 10.1371/journal.pone.0043749
- Fuke N, Aizawa K, Suganuma H, Takagi T, Naito Y. Effect of Combined Consumption of *Lactobacillus Brevis* KB290 and β -Carotene on Minor Diarrhoea-Predominant Irritable Bowel Syndrome-Like Symptoms in Healthy Subjects: A Randomised, Double-Blind, Placebo-Controlled, Parallel-Group Trial. *Int J Food Sci Nutr* (2017) 68:973–86. doi: 10.1080/09637486.2017
- Preston K, Krumian R, Hattner J, de Montigny D, Stewart M, Gaddam S. *Lactobacillus Acidophilus* CL1285, *Lactobacillus Casei* LBC80R and *Lactobacillus Rhamnosus* CLR2 Improve Quality-of-Life and IBS Symptoms: A Double-Blind, Randomised, Placebo-Controlled Study. *Benef Microbes* (2018) 9:697–706. doi: 10.3920/BM2017.0105
- Brigidi P, Vitali B, Swennen E, Bazzocchi G, Matteuzzi D. Effects of Probiotic Administration Upon the Composition and Enzymatic Activity of Human Fecal Microbiota in Patients With Irritable Bowel Syndrome or Functional Diarrhea. *Res Microbiol* (2001) 152:735–41. doi: 10.1016/s0923-2508(01)01254-2
- Sun J, Kong C, Qu X, Deng C, Lou Y, Jia L. Efficacy and Safety of Probiotics in Irritable Bowel Syndrome: A Systematic Review and Meta-Analysis. *Saudi J Gastroenterol* (2020) 26:66–77. doi: 10.4103/sjg.SJG_384_19
- Dale HF, Rasmussen SH, Asiller O, Lied GA. Probiotics in Irritable Bowel Syndrome: An Up-to-Date Systematic Review. *Nutrients* (2019) 11:2048. doi: 10.3390/nu11092048
- Whelan K. Probiotics and Prebiotics in the Management of Irritable Bowel Syndrome: A Review of Recent Clinical Trials and Systematic Reviews. *Curr Opin Clin Nutr Metab Care* (2011) 14:581–7. doi: 10.1097/MCO.0b013e32834b8082
- El-Salhy M, Patcharatrakul T, Hatlebakk JG, Hausken T, Gilja OH, Gonlachanvit S. Chromogranin A Cell Density in the Large Intestine of Asian and European Patients With Irritable Bowel Syndrome. *Scand J Gastroenterol* (2017) 52:691–7. doi: 10.1080/00365521.2017.1305123
- Yue Y, He Z, Zhou Y, Ross RP, Stanton C, Zhao J, et al. *Lactobacillus Plantarum* Relieves Diarrhea Caused by Enterotoxin-Producing *Escherichia Coli* Through Inflammation Modulation and Gut Microbiota Regulation. *Food Funct* (2020) 11:10362–74. doi: 10.1039/d0fo02670k
- Francis CY, Morris J, Whorwell PJ. The Irritable Bowel Severity Scoring System: A Simple Method of Monitoring Irritable Bowel Syndrome and Its Progress. *Aliment Pharmacol Ther* (1997) 11:395–402. doi: 10.1046/j.1365-2036.1997.142318000.x
- Patrick DL, Drossman DL, Frederick IO, Dicesare J, Puder KL. Quality of Life in Persons With Irritable Bowel Syndrome: Development and Validation of a New Measure. *Dig Dis Sci* (1998) 43:400–11. doi: 10.1023/a:1018831127942
- Han B, Shao Q, Cong Y, Guo S, Mao X, Wei R, et al. Transcutaneous Electric Nerve Stimulation Over Acupoints for Patients With Diarrhea-Predominant Irritable Bowel Syndrome: Protocol for Systematic Review and Meta-Analysis. *Med (Baltimore)* (2018) 97:e13267. doi: 10.1097/MD.00000000000013267
- Wang L, Hu L, Xu Q, Jiang T, Fang S, Wang G, et al. *Bifidobacteria* Exert Species-Specific Effects on Constipation in BALB/c Mice. *Food Funct* (2017) 8:3587–600. doi: 10.1039/c6fo01641c
- Tian P, Wang G, Zhao J, Zhang H, Chen W. *Bifidobacterium* With the Role of 5-Hydroxytryptophan Synthesis Regulation Alleviates the Symptom of Depression and Related Microbiota Dysbiosis. *J Nutr Biochem* (2019) 63:43–51. doi: 10.1016/j.jnutbio.2019.01.007
- Yan S, Yang B, Zhao J, Stanton C, Ross RP, Zhang H, et al. A Ropy Exopolysaccharide Producing Strain *Bifidobacterium Longum* Subsp.

- Longum YS108R Alleviates DSS-Induced Colitis by Maintenance of the Mucosal Barrier and Gut Microbiota Modulation. *Food Funct* (2019) 10:1595–608. doi: 10.1039/c9fo00014c
21. Ringel Y. The Gut Microbiome in Irritable Bowel Syndrome and Other Functional Bowel Disorders. *Gastroenterol Clin North Am* (2017) 46:91–101. doi: 10.1016/j.gtc.2016.09.014
 22. Martoni CJ, Srivastava S, Leyer GJ. *Lactobacillus Acidophilus* DDS-1 and *Bifidobacterium Lactis* UABla-12 Improve Abdominal Pain Severity and Symptomatology in Irritable Bowel Syndrome: Randomized Controlled Trial. *Nutrients* (2020) 12:363. doi: 10.3390/nu12020363
 23. Ishaque SM, Khosruzzaman SM, Ahmed DS, Sah MP. A Randomized Placebo-Controlled Clinical Trial of a Multi-Strain Probiotic Formulation (Bio-Kult®) in the Management of Diarrhea-Predominant Irritable Bowel Syndrome. *BMC Gastroenterol* (2018) 18:71. doi: 10.1186/s12876-018-0788-9
 24. Cha BK, Jung SM, Choi CH, Song ID, Lee HW, Joon Kim H, et al. The Effect of a Multispecies Probiotic Mixture on the Symptoms and Fecal Microbiota in Diarrhea-Dominant Irritable Bowel Syndrome: A Randomized, Double-Blind, Placebo-Controlled Trial. *J Clin Gastroenterol* (2012) 46:220–7. doi: 10.1097/MCG.0b013e31823712b1
 25. Shin SP, Choi YM, Kim WH, Hong SP, Park JM, Kim J, et al. A Double Blind, Placebo-Controlled, Randomized Clinical Trial That Breast Milk Derived-*Lactobacillus Gasseri* BNR17 Mitigated Diarrhea-Dominant Irritable Bowel Syndrome. *J Clin Biochem Nutr* (2018) 62:179–86. doi: 10.3164/jcbs.17-73
 26. Fang Z, Lu W, Zhao J, Zhang H, Qian L, Wang Q, et al. Probiotics Modulate the Gut Microbiota Composition and Immune Responses in Patients With Atopic Dermatitis: A Pilot Study. *Eur J Nutr* (2020) 59:2119–30. doi: 10.1007/s00394-019-02061-x
 27. Caviglia GP, Tucci A, Pellicano R, Fagoonee S, Rosso C, Abate ML, et al. Clinical Response and Changes of Cytokines and Zonulin Levels in Patients With Diarrhea Predominant Irritable Bowel Syndrome Treated With *Bifidobacterium Longum* ES1 for 8 or 12 Weeks: A Preliminary Report. *J Clin Med* (2020) 9:2353. doi: 10.3390/jcm9082353
 28. Chu C, Liaw Y. Hepatitis B Virus-Related Cirrhosis: Natural History and Treatment. *Semin Liver Dis* (2006) 26:142–52. doi: 10.1055/s-2006-939752
 29. Gao Z, Ji J, He X. Clinical and Experimental Study on Probiotics in the Treatment of Constipation Type Irritable Bowel Syndrome. *Biomark Applic* (2019) 3:138. doi: 10.29011/2576-9588.100038
 30. Harris LA, Chang L, Alossetron: An Effective Treatment for Diarrhea-Predominant Irritable Bowel Syndrome. *Womens Health (Lond)* (2007) 3:15–27. doi: 10.2217/17455057.3.1.15
 31. Liang X, Bi S, Yang W, Wang L, Cui G, Cui F, et al. Evaluation of the Impact of Hepatitis B Vaccination Among Children Born During 1992–2005 in China. *J Infect Dis* (2009) 200:39–47. doi: 10.1086/599332
 32. Alm P, Alumets J, Håkanson R, Owman O, Sjöberg NO, Sundler F, et al. Origin and Distribution of VIP (Vasoactive Intestinal Polypeptide)-Nerves in the Genitourinary Tract. *Cell Tissue Res* (1980) 205:337–47. doi: 10.1007/BF00232276
 33. Wong S, Jamous A, Driscoll JO, Sekhar R, Weldon M, Yau CY, et al. A *Lactobacillus Casei* Shirota Probiotic Drink Reduces Antibiotic-Associated Diarrhoea in Patients With Spinal Cord Injuries: A Randomised Con-Trolled Trial. *Br J Nutr* (2014) 111:672–8. doi: 10.1017/S0007114513002973
 34. Duscha A, Gisevius B, Hirschberg S, Yissachar N, Stangl GI, Eilers E, et al. Propionic Acid Shapes the Multiple Sclerosis Disease Course by an Immunomodulatory Mechanism. *Cell* (2020) 180:1067–80. doi: 10.1016/j.cell.2020.02.035
 35. Li M, van Esch B, Henricks PAJ, Garssen J, Folkerts G. Time and Concentration Dependent Effects of Short Chain Fatty Acids on Lipopolysaccharide- or Tumor Necrosis Factor α -Induced Endothelial Activation. *Front Pharmacol* (2018) 9:233. doi: 10.3389/fphar.2018.00233
 36. Hahn AW, Froerer C, VanAlstine S, Rathi N, Bailey EB, Stenehjem DD, et al. Targeting *Bacteroides* in Stool Microbiome and Response to Treatment With First-Line VEGF Tyrosine Kinase Inhibitors in Metastatic Renal-Cell Carcinoma. *Clin Genitourin Cancer* (2018) 16:365–8. doi: 10.1016/j.clgc.2018.05.001
 37. Lynch SV, Pedersen O. The Human Intestinal Microbiome in Health and Disease. *N Engl J Med* (2016) 375:2369–79. doi: 10.1056/NEJMra1600266
 38. Eeckhaut V, Van Immerseel F, Croubels S, De Baere S, Haesebrouck F, Ducatelle R, et al. Butyrate Production in Phylogenetically Diverse Firmicutes Isolated From the Chicken Caecum. *Microb Biotechnol* (2011) 4:503–12. doi: 10.1111/j.1751-7915.2010.00244.x
 39. Liu Q, Zhou Y, Li X, Ma D, Zhang M. Ammonia Induce Lung Tissue Injury in Broilers by Activating NLRP3 Inflammasome via *Escherichia/Shigella*. *Poult Sci* (2020) 99:3402–10. doi: 10.1016/j.psj.2020.03.019
 40. Liderot K, Ratcliffe P, Lüthje P, Thidholm E, Özenci V. Microbiological Diagnosis of Eggerthella Lenta Blood Culture Isolates in a Swedish Tertiary Hospital: Rapid Identification and Antimicrobial Susceptibility Profile. *Anaerobe* (2016) 38:21–4. doi: 10.1016/j.anaerobe.2015.11.005
 41. Wick EC, Sears CL. *Bacteroides* Spp. And Diarrhea. *Curr Opin Infect Dis* (2010) 23:470–4. doi: 10.1097/QCO.0b013e32833da1eb
 42. Shin NR, Lee JC, Lee HY, Kim MS, Whon TW, Lee MS, et al. An Increase in the *Akkermansia* Spp. Population Induced by Metformin Treatment Improves Glucose Homeostasis in Diet-Induced Obese Mice. *Gut* (2014) 63:727–35. doi: 10.1136/gutjnl-2012-303839
 43. Liu Y, Yu X, Yu L, Tian F, Chen W. *Lactobacillus Plantarum* CCFM8610 Alleviates Irritable Bowel Syndrome and Prevents Gut Microbiota Dysbiosis: A Randomized, Double-Blind, Placebo-Controlled, Pilot Clinical Trial. *Engineering* (2020) 7:376–85. doi: 10.1016/j.eng.2020.06.026
 44. Chen L, Zhou W, Zhou Y, Tan T, Du H, Feng L. Analysis of the Effects of Nanosilver on Bacterial Community in the Intestinal Fluid of Silkworms Using High-Throughput Sequencing. *Bull Entomol Res* (2020) 110:309–20. doi: 10.1017/S0007485319000634
 45. Xu H, Ma C, Zhao F, Chen P, Liu Y, Sun Z, et al. Adjunctive Treatment With Probiotics Partially Alleviates Symptoms and Reduces Inflammation in Patients With Irritable Bowel Syndrome. *Eur J Nutr* (2020) 60:1–13. doi: 10.1007/s00394-020-02437-4
 46. Liu Y, Yuan X, Li L, Lin L, Zuo X, Cong Y, et al. Increased Ileal Immunoglobulin A Production and Immunoglobulin A-coated Bacteria in Diarrhea Predominant Irritable Bowel Syndrome. *Clin Transl Gastroenterol* (2020) 11:e00146. doi: 10.14309/ctg.00000000000000146

Conflict of Interest: The authors declare that the research was conducted in the absence of any commercial or financial relationships that could be construed as a potential conflict of interest.

Publisher's Note: All claims expressed in this article are solely those of the authors and do not necessarily represent those of their affiliated organizations, or those of the publisher, the editors and the reviewers. Any product that may be evaluated in this article, or claim that may be made by its manufacturer, is not guaranteed or endorsed by the publisher.

Copyright © 2021 Yang, Yue, Chen, Ding, Li, Wang, Wang, Stanton, Ross, Zhao, Zhang and Chen. This is an open-access article distributed under the terms of the Creative Commons Attribution License (CC BY). The use, distribution or reproduction in other forums is permitted, provided the original author(s) and the copyright owner(s) are credited and that the original publication in this journal is cited, in accordance with accepted academic practice. No use, distribution or reproduction is permitted which does not comply with these terms.



Mannan Oligosaccharides Application: Multipath Restriction From *Aeromonas hydrophila* Infection in the Skin Barrier of Grass Carp (*Ctenopharyngodon idella*)

Zhiyuan Lu^{1†}, Lin Feng^{1,2,3†}, Wei-Dan Jiang^{1,2,3}, Pei Wu^{1,2,3}, Yang Liu^{1,2,3}, Jun Jiang^{1,2,3}, Sheng-Yao Kuang^{4,5}, Ling Tang^{4,5}, Shu-Wei Li^{4,5}, Xiang-An Liu⁴, Cheng-Bo Zhong⁴ and Xiao-Qiu Zhou^{1,2,3*}

OPEN ACCESS

Edited by:

Jiong-Wei Wang,
National University of Singapore,
Singapore

Reviewed by:

Dan Li,
National University of Singapore,
Singapore
Guoxing Nie,
Henan Normal University, China

*Correspondence:

Xiao-Qiu Zhou
xqzhouqq@tom.com;
zhouxq@scau.edu.cn

[†]These authors have contributed
equally to this work and share
first authorship

Specialty section:

This article was submitted to
Nutritional Immunology,
a section of the journal
Frontiers in Immunology

Received: 15 July 2021

Accepted: 27 September 2021

Published: 18 October 2021

Citation:

Lu Z, Feng L, Jiang W-D, Wu P, Liu Y,
Jiang J, Kuang S-Y, Tang L, Li S-W,
Liu X-A, Zhong C-B and Zhou X-Q
(2021) Mannan Oligosaccharides
Application: Multipath Restriction From
Aeromonas hydrophila Infection in
the Skin Barrier of Grass Carp
(*Ctenopharyngodon idella*).
Front. Immunol. 12:742107.
doi: 10.3389/fimmu.2021.742107

¹ Animal Nutrition Institute, Sichuan Agricultural University, Chengdu, China, ² Fish Nutrition and Safety Production University Key Laboratory of Sichuan Province, Sichuan Agricultural University, Chengdu, China, ³ Key Laboratory for Animal Disease-Resistance Nutrition of China Ministry of Education, Sichuan Agricultural University, Chengdu, China, ⁴ Sichuan Animal Science Academy, Sichuan Animtech Feed Co. Ltd, Chengdu, China, ⁵ Animal Breeding and Genetics Key Laboratory of Sichuan Province, Animal Nutrition Institute, Sichuan Academy of Animal Science, Chengdu, China

The objective of this study was to evaluate the efficacy of dietary Mannan oligosaccharides (MOS) supplementation on skin barrier function and the mechanism of on-growing grass carp (*Ctenopharyngodon idella*). Five hundred forty grass carp were fed for 60 days from the growing stage with six different levels of MOS diets (0, 200, 400, 600, 800, and 1,000 mg kg⁻¹). At the end of the growth trial, the 14-day *Aeromonas hydrophila* challenge experiment has proceeded. The obtained data indicate that MOS could (1) decline skin lesion morbidity after being challenged by the pathogenic bacteria; (2) maintain physical barrier function via improving antioxidant ability, inhibiting excessive apoptosis, and strengthening the tight junction between the epithelial cell and the related signaling pathway (Nrf2/Keap1, p38MAPK, and MLCK); and (3) regulate immune barrier function by modulating the production of antimicrobial compound and expression of involved cytokines and the related signaling pathway (TOR and NF-κB). Finally, we concluded that MOS supplementation reinforced the disease resistance and protected the fish skin barrier function from *Aeromonas hydrophila* infection.

Keywords: mannan oligosaccharides, antioxidant, apoptosis, tight junction, skin immune, grass carp (*Ctenopharyngodon idella*)

INTRODUCTION

Due to large-scale intensive production facilities, fish are exposed to potential various pathogens that often result in massive economic losses (1). The disease resistance of fish mainly depends on the main defense organs' immune function (2). Skin, an important mucosal defense organ in fish, has developed a better barrier system (including physical barriers and immune barriers) to protect the whole body from natural pathogen invasion (3). A previous report has confirmed that mechanical

skin barrier injury could further lead to high morbidity and mortality of fish (4). Therefore, a protected fish skin barrier function must be necessary for fish health. An effective strategy is to supplement the dietary with prebiotics. The current definition of prebiotics is, “Prebiotics are food constituents that well thought-out to be non-digestible selectively fermented, confers benefits of growth and activity of beneficial microbes present in gastrointestinal tract and improve the health of host” (5). In general, the prebiotics used in animal production are some functional oligosaccharides (6). Studies on fish reported that skin physical and immune barrier function could be improved by functional oligosaccharides such as xylooligosaccharides (XOS), galactooligosaccharides (GOS), fructooligosaccharides (FOS), and so on (7–9). Mannan oligosaccharide (MOS), a kind of functional oligosaccharide, is widely used in the feed formulation of aquatic (10). However, no systematic research has been conducted, and no in-depth exploration has been performed about the relationship between MOS and skin barrier function. Limited research on skin has shown that MOS supplementation promoted mucus production in rainbow trout (*Oncorhynchus mykiss*) and European sea bass (*Dicentrarchus labrax*), and upregulated *IFN γ* and *IL-10* expression in greater amberjack (*Seriola dumerili* Risso 1810) (11–13). Thus, a comprehensive understanding of the effect of MOS on fish skin barrier function and the in-depth possible mechanisms is necessary.

Previous studies have reported that cellular structure and intercellular junctions comprise skin physical barrier, which is mainly related to the antioxidant capacity, apoptosis levels, and tight junctions (1, 14). As far as we know, the NF-E2-related factor 2 (Nrf2) could eliminate excess free radicals by regulating the levels of antioxidant enzymes, while p38 mitogen-activated protein kinase (MAPK) could dynamically regulate apoptosis by regulating apoptosis promoter and effector, thus corporately protecting the cellular structure integrity (15, 16). Myosin light chain kinase (MLCK) is an important signaling molecule that could maintain intercellular junctions by regulating the expression of downstream tight junction protein molecules (17, 18). However, the research to date about the effects of MOS on fish skin cellular structure and intercellular junctions and their possible mechanism has not been investigated. It is worth noting that available evidence suggests a probable correlation between MOS and skin physical barrier. A study on chicken macrophages demonstrated that MOS could increase the production of nitric oxide (NO) (19), which could activate Nrf2 in PC12 cells (20). Furthermore, MOS supplementation could improve calcium (Ca^{2+}) absorption and retention in layer hens (21). Other reports revealed that Ca^{2+} induced apoptosis *via* activating p38MAPK signaling pathways in murine macrophage cells (22). Besides, IL-1 β gene expression was upregulated by MOS in European sea bass (23). And occludin expression could be decreased by IL-1 β in Caco-2 cells (24). These intriguing observations implicate a probably delicate link between MOS and fish skin physical barrier, and the underlying mechanism warrants further exploration.

Fish physical barrier function of the skin is also associated with the immune barrier function, which is closely related to

antimicrobial compounds [such as lysozyme (LZ), complement 3 (C3), and immunoglobulins (Ig)] and inflammatory cytokines (25–27). However, available literature describing the skin barrier's function affected by MOS supplementation after pathogen infections is particularly scarce. A study in human macrophages showed that cytokines were mediated by nuclear factor kappa B (NF κ B) (28) and the target of rapamycin (TOR) signaling pathways (29). It has been reported that MOS increased the digestibility of protein in the ileum of piglets (30). Our lab's previous work in grass carp confirmed that protein increased the activity of LZ and the concentration of C3 (31). A study on weaned piglets demonstrated that fed MOS diet could enhance the digestibility of phosphorus in ileum (30). Another study from our lab in grass carp described that phosphorus could upregulate interleukin 15 (IL-15) expression, which is regulated by the TOR signaling pathway (32). Furthermore, Pinheiro et al. (33) demonstrated that MOS increased butyrate concentration in growing rabbit cecum. It was of note that butyrate could inhibit the activation of the NF κ B signaling pathway in grass carp (34). All of these studies imply that MOS might regulate skin immune barrier function *via* acting on multiple pathways, the mechanism of which is worth in-depth exploration.

Based on the lab's previous MOS study of growth and intestinal health (35), the objectives of the present study were to elaborate on the protective effects of dietary MOS supplementation on the skin barrier function of on-growing grass carp under the condition of pathogen infection. For this purpose, this work explores the influence of MOS on antioxidant parameters, apoptosis parameters, tight junction (TJ) proteins, antibacterial compounds, and cytokines, as well as the possible signal molecule Nrf2, p38MAPK, MLCK, NF κ B, and TOR in the skin of grass carp after being challenged with *Aeromonas hydrophila* for the first time. Furthermore, as we all know, the grass carp is a broadly distributed species over the world (36). These results will shed new light on the understanding of freshwater fish defense mechanisms to bacterial pathogens, and also provide a more effective alternative reference for antibiotics.

MATERIALS AND METHODS

Study Design

The method of MOS (Sciphar Hi-Tech Industry, Xi'an, purity: 99.12%) diet preparation and storage was based on our published work (35, 37). The experimental diet formulation and proximate composition analyses are displayed in **Supplementary Table 1**. The different levels of MOS (0, 200, 400, 600, 800, and 1,000 mg kg⁻¹) were added to the control diet in place of cornstarch. All completed diets were stored at 4°C until feeding.

Determination of Antioxidant Properties

MOS antioxidant properties were determined mainly by the kit list in **Supplementary Table 2**. In short, DPPH, $\cdot\text{O}_2^{\cdot-}$ (ASA), and $\cdot\text{OH}$ (AHR) radical scavenging activities of MOS at different levels were determined to reflect the antioxidant properties of MOS *in vitro*.

The method used is spectrophotometry as previously described (38, 39).

Animals and Experimental Management

The guidelines for the Laboratory Animals Care and Use of Animal Nutrition Institute (LACUANI), Sichuan Agricultural University were strictly followed (permit no. LZY-2018114005) during the whole feeding trial. All healthy on-growing grass carp were obtained from Tong Wei fisheries (Sichuan, China) and acclimated to the fishpond culture condition for a month before the experiment. A total of 540 individuals (215.85 ± 0.30 g) were randomized to 18 nylon cages ($n=30$), and the feeding frequency and experimental period had the same description as our previous study (35). Routine test control parameters were as follows: dissolved oxygen > 6.0 mg L^{-1} , water temperature at $28.5 \pm 2.0^{\circ}C$, pH value 7.5 ± 0.3 , and experiment condition with a natural light cycle during the whole experimental period.

Challenge Test

After the growth trial, a 14-day challenge test (CT) was conducted to study the effect of dietary MOS on the fish skin barrier function according to our published work (35). Briefly, randomly selected five fish per replicates from each MOS group were intraperitoneally injected with 1.0 ml *A. hydrophila* (FDL20120711), and the concentration of bacteria is 2.5×10^8 colony-forming units (CFU) ml^{-1} . Concurrently, the saline group was injected with the same amount of normal saline. The situation and management were in line with the feeding trial. In a previous study, we successfully establish the *A. hydrophila* challenge model.

Sampling and Biochemical Parameter Analysis

At the end of the CT, all grass carp were anesthetized in a benzocaine bath according to LACUANI requirements. Then fish skin was rapidly collected and temporarily stored in liquid nitrogen. Finally, the sample was stored at $-80^{\circ}C$ for later analysis. The methods of the skin lesion morbidity scoring system were from a previous study (40). For the determination of physical and immune barrier-related parameters, 10% (w/v) of skin tissue homogenates were prepared with saline ($4^{\circ}C$) and centrifuged (6,000 g, 20 min). Then the supernatant was collected. The biomarkers and related enzyme activity analysis methods are shown in **Supplementary Table 2**.

DNA Fragment Analysis

The fragmented DNA of the skin tissue was isolated as previously described (41). And then, DNA was extracted following the instructions and analyzed on a 2% agarose gel to verify DNA fragmentation. Electrophoresis duration and related parameters were 90 min and 80 V, respectively. Finally, Gene Genius (Syngene, Frederick, MD, USA) is used to analyze the results of visualizations.

Real-Time PCR

qRT-PCR was conducted to refer to the method from our previous work (35). In short, the total RNA of skin samples

was isolated by using an RNAiso Plus Kit (Takara, Dalian, China). RNA quality was assessed by 1% agarose gel electrophoresis and quantified by spectrophotometry at 260/280 nm using Nanodrop 2000 (Thermo Scientific, USA). Afterward, RNA was reverse-transcribed into cDNA by using a PrimeScriptTM RT reagent kit (Takara, Dalian, China). For qRT-PCR, specific primers were designed according to the sequences we cloned (**Supplementary Table 3**). Our preliminary experiment screened four internal reference genes and finally selected β -Actin and GAPDH as previously described (35, 42). Preparation of melting curves and calculation of amplification efficiency of target genes were according to the manufacturer's instruction. The gene transcription level was calculated as described by the method ($2^{-\Delta\Delta CT}$) from Livak and Schmittgen (43).

Western Blot Analysis

Preparation method-related parameters of skin homogenates, primary and second antibodies, and blotting analysis were performed as our lab previously described (35, 44, 45). Extraction and determination of tissue protein were performed by using the RIPA and BCA assay kit (Beyotime). The prepared sample (40 μ g lane⁻¹) was separated by SDS-PAGE (10%) and transferred to a PVDF membrane. Membranes were incubated overnight with primary antibody (14 h, $4^{\circ}C$). Afterward, membranes were washed and secondary antibody was incubated (90 min, room temperature). Then, protein signals were visualized and quantified (NIH Image J, 1.42q) as previously described (35, 37). All antibodies' detailed information in the current study is listed in **Supplementary Table 4**.

Statistical Analysis Method

Before statistical analysis, the Shapiro–Wilk test of normality, as well as Levene's test of variance homogeneity, was conducted. All data underwent one-way analysis of variance (ANOVA) followed by Duncan's multiple comparisons at $P < 0.05$ with SPSS 25.0 (SPSS Inc., Chicago, IL, USA). Data visualization was done using the GraphPad 8.0 software (GraphPad Software, Inc.), R (v4.0.2), and Hiplot platform (<https://hiplot.com.com>).

RESULTS

Skin Morbidity and Phenotype

To investigate the effect of MOS on fish skin morbidity and phenotype with *A. hydrophila* challenge, we performed intraperitoneal injection of bacteria solution. We obtained the results of skin morbidity and phenotype as showed in **Figure 1**; compared to the control (14.40%), the morbidity of skin hemorrhages and lesions after being challenged was significantly decreased with MOS at 400 mg kg^{-1} diet. At this optimal MOS supplementation, the skin morbidity was reduced to a minimum 8.27% ($P < 0.05$). Then, it showed an upward trend (from 9.87% to 13.33%, $P < 0.05$) with the increase in MOS (600–1000 mg kg^{-1}). These results suggest that the optimal level of MOS could effectively reduce skin morbidity.

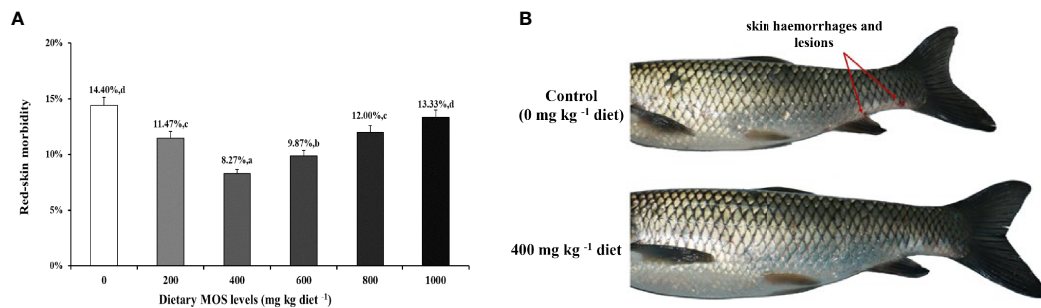


FIGURE 1 | MOS alleviates skin damage of on-growing grass carp after infection of *Aeromonas hydrophila*. **(A)** The red-skin morbidity of fish. Data were represented as the mean \pm SD. N = 15 for each MOS level; different letters above bars indicate significant differences ($P < 0.05$). **(B)** The apparent symptoms (red arrow, hemorrhages, and lesions) of fish skin.

Antioxidant Properties of MOS

To investigate whether MOS have antioxidant properties *in vitro*, we designed MOS with different concentrations to test their antioxidant properties (**Supplementary Figure 1**). Our results showed that the free radical scavenging rate (DPPH, ASA, and AHR) increased gradually (from 0 to 60%) with the increase in the dosage of MOS (from 0 to 5 mg ml⁻¹) in a dose-dependent manner. These data suggest that MOS has excellent antioxidant properties.

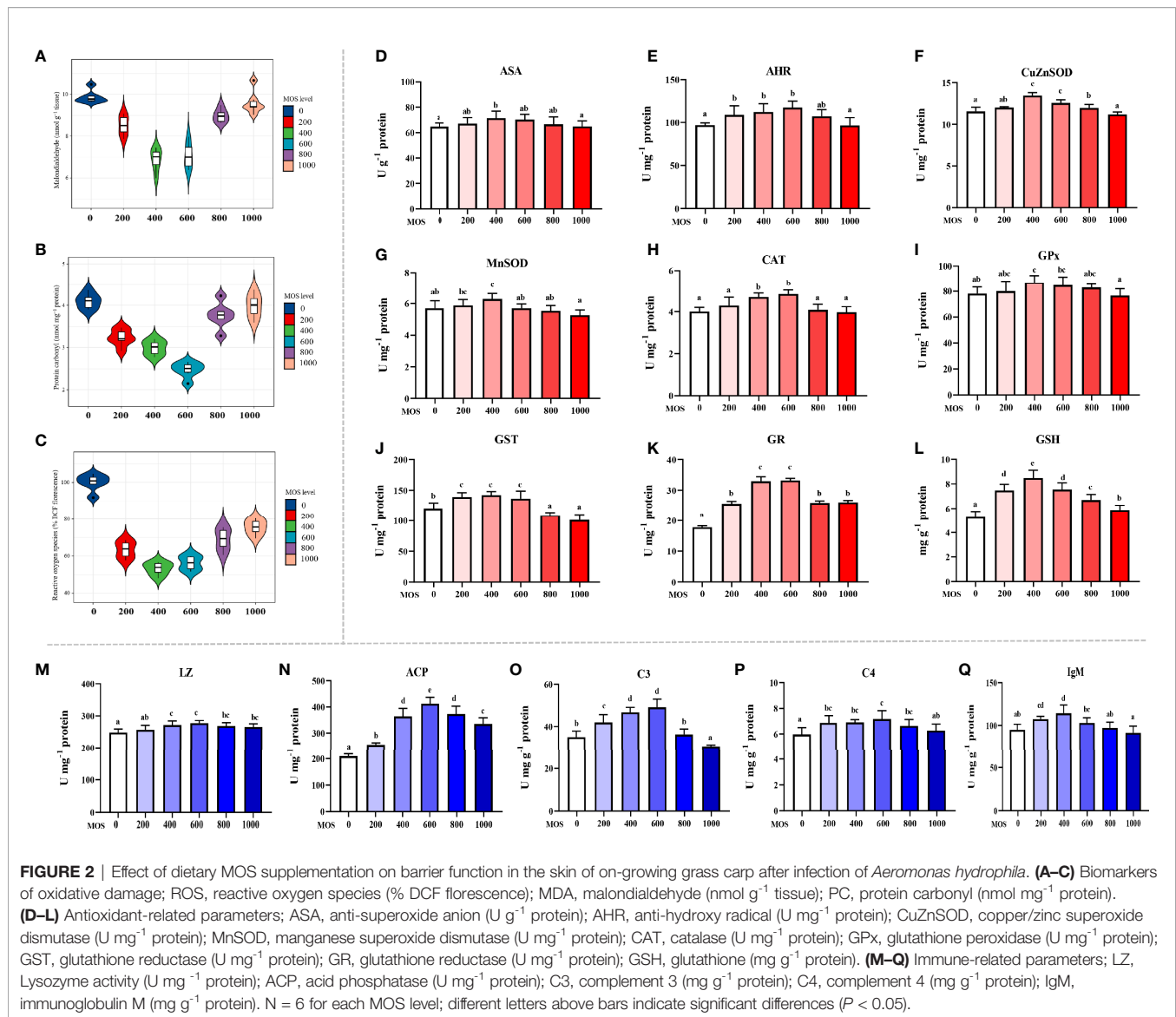
Biochemical Analysis Parameters

To uncover the MOS effect on fish skin antioxidant capacity with *A. hydrophila* challenge, we determined the content of oxidative damage biomarkers and the activity of key antioxidant enzymes (**Figures 2A–L**). Oxidative damage biomarkers are indicators that reflect the state of oxidative damage. In **Figures 2A–E**, compared with the control diet (ROS: 100% DCF fluorescence; MDA: 9.88 nmol g⁻¹ tissue; ASA: 64.71 U g⁻¹ protein), the ROS and MDA contents were decreased, the ASA were increased with the MOS supplementation, and ROS and MDA reached their minimum value (ROS: 53.20% DCF fluorescence; MDA: 6.88 nmol g⁻¹ tissue, $P < 0.05$), whereas ASA reached its maximum value (ASA: 71.46 U g⁻¹ protein, $P < 0.05$) with 400 mg kg⁻¹ MOS supplementation. Then ROS and MDA showed an upward trend (ROS: from 56.08 to 75.50% DCF fluorescence, $P < 0.05$; MDA: from 7.07 to 9.60 nmol g⁻¹ tissue), and ASA showed a downward trend (ASA: from 70.28 to 64.94 U g⁻¹ protein) with the increase in MOS (600–1,000 mg kg⁻¹). The PC contents were significantly decreased, and the AHR were increased with MOS supplementation with MOS at 600 mg kg⁻¹ diet; at this optimal MOS supplementation, the PC content was obviously reduced to a minimum 2.47 nmol mg⁻¹ protein, and AHR was increased to a maximum 117.4 U mg⁻¹ protein ($P < 0.05$) compared with the control group (PC: 4.10 nmol mg⁻¹ protein; AHR: 97.12 U mg⁻¹ protein). Then PC showed an upward trend (from 3.76 to 3.98 nmol mg⁻¹ protein), and AHR showed a downward trend (from 66.52 to 64.94 U mg⁻¹ protein) with the increase in MOS (800–1,000 mg kg⁻¹). These data suggest that the MOS could effectively alleviate oxidative damage caused by *A. hydrophila*.

Antioxidant enzymes are key proteins that scavenge free radicals, and their activities reflect antioxidant capacity.

Figures 2F–L presents the results obtained from the biochemical analysis of the antioxidant enzymes and non-enzymatic antioxidants (GSH). Compared with the control diet (CuZnSOD: 5.85 U mg⁻¹ protein; MnSOD: 5.70 U mg⁻¹ protein; GPx: 78.00 U g⁻¹ protein; GST: 120.54 U mg⁻¹ protein, GSH: 5.28 mg g⁻¹ protein), the activity of CuZnSOD, MnSOD, GPx, and GST and the content of GSH were increased with the MOS supplementation, and all of them reached their maximum value (CuZnSOD: 7.18 U mg⁻¹ protein; MnSOD: 6.28 U mg⁻¹ protein; GPx: 87.11 U g⁻¹ protein; GST: 142.34 U mg⁻¹ protein, GSH: 8.49 mg g⁻¹ protein, $P < 0.05$) with 400 mg kg⁻¹ MOS supplementation. Then all of them showed a downward trend (CuZnSOD: from 6.84 to 5.94 U mg⁻¹ protein; MnSOD: from 5.71 to 5.26 U mg⁻¹ protein; GPx: from 84.77 to 76.73 U mg⁻¹ protein; GST: from 136.80 to 101.19 U mg⁻¹ protein; GSH: from 7.55 to 5.88 mg g⁻¹ protein) with the increase in MOS (600–1,000 mg kg⁻¹). The activity of CAT and GR increased with the MOS supplementation, and both of them reached their maximum value (CAT: 4.85 U mg⁻¹ protein; GR: 33.23 U mg⁻¹ protein, $P < 0.05$) with 600 mg kg⁻¹ MOS supplementation compared with the control group (CAT: 4.01 U mg⁻¹ protein; GR: 17.79 U mg⁻¹ protein). Then both of them showed a downward trend (CAT: from 4.09 to 3.98 U mg⁻¹ protein; GR: from 25.90 to 26.12 U mg⁻¹ protein) with the increase in MOS (800–1,000 mg kg⁻¹).

The antimicrobial compound-related parameters are displayed in **Figures 2M–Q**. Compared with the control (LZ: 248.64 U mg⁻¹ protein; ACP: 209.33 U mg⁻¹ protein; C3: 35.01 mg g⁻¹ protein; C4: 5.97 mg g⁻¹ protein), the activity of LZ and ACP and the contents of C3 and C4 were increased with the MOS supplementation. And all of them reached their maximum value (LZ: 277.72 U mg⁻¹ protein; ACP: 412.41 U mg⁻¹ protein; C3: 49.19 mg g⁻¹ protein; C4: 7.17 mg g⁻¹ protein, $P < 0.05$) with 600 mg kg⁻¹ MOS supplementation. Then all of them showed a downward trend (LZ: from 269.13 to 265.80 U mg⁻¹ protein; ACP: from 373.30 to 335.22 U mg⁻¹ protein; C3: from 36.29 to 30.57 mg g⁻¹ protein; C4: from 6.65 to 6.28 mg g⁻¹ protein) with the increase in MOS (800–1,000 mg kg⁻¹). The IgM content was significantly increased with MOS supplementation with MOS at



400 mg kg⁻¹ diet; at this optimal MOS supplementation, the IgM content was obviously increased to a maximum 114.49 mg g⁻¹ protein ($P < 0.05$) compared with the control group (IgM: 94.90 mg g⁻¹ protein). Then it showed a downward trend (IgM: from 103.00 to 91.59 mg g⁻¹ protein) with the increase in MOS (600–1,000 mg kg⁻¹).

Skin Physic Barrier Function Gene Expression

To further determine the MOS effect on fish skin physic barrier function with *A. hydrophila* challenge, the mRNA expression of the antioxidant, apoptosis, and tight junction-related gene was examined by real-time RT-PCR (**Figures 3A–C**). The enzymatic antioxidant pathway is an important part of the antioxidant system in fish (46). **Figure 3A** provides the heat map of the antioxidant-related gene expression. In comparison with the control group, almost all antioxidant enzyme-related isoforms,

CuZnSOD (1.84-fold change), *MnSOD* (1.70-fold change), *CAT* (1.98-fold change), *GR* (1.79-fold change), *GPx1a* (1.69-fold change), *GPx1b* (1.63-fold change), *GPx4a* (1.69-fold change), *GSTp1* (1.49-fold change), *GSTp2* (1.61-fold change), and *GSTo1* (1.65-fold change), were significantly upregulated with optimal MOS supplementation up to 400 mg kg⁻¹ ($P < 0.05$), and *GPx4b* (1.87-fold change), *GSTo2* (1.81-fold change), and *GSTR* (1.53-fold change) were significantly upregulated with optimal MOS supplementation up to 600 mg kg⁻¹ ($P < 0.05$); then all of them followed a gradual downward trend with the increase in MOS (600–1,000 mg kg⁻¹ or 800–1,000 mg kg⁻¹). Furthermore, the key transcriptional factor *Nrf2* mRNA levels (1.88-fold change) were significantly upregulated with optimal MOS supplementation up to 400 mg kg⁻¹ ($P > 0.05$), followed by a gradual downward trend with the increase in MOS (600–1,000 mg kg⁻¹). Conversely, the *keap1a* (0.56-fold change) mRNA level had a significant downward trend with 400 mg kg⁻¹ MOS supplementation ($P > 0.05$).

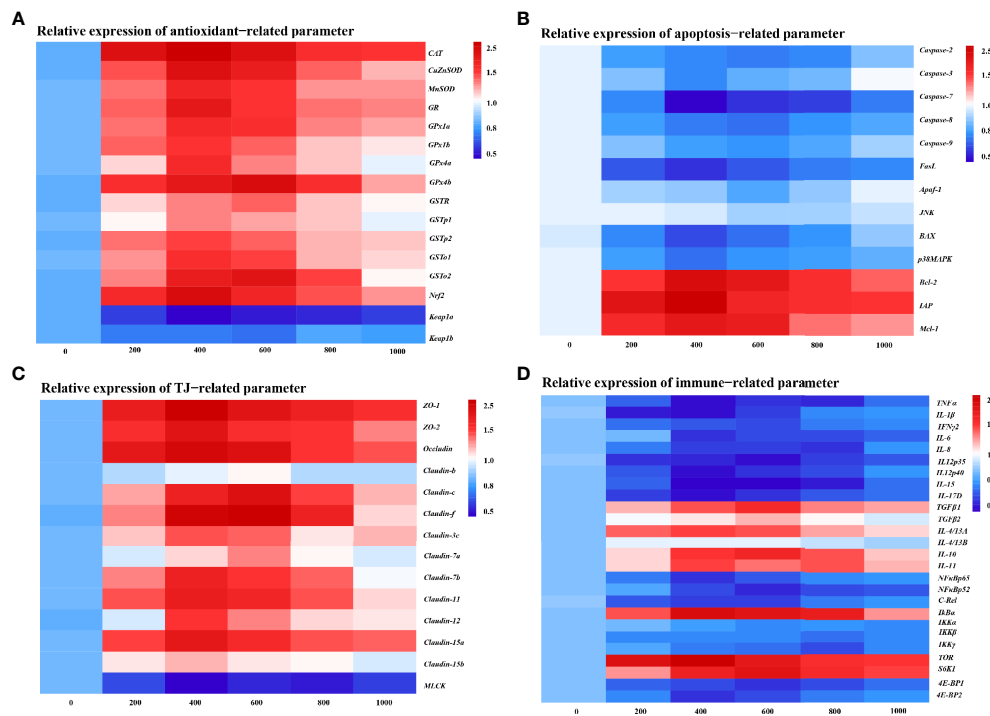


FIGURE 3 | Heat map of MOS (mg kg⁻¹ diet) changed expression of antioxidant (A), apoptosis (B), TJs (C), and immune (D) related parameters in the skin of on-growing grass carp after infection of *Aeromonas hydrophila*. The signal values of upregulation (red) and downregulation (blue) were expressed and ranged from 0.5 to 2.5 folds.

and then plateaued. However, one of the interesting results we found was that the MOS supplementation did not affect *keap1b* mRNA levels. As expected, our antioxidant gene expression data were consistent with enzyme activities results, suggesting that the optimal level of MOS could enhance the antioxidant capacity of fish skin under *A. hydrophila* challenge.

We investigated the effect of MOS on the apoptosis level by DNA fragmentation and determination of apoptotic pathway gene expression (Supplementary Figure 2 and Figure 3B). Supplementary Figure 2 provides the visualization results that revealed that skin DNA showed an obvious fragmentation after being challenged (control group). Interestingly, MOS supplementation (600 and 800 mg kg⁻¹) performed the obvious reduction of DNA fragmentation. In Figure 3B, our results showed that compared with the control, the pro-apoptotic factors, *Caspase-3* (0.67-fold change), *Caspase-7* (0.31-fold change), *FasL* (0.44-fold change), *BAX* (0.51-fold change), and *p38MAPK* (0.61-fold change), were significantly downregulated with optimal MOS supplementation up to 400 mg kg⁻¹ ($P < 0.05$), and *Caspase-2* (0.62-fold change), *Caspase-8* (0.61-fold change), *Caspase-9* (0.68-fold change), and *Apaf-1* (0.75-fold change) were significantly downregulated with optimal MOS supplementation up to 600 mg kg⁻¹ ($P < 0.05$); then all of them followed a gradual upward trend with the increase in MOS (600–1,000 mg kg⁻¹ or 800–1,000 mg kg⁻¹). The anti-apoptotic factors, *Bcl-2* (1.73-fold change), *IAP* (1.83-fold change), and *Mcl-1* (1.62-fold change), were significantly

upregulated with optimal MOS supplementation up to 400 mg kg⁻¹ ($P < 0.05$), and then all of them followed a gradual downward trend with the increase in MOS (600–1,000 mg kg⁻¹) compared with the control group. However, we found that the MOS supplementation did not affect *JNK* mRNA levels. These data suggest that the MOS could effectively inhibit fish skin excessive apoptosis caused by *A. hydrophila*.

The tight junction proteins contribute to the skin barrier function (47). In Figure 3C, our results showed that compared with the control, most TJ protein genes, *ZO-1* (1.95-fold change), *ZO-2* (1.80-fold change), *Occludin* (1.87-fold change), *Claudin-3c* (1.56-fold change), *Claudin-7b* (1.73-fold change), *Claudin-11* (1.74-fold change), *Claudin-12* (1.61-fold change), *Claudin-15a* (1.77-fold change), and *Claudin-15b* (1.39-fold change), were significantly upregulated with optimal MOS supplementation up to 400 mg kg⁻¹ ($P < 0.05$), and *Claudin-c* (1.83-fold change), *Claudin-f* (1.93-fold change), and *Claudin-7a* (1.46-fold change) were significantly upregulated with optimal MOS supplementation up to 600 mg kg⁻¹ ($P < 0.05$); then all of them followed a gradual downward trend with the increase in MOS (600–1,000 mg kg⁻¹ or 800–1,000 mg kg⁻¹). Furthermore, the key regulation molecules *MLCK* mRNA levels (0.58-fold change) were significantly downregulated with optimal MOS supplementation up to 400 mg kg⁻¹ ($P > 0.05$) and plateaued with the increase in MOS (600–1,000 mg kg⁻¹) compared with the control group. We also found that the MOS supplementation did not affect *Claudin-b* mRNA levels. These data suggest that MOS

could enhance tight junctions of fish skin under *A. hydrophila* challenge.

Skin Immune Barrier Function Gene Expression

To investigate the effect of MOS on fish skin immune barrier function with *A. hydrophila* challenge, the mRNA expression of the pro-inflammatory cytokines and anti-inflammatory cytokines and key signaling molecule gene was examined by real-time RT-PCR (**Figure 3D**). As is well known, inflammatory cytokines are crucial for fighting off infections and are involved in immune responses (48). In **Figure 3D**, compared with the control, the expression of pro-inflammatory cytokines, *IL-1 β* (0.48-fold change), *TNF- α* (0.50-fold change), *IL-6* (0.57-fold change), *IL-12p40* (0.48-fold change), *IL-15* (0.43-fold change), and *IL-17D* (0.47-fold change), was significantly downregulated with MOS supplementation up to 400 mg kg⁻¹ ($P < 0.05$), that of *IFN γ 2* (0.65-fold change) and *IL-12p35* (0.47-fold change) was significantly downregulated with MOS supplementation up to 600 mg kg⁻¹ ($P < 0.05$), and *IL-8* (0.58-fold change) was significantly downregulated with MOS supplementation up to 800 mg kg⁻¹ ($P < 0.05$), followed by a gradual upward trend or plateau with the increase in MOS (600–1,000 mg kg⁻¹). Besides, the anti-inflammatory cytokine factors *IL-4/13A* (1.64-fold change) and *IL-11* (1.66-fold change) were significantly upregulated with MOS supplementation up to 400 mg kg⁻¹ ($P > 0.05$), and *TGF β 1* (1.76-fold change), *TGF- β 2* (1.42-fold change), and *IL-10* (1.79-fold change) were significantly upregulated with MOS supplementation up to 600 mg kg⁻¹ ($P > 0.05$), followed by a gradual downward trend with the increase in MOS (600–1,000 mg kg⁻¹ or 800–1,000 mg kg⁻¹), compared with the control group. Our results showed that the MOS supplementation did not affect *IL-4/13B* mRNA levels.

Many inflammatory cytokines could be mediated by NF κ B and the TOR signaling pathway (29, 49). The present study displayed that compared with the control, the expression of inflammatory signal molecular-related genes, *NF κ Bp65* (0.57-fold change) and *4E-BP2* (0.59-fold change), was significantly downregulated with MOS supplementation up to 400 mg kg⁻¹, that of *NF κ Bp52* (0.55-fold change), *c-Rel* (0.61-fold change), and *4E-BP1* (0.58-fold change) was significantly downregulated with MOS supplementation up to 600 mg kg⁻¹, and that of *IKK β* (0.75-fold change) and *IKK γ* (0.64-fold change) was significantly downregulated with MOS supplementation up to 800 mg kg⁻¹, followed by a gradual upward trend with the increase in MOS (600–1,000 mg kg⁻¹). Besides, *I κ B α* (1.98-fold change) and *TOR* (2.11-fold change) were significantly upregulated with MOS supplementation up to 400 mg kg⁻¹, and *S6K1* (1.92-fold change) was significantly upregulated with MOS supplementation up to 600 mg kg⁻¹, followed by a gradual downward trend with the increase in MOS (600–1,000 mg kg⁻¹), compared with the control group. Our results showed that the MOS supplementation did not affect *IKK α* mRNA levels. These results suggest that MOS is involved in the regulation of inflammatory cytokines under *A. hydrophila* challenge.

Correlation Analysis

To investigate the correlation between the expression of genes related to the skin barrier function and the signal molecules involved in regulation, correlation analysis was performed. **Figures 4A–D** provides the diagram of the correlation analysis. These data showed the gene expression correlation analyses of physic barrier-related parameters and immune barrier-related parameters. Gene expression of studied antioxidant enzymes revealed a positive correlation with *Nrf2* mRNA levels, whereas *Keap1a* and *Keap1b* revealed a negative correlation. Gene expression of the studied pro-apoptotic factor showed a positive correlation with p38MAPK, whereas the anti-apoptotic factor showed a negative correlation. Gene expression of studied TJ proteins (except *Claudin-b*) showed a negative correlation with *MLCK*. Besides, gene expression of studied pro-inflammatory cytokine factors presented a positive correlation with NF κ B, and the anti-inflammatory cytokine presented a positive correlation with *TOR*.

Key Role Protein Levels of Skin Barrier Function

To verify the results of skin barrier gene expression, we further performed Western blot analysis to test several key regulatory signaling molecules. The protein expression of Nrf2, TOR, and NF κ B p65 in the skin of fish is exhibited in **Figures 5A–C**, respectively.

Compared with the control group, the nuclear Nrf2 (1.42-fold change) in the skin of fish was elevated with MOS supplementation up to 400 mg kg⁻¹ ($P > 0.05$) and then plateaued with MOS supplementation up to 1,000 mg kg⁻¹. Besides, fish fed with 600 and 400 mg kg⁻¹ MOS presented the maximum p-TOR Ser2448 (1.80-fold change) and total TOR (T-TOR) (1.33-fold change) expression ($P < 0.05$), respectively, and then gradually decreased with MOS supplementation up to 1,000 mg kg⁻¹ compared with the control group. With dietary MOS supplementation up to 600 mg kg⁻¹, NF κ B p65 expression (0.70-fold change) weakened obviously ($P < 0.05$) and then gradually increased with MOS supplementation up to 1,000 mg kg⁻¹. As expected, these results of protein expression were consistent with those of gene expression.

DISCUSSION

This research used the same growth trial from our previous work in grass carp (35), which is a part of a larger study conducted to investigate the protective effect of fish skin barrier function by MOS supplementation. Our previous works have demonstrated that optimal MOS supplementation could promote fish growth and improve multiple functional organs (such as intestine, head-kidney, and spleen) health (35, 37). As is well known, fish growth and development are closely related to skin health (1). Therefore, to investigate the effects of prebiotics on fish skin health, we conducted relevant experiments based on previous studies.

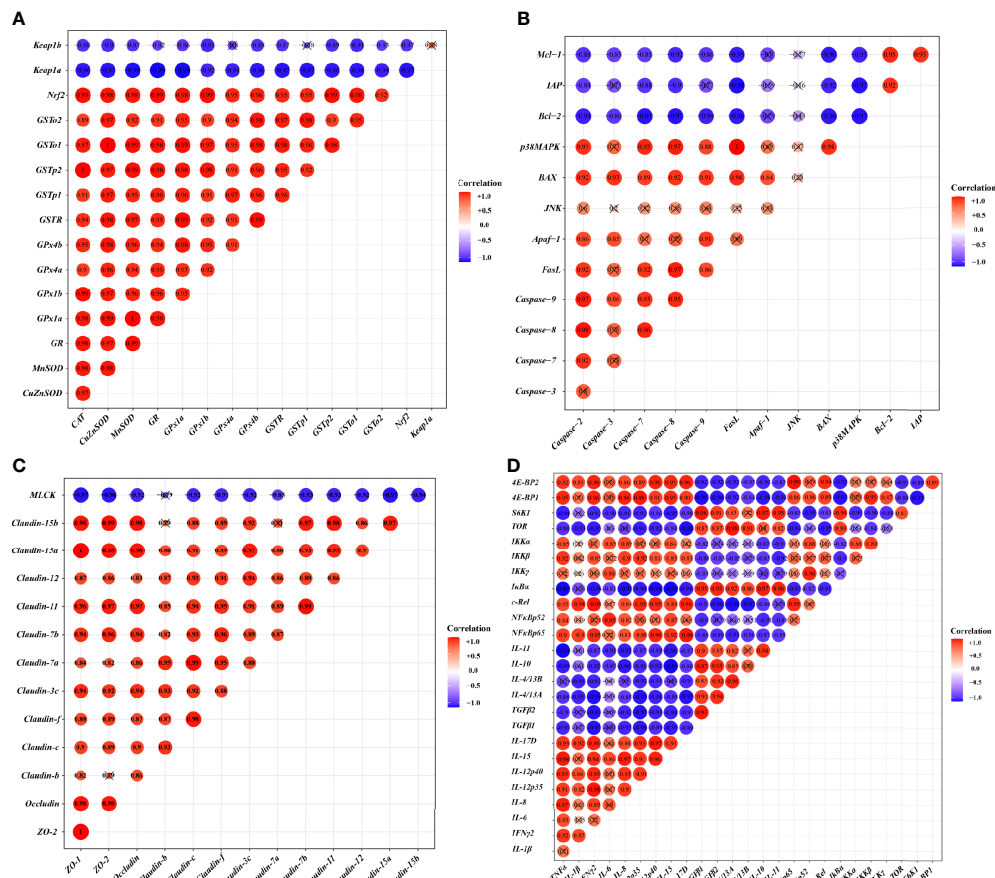


FIGURE 4 | Correlation analysis of parameters in the skin of on-growing grass carp after infection of *Aeromonas hydrophila*. Antioxidant (A), apoptosis (B), TJs (C), and immune (D) of on-growing grass carp after infection of *Aeromonas hydrophila*.

MOS Supplementation Enhanced Skin Disease Resistance

As is well known, skin health is mainly reflected by disease resistance (50). *Aeromonas hydrophila* is one of the most common pathogenic microorganisms associated with the aquatic environment, which could cause skin lesions in fish (51). In this study, our results displayed that optimal MOS (400 mg kg⁻¹) could decrease skin lesion morbidity (8.27%) after being challenged while the control group caused skin lesion morbidity (14.40%), indicating that MOS supplementation enhanced fish resistance against skin lesions. Our data also showed that MOS supplementation attenuated skin hemorrhages and lesions, which suggested that MOS supplementation enhanced the ability to resist *A. hydrophila* invasion. Based on the quadratic regression analysis, the recommend suitable MOS supplementation against skin lesions morbidity was estimated to be 508.2 mg kg⁻¹. Generally, skin health is closely related to physical barriers and immune barriers in fish (1). Therefore, at first, we investigated the effects of MOS supplementation on physical barrier function in the skin of on-growing grass carp.

MOS Supplementation Enhanced Skin Physical Barrier Function

As mention above, the physical barrier function of the skin is related to cellular integrity and intercellular integrity, which were related to antioxidant capacity, apoptosis, and tight junction. Generally, MDA and PC were usually recognized to reflect the level of cell damage resulting from reactive oxygen (ROS) metabolites, which could be reduced by the antioxidant system (52, 53). We found that optimal MOS dosage decreased the biomarker content of oxidative damage of lipid and protein, whereas it enhanced the antioxidant enzyme activities. These data implied that MOS supplementation enhanced the antioxidant capacity to inhibit oxidative damage in fish skin. In general, antioxidant enzyme activities were strongly associated with their corresponding mRNA gene expression (54). We found that antioxidant enzymes and related isoform gene expression were upregulated by optimal MOS supplementation in the skin, indicating that MOS-enhanced activity of the antioxidant enzyme might be partly related to the upregulation of their mRNA levels. To our knowledge, Nrf2 is a major factor accounting for promoting the expression of various antioxidant

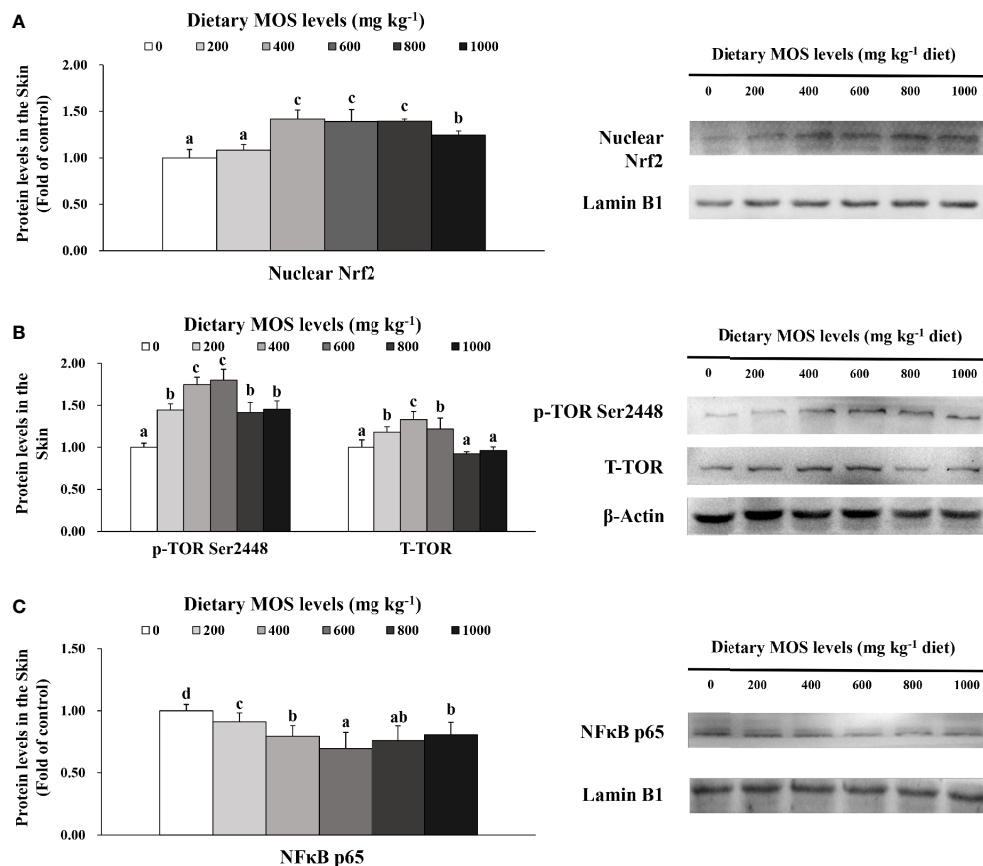


FIGURE 5 | Western blot analysis of nuclear Nrf2 (A), p-TOR Ser2448 (B) and NFκBp65 (C) protein levels in the skin of on-growing grass carp after infection of *Aeromonas hydrophila*. Data represent means of three fish in each group, error bars indicate S.D. Values having different letters are significantly different ($P < 0.05$).

enzyme genes to defend against oxidative stress, which is degenerated by Keap1 in the nucleus (55, 56). A study on mice liver showed that the Nrf2 protein level in the nucleus could evaluate the nuclear translocation of Nrf2 (57). Our result showed that MOS supplementation upregulated *Nrf2* and downregulated *Keap1a* (rather than *Keap1b*) and increased the protein levels of nucleus Nrf2, suggesting that MOS supplementation activated the Nrf2 signaling pathway by the activation of Nrf2 nuclear translocation in the skin. Notably, we found that MOS only downregulated the *Keap1a* expression in the skin, which might be partly relevant to threonine. A study on piglets revealed that threonine absorbed from the intestine could be enhanced by MOS supplementation (58). Our lab previously has confirmed that threonine has no influence on *Keap1b* gene expression in the grass carp gill (59). Thus, these data might partially support our hypothesis. However, the specific mechanism needs further investigation. In addition, a study reported that excessive oxidative damage could induce cell apoptosis in MN9D cells (60). Therefore, we further examined the effects of MOS supplementation on fish skin apoptosis.

Apoptosis, a tightly controlled physiological process, and internal environment homeostasis, plays important roles not only in the normal development and homeostasis of organisms

but also in the pathogenesis of bacterial infections (61). However, excessive apoptosis could destroy the physical barrier of the skin in fish (62). In mammals, there are two major apoptosis pathways, the death receptor pathway (FasL/caspase-8) and the mitochondria pathway [(Bcl-2, Mcl-1, and Bax)/Apaf-1/caspase-9], which were modulated by signal molecule p38MAPK and JNK (63–65). These two apoptosis pathways converge on caspase-3 activation, which is the key apoptotic protein. As is well known, the apoptosis-related protein includes the apoptotic promoter (caspase-8 and caspase-9) and effector (caspase-3 and caspase-7). In addition, DNA fragmentation is a hallmark of apoptosis (66). The visualization of apparent index results clearly showed that the level of apoptosis was significantly reduced with MOS supplementation. Our gene expression results also displayed that the optimal MOS supplementation could suppress the excess apoptosis process under-challenged, which was partly associated with p38MAPK (not JNK), leading to the inhibition of both apoptosis pathways in fish skin. As mentioned above, intercellular structure integrity also played a crucial role in the physical barrier, which is associated with TJ proteins (67). Thus, we next examined the influences of MOS supplementation on TJs as well as the related signaling pathway in fish skin.

The intercellular junction complex function has maintained the integrity of the skin barrier, which mainly consists of TJ proteins (68, 69). It has been reported that inhibition of *MLCK* expression could improve epithelial TJ barrier function in Caco-2 cells (70). Our result displayed that optimal MOS upregulated the expression of most of the tight junction proteins (except *claudin-b*) and downregulated *MLCK*, suggesting that MOS improved tight junction partly by inhibiting the *MLCK* signaling pathway. We surprisingly found that MOS did not affect *claudin-b* gene expression, which could involve both IL-6 and cortisol. Our result exhibited that MOS supplementation could downregulate *IL-6* gene expression. Steensberg et al. (71) confirmed that IL-6 could increase the content of cortisol in humans. Studies showed that cortisol did not affect *claudin-b* mRNA levels in the gill epithelial cell of pufferfish and goldfish (72, 73), which supports our hypothesis. However, determining the underlying mechanism warrants further investigation.

MOS Supplementation Enhanced Skin Immune Barrier Function

To our knowledge, the existence and function of the secretory cell in teleost skin (such as mucous goblet cells, squamous cells, pigment cells, and so on) have been confirmed and provided the first line of defense against pathogen invasion (1, 74). The mucus secreted by these cells contains a large number of antimicrobial substances (75, 76). Previous studies have demonstrated that MOS can increase the LZ activity and bactericidal activity in the skin of greater amberjack (13). The present study focuses on antibacterial compounds, and the results revealed that MOS could promote LZ production in the skin of grass carp, agreeing with previous findings in the skin of greater amberjack. Coincidentally, we also found a study that showed that other prebiotics also has antimicrobial properties, which reported the antimicrobial ability to be enhanced in the skin of Caspian white fish (*Rutilus frisii kutum*) with xylooligosaccharide (77). These interesting results partly reflect the commonality of prebiotic to improve skin antimicrobial capacity. In addition, the skin immune function is closely related to the inflammatory response mediated by cytokines (14). Thus, we next examined the effects of MOS supplementation on fish skin immune barrier function.

In the immune system, there is a dynamic balance between pro-inflammatory cytokines and anti-inflammatory cytokines. The imbalance of inflammatory cytokines caused by external stimuli (pathogenic bacteria) is one of the causes of the excessive inflammatory response (78). A study on channel catfish, *Ictalurus punctatus*, revealed that Actigen® (a commercial MOS product from Alltech) could improve inflammatory cytokine balance in multiple mucosal immune organs by using RNA-seq, indicating that MOS additives may provide protection extending beyond the intestine to surface mucosa (79). As we expected, our result displayed that optimal MOS dosage downregulated pro-inflammatory cytokine expression; in contrast to the former, the anti-inflammatory cytokine (except *IL-4/13B*) expression was upregulated, indicating that MOS supplementation attenuated the inflammation in fish skin. Notably, part of these data differed with other similar studies

(parasite challenged) in the skin of greater amberjack, which found that *TNF α* , *IL-1 β* , *IFN γ* , and *IL-8* were upregulated by MOS supplementation (2 g kg⁻¹) (13). Differences in species, MOS purity, and challenged type might account for this disparity. Notably, another interesting result showed that dietary MOS only upregulated *IL-4/13A* expression in the skin. This phenomenon might be associated with the content of phosphorus. A study on weaned piglets confirmed that MOS increased the digestibility of phosphorus (30). Past work in our lab has confirmed that phosphorus has no effect on the *IL-4/13B* expression, and our results also showed that dietary MOS did the same effect on *IL-4/13B* expression (32). Thus, we speculated that MOS supplementation upregulates the *IL-4/13A* (rather than *IL-4/13B*), which might relate to improving the digestibility of phosphorus, thus leading to a disposition of only upregulated *IL-4/13A* in fish.

As we all know, the pro-inflammatory cytokines could be activated by the NF κ B family of transcription factors (such as NF κ B p65, p52, and c-Rel), which required a sequestering protein named I κ B α that could be catalyzed by the IKK complex (IKK α , IKK β , and IKK γ) (80, 81). We found that optimal MOS supplementation downregulated NF κ B-related signal molecule (rather than IKK α) gene expression and decreased the protein levels of NF κ B p65, suggesting that MOS supplementation activated the NF κ B signaling pathway by decreasing the nuclear NF κ B p65 protein expression in the skin. Interestingly, what is noteworthy of this study is that MOS supplementation did not have influence on IKK α in the skin; the possible reasons for this difference might be due to TNF- α and PKC ζ . Our result revealed that MOS could downregulate TNF- α expression. A study on rat showed that downregulated TNF- α expression could decrease the activity of PKC ζ (82), which could downregulate IKK β and IKK γ (rather than IKK α) expression in Kupffer cells, and did not have an effect on IKK α expression (83), supporting our hypothesis. However, the underlying molecular mechanism is still unknown and warrants further investigation. In addition, it has been reported that anti-inflammatory cytokines could be modulated by the mTOR/(S6K1, 4EBP-1) signaling cascades in humans (84). One study on rainbow trout reported that the phosphorylation of TOR on residue Ser2448 can be used to monitor the activation of TOR signaling (85). We found that MOS supplementation downregulated *4EBP-1* and *4EBP-2* gene expression and upregulated *TOR* and *S6K1* expression, and increased the protein levels of TOR and p-TOR Ser2448, suggesting that MOS supplementation upregulated the anti-inflammatory cytokine mRNA levels partly due to the activation of the TOR signaling pathway cascades in fish skin.

In summary, the current work presented a clear outline of dietary MOS enhanced fish skin immune barrier and physical barrier function after infection with *A. hydrophila*. Our study confirmed that dietary MOS supplementation could improve the status of skin health, as demonstrated by the following findings (1): MOS supplementation enhanced the immune barrier function *via* increasing the skin disease resistance, producing antibacterial compounds and immunoglobulins, upregulating anti-

inflammatory cytokines (except *IL-4/13B*), and downregulating pro-inflammatory cytokines gene expression (2). MOS supplementation protected the physical barrier function *via* increasing the antioxidant capacity, inhibited excessive apoptosis, and enhanced the tight junction barriers (except *claudin-b*). Moreover, MOS supplementation improved fish physical and immune barrier function by modulating multiple signaling pathways (such as Nrf2, TOR, NFκB, and so on).

DATA AVAILABILITY STATEMENT

The original contributions presented in the study are included in the article/**Supplementary Material**. Further inquiries can be directed to the corresponding author.

ETHICS STATEMENT

The animal study was reviewed and approved by Laboratory Animals Care and Use of Animal Nutrition Institute of Sichuan Agricultural University.

AUTHOR CONTRIBUTIONS

ZyL performed formal analysis, investigation and writing original draft. LF performed conceptualization, funding acquisition and supervision. W-DJ performed data curation, validation, project administration and writing review & editing. PW performed conceptualization, methodology, validation, data curation and project administration. YL and JJ performed project

administration. S-YK, LT, S-WL, C-BZ performed resources. X-QZ performed conceptualization, designed experiment, supervision and funding acquisition. All authors contributed to the article and approved the submitted version.

FUNDING

This research was financially supported by the National Key R&D Program of China (2019YFD0900200 and 2018YFD0900400), the National Natural Science Foundation of China for Outstanding Youth Science Foundation (31922086), and the Young Top-Notch Talent Support Program, Supported by China Agriculture Research System of MOF and MARA (CARS-45), and supported by Sichuan Science and Technology Program (2019YFN0036). The authors would like to thank the personnel of these teams for their kind assistance.

SUPPLEMENTARY MATERIAL

The Supplementary Material for this article can be found online at: <https://www.frontiersin.org/articles/10.3389/fimmu.2021.742107/full#supplementary-material>

Supplementary Figure 1 | Antioxidative activities of MOS with different levels.

(A) 2,2-diphenyl-1-picrylhydrazyl (DPPH) radical scavenging activity. (B) $\cdot\text{O}_2$ radical scavenging activity. (C) $\cdot\text{OH}$ scavenging activity.

Supplementary Figure 2 | DNA fragmentation analysis in the skin of on-growing grass carp after infection of *Aeromonas hydrophila*. Lane 1: maker. Lane 2–Lane 6: levels of dietary MOS were 0, 200, 400, 600, 800 and 1000 mg kg^{-1} , respectively. This experiment was repeated three times with similar results achieved.

REFERENCES

- Ángeles Esteban M. An Overview of the Immunological Defenses in Fish Skin. *ISRN Immunol* (2012) 2012:1–29. doi: 10.5402/2012/853470
- Alvarez-Pellitero P. Fish Immunity and Parasite Infections: From Innate Immunity to Immunoprophylactic Prospects. *Vet Immunol Immunopathol* (2008) 126:171–98. doi: 10.1016/j.vetimm.2008.07.013
- Fast MD, Sims DE, Burka JF, Mustafa A, Ross NW. Skin Morphology and Humoral non-Specific Defence Parameters of Mucus and Plasma in Rainbow Trout, Coho and Atlantic Salmon. *Comp Biochem Physiol Part A Mol Integr Physiol* (2002) 132:645–57. doi: 10.1016/s1095-6433(02)00109-5
- Noga EJ. Skin Ulcers in Fish: Pfiesteria and Other Etiologies. *Toxicol Pathol* (2000) 28:807–23. doi: 10.1177/019262330002800607
- Bindels LB, Delzenne NM, Cani PD, Walter J. Towards a More Comprehensive Concept for Prebiotics. *Nat Rev Gastroenterol Hepatol* (2015) 12:303–10. doi: 10.1038/nrgastro.2015.47
- Nawaz A, Bakhsh Javaid A, Irshad S, Hoseinifar SH, Xiong H. The Functionality of Prebiotics as Immunostimulant: Evidences From Trials on Terrestrial and Aquatic Animals. *Fish Shellfish Immunol* (2018) 76:272–8. doi: 10.1016/j.fsi.2018.03.004
- Hoseinifar SH, Ahmadi A, Raeisi M, Hoseini SM, Khalili M, Behnampour N. Comparative Study on Immunomodulatory and Growth Enhancing Effects of Three Prebiotics (Galactooligosaccharide, Fructooligosaccharide and Inulin) in Common Carp (*Cyprinus Carpio*). *Aquacult Res* (2017) 48:3298–307. doi: 10.1111/are.13156
- Modanloo M, Soltanian S, Akhlaghi M, Hoseinifar SH. The Effects of Single or Combined Administration of Galactooligosaccharide and Pediococcus Acidilactici on Cutaneous Mucus Immune Parameters, Humoral Immune Responses and Immune Related Genes Expression in Common Carp (*Cyprinus Carpio*) Fingerlings. *Fish Shellfish Immunol* (2017) 70:391–7. doi: 10.1016/j.fsi.2017.09.032
- Van Doan H, Hoseinifar SH, Faggio C, Chitmanat C, Mai NT, Jaturasitha S, et al. Effects of Corn Cob Derived Xylooligosaccharide on Innate Immune Response, Disease Resistance, and Growth Performance in Nile Tilapia (*Oreochromis Niloticus*) Fingerlings. *Aquaculture* (2018) 495:786–93. doi: 10.1016/j.aquaculture.2018.06.068
- Gelibolu S, Yanar Y, Genc MA, Genc E. The Effect of Mannan-Oligosaccharide (MOS) as a Feed Supplement on Growth and Some Blood Parameters of Gilthead Sea Bream (*Sparus Aurata*). *Turkish J Fisheries Aquat Sci* (2018) 18:817–23. doi: 10.4194/1303-2712-v18_6_08
- Uriel R. Effects of Single and Combined Supplementation of Enterococcus Faecalis, Mannan Oligosaccharide and Polyhydroxybutyrate Acid on Growth Performance and Immune Response of Rainbow Trout *Oncorhynchus Mykiss*. *Aquaculture* (2009) 57:609–14. doi: 10.1123/aquaculturesci.57.609
- Torreillas S, Montero D, Caballero MJ, Pittman KA, Custodio M, Campo A, et al. Dietary Mannan Oligosaccharides: Counteracting the Side Effects of Soybean Meal Oil Inclusion on European Sea Bass (*Dicentrarchus Labrax*) Gut Health and Skin Mucosa Mucus Production? *Front Immunol* (2015) 6:397. doi: 10.3389/fimmu.2015.00397
- Fernandez-Montero A, Torreillas S, Izquierdo M, Caballero MJ, Milne DJ, Secombes CJ, et al. Increased Parasite Resistance of Greater Amberjack (*Seriola Dumerili* Risso 1810) Juveniles Fed a cMOS Supplemented Diet is Associated With Upregulation of a Discrete Set of Immune Genes in Mucosal Tissues. *Fish Shellfish Immunol* (2019) 86:35–45. doi: 10.1016/j.fsi.2018.10.034
- Zheng L, Feng L, Jiang W-D, Wu P, Tang L, Kuang S-Y, et al. Selenium Deficiency Impaired Immune Function of the Immune Organs in Young

- Grass Carp (*Ctenopharyngodon Idella*). *Fish Shellfish Immunol* (2018) 77:53–70. doi: 10.1016/j.fsi.2018.03.024
15. Homma S, Ishii Y, Morishima Y, Yamadori T, Matsuno Y, Haraguchi N, et al. Nrf2 Enhances Cell Proliferation and Resistance to Anticancer Drugs in Human Lung Cancer. *Clin Cancer Res* (2009) 15:3423–32. doi: 10.1158/1078-0432.CCR-08-2822
 16. Ki YW, Park JH, Lee JE, Shin IC, Koh HC. JNK and P38 MAPK Regulate Oxidative Stress and the Inflammatory Response in Chlorpyrifos-Induced Apoptosis. *Toxicol Lett* (2013) 218:235–45. doi: 10.1016/j.toxlet.2013.02.003
 17. Ma TY, Boivin MA, Ye D, Pedram A, Said HM. Mechanism of TNF- α Modulation of Caco-2 Intestinal Epithelial Tight Junction Barrier: Role of Myosin Light-Chain Kinase Protein Expression. *Am J Physiol Gastrointest Liver Physiol* (2005) 288:G422. doi: 10.1152/ajpgi.00412.2004
 18. Baker OJ, Camden JM, Redman RS, Jones JE, Seye CI, Erb L, et al. Proinflammatory Cytokines Tumor Necrosis Factor- α and Interferon- γ Alter Tight Junction Structure and Function in the Rat Parotid Gland Par-C10 Cell Line. *Am J Physiol Cell Physiol* (2008) 295:C1191. doi: 10.1152/ajpcell.00144.2008
 19. Ibuki M, Kovacs-Nolan J, Fukui K, Kanatani H, Mine Y. Beta 1-4 Mannobiose Enhances Salmonella-Killing Activity and Activates Innate Immune Responses in Chicken Macrophages. *Vet Immunol Immunopathol* (2011) 139:289–95. doi: 10.1016/j.vetimm.2010.10.011
 20. Um HC, Jang JH, Kim DH, Lee C, Surh YJ. Nitric Oxide Activates Nrf2 Through S-Nitrosylation of Keap1 in PC12 Cells. *Nitric Oxide: Biol Chem* (2011) 25:161–8. doi: 10.1016/j.niox.2011.06.001
 21. Hassanein SM, Soliman NK. Effect of Probiotic (*Saccharomyces Cerevisiae*) Adding to Diets on Intestinal Microflora and Performance of Hy-Line Layers Hens. *J Am Sci* (2010) 6:159–69. doi: 10.1016/j.jamsci.2010.06.011
 22. Kim SH, Sharma RP. Mercury-Induced Apoptosis and Necrosis in Murine Macrophages: Role of Calcium-Induced Reactive Oxygen Species and P38 Mitogen-Activated Protein Kinase Signaling. *Toxicol Appl Pharmacol* (2004) 196:47–57. doi: 10.1016/j.taap.2003.11.020
 23. Torrecillas S, Montero D, Caballero MJ, Robaina L, Zamorano MJ, Sweetman J, et al. Effects of Dietary Concentrated Mannan Oligosaccharides Supplementation on Growth, Gut Mucosal Immune System and Liver Lipid Metabolism of European Sea Bass (*Dicentrarchus Labrax*) Juveniles. *Fish Shellfish Immunol* (2015) 42:508–16. doi: 10.1016/j.fsi.2014.11.033
 24. Alsadi RM, Ma TY. IL-1 β Causes an Increase in Intestinal Epithelial Tight Junction Permeability. *J Immunol* (2007) 178:4641–9. doi: 10.1049/jimmunol.178.7.4641
 25. Tort LBJ, Balasch JC, Mackenzie S. Fish Immune System. A Crossroads Between Innate and Adaptive Responses. *Immunologia* (2003) 22:824. doi: 10.3389/fimmu.2020.00824
 26. Esteban MÁ, Cerezuela R. Fish Mucosal Immunity: Skin. *Mucosal Health Aquacult* (2015) 67–92. doi: 10.1016/B978-0-12-417186-2.00004-2
 27. Secombes CJ, Belmonte R. Overview of the Fish Adaptive Immune System. Springer Basel (2016). doi: 10.1007/978-3-0348-0980-1_2
 28. Bondeson J, Browne KA, Brennan FM, Foxwell BM, Feldmann M. Selective Regulation of Cytokine Induction by Adenoviral Gene Transfer of IkappaBalpha Into Human Macrophages: Lipopolysaccharide-Induced, But Not Zymosan-Induced, Proinflammatory Cytokines are Inhibited, But IL-10 is Nuclear factor-kappaB Independent. *J Immunol* (1999) 162:2939–45. doi: 10.1007/s11910-003-0047-4
 29. Weichhart T, Costantino G, Poglitsch M, Rosner M, Zeyda M, Stuhlmeier KM, et al. The TSC-mTOR Signaling Pathway Regulates the Innate Inflammatory Response. *Immunity* (2008) 29:565–77. doi: 10.1016/j.immuni.2008.08.012
 30. Nohta I, Halas V, Tossenberger J, Babinszky L. Effect of Different Levels of Mannan-Oligosaccharide Supplementation on the Apparent Ileal Digestibility of Nutrients, N-Balance and Growth Performance of Weaned Piglets. *J Anim Physiol Anim Nutr* (2010) 94:747–56. doi: 10.1111/j.1439-0396.2009.00957.x
 31. Jiang WD, Xu J, Zhou XQ, Wu P, Liu Y, Jiang J, et al. Dietary Protein Levels Regulated Antibacterial Activity, Inflammatory Response and Structural Integrity in the Head Kidney, Spleen and Skin of Grass Carp (*Ctenopharyngodon Idella*) After Challenged With *Aeromonas Hydrophila*. *Fish Shellfish Immunol* (2017) 68:154–72. doi: 10.1016/j.fsi.2017.07.019
 32. Chen K, Jiang WD, Wu P, Liu Y, Kuang SY, Tang L, et al. Effect of Dietary Phosphorus Deficiency on the Growth, Immune Function and Structural Integrity of Head Kidney, Spleen and Skin in Young Grass Carp (*Ctenopharyngodon Idella*). *Fish Shellfish Immunol* (2017) 63:103–26. doi: 10.1016/j.fsi.2017.02.007
 33. Pinheiro V, Alves A, Mourão JL, Guedes CM, Pinto L, Spring P, et al. (2004). Effect of Mannan Oligosaccharides on the Ileal Morphometry and Cecal Fermentation of Growing Rabbits, in: *Proceedings of the 8th World Rabbit Congress*, Pueblo, Mexico, September 7–10, 2004. pp. 936–41.
 34. Tian L, Zhou XQ, Jiang WD, Liu Y, Wu P, Jiang J, et al. Sodium Butyrate Improved Intestinal Immune Function Associated With NF-kappaB and P38mapk Signalling Pathways in Young Grass Carp (*Ctenopharyngodon Idella*). *Fish Shellfish Immunol* (2017) 66:548–63. doi: 10.1016/j.fsi.2017.05.049
 35. Lu Z-Y, Feng L, Jiang W-D, Wu P, Liu Y, Kuang S-Y, et al. Mannan Oligosaccharides Improved Growth Performance and Antioxidant Capacity in the Intestine of on-Growing Grass Carp (*Ctenopharyngodon Idella*). *Aquacult Rep* (2020) 17:100313. doi: 10.1016/j.aqrep.2020.100313
 36. Tacon AGJ. Trends in Global Aquaculture and Aquafeed Production: 2000–2017. *Rev Fisheries Sci Aquacult* (2019) 28:43–56. doi: 10.1080/23308249.2019.1649634
 37. Lu ZY, Jiang WD, Wu P, Liu Y, Kuang SY, Tang L, et al. Mannan Oligosaccharides Supplementation Enhanced Head-Kidney and Spleen Immune Function in on-Growing Grass Carp (*Ctenopharyngodon Idella*). *Fish Shellfish Immunol* (2020) 106:596–608. doi: 10.1016/j.fsi.2020.08.035
 38. Xu S, Zhang Y, Jiang K. Antioxidant Activity *In Vitro* and *In Vivo* of the Polysaccharides From Different Varieties of Auricularia Auricularia. *Food Funct* (2016) 7:3868–79. doi: 10.1039/c6fo00686h
 39. Zhang YH, Song XN, Lin Y, Xiao Q, Du XP, Chen YH, et al. Antioxidant Capacity and Prebiotic Effects of Gracilaria Neoagaro Oligosaccharides Prepared by Agarase Hydrolysis. *Int J Biol Macromol* (2019) 137:177–86. doi: 10.1016/j.ijbiomac.2019.06.207
 40. Seguin MJ, Barney D, Widowski TM. Assessment of a Group-Housing System for Gestating Sows: Effects of Space Allowance and Pen Size on the Incidence of Superficial Skin Lesions, Changes in Body Condition, and Farrowing Performance. *J Swine Health Product* (2006) 14:89–96. doi: 10.1111/j.1748-5827.2006.00023.x
 41. Wang B, Feng L, Jiang WD, Wu P, Kuang SY, Jiang J, et al. Copper-Induced Tight Junction mRNA Expression Changes, Apoptosis and Antioxidant Responses via NF-Kappab, TOR and Nrf2 Signaling Molecules in the Gills of Fish: Preventive Role of Arginine. *Aquat Toxicol* (2015) 158:125–37. doi: 10.1016/j.aquatox.2014.10.025
 42. Su J, Zhang R, Dong J, Yang C. Evaluation of Internal Control Genes for qRT-PCR Normalization in Tissues and Cell Culture for Antiviral Studies of Grass Carp (*Ctenopharyngodon Idella*). *Fish Shellfish Immunol* (2011) 30:830–5. doi: 10.1016/j.fsi.2011.01.006
 43. Livak KJ, Schmittgen TD. Analysis of Relative Gene Expression Data Using Real-Time Quantitative PCR and the 2 \times (-Delta Delta C(T)) Method. *Methods* (2001) 25:402–8. doi: 10.1006/meth.2001.1262
 44. Hu K, Zhang JX, Feng L, Jiang WD, Wu P, Liu Y, et al. Effect of Dietary Glutamine on Growth Performance, non-Specific Immunity, Expression of Cytokine Genes, Phosphorylation of Target of Rapamycin (TOR), and Anti-Oxidative System in Spleen and Head Kidney of Jian Carp (*Cyprinus Carpio* Var. Jian). *Fish Physiol Biochem* (2015) 41:635–49. doi: 10.1007/s10695-015-0034-0
 45. Jiang WD, Liu Y, Jiang J, Wu P, Feng L, Zhou XQ. Copper Exposure Induces Toxicity to the Antioxidant System via the Destruction of Nrf2/ARE Signaling and Caspase-3-Regulated DNA Damage in Fish Muscle: Amelioration by Myo-Inositol. *Aquat Toxicol* (2015) 159:245–55. doi: 10.1016/j.aquatox.2014.12.020
 46. Martínez-Alvarez RM, Morales AE, Sanz A. Antioxidant Defenses in Fish: Biotic and Abiotic Factors. *Rev Fish Biol Fisheries* (2005) 15:75–88. doi: 10.1007/s11160-005-7846-4
 47. Kalailingam P, Tan HB, Jain N, Sng MK, Chan JSK, Tan NS, et al. Conditional Knock Out of N-WASP in Keratinocytes Causes Skin Barrier Defects and Atopic Dermatitis-Like Inflammation. *Sci Rep* (2017) 7:7311. doi: 10.1038/s41598-017-07125-8
 48. Lowry SF. Cytokine Mediators of Immunity and Inflammation. *Arch Surg* (1993) 128:1235–41. doi: 10.1001/archsurg.1993.01420230063010
 49. Ghosh S, May MJ, Kopp EB. NF- κ B AND REL PROTEINS: Evolutionarily Conserved Mediators of Immune Responses. *Annu Rev Immunol* (1998) 16:225–60. doi: 10.1146/annurev.immunol.16.1.225

50. Bunnay A, Na-Nakorn U, Srisapoom P. Probiotic Effects of a Novel Strain, *Acinetobacter* KU011TH, on the Growth Performance, Immune Responses, and Resistance Against *Aeromonas Hydrophila* of Bighead Catfish (*Clarias Macrocephalus* Gunther, 1864). *Microorganisms* (2019) 7:1–30. doi: 10.3390/microorganisms7120613
51. Turutoglu H, Ercelik S, Corlu M. *Aeromonas Hydrophila*-Associated Skin Lesions and Septicaemia in a Nile Crocodile (*Crocodylus Niloticus*). *J South Afr Vet Assoc* (2012) 76:40–2. doi: 10.4102/jsava.v76i1.393
52. Marnett LJ. Lipid Peroxidation-DNA Damage by Malondialdehyde. *Mutat Res/fundamental Mol Mech Mutagene* (1999) 424:83–95. doi: 10.1016/s0027-5107(99)00010-x
53. Birben E, Sahiner UM, Sackesen C, Erzurum S, Kalayci O. Oxidative Stress and Antioxidant Defense. *World Allergy Organ J* (2012) 5:9–19. doi: 10.1097/WOX.0b013e3182439613
54. Hatao H, Oh-ishi S, Itoh M, Leeuwenburgh C, Ohno H, Ookawara T, et al. Effects of Acute Exercise on Lung Antioxidant Enzymes in Young and Old Rats. *Mech Ageing Dev* (2006) 127:384–90. doi: 10.1016/j.mad.2005.12.008
55. Kobayashi A, Kang MI, Okawa H, Ohtsui M, Zenke Y, Chiba T, et al. Oxidative Stress Sensor Keap1 Functions as an Adaptor for Cul3-Based E3 Ligase to Regulate Proteasomal Degradation of Nrf2. *Mol Cell Biol* (2004) 24:7130–9. doi: 10.1128/MCB.24.16.7130-7139.2004
56. Kaspar JW, Niture SK, Jaiswal AK. Nrf2:INrf2 (Keap1) Signaling in Oxidative Stress. *Free Radical Biol Med* (2009) 47:1304–9. doi: 10.1016/j.freeradbiomed.2009.07.035
57. Tomobe K, Shinozuka T, Kuroiwa M, Nomura Y. Age-Related Changes of Nrf2 and Phosphorylated GSK-3 β in a Mouse Model of Accelerated Aging (SAMP8). *Arch Gerontol Geriatr* (2012) 54:e1–7. doi: 10.1016/j.archger.2011.06.006
58. Kim JD, Hyun Y, Sohn KS, Woo HJ, Kim TJ, Han IK. Effects of Immunostimulators on Growth Performance and Immune Response in Pigs Weaned at 21 Days of Age. *J Anim Feed Sci* (2000) 9:333–46. doi: 10.1016/S0739-7240(99)00071-5
59. Dong YW, Feng L, Jiang WD, Liu Y, Wu P, Jiang J, et al. Dietary Threonine Deficiency Depressed the Disease Resistance, Immune and Physical Barriers in the Gills of Juvenile Grass Carp (*Ctenopharyngodon Idella*) Under Infection of *Flavobacterium Columnare*. *Fish Shellfish Immunol* (2018) 72:161–73. doi: 10.1016/j.fsi.2017.10.048
60. Choi WS, Eom DS, Han BS, Kim WK, Han BH, Choi EJ, et al. Phosphorylation of P38 MAPK Induced by Oxidative Stress is Linked to Activation of Both Caspase-8- and -9-Mediated Apoptotic Pathways in Dopaminergic Neurons. *J Biol Chem* (2004) 279:20451–60. doi: 10.1074/jbc.M311164200
61. Shi Y. Mechanisms of Caspase Activation and Inhibition During Apoptosis. *Mol Cell* (2002) 9:459–70. doi: 10.1016/s1097-2765(02)00482-3
62. Bakke-Mckellep AM, Penn MH, Salas PM, Refstie S, Sperstad S, Landsverk T, et al. Effects of Dietary Soybean Meal, Inulin and Oxytetracycline on Intestinal Microbiota and Epithelial Cell Stress, Apoptosis and Proliferation in the Teleost Atlantic Salmon (*Salmo Salar* L.). *Br J Nutr* (2007) 97:699–713. doi: 10.1017/S0007114507381397
63. Wang X. The Expanding Role of Mitochondria in Apoptosis. *Genes Dev* (2001) 15:2922–33. doi: 10.1101/gad.949001
64. Villunger A, Scott C, Bouillet P, Strasser A. Essential Role for the BH3-Only Protein Bim But Redundant Roles for Bax, Bcl-2, and Bcl-W in the Control of Granulocyte Survival. *Blood* (2003) 101:2393–400. doi: 10.1182/blood-2002-07-2132
65. Lin HH, Chen JH, Kuo WH, Wang CJ. Chemopreventive Properties of Hibiscus Sabdariffa L. @ on Human Gastric Carcinoma Cells Through Apoptosis Induction and JNK/p38 MAPK Signaling Activation. *Chemico-biol Interact* (2007) 165:59–75. doi: 10.1016/j.cbi.2006.10.011
66. Hussain A, Lahiri D, Ameerunisha Begum MS, Saha S, Majumdar R, Dighe RR, et al. Photocytotoxic Lanthanum(III) and Gadolinium(III) Complexes of Phenanthroline Bases Showing Light-Induced DNA Cleavage Activity. *Inorg Chem* (2010) 49:4036–45. doi: 10.1021/ic901791f
67. Niklasson L. Intestinal Mucosal Immunology of Salmonids Response to Stress and Infection and Crosstalk with the Physical Barrier. *J Jiaxing Univ* (2013) 280:2805–8.
68. Furuse M, Hirase T, Itoh M, Nagafuchi A, Yonemura S, Tsukita S, et al. Occludin: A Novel Integral Membrane Protein Localizing at Tight Junctions. *J Cell Biol* (1993) 123:1777–88. doi: 10.1083/jcb.123.6.1777
69. Furuse M, Fujita K, Hiiiragi T, Fujimoto K, Tsukita S. Claudin-1 and -2: Novel Integral Membrane Proteins Localizing at Tight Junctions With No Sequence Similarity to Occludin. *J Cell Biol* (1998) 141:1539–50. doi: 10.1083/jcb.141.7.1539
70. Shen L, Black ED, Witkowski ED, Lencer WI, Guerriero V, Schneeberger EE, et al. Myosin Light Chain Phosphorylation Regulates Barrier Function by Remodeling Tight Junction Structure. *J Cell Sci* (2006) 119:2095–106. doi: 10.1242/jcs.02915
71. Steensberg A, Fischer CP, Keller C, Möller K, Pedersen BK. IL-6 Enhances Plasma IL-1ra, IL-10, and Cortisol in Humans. *Am J Physiol Endocrinol Metab* (2003) 285:E433. doi: 10.1186/s12970-020-00375-4
72. Bui P, Bagherielachidan M, Kelly SP. Cortisol Differentially Alters Claudin Isoforms in Cultured Puffer Fish Gill Epithelia. *Mol Cell Endocrinol* (2010) 317:120–6. doi: 10.1016/j.mce.2009.12.002
73. Chasiotis H, Kelly SP. Effect of Cortisol on Permeability and Tight Junction Protein Transcript Abundance in Primary Cultured Gill Epithelia From Stenohaline Goldfish and Euryhaline Trout. *Gen Comp Endocrinol* (2011) 172:494. doi: 10.1016/j.mce.2009.12.002
74. Magnadóttir B. Innate Immunity of Fish (Overview). *Fish Shellfish Immunol* (2006) 20:137. doi: 10.1016/j.fsi.2004.09.006
75. Shirdel I, Kalbassi MR, Hosseinkhani S, Paknejad H, Wink M. Cloning, Characterization and Tissue-Specific Expression of the Antimicrobial Peptide Hepcidin From Caspian Trout (*Salmo Caspius*) and the Antibacterial Activity of the Synthetic Peptide. *Fish Shellfish Immunol* (2019) 90:288–96. doi: 10.1016/j.fsi.2019.05.010
76. Ahmadiyeh Motlagh H, Javadmanesh A, Safari O. Improvement of non-Specific Immunity, Growth, and Activity of Digestive Enzymes in *Carassius Auratus* as a Result of Apple Cider Vinegar Administration to Diet. *Fish Physiol Biochem* (2020) 46:1387–95. doi: 10.1007/s10695-020-00797-6
77. Hoseinifar SH, Sharifian M, Vesaghi MJ, Khalili M, Esteban MA. The Effects of Dietary Xylooligosaccharide on Mucosal Parameters, Intestinal Microbiota and Morphology and Growth Performance of Caspian White Fish (*Rutilus Frisii Kutum*) Fry. *Fish Shellfish Immunol* (2014) 39:231–6. doi: 10.1016/j.fsi.2014.05.009
78. Clark IA, Alleva LM, Budd AC, Cowden WB. Understanding the Role of Inflammatory Cytokines in Malaria and Related Diseases. *Travel Med Infect Dis* (2008) 6:67–81. doi: 10.1016/j.tmaid.2007.07.002
79. Zhao H, Li C, Beck BH, Zhang R, Thongda W, Davis DA, et al. Impact of Feed Additives on Surface Mucosal Health and Columnaris Susceptibility in Channel Catfish Fingerlings. *Ictalurus Punctatus Fish Shellfish Immunol* (2015) 46:624–37. doi: 10.1016/j.fsi.2015.07.005
80. Tan P, Dong X, Mai K, Xu W, Ai Q. Vegetable Oil Induced Inflammatory Response by Altering TLR-NF- κ B Signalling, Macrophages Infiltration and Polarization in Adipose Tissue of Large Yellow Croaker (*Larimichthys Crocea*). *Fish Shellfish Immunol* (2016) 59:398–405. doi: 10.1016/j.fsi.2016.11.009
81. Ko EY, Cho SH, Kwon SH, Eom CY, Jeong MS, Lee W, et al. The Roles of NF- κ B and ROS in Regulation of Pro-Inflammatory Mediators of Inflammation Induction in LPS-Stimulated Zebrafish Embryos. *Fish Shellfish Immunol* (2017) 68:525–9. doi: 10.1016/j.fsi.2017.07.041
82. Estève PO, Chicoine É, Robledo O, Aoudjit F, Descoteaux A, Potworowski EF, et al. Protein Kinase C- ζ Regulates Transcription of the Matrix Metalloproteinase-9 Gene Induced by IL-1 and TNF- α in Glioma Cells via NF- κ B. *J Biol Chem* (2002) 277:35150–5. doi: 10.1074/jbc.M108600200
83. Peng Y, Sigua CA, Gallagher SF, Murr MM. Protein Kinase C-Zeta is Critical in Pancreatitis-Induced Apoptosis of Kupffer Cells. *J Gastrointest Surg* (2007) 11:1253–61. doi: 10.1007/s11605-007-0193-0
84. Zhao J, Benakanakere MR, Hosur KB, Galicia JC, Martin M, Kinane DF. Mammalian Target of Rapamycin (mTOR) Regulates TLR3 Induced Cytokines in Human Oral Keratinocytes. *Mol Immunol* (2010) 48:294–304. doi: 10.1016/j.molimm.2010.07.014
85. Seiliez I, Gabillard JC, Skibacassy S, Garciaserrana D, Gutiérrez J, Kaushik S, et al. An *In Vivo* and *In Vitro* Assessment of TOR Signaling Cascade in

Rainbow Trout (*Oncorhynchus Mykiss*). *Am J Physiol* (2008) 295:329–35. doi: 10.1152/ajpregu.00146.2008

Conflict of Interest: S-YK, LT, S-WL, X-AL and C-BZ were employed by Sichuan Animtech Feed Co. Ltd.

The remaining authors declare that the research was conducted in the absence of any commercial or financial relationships that could be construed as a potential conflict of interest.

Publisher's Note: All claims expressed in this article are solely those of the authors and do not necessarily represent those of their affiliated organizations, or those of

the publisher, the editors and the reviewers. Any product that may be evaluated in this article, or claim that may be made by its manufacturer, is not guaranteed or endorsed by the publisher.

Copyright © 2021 Lu, Feng, Jiang, Wu, Liu, Jiang, Kuang, Tang, Li, Liu, Zhong and Zhou. This is an open-access article distributed under the terms of the Creative Commons Attribution License (CC BY). The use, distribution or reproduction in other forums is permitted, provided the original author(s) and the copyright owner(s) are credited and that the original publication in this journal is cited, in accordance with accepted academic practice. No use, distribution or reproduction is permitted which does not comply with these terms.



A Potential Probiotic for Diarrhea: *Clostridium tyrobutyricum* Protects Against LPS-Induced Epithelial Dysfunction via IL-22 Produced By Th17 Cells in the Ileum

Zhiping Xiao¹, Lujie Liu¹, Xun Pei¹, Wanjing Sun¹, Yuyue Jin¹, Shang-Tian Yang² and Minqi Wang^{1*}

¹ The key Laboratory of Molecular Animal Nutrition, Ministry of Education, College of Animal Sciences, Zhejiang University, Hangzhou, China, ² Department of Chemical and Biomolecular Engineering, The Ohio State University, Columbus, OH, United States

OPEN ACCESS

Edited by:

Huaxi Yi,
Ocean University of China, China

Reviewed by:

Huizi Tan,
Nanchang University, China
Jufang Wang,
South China University of Technology,
China

*Correspondence:

Minqi Wang
wangmq@zju.edu.cn

Specialty section:

This article was submitted to
Nutritional Immunology,
a section of the journal
Frontiers in Immunology

Received: 13 August 2021

Accepted: 08 November 2021

Published: 30 November 2021

Citation:

Xiao Z, Liu L, Pei X, Sun W, Jin Y,
Yang S-T and Wang M (2021) A
Potential Probiotic for Diarrhea:
Clostridium tyrobutyricum Protects
Against LPS-Induced Epithelial
Dysfunction via IL-22 Produced
By Th17 Cells in the Ileum.
Front. Immunol. 12:758227.
doi: 10.3389/fimmu.2021.758227

Probiotics are clinically used for diarrhea and inflammatory bowel diseases in both humans and animals. Previous studies have shown that *Clostridium tyrobutyricum* (Ct) protects against intestinal dysfunction, while its regulatory function in the gut needs further investigation and the related mechanisms are still not fully elucidated. This study aims to further verify the protective function of Ct and reveal its underlying mechanisms in alleviating diarrhea and intestinal inflammation. Ct inhibited LPS-induced diarrhea and intestinal inflammation in the ileum. IL-22 was identified and the protective role of Ct in the ileum presented an IL-22-dependent manner according to the transcriptomic analysis and *in vivo* interference mice experiments. The flow cytometric analysis of immune cells in the ileum showed that Ct enhanced the proportions of Th17 cells in response to LPS. The results of *in situ* hybridization further verified that Ct triggered Th17 cells to produce IL-22, which combined with IL-22RA1 expressed in the epithelial cells. Moreover, Ct was unable to enhance the levels of short-chain fatty acids (SCFAs) in the ileum, suggesting that the protective role of Ct in the ileum was independent of SCFAs. This study uncovered the role of Ct in alleviating diarrhea and inflammation with the mechanism of stimulating Th17 cells in the lamina propria to produce IL-22, highlighting its potential application as a probiotic for diarrhea and inflammation in the ileum.

Keywords: *Clostridium tyrobutyricum*, diarrhea, intestinal barrier function, IL-22, Th17 cells

INTRODUCTION

Diarrhea is a gastrointestinal condition with high morbidity and mortality. Generally, diarrhea results from the decreased absorption of Cl⁻ and Na⁺ and movement of water, leading to the imbalance of ions and solute across the gut epithelium (1). When diarrhea occurs, the enteric pathogens easily disseminate into the intestinal microenvironment, disturbing homeostasis of the

epithelial barrier, host flora, and immune cells, inducing intestinal inflammation, causing intestinal inflammation, and gastrointestinal diseases like inflammatory bowel disease (IBD).

Alleviation of diarrhea and intestinal inflammation requires an ingenious intestinal barrier system concerting the crosstalk between the microbiota and immune cells to avoid excessive immune responses to commensal microbes or pathogens. This process involves a series of mechanisms, including the secretion of cytokines, chemokines, and immunomodulatory molecules, such as thymic stromal lymphopoietin, TGF- β , retinoic acid, IL-10, and IL-5 produced by intestinal epithelial cells (IECs) (2). The mechanisms involved in microbiota-IECs-immune cell interactions are still being elucidated because of the cell culture systems imitating the physiological cues of the complex gastrointestinal mucosa microenvironment. However, equilibrium of the gut microbiota, IECs, and immune cells is crucial for intestinal homeostasis.

Clostridium tyrobutyricum (*C. tyrobutyricum*/Ct) is one of the anaerobic *Clostridium* strains. Compared with other gram-positive bacteria, the cell wall of *C. tyrobutyricum* is mainly made up of higher protein (35–40% dry weight), lower insoluble peptidoglycan (10–12% dry weight), and neutral sugar, and absent teichuronic acids (3, 4). Numerous studies have revealed that *Clostridium tyrobutyricum* could be used to produce higher butyric acid via bacterial fermentation (5–7). Recently, *C. tyrobutyricum* has been revealed to protect barrier function in different tissues, including the gut (8), testis (9), and endometrium (10). A new study about the genomic analysis of *C. tyrobutyricum* pointed out that *C. tyrobutyricum* is a potential bacteria in regulating health in human beings (11). Our earlier study has shown that *C. tyrobutyricum* protects against lipopolysaccharide (LPS)-induced epithelial dysfunction in IPEC-J2 cells (12). Moreover, *C. tyrobutyricum* has been revealed in alleviating LPS-induced inflammation via regulating immune cells in the intestinal sections (13, 14). However, the regulatory function of *C. tyrobutyricum* in the gut needs further elucidation and its underlying mechanism in maintaining intestinal homeostasis is still not fully understood.

In this study, we aimed to investigate the role and possible mechanisms of *C. tyrobutyricum* in the ileum based on our previous study (14). We further proved that *C. tyrobutyricum* prevented diarrhea and protected against LPS-induced ileal barrier dysfunction *in vivo*. IL-22 was identified according to the transcriptomic analysis of the ileum. *C. tyrobutyricum* alleviated LPS-induced epithelial destruction depending on IL-22 produced according to the *in vivo* interference experiments. We also revealed that *C. tyrobutyricum* enhanced the MHC-II process, thereby stimulating Th17 cells to produce IL-22 which combined with IL-22RA1 expressed in the epithelial cells. Strikingly, *C. tyrobutyricum* decreased the levels of short-chain fatty acids (SCFAs) in response to LPS, suggesting that the regulatory function of *C. tyrobutyricum* in the gut was independent of SCFAs. Our studies revealed the role of *C. tyrobutyricum* in the crosstalk between epithelial cells and immune cells mediated by IL-22 and identifies the potential application of *C. tyrobutyricum* as a probiotic for diarrhea and inflammation in the ileum.

MATERIALS AND METHODS

Antibodies and Reagents

LPS (derived from *Escherichia coli* strain O55:B5) and Collagenase VIII from *Clostridium histolyticum* (C2139) were from Sigma-Aldrich (USA). The antibodies in the flow cytometry were described as our previous studies (13, 14). All antibodies used in the flow cytometric analysis, immunoblotting, and immunohistochemistry were shown in **Supplemental Table 1**. Transcription Factor Staining Buffer Set (562574) and Stain Buffer FBS (554656) were from BD (USA). HEPES was from Gibco (USA). EDTA and BacLight™ Green Bacterial Stain (B-35000) were from Invitrogen (USA). Fetal Bovine Serum was purchased from Gemini (USA). RMP1 1640 was from BI (Israel). TRIzol reagent, The PrimeScript RT reagent kit with gDNA Erase, and SYBR Green qPCR reagent were from Takara (Japan). DNase (D8070), 5% BSA (SW3015), Triton X-100 (P1080) and DAPI (C0065) were from Solarbio (China). The Opal 7-color Manual IHC kit (NEL811001KT) was purchased from PerkinElmer (USA). Polybrene was provided by HanBio (China). The whole cell lysis assay (KGP2100) was from KeyGEN (China).

Mice

Four-week-old C57BL/6 male mice were purchased from Shanghai SLAC Laboratory Animal Co., Ltd and bred at the Zhejiang University Laboratory Animal Center (25°C, 12/12-h light/dark cycle) allowing unrestricted access to standard mice diet and water. The mice experiments were performed following the protocol approved by the Institutional Animal Care and Use Committee of Zhejiang University. For the mice feeding trial, four-week C57BL/6 male mice were treated with PBS (Control, mice were treated with PBS by gavage for 20 days followed by intraperitoneal injection with PBS, n=10), Ct (mice were treated with 10⁸ CFU/mL Ct for 20 days followed by intraperitoneal injection with PBS, n=10), LPS (mice were treated with PBS for 20 days followed by intraperitoneal injection with 10 mg/kg BW LPS, n=12), and Ct + LPS (mice were treated with 10⁸ CFU/mL Ct for 20 days followed by intraperitoneal injection with 10 mg/kg BW LPS, n=12). For the *in vivo* interference feeding experiment, adeno-associated virus 2/2-m-shIL22 labeled with GFP (AAV-shIL22) and AAV-shNC were generated by Hanbio (Shanghai, China). The sequences of AAV-shNC and AAV-shIL22 were designed as the previous study, namely 5'-TTCTCCGAAC GTGTCACGTA-3' and 5'-GCTAAGGATCAGTGCTACCTG ATGA-3' (13). Four-week C56BL/6 male mice were first intraperitoneally injected with 200 μ L AAV-shIL22/AAV-shILNC at a concentration of at least 2.4×10^{11} vg/mL. After 14 days, mice were treated with PBS (AAV-shNC-Control, n=19; AAV-shIL22-Control, n=17), Ct (AAV-shNC-Ct, n=14, AAV-shIL22-Ct, n=12), LPS (AAV-shNC-LPS, n=20; AAV-shIL22-LPS, n=18), and Ct + LPS (AAV-shNC-Ct + LPS, n=17; AAV-shIL22-Ct + LPS, n=12), respectively as described above.

Bacterial Culturing

C. tyrobutyricum was provided by Prof. Shang-Tian Yang, from The Ohio State University and was cultured as our previous

study (5). Simply, *C. tyrobutyricum* was cultured anaerobically at 37°C in a clostridial growth medium (CGM), collected after centrifugation at 12,000 rpm for 5 min, and suspended in PBS.

Bacterial Colonization

For the colonization of *C. tyrobutyricum* in the intestine, 10^8 CFU/mL *C. tyrobutyricum* was first mixed with 100 μ M working solution of the BacLight bacterial stain, incubated for 15 min at room temperature, and washed with PBS. C57BL/6 mice were then treated with *C. tyrobutyricum* by gavage and the intestinal samples were collected, frozen with liquid nitrogen, embedded with OCT, and sectioned. The fluorescence was visualized using a confocal microscope LSM 880 and captured using ZEN 2.3 software (Carl Zeiss, Germany).

RNA-Sequencing

Total RNA of ileal samples from the Control, LPS, Ct, and Ct + LPS groups (n=6) were isolated for RNA-Sequencing. RNA sequencing was performed by Novogene using an Illumina sequencer. Clean reads obtained by removing reads containing adapter, poly-N and low-quality reads were aligned to the reference genome using Tophat2 RNA-Seq alignment software. HTSeq was used to count the read numbers mapped to each gene. Differential expression analysis was conducted using the DESeq R package. The P values were adjusted using the Benjamini & Hochberg method (FDR). Corrected P-value of 0.05 and fold-change of at 1 was set as the threshold for significantly differential expression.

Immune Cells Isolation and Flow Cytometric Analysis

The isolation of immune cells from the ileal lamina propria was performed as previously described (15, 16). The steps of cell isolation and antibodies staining were conducted according to our previous studies (13, 14). Simply, the ileal sections were isolated from the mice, washed with PBS, cut into 5-cm pieces after removing the fat tissue, mesenteric, and Peyer's patches, and shaken in PBS containing 2% FBS, 10 mM HEPES, and 2 mM EDTA at 37°C for 30 min for two to three cycles. The intestinal pieces were then shaken in RPMI 1640 medium containing 10% FBS, 2 mM L-glutamine, 100 U/mL penicillin, 100 μ g/mL streptomycin, 0.6 mg/mL collagenase VIII, and 150 μ g/mL DNase at 37°C for 30 min for two cycles, passed through 100 μ m and 40 μ m cell strainers, and centrifuged at $400 \times g$ for 10 min. Cells were then stained with Live/Dead (FVS780) for 20 min followed by CD16/32 antibody for 15 min, washed with PBS, stained with surface antibodies for 20 min, and washed with PBS. For the intracellular antibodies, cells were fixed and permeabilized for 2 h followed by staining the intracellular antibodies for 2 h, washed with PBS, and suspended in PBS before processing. The data were analyzed with FlowJo software (BD, USA).

Transmission Electron Microscopy and Scanning Electron Microscopy

Ileal sections were washed in PBS and fixed in 2.5% GA overnight. All samples were washed in PBS and postfixed in 1% osmic acid for 1-2 h. Then the samples were washed in PBS

and dehydrated in a series of gradient ethanol solutions (50%, 75%, 85%, 95%, and 100% ethanol), each for 15 min. For SEM, the samples were dehydrated in a Hitachi Model HCP-2 critical point dryer with liquid CO₂ and visualized using a Philips Model SU8010 FASEM (Hitachi, Japan). For TEM, samples were embedded in Epon resin and cut into 60 nm ultrathin sections. Sections were counterstained with uranyl acetate and lead citrate. All the samples were observed using a Hitachi HT7650 electron microscope (Hitachi, Japan).

Histology and Immunohistochemistry

Ileal samples were fixed overnight in 4% PFA, and then dehydrated in 30% sucrose in PBS solution for 48 h until sunk to the bottom. Ileal sectioning, H&E, and ZO-1 staining were performed by Zhejiang Chinese Medical University. The scanning was conducted on Nikon Eclipse 80i (Nikon, Japan). The intestinal morphology was evaluated with NDP. View2 (Hamamatsu, China). The average of density (AOD) of ZO-1 was obtained with ImageJ software.

In situ Hybridization

For tissue fluorescence *in situ* hybridization, the Opal 7-color Manual IHC kit was used according to the manual provided. The sections were dewaxed with xylene, rehydrated through a graded series of ethanol solutions, and fixed in 10% neutral buffered formalin. After microwave treatment and blocking, the ileal sections were sequentially stained with primary antibodies and HRP-conjugated secondary antibodies. One of four Opal reagents was used for staining followed by microwave treatments and another round of staining. Slides were finally stained with DAPI for 5 min and mounted before image acquisition. CD45, EpCAM, CD3e, ROR γ t, IL-22, and IL-22RA1 were used as primary antibodies. The dyes Opal 520, Opal540, Opal570, and Opal 590 were used for staining. Images were visualized using confocal microscope LSM 880 and captured using ZEN 2.3 software (Carl Zeiss, Germany). Considering the autofluorescence of tissues, the contrast/brightness with consistent parameters was regulated in all images using ZEN 2.3 software. All images were analyzed with ImageJ software.

RT-qPCR

Total RNA was extracted using TRIzol reagent. cDNA was synthesized with PrimeScript RT reagent kit with gDNA Eraser according to the manufacturer's instructions. RT-qPCR was performed on the CFX96™ Real-Time System (Bio-Rad) in duplicate or triplicate. Data were analyzed according to the $2^{-\Delta\Delta Ct}$ method and normalized to the expression of GAPDH. PCR primers are shown in **Supplemental Table 2**.

Immunoblotting

Whole-cell lysates of ileum was prepared using Whole Cell Lysis Assay. After electrophoresis with 10% SDS-PAGE, proteins were transferred to PVDF membranes. The membranes were blocked with 5% non-fat milk for 1h at room temperature, incubated with specific primary antibodies followed by HRP-conjugated secondary antibodies, and detected by the ECL reagent.

Gas Chromatographic Analysis

The concentrations of SCFAs were analysed *via* gas chromatography (17, 18). The ileal contents were mixed with 5 mL double distilled water for 1 h. The supernatant was collected after centrifugation at 10,000 g for 15 min and mixed with 85% orthophosphoric acid for 1 h. The supernatant was then collected, passed by 0.22 μ m strainers, and transferred into the gas chromatography vial. The concentrations of SCFAs in the ileal contents of mice were measured by GC-8A gas chromatography (Shimadzu, Kyoto, Japan).

Statistical Analysis

All statistical tests were performed with Prism 8.0 software and analyzed using two-tail unpaired t-test. All data are expressed as mean \pm SEM and $P < 0.05$ was considered significant and the level of significance was indicated as * $P < 0.05$, ** $P < 0.01$.

RESULTS

Ct Alleviates LPS-Induced Ileal Barrier Dysfunction

Our previous studies have investigated the most efficient concentration of Ct in alleviating intestinal dysfunction and suggested that 10^8 CFU/mL Ct effectively alleviated LPS-induced inflammation in different sections of the intestine including the duodenum, ileum, and colon (13, 14). To further understand the role of Ct in alleviating diarrhea and intestinal inflammation *in vivo*, we first evaluated the colonization of Ct *in vivo* via staining Ct with BacLight™ green. Mice were treated with 10^8 CFU/mL Ct by gavage. After 4 h, faint fluorescence was observed on the lumen and the villus surface of the small intestines (Supplemental Figure 1), indicating that Ct could colonize in the small intestines, while its colonization capacity in the intestine was weak.

Mice were then treated with 10^8 CFU/mL Ct by gavage followed by LPS injection. Compared with LPS group, Ct maintained the body weight gain (Figure 1A) and inhibited diarrhea (Figure 1B) in response to LPS. In response to LPS, Ct improved the ileal morphology, enhanced the villus height, and villus height/crypt depth ratio (Figure 1C), which were consistent with our previous study (14). Compared with LPS group, Ct significantly increased the expression of ZO-1 (a typical tight junction protein) in the ileum in response to LPS (Figure 1D). Under electron microscopy, we observed that LPS induced the destruction of villi, microvilli, and tight junction structures, while Ct improved these phenomena in response to LPS (Figures 1E, F). These results further verified that Ct effectively inhibited diarrhea and alleviated ileal barrier dysfunction induced by LPS.

Ct Enhances the Expression of IL-22 in the Ileum

The ileal samples were collected after the feeding experiment and transcriptomic analysis was conducted to elucidate the molecular mechanism of Ct in the ileum. A total of 19 differentially expressed

genes were identified between the Ct and Control groups according to $\text{padj} < 0.05$ and $|\log_2(\text{FoldChange})| > 1$ (Figure 2A and Supplemental Table 3). Ct up-regulated genes like Ahsg and Alb, which have been revealed in inhibiting intestinal diseases such as ulcerative colitis (19, 20). In addition, Ct down-regulated genes including Tacr2, Cav1, Adrb3, Csf3, and Cxcl2, which enriched in 'Neuroactive ligand-receptor interaction', 'Calcium signaling pathway', 'Endocytosis', and 'Cytokine-cytokine receptor' processes (Supplemental Figure 2A and Supplemental Table 4). These results indicated that Ct inhibited intestinal inflammation and regulated intestinal nervous response. A total of 145 differentially expressed genes were identified between the LPS and Ct + LPS groups (Figure 2B, Supplemental Table 5). Compared with the LPS group, genes including Maf, IL-18, H2-Ab1, H2-DMA, H2-Eb1, Gsdmd, Ahsg, Alb, and Gc enriching in 'Intestinal bowel disease' and bacterial infection were enhanced in the Ct + LPS group. In addition, Ct regulated the intestinal metabolism, especially fatty acid metabolism in response to LPS (Supplemental Figure 2B and Supplemental Table 6). Altogether, we suggested three possible mechanisms of Ct in regulating intestinal immune response, namely neuro-, metabolism-, and cytokines-immune regulation. In this study, we focused on the mechanism of cytokines-immune regulation.

The mRNA expression of Csf3, Gsdmd, and Maf was first determined. No differences in the mRNA expression of Csf3, Gsdmd, and Maf were observed between the LPS and Ct + LPS groups (Figure 2C), which were inconsistent with the transcriptomic analysis. In the innate immune system, pathogens/extracellular stimuli are recognized by pattern-recognition receptors (PRRs) like Toll-like receptors (TLRs) and NOD-like receptors (NLRs) to induce the recruitment of monocytes, thereby producing cytokines and chemokines (21, 22). According to the transcriptomic analysis, we also noticed that Ct decreased the expression of TLRs such as TLR4, a well-known receptor of LPS (Supplemental Figure 3A, Supplemental Table 7). *Clostridium butyricum*, another *Clostridium* strain, which has been clinically used in regulating intestinal health with the mechanism *via* activating TLR2/MyD88 signaling pathway in colitis (23). Unlike *Clostridium butyricum*, Ct decreased the expression of TLR2 in response to LPS, indicating that Ct regulated intestinal health in a TLR2-independent manner. NLRP9b is highly expressed in the ileal epithelial cells and restricts rotavirus infection (24). In this study, Ct decreased the mRNA expression of NLRP6 and NLRP9b in response to LPS (Supplemental Figure 3B).

To address whether Ct regulated intestinal immune response *via* cytokines. Herein, some differentially expressed cytokines and chemokines were identified among the Control, Ct, LPS, and Ct + LPS groups (Figure 2D and Supplemental Tables 8, 9). We then analyzed the mRNA expression of these cytokines and chemokines in the ileum using RT-qPCR. Ct decreased the mRNA expression of IL-1 β , IL-6, TNF- α , Ccl2, Ccl9, and Ccl11 in response to LPS (Figure 2E and Supplemental Figure 3D). Besides, in response to LPS, Ct decreased the levels of IL-6, IL-1 β , TNF- α , and IFN- γ in the ileum according to ELISA analysis (Figure 2F). The above results showed that Ct inhibited LPS-induced inflammation in the ileum. We also

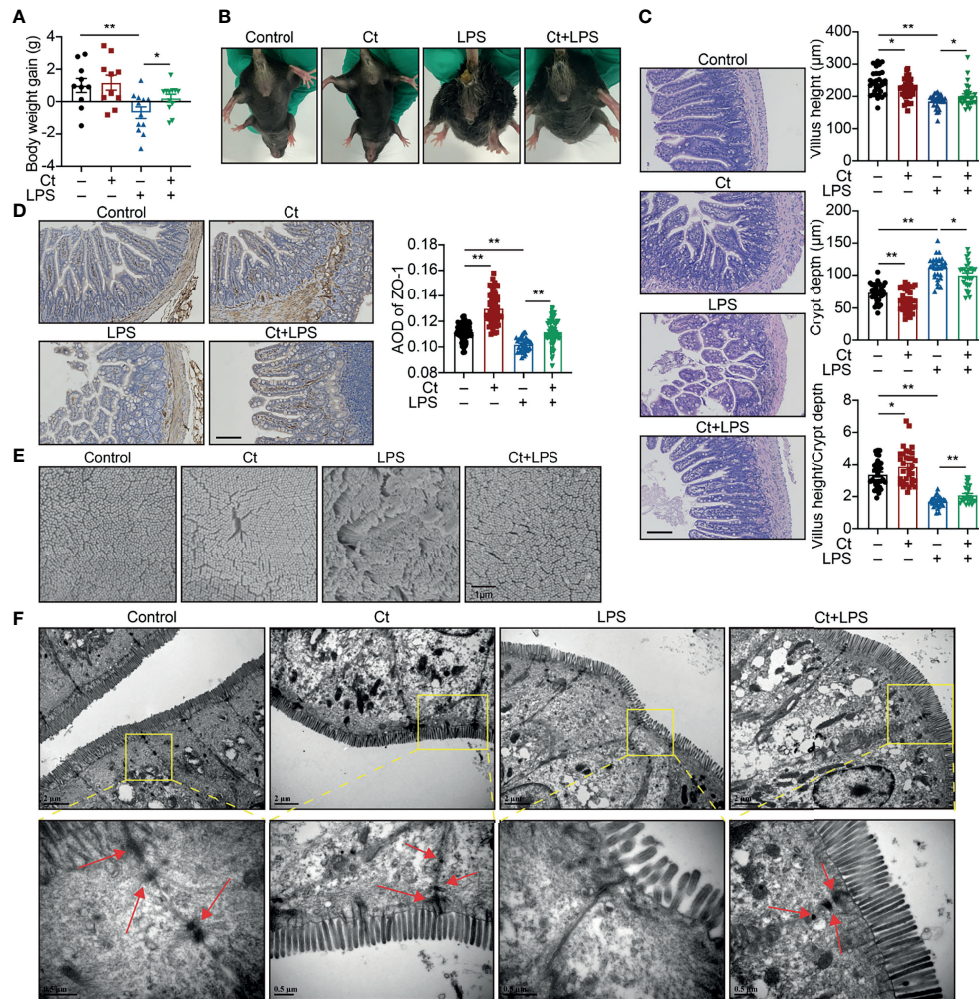


FIGURE 1 | Ct alleviates LPS-induced diarrhea and ileal barrier function *in vivo*. C57BL/6 were randomly divided into 4 groups, including the Control (n=10), Ct (n=10), LPS (n=12), Ct + LPS (n=12). All samples were collected after 24 h. **(A)** Body weight gain. **(B)** Diarrhea. **(C, D)** H&E staining **(C)** and ZO-1 expression **(D)**. The presented figures of H&E and ZO-1 staining in each group were from the same sample. Scale bar: 500 μm. **(E)** Visualization of villus morphology under SEM. Scale bar: 1 μm. **(F)** Visualization of microvilli and structure of tight junctions under TEM. Scale bar: 2 μm. Data were presented as mean ± SEM. The significant difference was analyzed by two-way unpaired t-tests. * $P < 0.05$, ** $P < 0.01$.

noticed that Ct enhanced the mRNA expression of IL-18, IL-17rc, and IL-22 in response to LPS (**Figure 2E**). Some earlier studies have shown that these three cytokines (IL-18, IL-17, and IL-22) induce intestinal inflammation (25–27), while recent studies show the protective roles of these cytokines in the gut (28–30). These guided us to hypothesize that Ct might regulate intestinal inflammation *via* enhancing IL-18, IL-17, and IL-22 in the ileum.

According to the results of RNA-seq and RT-qPCR verification, in response to LPS, Ct enhanced the mRNA expression of H2-Eb1 and H2-DMA in the ileum (**Figure 2G**), which have been defined as major histocompatibility complex class II-related transcripts (MHC-II) (31). Generally, MHC-II is constitutively expressed on antigen-presenting cells and epithelial cells, recognizing the antigen derived from nutrients, commensal bacteria, or pathogens, and is sensitized by CD4⁺ T

cells, thereby promoting immune response (32–35). MHC-II deficiency accounts for higher susceptibility to enteric infections, leading to intestinal inflammation and gastrointestinal disease like IBD (36). We then analyzed the proportions of MHC-II⁺ cells in the ileum. Compared with LPS group, Ct significantly enhanced the proportion of MHC-II⁺ cells in response to LPS (**Figure 2H**). It has been reported that MHC-II, IL-22, and type 3 innate lymphoid cells (ILC3s) partially overlap in the intestine according to the single-cell RNA-sequencing (37), which guided us to assume that Ct might regulate intestinal immune response *via* IL-22. We then measured the protein expression of IL-22 in the ileum and found that Ct enhanced the IL-22 expression in response to LPS (**Figure 2I**). The level of IL-22 in the ileum was also measured using ELISA. In response to LPS, Ct enhanced the level of IL-22 in the ileum (**Figure 2J**). Altogether, Ct might alleviate LPS-induced inflammation *via* IL-22 in the ileum.

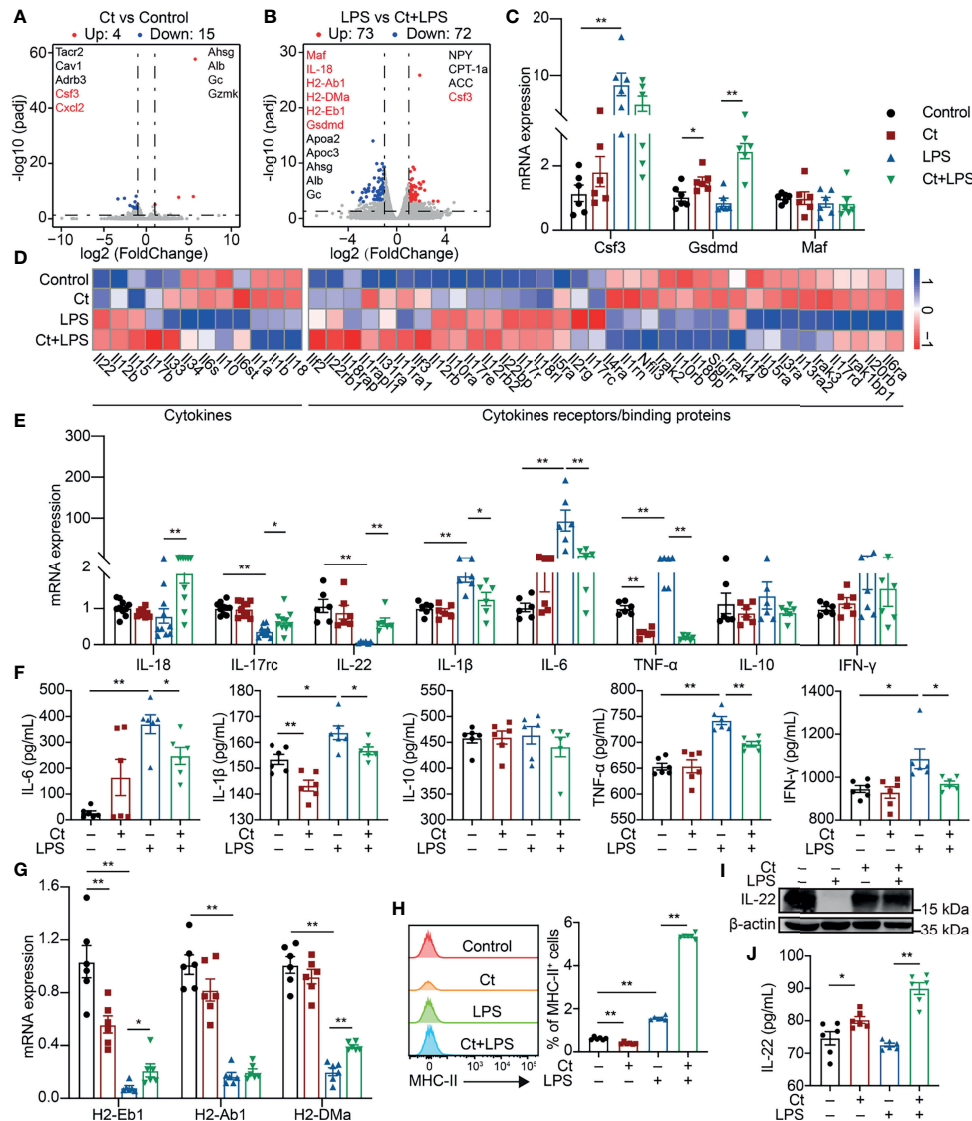


FIGURE 2 | Ct enhances the expression of IL-22 in response to LPS. **(A)** Volcano plots of differentially expressed genes between the Control and Ct group (Ct vs Control, $n=6$). **(B)** Volcano plots of differentially expressed genes between the LPS and Ct + LPS group (LPS vs Ct + LPS, $n=6$). **(C)** RT-qPCR analysis of Csf3, Gsdmd, and Maf in the ileum ($n=6$). **(D)** Heat-map of differentially expressed genes enriched in cytokines and cytokine receptors/binding proteins. **(E)** RT-qPCR analysis of cytokines including IL-18, IL-17rc, IL-22, IL-1 β , IL-6, TNF- α , IL-10, and IFN- γ in the ileum (IL-18 and IL-17rc, $n=10$, others, $n=6$). **(F)** The levels of inflammatory cytokines including IL-6, IL-1 β , IL-10, TNF- α , and IFN- γ in the ileum ($n=6$). **(G)** RT-qPCR analysis of MHC-II transcripts in the ileum ($n=6$). **(H)** Proportions of MHC-II $^{+}$ cell in the ileum ($n=6$). **(I)** Immunoblotting analysis of IL-22 in the ileum. **(J)** ELISA analysis of IL-22 levels in the ileum ($n=6$). Data were presented as mean \pm SEM. The significant difference was analyzed by two-way unpaired t-tests. * $P < 0.05$, ** $P < 0.01$.

Ct Protects LPS-Induced Inflammation Depending on IL-22 in the Ileum

To investigate whether Ct protected intestinal barrier function and alleviated LPS-induced intestinal inflammation depending on IL-22. An RNA interference experiment *in vivo* with adeno-associated virus-shIL22 labeled with GFP (AAV-shIL22) by intraperitoneal injection was conducted to knock down IL-22 in the intestine. The fluorescence was observed on the surface of both ileum and colon, offering the possibility for AAV-shIL22 to target the intestine (Supplemental Figure 4A). The mRNA

expression of IL-22 in the ileum was reduced in mice treated with AAV-shIL22 and the efficiency of *in vivo* interference reached 64.19% (Supplemental Figure 4B).

After knocking down IL-22, Ct was unable to maintain the body weight gain (Figure 3A), while Ct decreased the diarrhea incidence in response to LPS (Figure 3B). In mice treated with AAV-shNC, Ct maintained the whole length of the intestine in response to LPS, while no differences were observed between LPS and Ct + LPS groups after knocking down IL-22 (Figure 3C). We also observed the above phenomenon in the colon and

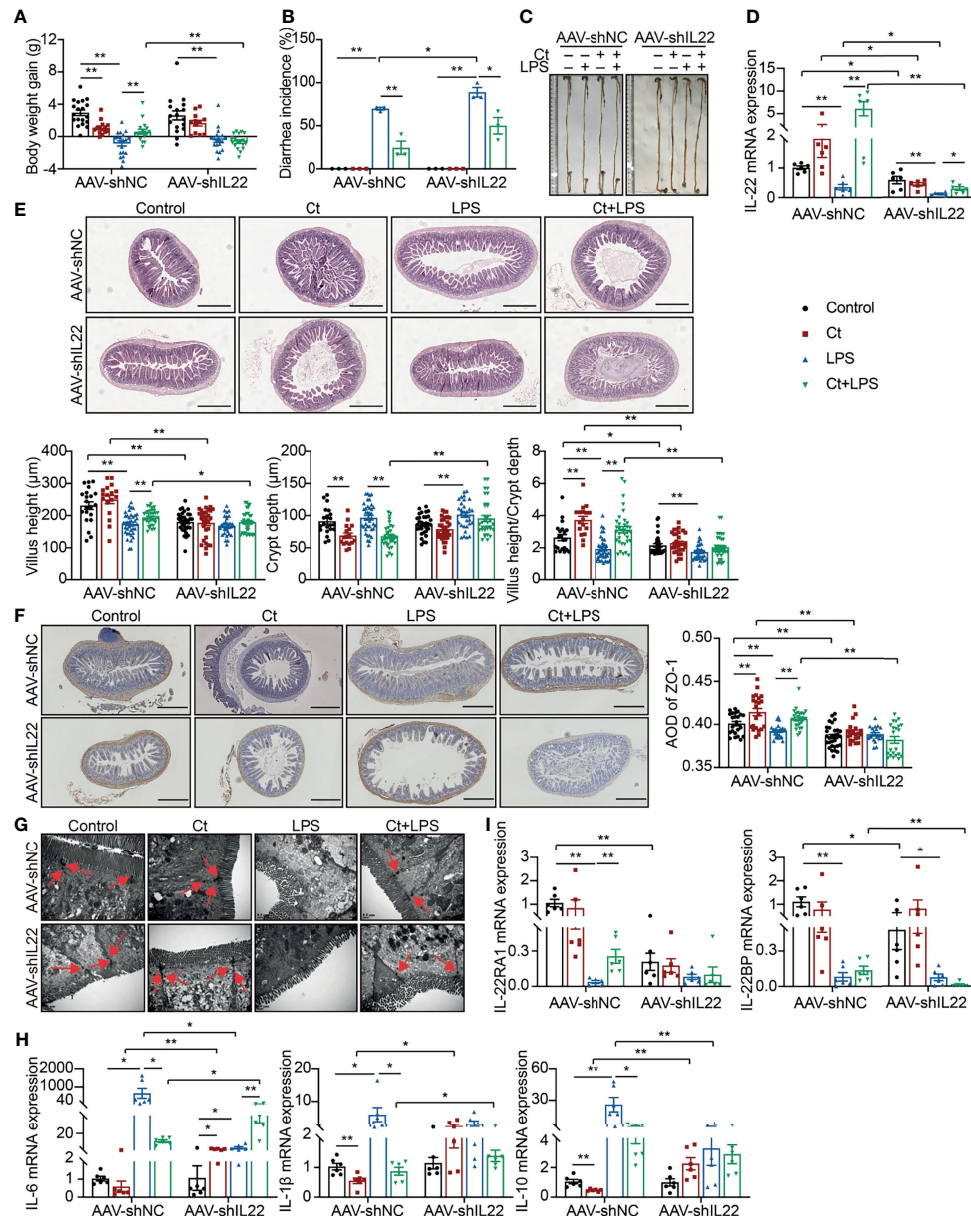


FIGURE 3 | Ct alleviates intestinal barrier dysfunction in an IL-22-dependent manner. C57BL/6 mice were first intraperitoneally injected with AAV-shNC ($n=70$) and AAV-shIL22 ($n=59$), after 14 days, mice were randomly divided into 8 groups, namely AAV-shNC-Control ($n=19$), AAV-shNC-Ct ($n=14$), AAV-shNC-LPS ($n=20$), AAV-shNC-Ct + LPS ($n=17$), AAV-shIL22-Control ($n=17$), AAV-shIL22-Ct ($n=12$), AAV-shIL22-LPS ($n=18$), AAV-shIL22-Ct + LPS ($n=12$). All samples were collected after 24 h. **(A)** Body weight gain. **(B)** Diarrhea incidence. **(C)** Intestinal length. **(D)** RT-qPCR analysis of IL-22 in the ileum ($n=6$). **(E)** H&E staining. Scale bar: 500 μm . **(F)** ZO-1 expression. Scale bar: 500 μm . **(G)** Visualization of microvilli and structure of tight junctions under TEM. Scale bar: 0.5 μm . **(H)** RT-qPCR analysis of inflammatory cytokines including IL-6, IL-1 β , and IL-10 in the ileum ($n=6$). **(I)** RT-qPCR analysis of IL-22 and IL-22BP in the ileum ($n=6$). Data were presented as mean \pm SEM. The significant difference was analyzed by two-way unpaired t-tests. * $P < 0.05$, ** $P < 0.01$.

demonstrated that Ct alleviated colonic dysfunction in an IL-22-dependent manner (13). After knocking down IL-22, compared with LPS group, Ct still enhanced the mRNA expression of IL-22 in the ileum in response to LPS (**Figure 3D**). Fragmentary villi were observed after knocking down IL-22 in the ileum, and in response to LPS, Ct dramatically decreased the villus height and villus height/crypt depth ratio after knocking down IL-22

compared with that in AAV-shNC-Ct + LPS group. After knocking down IL-22, Compared with LPS group, Ct was unable to enhance the villus height and villus height/crypt depth ratio in response to LPS (**Figure 3E**).

Compared with mice treated with AAV-shNC, the expression of ZO-1 in the Control, Ct, and Ct + LPS groups was decreased after knocking down IL-22, and Ct was unable to maintain ZO-1

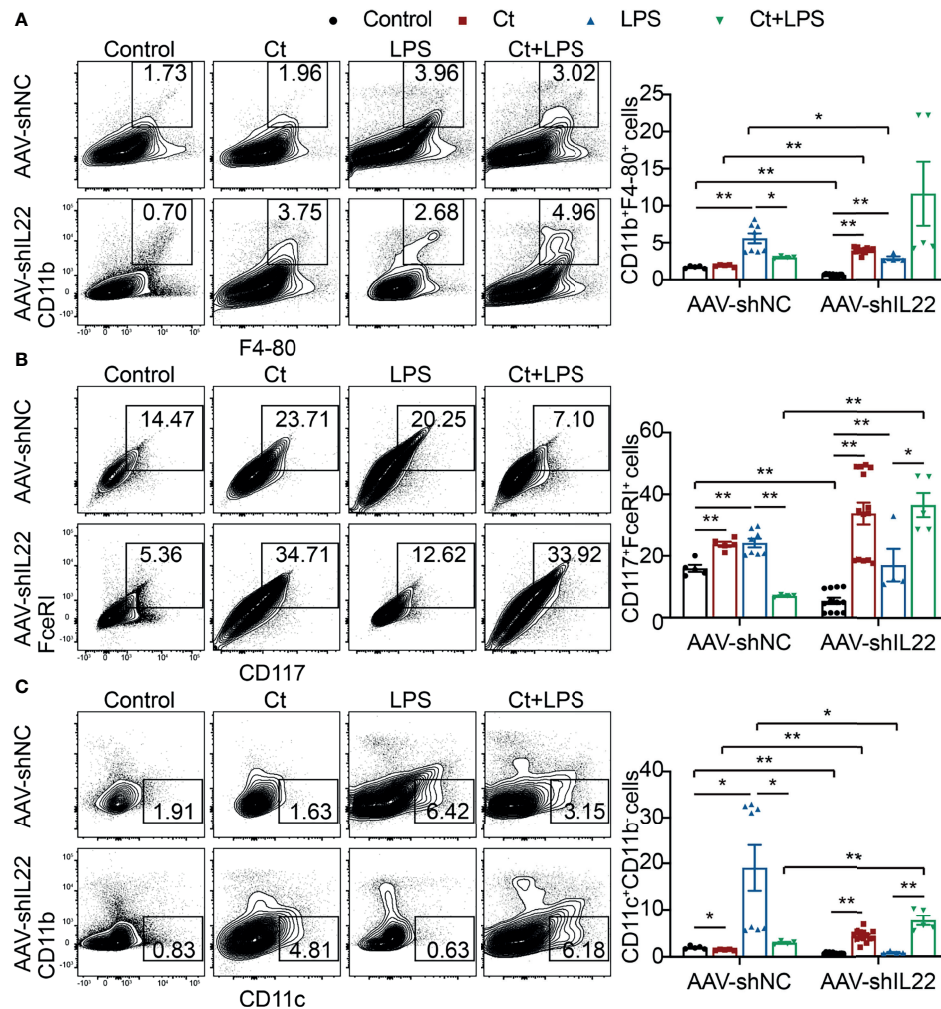


FIGURE 4 | Effects of Ct on the proportions of macrophages, mast cells, and DCs in the ileum. Flow cytometric analyses were conducted on 8-colour FACS Verse and three panels were used to analyzing the intestinal immune cells. The single cells were first gated on SSC-A vs FSC-A and FSC-A vs FSC-H, and then CD45⁺FVS780⁻ cells (CD45⁺Live⁺ cells) were gated out. CD11b⁺F4-80⁺ cells, CD117⁺FceRI⁺ cells, and CD11c⁺CD11b⁻ cells were gated out from CD45⁺Live⁺ cells. **(A)** Proportions of macrophages (CD11b⁺F4-80⁺ cells). **(B)** Proportions of mast cells (CD117⁺FceRI⁺ cells). **(C)** Proportions of DCs (CD11c⁺CD11b⁻ cells). Each point presented a mouse. Data were presented as mean \pm SEM. The significant difference was analyzed by two-way unpaired t-tests. * $P < 0.05$, ** $P < 0.01$.

expression in mice treated AAV-shIL22 in response to LPS (**Figure 3F**). Although the structure of TJs was observed, the microvilli was damaged in the AAV-shIL22-Ct + LPS group (**Figure 3G**). Besides, after knocking down IL-22, Ct enhanced the mRNA expression of IL-6 and had no effects on IL-1 β and IL-10 in response to LPS (**Figure 3H**). Collectively, these findings indicated that Ct protected against LPS-induced dysfunction depending on IL-22 in the ileum.

The IL-22 receptor (IL-22R), composed of two heterodimeric subunits including IL-22RA1 and IL-10R2, is one of the IL-10 family of receptors (38). According to binding studies, IL-22 initially binds to IL-22RA1 since IL-22 has a high affinity for IL-22RA1, and as such, the formation of the IL-22-IL-22RA1 complex enables secondary binding of the IL-10R2 subunit to activate downstream signaling (39). In this study, after knocking

down IL-22, although Ct enhanced the mRNA expression of IL-22 in response to LPS, no differences in the mRNA expression of IL-22RA1 in the ileum were observed between the LPS and Ct + LPS groups. IL-22BP, a soluble form of the IL-22RA1 subunit with a higher affinity to IL-22 than the membrane-bound IL-22RA1 form, binds to IL-22 at an overlapping site to IL-22RA1 (40, 41). Compared with LPS group, Ct had no effects on mRNA expression of IL-22BP in response to LPS (**Figure 3I**).

Ct Stimulates Th17 Cells to Produce IL-22 in the Lamina Propria

IL-22, identified as one of the IL-10 members, is generally produced by a series of immune cells such as Th17 cells, ILC cells, and dendritic cells (DCs) (42, 43). According to the transcriptomic analyses, we identified some differentially

expressed genes enriched in the cluster of differentiation (Supplemental Figure 3E), some of which have been defined as the surface biomarkers of immune cells, indicating that Ct might specifically regulate the function of intestinal immune cells. Our previous study also points out that Ct mainly targets Th17 cells in the ileum and supposes that Ct may stimulate Th17 cells to produce IL-22 in the ileum (14).

To investigate whether Ct regulates ileal immune cells in the *in vivo* interference feeding experiment, we isolated ileal lamina propria cells from AAV-shNC- and AAV-shIL22-treated mice to analyze the proportions of immune cells including macrophages, mast cells, DCs, ILC3s, CD4⁺ T cells, and T cell subsets in the ileum. As shown in Figure 4 and Supplemental Table 10, in the innate immune system, In mice treated with AAV-shNC, compared with LPS group, Ct decreased the proportions of macrophages, mast cells, and DCs in response to LPS in the ileum, which were consistent with our previous study (14). After knocking down IL-22, Ct enhanced the frequencies of mast cells and DCs in response to LPS. Numerous studies have revealed that IL-22 is induced by immune cells such as Th17 cells and ILC3s, thereby repairing epithelial damage (38, 44–48). Herein, as shown in Figure 5A, Supplemental Tables 11, 12 and Supplemental Figure 5, in mice treated with AAV-shNC, in response to LPS, Ct increased the proportions of Th1 cells, Tregs, and Th17 cells, while after knocking down IL-22, Ct decreased

the numbers of Th1 cells and Tregs and had no effects on Th17 cells number. Besides, compared with LPS, Ct had no effects on the proportions of ILC3s in response to LPS (Figure 5B), indicating that Ct triggered Th17 cells rather than ILC3s in the ileum.

To better understand the origin and position of IL-22 production in the intestine, the ileal slices were stained with EpCAM, CD45, IL-22, and IL-22RA1 (Figure 6A). We first analyzed the colocalization of EpCAM, CD45, and IL-22 in the ileum (Figures 6B, C). IL-22⁺EpCAM⁺CD45⁺ cells were observed in the intraepithelial lymphocyte and crypt, especially the crypt where IL-22 is highly expressed to promote the proliferation of intestinal stem cells (29, 49). According to the colocalization analysis of EpCAM and IL-22 using Pearson's R value. In response to LPS, Ct enhanced the colocalization of EpCAM and IL-22, suggesting that the IL-22 colocalized with EpCAM might be from the intraepithelial lymphocytes. Moreover, IL-22⁺CD45⁺ cells were observed in the lamina propria after Ct treatment and Ct enhanced the whole number of CD45⁺IL-22⁺ cells in response to LPS. Ligation of the IL-22-IL-22RA1-IL-10R2 complex is an essential step to mediate the biological effects of IL-22, thereby activating the downstream signaling pathways like the JAK-STAT pathway in epithelial cells and inducing renewal of epithelial cells (38, 50, 51). In the above process, the IL-22RA1 determines the cellular sensitivity to IL-22

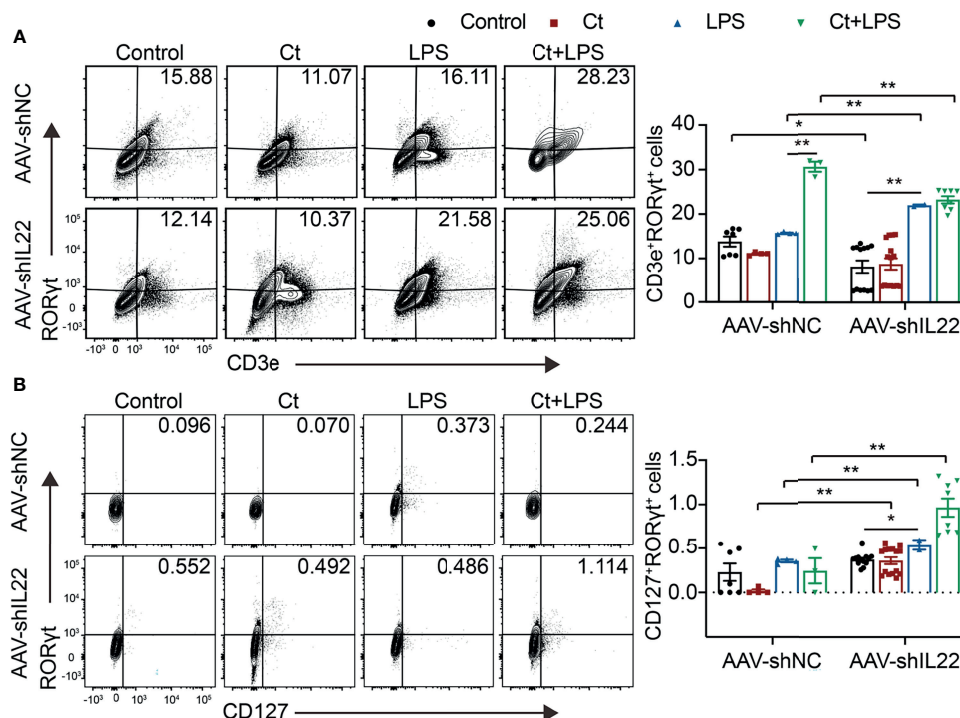


FIGURE 5 | Ct stimulates Th17 cells rather than ILC3s in the ileum. Flow cytometric analyses were conducted on 8-colour FACS Verse and three panels were used to analyzing the intestinal immune cells. The single cells were first gated on SSC-A vs FSC-A and FSC-A vs FSC-H, and then CD45⁺FVS780⁻ cells (CD45⁺Live⁺ cells) were gated out. CD3e⁺RORyt⁺ cells were gated out from CD45⁺CD3e⁺ cells. CD45⁺CD3e⁺ cells were gated out from CD45⁺FVS780⁻ cells and CD127⁺RORyt⁺ cells were gated out from CD45⁺CD3e⁺ cells. **(A)** Proportions of Th17 cells (CD45⁺CD3e⁺RORyt⁺ cells). **(B)** Proportions of ILC3s (CD45⁺CD3e⁺CD127⁺RORyt⁺). Each point presented a mouse. Data were presented as mean \pm SEM. The significant difference was analyzed by two-way unpaired t-tests. * P < 0.05, ** P < 0.01.

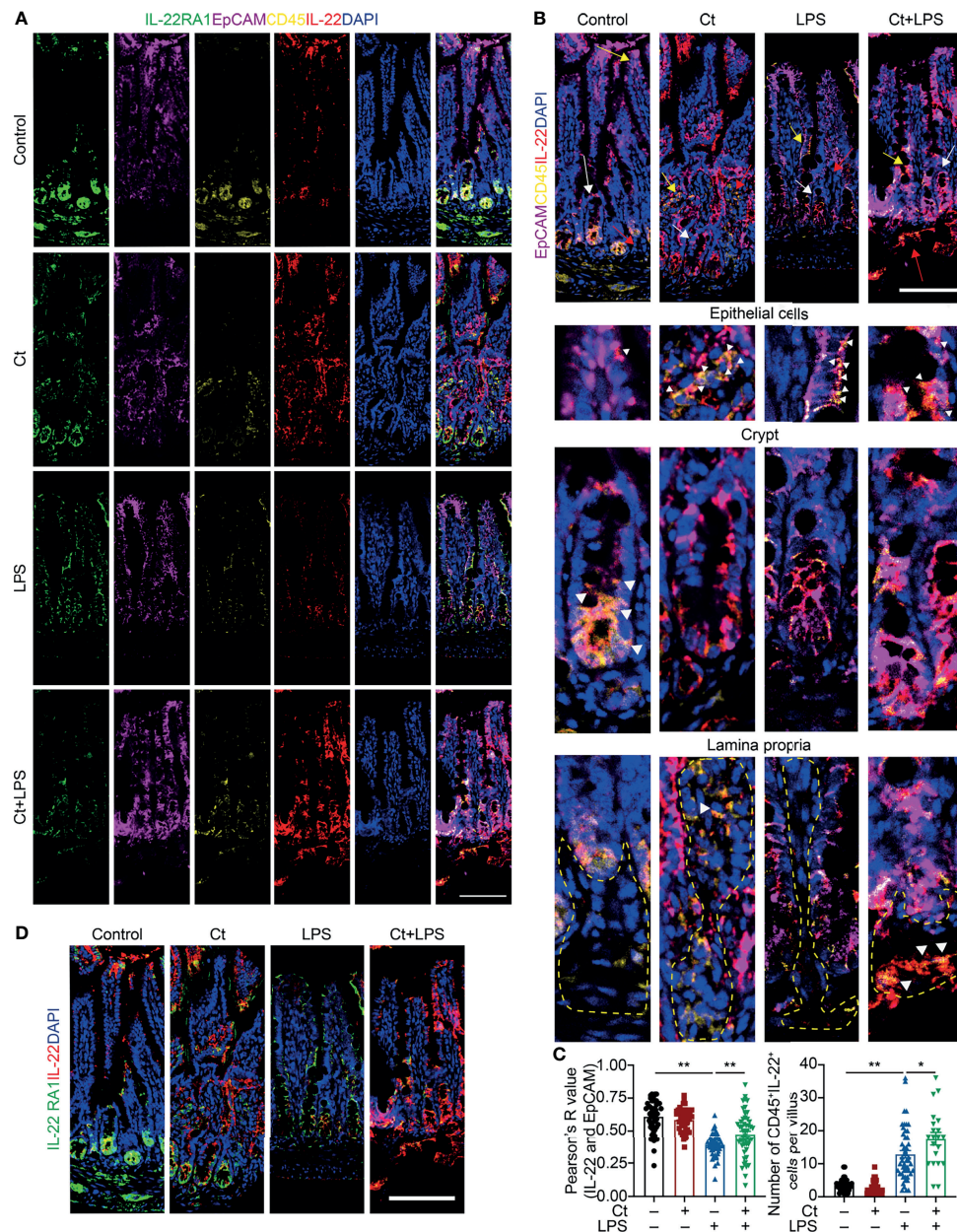


FIGURE 6 | Ct triggers immune cells to enhance the production of IL-22 in the ileal lamina propria. Ileal slices were stained with IL-22 (red), IL-22RA1 (green), EpCAM (violet), CD45 (yellow), and DAPI (blue). **(A)** *In situ* hybridization of IL-22, IL-22RA1, EpCAM, and CD45. **(B)** Colocalization of EpCAM, CD45, and IL-22 in the epithelial position, crypt, and lamina propria, respectively. White triangle: localization, yellow arrow: epithelial cells, white arrow: crypt, red arrow: lamina propria. **(C)** Analysis of IL-22⁺EpCAM⁺ and CD45⁺IL-22⁺ cells. **(D)** Colocalization of IL-22 and IL-22RA1. Scale bar: 100 μ m. Data were presented as mean \pm SEM. The significant difference was analyzed by two-way unpaired t-tests. * $P < 0.05$, ** $P < 0.01$.

and is mainly expressed in outer body barriers of respiratory like lungs, the gastrointestinal like stomach and intestine, the liver, the kidney, but not expressed in the bone marrow, spleen, or thymus containing high proportions of immune cells (52, 53). Herein, we observed that Ct induced higher colocalization of IL-22 and IL-22RA1 in the epithelial cells (Figure 6D). Altogether, Ct stimulated the intestinal immune cells to produce IL-22 and

triggered the combination of IL-22 with IL-22RA1. The ileal slices were then stained with ROR γ t, EpCAM, CD3e, and IL-22 to determine whether IL-22 was produced by Th17 cells (Figure 7). In response to LPS, Ct enhanced the number of ROR γ t⁺CD3e⁺IL-22⁺ cells. These results further suggested that Ct enhanced the level of IL-22 induced by Th17 cells in the lamina propria.

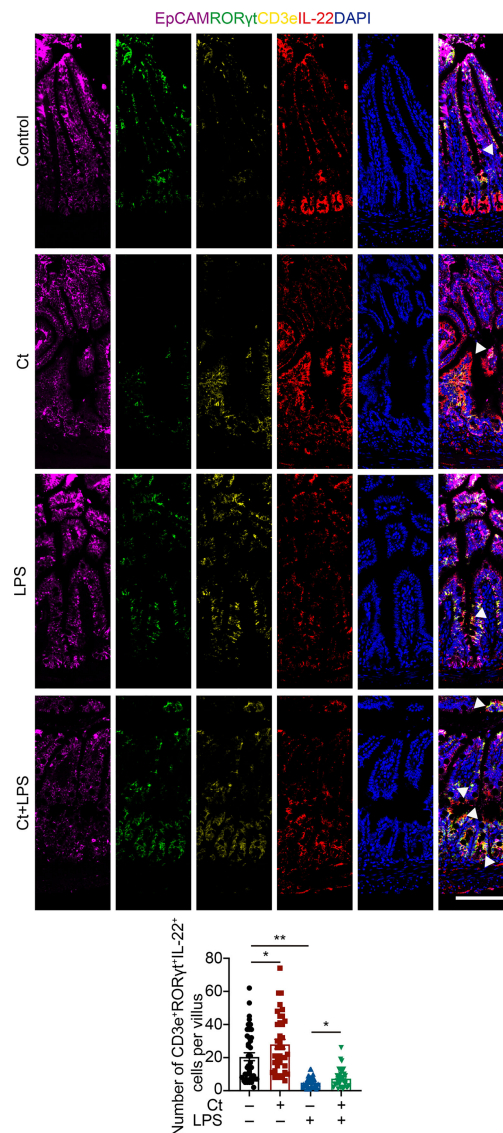


FIGURE 7 | Ct stimulates intestinal Th17 cells to enhance the production of IL-22 in the ileum. Ileal slices were stained with EpCAM (violet), RORγt (green), CD3e (yellow), IL-22 (red), and DAPI (blue). The samples were from the continuous slices in Fig. 6. White triangle: localization. Scale bar: 100 μm. Data were presented as mean ± SEM. The significant difference was analyzed by two-way unpaired t-tests. * $P < 0.05$, ** $P < 0.01$.

The Role of Ct in Regulating Intestinal Health Was Independent of SCFAs

Most probiotics regulate intestinal health *via* their metabolites like short-chain fatty acids (SCFAs) in the gut. Bacterial metabolites including short-chain acids (SCFAs), bile acids (BAs), and tryptophan metabolites, bacterial components, and bacteria themselves have been shown to play vital roles in maintaining epithelial integrity and modulating immune responses (54–56). Butyrate acid-producing *Clostridia* like *Clostridium butyrium* has been well studied in regulating intestinal health and inhibiting intestinal tumor development in both patients with IBD and animals with the mechanism of inhibiting histone deacetylase (HDAC) *via* SCFAs (23, 57).

Herein, we found that Ct dramatically decreased the levels of SCFAs in the intestine in response to LPS and the decreasing of SCFAs by Ct was independent on IL-22 (**Figure 8**), indicating that Ct protected against intestinal injury in a butyrate acid-independent manner.

DISCUSSION

Probiotics have been widely used in both humans and production animals. However, some inevitable problems must be considered for probiotics, mainly including the safety, the efficiency in treating intestinal diseases, the colonization in the gut, the

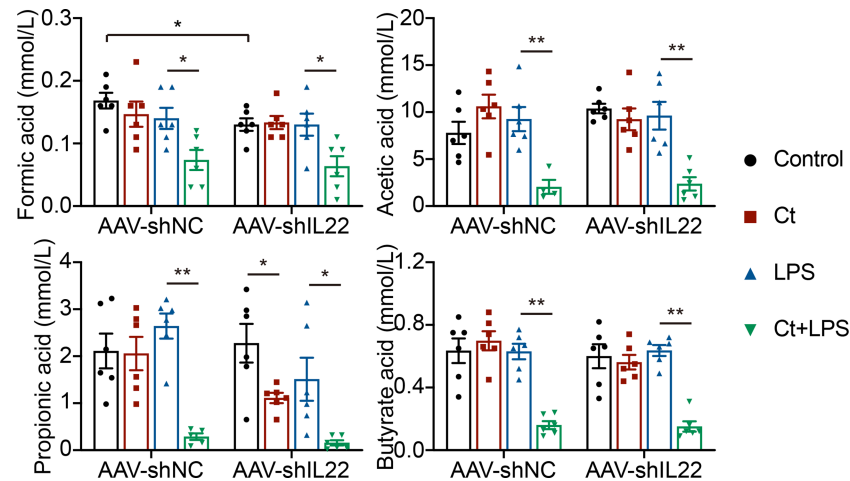


FIGURE 8 | Ct decreases the ileal levels of SCFAs in response to LPS. Data were presented as mean \pm SEM (n=6). The significant difference was analyzed by two-way unpaired t-tests. *P < 0.05, **P < 0.01.

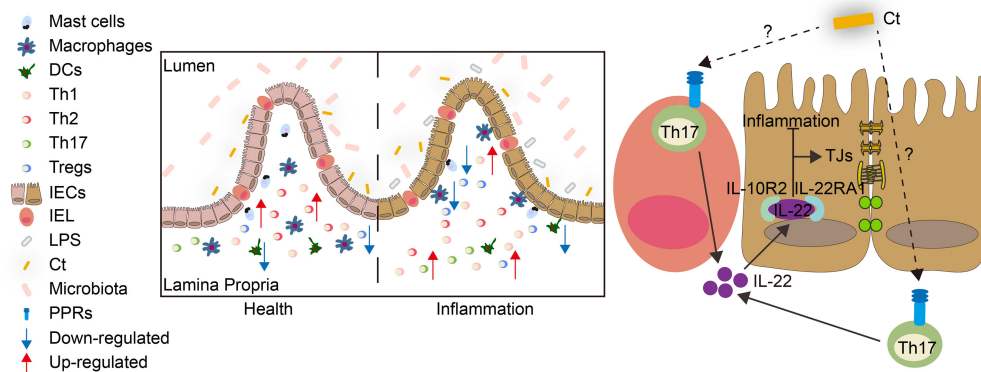


FIGURE 9 | Model for the function and mechanism of Ct in regulating intestinal health. Ct inhibited LPS-induced intestinal inflammation in the ileum. The protective role of Ct in the ileum presented an IL-22-dependent manner *in vivo*. In response to LPS, Ct enhanced the proportions of Th17 cells to produce IL-22, which combined with IL-22RA1 expressed in the epithelial cells, thereby maintaining the barrier function and alleviating inflammation in the ileum.

viability after passing through the gastrointestinal tract, and the effects on commensal microbiota (58). As for *C. tyrobutyricum*, our previous study has shown that 10^8 CFU/mL *C. tyrobutyricum* could effectively alleviate LPS-induced inflammation in both the ileum and colon (13, 14). Moreover, the viability of *C. tyrobutyricum* reaches 90.03% after treatment in the simulated gastric fluid *in vitro* (pH 1.2) for 2 h and its viability reaches 62.12% after continuous treatment in the simulated intestinal fluid (pH 7.4) for 4 h (59), suggesting that *C. tyrobutyricum* has considerable high gastrointestinal tolerance. Colonization is an essential characteristic of probiotics. Two decades-long debate views on colonization are existed, namely the colonization of the mucosa during supplementation and the post-supplementation persistence in the gut, which are limited by the abundance of probiotics in the assessment methods directly reflecting their colonization in the gut (58). Herein, we noticed

that *C. tyrobutyricum* had the colonization capacity in the small intestine, while the accurate quantitative of viability was not fully revealed because of its weak colonization in the gut. Considering that *C. tyrobutyricum* effectively alleviated intestinal inflammation and prevented LPS-induced diarrhea, how to enhance the colonization or adhesion of *C. tyrobutyricum* on the gut mucosa is an imperative problem in the IBD therapy and the application in preventing diarrhea. A recent study revealed that the bacteria-derived biofilm contributes to the defense of bacteria under extreme conditions, such as physical forces and environmental attacks. The biofilm-coated probiotics present improved gastrointestinal tract tolerance and mucosal adhesion in animals and exhibit higher oral bioavailability and colonization than uncoated bacteria in the intestine (60), providing a feasible method to enhance the colonization or adhesion of *C. tyrobutyricum* *in vivo*.

According to the transcriptomic analysis, compared with the Control, *C. tyrobutyricum* treatment alone decreased the expression of Cav1, Tacr2, and Adrb3, which were enriched in the process of neuro regulation and calcium signaling pathway according to the KEGG analysis. Moreover, we noticed that mice presented slowly in action during the gavage of *C. tyrobutyricum*. Whether *C. tyrobutyricum* alleviating intestinal dysfunction via the brain-gut axis or intestinal nervous regulation needs further study. Considering that LPS induced the metabolic disorder and *C. tyrobutyricum* reversed the metabolic processes like fatty acids synthesis and degradation in response to LPS, whether *C. tyrobutyricum* orchestrating the immune response and metabolism needs to be revealed in the future study.

IL-22, discovered by Gurney's group and Renault's group in 2000 (61, 62), is highly expressed in some gastrointestinal diseases like IBD (27, 63–65). However, IL-22 repairs tissue damage and prevents pathogens via promoting the regeneration of epithelial cells and the production of antimicrobial molecules when it is under proper control (38, 45, 46). The fuzzy boundary of IL-22 between inhibitor and inducer for colitis may present a dose-/time-dependent manner in the intestine. In this study, we found that *C. tyrobutyricum* alleviated intestinal inflammation depending on IL-22 produced by Th17 cells. Strangely, LPS stimulation decreased the mRNA expression of IL-6 and proportions of immune cells like macrophages and DCs in the ileum after knocking down IL-22. Some similar results were also observed in the colon (13). Unlike the earlier study in which IL-22 level in the intestine is enhanced in response to LPS (64), herein, the expression of IL-22 in the ileum was decreased in response to LPS. Thus, whether LPS-induced intestinal inflammation depending on IL-22 needs further investigation. More importantly, to fully understand the role of *C. tyrobutyricum* in the intestine, chemical methods like DSS should be considered to induce IBD in our future research.

IECs receive signals from nutrients, commensal microbes, or pathogens, orchestrating the communication between the commensal microorganisms and immune cells under physiological and inflammatory conditions. These signals are classified into three types, namely the microbiota, the microbial components, and the microbial metabolites (2). For most studies, probiotics regulate intestinal health via their metabolites like SCFAs, bile acids, and tryptophan metabolites, which have been revealed to maintain the interactions among microbiota, epithelial cells, and immune cells in the gut. The SCFAs activate the G protein-coupled receptors (GPRs) expressed in the epithelial cells to inhibit inflammation via producing cytokines like IL-18 (66), concerting the communication between microbiota and IECs. The SCFAs can also regulate the interactions between microbiota and immune cells with the mechanism of stimulating the IL-10 producing Foxp3⁺ Tregs via inhibiting HDAC, thereby alleviating colitis (56, 66). As one of *Clostridium* strains producing high levels of butyrate acid *in vitro*, *C. tyrobutyricum* was unable to enhance the levels of SCFAs in the ileum in response to LPS. In this study, we suggested that *C. tyrobutyricum* might play a protective role in the intestine via stimulating the metabolites except for SCFAs. Further investigation in whether

C. tyrobutyricum could trigger the production of metabolites contributing to the stimulation of Th17 cells to produce IL-22 in the gut based on metabolome should be considered.

The present study revealed that *C. tyrobutyricum* alleviated LPS-induced intestinal inflammation and prevented diarrhea in mice with the mechanism of triggering Th17 cells in the lamina propria to induce IL-22 production, which combined with IL-22RA1 expressed in the epithelial cells (Figure 9). The results indicated that *C. tyrobutyricum* could be a potential probiotic in regulating intestinal health and provided a scientific basis for its application in preventing diarrhea and inflammation in the ileum.

DATA AVAILABILITY STATEMENT

The original contributions presented in the study are publicly available. This data can be found here: <https://www.ncbi.nlm.nih.gov/sra/?term=PRJNA756726>.

ETHICS STATEMENT

The animal study was reviewed and approved by The Institutional Animal Care and Use Committee of Zhejiang University (Approval numbers: ZJU20200005, ZJU20200040).

AUTHOR CONTRIBUTIONS

MW took charge of the project administration. ZX designed the whole experiment. ZX and LL performed all *in vivo* and *in vitro* experiments. ZX and LL analyzed and checked the data. ZX wrote the original manuscript. LL revised the manuscript. XP and WS performed the bacterial colonization experiment and cultured the bacteria. YJ performed flow cytometry experiments. ZX, LL, XP, and WS collected the tissue samples. S-TY revised and copy-edited the paper. All authors contributed to the article and approved the submitted version.

FUNDING

This study was jointly funded by the National Key Research & Development Program of China (No. 2018YFE0112700) and Key Research & Development Program of Zhejiang Province (No. 2019C02005).

ACKNOWLEDGMENTS

We would like to thank all members from Laboratory Animal Center, Zhejiang University for taking care of all experimental mice. We show great thanks to all members from the Bio-ultrastructure analysis Lab. of Analysis Center of Agrobiology and Environmental Sciences, Zhejiang University for their supports in electron microscopy and confocal microscopy.

We would like to thank Bojing Liu from Institute of Feed Science, Zhejiang University for her kind help in SCFAs measurement. We would also like to thank Weiren Dong, Junhong Wang, and Yuanyuan Zhang from lab platform of College of Animal Sciences, Zhejiang University for their technical supports.

REFERENCES

- Viswanathan VK, Hodges K, Hecht G. Enteric Infection Meets Intestinal Function: How Bacterial Pathogens Cause Diarrhoea. *Nat Rev Microbiol* (2009) 7:110–9. doi: 10.1038/nrmicro2053
- Kayama H, Okumura R, Takeda K. Interaction Between the Microbiota, Epithelia, and Immune Cells in the Intestine. *Annu Rev Immunol* (2020) 38:23–48. doi: 10.1146/annurev-immunol-070119-115104
- Helene H, Jacqykube C, Bergere J. A High-Molecular-Mass Cell Wall Protein Released From *Clostridium Tyrobutyricum* by Heat Treatment. *FEBS Lett* (1984) 174:284–8. doi: 10.1016/0014-5793(84)81174-6
- Bergere JL, Commissaire H, Hayes J. Major Protein Components in the Cell Envelope of *Clostridium Tyrobutyricum*. *Annu Inst pasteur Microbiol* (1986) 127:271–82. doi: 10.1016/s0769-2609(86)80117-x
- Xiao Z, Cheng C, Bao T, Liu L, Wang B, Tao W, et al. Production of Butyric Acid From Acid Hydrolysate of Corn Husk in Fermentation by *Clostridium Tyrobutyricum*: Kinetics and Process Economic Analysis. *Biotechnol Biofuels* (2018) 11:164. doi: 10.1186/s13068-018-1165-1
- Fu H, Yu L, Lin M, Wang J, Xiu Z, Yang ST. Metabolic Engineering of *Clostridium Tyrobutyricum* for Enhanced Butyric Acid Production From Glucose and Xylose. *Metab Eng* (2017) 40:50–8. doi: 10.1016/j.ymben.2016.12.014
- Zhang J, Yu L, Lin M, Yan Q, Yang ST. N-Butanol Production From Sucrose and Sugarcane Juice by Engineered *Clostridium Tyrobutyricum* Overexpressing Sucrose Catabolism Genes and Adhe2. *Bioresour Technol* (2017) 233:51–7. doi: 10.1016/j.biortech.2017.02.079
- Hudcovic T, Kolinska J, Klepetar J, Stepankova R, Rezanka T, Srutkova D, et al. Protective Effect of *Clostridium Tyrobutyricum* in Acute Dextran Sodium Sulphate-Induced Colitis: Differential Regulation of Tumour Necrosis Factor- α and Interleukin-18 in BALB/C and Severe Combined Immunodeficiency Mice. *Clin Exp Immunol* (2012) 167:356–65. doi: 10.1111/j.1365-2249.2011.04498.x
- Al-Asmakh M, Stukenborg JB, Reda A, Anuar F, Strand ML, Hedin L, et al. The Gut Microbiota and Developmental Programming of the Testis in Mice. *PLoS One* (2014) 9:e103809. doi: 10.1371/journal.pone.0103809
- Hu X, Guo J, Xu M, Jiang P, Yuan X, Zhao C, et al. *Clostridium Tyrobutyricum* Alleviates *Staphylococcus Aureus*-Induced Endometritis in Mice by Inhibiting Endometrial Barrier Disruption and Inflammatory Response. *Food Funct* (2019) 10:6699–710. doi: 10.1039/c9fo00654k
- Liu T, Zhu L, Zhu Z, Jiang L. Genome Sequence Analysis of *Clostridium Tyrobutyricum*, a Promising Microbial Host for Human Health and Industrial Applications. *Curr Microbiol* (2020) 77:3685–94. doi: 10.1007/s00284-020-02175-0
- Xiao Z, Liu L, Tao W, Pei X, Wang G, Wang M. *Clostridium Tyrobutyricum* Protect Intestinal Barrier Function From LPS-Induced Apoptosis via P38/JNK Signaling Pathway in IPEC-J2 Cells. *Cell Physiol Biochem* (2018) 46:1779–92. doi: 10.1159/000489364
- Xiao Z, Liu L, Jin Y, Pei X, Sun W, Wang M. *Clostridium Tyrobutyricum* Protects Against LPS-Induced Colonic Inflammation via IL-22 Signaling in Mice. *Nutrients* (2021) 13:215. doi: 10.3390/nu13010215
- Xiao Z, Liu L, Jin Y, Pei X, Sun W, Wang M. A Potential Prophylactic Probiotic for Inflammatory Bowel Disease: The Overall Investigation of *Clostridium Tyrobutyricum* ATCC25755 Attenuates LPS-Induced Inflammation via Regulating Intestinal Immune Cells. *Mol Nutr Food Res* (2021) 65:e2001213. doi: 10.1002/mnfr.202001213
- Scott CL, Bain CC, Mowat AM. Isolation and Identification of Intestinal Myeloid Cells. *Methods Mol Biol* (2017) 1559:223–39. doi: 10.1007/978-1-4939-6786-5_15
- Heli UH, Emma P, Petra N, William A. Isolation of Cells From Human Intestinal Tissue. *Bio-Protocol* (2014) 4:1–8. doi: 10.21769/BioProtoc.1092
- Hoving LR, Heijink M, van Harmelen V, van Dijk KW, Giera M. Gc-MS Analysis of Short-Chain Fatty Acids in Feces, Cecum Content, and Blood Samples. *Methods Mol Biol* (2018) 1730:247–56. doi: 10.1007/978-1-4939-7592-1_17
- Niccolai E, Baldi S, Ricci F, Russo E, Nannini G, Menicatti M, et al. Evaluation and Comparison of Short Chain Fatty Acids Composition in Gut Diseases. *World J Gastroenterol* (2019) 25:5543–58. doi: 10.3748/wjg.v25.i36.5543
- Swallow CJ, Partridge EA, Macmillan JC, Tajirian T, DiGuglielmo GM, Hay K, et al. Alpha2hs-Glycoprotein, an Antagonist of Transforming Growth Factor Beta *In Vivo*, Inhibits Intestinal Tumor Progression. *Cancer Res* (2004) 64:6402–9. doi: 10.1158/0008-5472.CAN-04-1117
- Hu LH, Fan YJ, Li Q, Guan JM, Qu B, Pei FH, et al. Bortezomib Protects Against Dextran Sulfate Sodium-induced Ulcerative Colitis in Mice. *Mol Med Rep* (2017) 15:4093–9. doi: 10.3892/mmr.2017.6524
- Nowarski R, Gagliani N, Huber S, Flavell RA. Innate Immune Cells in Inflammation and Cancer. *Cancer Immunol Res* (2013) 1:77–84. doi: 10.1158/2326-6066.CIR-13-0081
- Iwasaki A, Medzhitov R. Control of Adaptive Immunity by the Innate Immune System. *Nat Immunol* (2015) 16:343–53. doi: 10.1038/ni.3123
- Hayashi A, Sato T, Kamada N, Mikami Y, Matsuoka K, Hisamatsu T, et al. A Single Strain of *Clostridium Butyricum* Induces Intestinal IL-10-Producing Macrophages to Suppress Acute Experimental Colitis in Mice. *Cell Host Microbe* (2013) 13:711–22. doi: 10.1016/j.chom.2013.05.013
- Zhu S, Ding S, Wang P, Wei Z, Pan W, Palm NW, et al. Nlrp9b Inflammasome Restricts Rotavirus Infection in Intestinal Epithelial Cells. *Nature* (2017) 546:667–70. doi: 10.1038/nature22967
- Chikano S, Sawada K, Shimoyama T, Kashiwamura S-I, Sugihara A, Sekikawa K, et al. IL-18 and IL-12 Induce Intestinal Inflammation and Fatty Liver in Mice in an IFN- γ Dependent Manner. *Gut* (2000) 47:779–86. doi: 10.1136/gut.47.6.779
- Sivakumar PV, Westrich GM, Kanaly S, Garka K, Born TL, Derry JMJ, et al. Interleukin 18 Is a Primary Mediator of the Inflammation Associated With Dextran Sulphate Sodium Induced Colitis: Blocking Interleukin 18 Attenuates Intestinal Damage. *Gut* (2002) 50:812–20. doi: 10.1136/gut.50.6.812
- Brand S, Beigel F, Olszak T, Zitzmann K, Eichhorst ST, Otte JM, et al. IL-22 Is Increased in Active Crohn's Disease and Promotes Proinflammatory Gene Expression and Intestinal Epithelial Cell Migration. *Am J Physiol Gastrointest Liver Physiol* (2006) 290:G827–38. doi: 10.1152/ajpgi.00513.2005
- Lee JS, Tato CM, Joyce-Shaikh B, Gulen MF, Cayatte C, Chen Y, et al. Interleukin-23-Independent IL-17 Production Regulates Intestinal Epithelial Permeability. *Immunity* (2015) 43:727–38. doi: 10.1016/j.immuni.2015.09.003
- Hanash AM, Dudakov JA, Hua G, O'Connor MH, Young LF, Singer NV, et al. Interleukin-22 Protects Intestinal Stem Cells From Immune-Mediated Tissue Damage and Regulates Sensitivity to Graft Versus Host Disease. *Immunity* (2012) 37:339–50. doi: 10.1016/j.immuni.2012.05.028
- Nowarski R, Jackson R, Gagliani N, de Zoete MR, Palm NW, Bailis W, et al. Epithelial IL-18 Equilibrium Controls Barrier Function in Colitis. *Cell* (2015) 163:1444–56. doi: 10.1016/j.cell.2015.10.072
- Jakovcevski M, Bharadwaj R, Straubhaar J, Gao G, Gavin DP, Jakovcevski I, et al. Prefrontal Cortical Dysfunction After Overexpression of Histone Deacetylase 1. *Biol Psychiatry* (2013) 74:696–705. doi: 10.1016/j.biopsych.2013.03.020
- Fagarasan S, Kawamoto S, Kanagawa O, Suzuki K. Adaptive Immune Regulation in the Gut: T Cell-Dependent and T Cell-Independent IgA Synthesis. *Annu Rev Immunol* (2010) 28:243–73. doi: 10.1146/annurev-immunol-030409-101314
- Mowat AM. Anatomical Basis of Tolerance and Immunity to Intestinal Antigens. *Nat Rev Immunol* (2003) 3:331–41. doi: 10.1038/nri1057
- Neeffes J, Jongsma ML, Paul P, Bakke O. Towards a Systems Understanding of MHC Class I and MHC Class II Antigen Presentation. *Nat Rev Immunol* (2011) 11:823–36. doi: 10.1038/nri3084
- Unanue ER, Turk V, Neefjes J. Variations in MHC Class II Antigen Processing and Presentation in Health and Disease. *Annu Rev Immunol* (2016) 34:265–97. doi: 10.1146/annurev-immunol-041015-055420

SUPPLEMENTARY MATERIAL

The Supplementary Material for this article can be found online at: <https://www.frontiersin.org/articles/10.3389/fimmu.2021.758227/full#supplementary-material>

36. Posovszky C, Sirin M, Jacobsen E, Lorenz M, Schwarz K, Schmidt-Choudhury A, et al. Persisting Enteropathy and Disturbed Adaptive Mucosal Immunity Due to MHC Class II Deficiency. *Clin Immunol* (2019) 203:125–33. doi: 10.1016/j.clim.2019.04.012
37. Meital GB, Christoph AT, Serafini N, Winter DR, Giladi A, Lara-Astiaso D, et al. The Spectrum and Regulatory Landscape of Intestinal Innate Lymphoid Cells Are Shaped by the Microbiome. *Cell* (2016) 166:1231–46.e13. doi: 10.1016/j.cell.2016.07.043
38. Dudakov JA, Hanash AM, van den Brink MR. Interleukin-22: Immunobiology and Pathology. *Annu Rev Immunol* (2015) 33:747–85. doi: 10.1146/annurev-immunol-032414-112123
39. Bleicher L, de Moura P, Watanabe L, Colau D, Dumoutier L, Renaud J, et al. Crystal Structure of the IL-22/IL-22R1 Complex and Its Implications for the IL-22 Signaling Mechanism. *FEBS Lett* (2008) 582:2985–92. doi: 10.1016/j.febslet.2008.07.046
40. Jones BC, Logsdon NJ, Walter MR. Structure of IL-22 Bound to Its High-Affinity IL-22R1 Chain. *Structure* (2008) 16:1333–44. doi: 10.1016/j.str.2008.06.005
41. Wu PW, Li J, Kodagattil SR, Luxenberg DP, Bennett F, Martino M, et al. IL-22r, IL-10R2, and IL-22bp Binding Sites Are Topologically Juxtaposed on Adjacent and Overlapping Surfaces of IL-22. *J Mol Biol* (2008) 382:1168–83. doi: 10.1016/j.jmb.2008.07.046
42. Shabgah AG, Navashenaq JG, Shabgah OG, Mohammadi H, Sahebkar A. Interleukin-22 in Human Inflammatory Diseases and Viral Infections. *Autoimmun Rev* (2017) 16:1209–18. doi: 10.1016/j.autrev.2017.10.004
43. Ouyang W, Rutz S, Crellin NK, Valdez PA, Hymowitz SG. Regulation and Functions of the IL-10 Family of Cytokines in Inflammation and Disease. *Annu Rev Immunol* (2011) 29:71–109. doi: 10.1146/annurev-immunol-031210-101312
44. Perez LG, Kempinski J, McGee HM, Pelczar P, Agaloti T, Giannou A, et al. TGF- β Signaling in Th17 Cells Promotes IL-22 Production and Colitis-Associated Colon Cancer. *Nat Commun* (2020) 11:2608. doi: 10.1038/s41467-020-16363-w
45. Wolk K, Witte E, Wallace E, Docke WD, Kunz S, Asadullah K, et al. IL-22 Regulates the Expression of Genes Responsible for Antimicrobial Defense, Cellular Differentiation, and Mobility in Keratinocytes: A Potential Role in Psoriasis. *Eur J Immunol* (2006) 36:1309–23. doi: 10.1002/eji.200535503
46. Liang SC, Tan XY, Luxenberg DP, Karim R, Kyriaki DJ, Collins M, et al. Interleukin (IL)-22 and IL-17 Are Coexpressed by Th17 Cells and Cooperatively Enhance Expression of Antimicrobial Peptides. *J Exp Med* (2006) 203:2271–9. doi: 10.1084/jem.20061308
47. Zelante T, Iannitti RG, Cunha C, De Luca A, Giovannini G, Pieraccini G, et al. Tryptophan Catabolites From Microbiota Engage Aryl Hydrocarbon Receptor and Balance Mucosal Reactivity via Interleukin-22. *Immunity* (2013) 39:372–85. doi: 10.1016/j.immuni.2013.08.003
48. Yang W, Yu T, Huang X, Bilotta AJ, Xu L, Lu Y, et al. Intestinal Microbiota-Derived Short-Chain Fatty Acids Regulation of Immune Cell IL-22 Production and Gut Immunity. *Nat Commun* (2020) 11:4457. doi: 10.1038/s41467-020-18262-6
49. Diefenbach A. Interleukin-22, the Guardian of the Intestinal Stem Cell Niche? *Immunity* (2012) 37:196–8. doi: 10.1016/j.immuni.2012.08.007
50. Hou Q, Ye L, Liu H, Huang L, Yang Q, Turner JR, et al. Lactobacillus Accelerates Iscs Regeneration to Protect the Integrity of Intestinal Mucosa Through Activation of STAT3 Signaling Pathway Induced by LPLs Secretion of IL-22. *Cell Death Differ* (2018) 25:1657–70. doi: 10.1038/s41418-018-0070-2
51. Aden K, Tran F, Ito G, Sheibani-Tezerji R, Lipinski S, Kuiper JW, et al. Atg16L1 Orchestrates Interleukin-22 Signaling in the Intestinal Epithelium via cGAS-STING. *J Exp Med* (2018) 215:2868–86. doi: 10.1084/jem.20171029
52. Witte E, Witte K, Warszawska K, Sabat R, Wolk K. Interleukin-22: A Cytokine Produced by T, NK and NKT Cell Subsets, With Importance in the Innate Immune Defense and Tissue Protection. *Cytokine Growth Factor Rev* (2010) 21:365–79. doi: 10.1016/j.cytogfr.2010.08.002
53. Wolk K, Kunz S, Witte E, Friedrich M, Asadullah K, Sabat R. IL-22 Increases the Innate Immunity of Tissues. *Immunity* (2004) 21:241–54. doi: 10.1016/j.immuni.2004.07.007
54. Furusawa Y, Obata Y, Fukuda S, Endo TA, Nakato G, Takahashi D, et al. Commensal Microbe-Derived Butyrate Induces the Differentiation of Colonic Regulatory T Cells. *Nature* (2013) 504:446–50. doi: 10.1038/nature12721
55. Park J, Kim M, Kang SG, Jannasch AH, Cooper B, Patterson J, et al. Short-Chain Fatty Acids Induce Both Effector and Regulatory T Cells by Suppression of Histone Deacetylases and Regulation of the Mtor-S6k Pathway. *Mucosal Immunol* (2015) 8:80–93. doi: 10.1038/mi.2014.44
56. Smith PM, Howitt MR, Panikov N, Michaud M, Gallini CA, Bohlooly YM, et al. The Microbial Metabolites, Short-Chain Fatty Acids, Regulate Colonic Treg Cell Homeostasis. *Science* (2013) 341:569–73. doi: 10.1126/science.1241165
57. Chen DF, Jin DC, Huang SM, Wu JY, Xu MQ, Liu TY, et al. Clostridium Butyricum, a Butyrate-Producing Probiotic, Inhibits Intestinal Tumor Development Through Modulating Wnt Signaling and Gut Microbiota. *Cancer Lett* (2020) 469:456–67. doi: 10.1016/j.canlet.2019.11.019
58. Suez J, Zmora N, Segal E, Elinav E. The Pros, Cons, and Many Unknowns of Probiotics. *Nat Med* (2019) 25:716–29. doi: 10.1038/s41591-019-0439-x
59. Yaqoob MU, Wang B, Pei X, Xiao Z, Sun W, Jin Y, et al. Microencapsulation of Clostridium Tyrobutyricum by Spray Drying Method and Its Characteristics in-Vitro. *Pakistan Veterinary J* (2020) 40:419–24. doi: 10.29261/pakvetj/2020.046
60. Wang X, Cao Z, Zhang M, Meng L, Ming Z, Liu J. Bioinspired Oral Delivery of Gut Microbiota by Self-Coating With Biofilms. *Sci Adv* (2020) 6:eabb1952. doi: 10.1126/sciadv.abb1952.eCollection2020Jun
61. Xie MH, Aggarwal S, Ho WH, Foster J, Zhang Z, Stinson J, et al. Interleukin (IL)-22, a Novel Human Cytokine That Signals Through the Interferon Receptor-Related Proteins Crf2-4 and IL-22r. *J Biol Chem* (2000) 275:31335–9. doi: 10.1074/jbc.M005304200
62. Dumoutier L, Roost L, Ameye G, Michaux L, Renaud J. IL-TIF/IL-22: Genomic Organization and Mapping of the Human and Mouse Genes. *Genes Immun* (2000) 1:488–94. doi: 10.1038/sj.gene.6363716
63. Kamanaka M, Huber S, Zenewicz LA, Gagliani N, Rathinam C, Connor WO Jr, et al. Memory/Effector (Cd45rb(Lo)) CD4 T Cells Are Controlled Directly by IL-10 and Cause IL-22-Dependent Intestinal Pathology. *J Exp Med* (2011) 208:1027–40. doi: 10.1084/jem.20102149
64. Wolk K, Witte E, Hoffmann U, Doecke WD, Endesfelder S, Asadullah K, et al. IL-22 Induces Lipopolysaccharide-Binding Protein in Hepatocytes: A Potential Systemic Role of IL-22 in Crohn's Disease. *J Immunol* (2007) 178:5973–81. doi: 10.4049/jimmunol.178.9.5973
65. Mortha A, Chudnovskiy A, Hashimoto D, Bogunovic M, Spencer SP, Belkaid Y, et al. Microbiota-Dependent Crosstalk Between Macrophages and Ilc3 Promotes Intestinal Homeostasis. *Science* (2014) 343:1249288. doi: 10.1126/science.1249288
66. Singh N, Gurav A, Sivaprakasam S, Brady E, Padia R, Shi H, et al. Activation of GPR109a, Receptor for Niacin and the Commensal Metabolite Butyrate, Suppresses Colonic Inflammation and Carcinogenesis. *Immunity* (2014) 40:128–39. doi: 10.1016/j.immuni.2013.12.007

Conflict of Interest: The authors declare that the research was conducted in the absence of any commercial or financial relationships that could be construed as a potential conflict of interest.

Publisher's Note: All claims expressed in this article are solely those of the authors and do not necessarily represent those of their affiliated organizations, or those of the publisher, the editors and the reviewers. Any product that may be evaluated in this article, or claim that may be made by its manufacturer, is not guaranteed or endorsed by the publisher.

Copyright © 2021 Xiao, Liu, Pei, Sun, Jin, Yang and Wang. This is an open-access article distributed under the terms of the Creative Commons Attribution License (CC BY). The use, distribution or reproduction in other forums is permitted, provided the original author(s) and the copyright owner(s) are credited and that the original publication in this journal is cited, in accordance with accepted academic practice. No use, distribution or reproduction is permitted which does not comply with these terms.



Evaluation of the Anti-Aging Effects of a Probiotic Combination Isolated From Centenarians in a SAMP8 Mouse Model

Xin Fang¹, Mengyun Yue¹, Jing Wei², Yun Wang¹, Daojun Hong¹, Bo Wang¹, Xiaoting Zhou^{1*} and Tingtao Chen^{1,2*}

¹ Department of Neurology, The First Affiliated Hospital of Nanchang University, Nanchang, China, ² National Engineering Research Center for Bioengineering Drugs and the Technologies, Institute of Translational Medicine, Nanchang University, Nanchang, China

OPEN ACCESS

Edited by:

Qixiao Zhai,
Jiangnan University, China

Reviewed by:

Zhenxing Wang,
Southwest Forestry University, China
Menghao Huang,
Indiana University School of Medicine,
United States

Ming Li,
Dalian Medical University, China

*Correspondence:

Tingtao Chen
chentingtao1984@163.com
Xiaoting Zhou
914113072@qq.com

Specialty section:

This article was submitted to
Nutritional Immunology,
a section of the journal
Frontiers in Immunology

Received: 11 October 2021

Accepted: 16 November 2021

Published: 02 December 2021

Citation:

Fang X, Yue M, Wei J, Wang Y,
Hong D, Wang B, Zhou X and Chen T
(2021) Evaluation of the Anti-Aging
Effects of a Probiotic Combination
Isolated From Centenarians in a
SAMP8 Mouse Model.
Front. Immunol. 12:792746.
doi: 10.3389/fimmu.2021.792746

Population aging is a prominent global problem in today's society. However, there are currently no good methods to treat or prevent aging, so anti-aging research has crucial implications. In this research, we screened bacteria from centenarians, and finally selected four probiotics (*Lactobacillus fermentum* SX-0718, *L. casei* SX-1107, *Bifidobacterium longum* SX-1326, and *B. animalis* SX-0582) to form a probiotic combination. By using the senescence accelerated mouse prone 8 (SAMP8) model, the anti-aging effects of the probiotic combination were evaluated by using behavioural testing, neuroinflammation, intestinal inflammation, and intestinal microbiota. The results showed that probiotic combination improved the impaired spatial memory, motor dysfunction, and decreased exploratory behavior in aging mice. The probiotic combination inhibited Toll-like receptor 4 (TLR4)/nuclear factor kappa B (NFκB)-induced neuroinflammation and up-regulated the expression of Sirt 1 to protect hippocampal neurons. At the same time, the probiotic combination regulated the intestinal microbiota, reduced the relative abundance of *Alistipes* and *Prevotella* in SAMP8 mice, inhibited TLR4/NFκB-induced intestinal inflammation, and increased the expression of intestinal permeability related proteins zonula occludens-1 (ZO-1) and Occludin. The anti-aging effects of the probiotic combination may be through the regulating intestinal microbiota and inhibiting TLR4/NFκB-induced inflammation. This research provides the basis and technical support for the future production and application of the probiotic combination.

Keywords: aging, SAMP8 mice, TLR4/NFκB, neuroinflammation, probiotic combination

INTRODUCTION

Aging is a process that almost all living organisms go through, characterised by the gradual decline of in the body's cell, tissue, and organ functions over time, as well as reduced cognitive and memory functions (1). Globally, the population over the age of 65 is 617 million (8.5%), and this number may reach 1.6 billion by 2050 (2). With the aging of China's population, the incidence of aging-related

diseases - Parkinson's disease (PD), Alzheimer's disease (AD), malignant tumours, and others - continues to rise, causing a heavy financial burden on the country and the families of patients (3, 4). Although many drugs such as metformin, resveratrol, and rapamycin have been proven to have anti-aging effects, they have not been promoted widely due to high cost, difficulty in extraction, and serious side effects (5). Therefore, finding or developing anti-aging active substances and exploring their mechanisms of action has become a current research hotspot in response to the reality of population aging.

In recent years, inflammatory aging has become a new topic in aging research (6). These studies have shown that inflammatory aging is closely related to the occurrence and development of many senile diseases such as AD, atherosclerosis, PD and osteoporosis (7). Inflammatory aging refers to the chronic and progressive increase in the pro-inflammatory state of the body during the natural aging process. The main reason is the imbalance between pro-inflammatory and anti-inflammatory cytokines in the body, which ultimately leads to an increase in the pro-inflammatory response (8). Pro-inflammatory cytokines can induce stem cell senescence, which is the cellular basis for the aging of tissues and organs. Senescent cells secrete cytokines, growth factors, proteases, and other substances that cause inflammation and destroy the cellular microenvironment, leading to reduced cell survival. It affects the proliferation and differentiation of cells and induces stem cell senescence and aging-related diseases (9). Research has shown that in the elderly, increased levels of serum inflammatory factors such as tumour necrosis factor- α (TNF- α), interleukin-6 (IL-6) and C-reactive protein (CRP) are considered to be risk factors of cardiovascular and degenerative diseases (10). Bruunsgaard et al. (11) found that the increased of TNF- α is correlated positively with the all-cause mortality of elderly men in a follow-up study of 333 relatively healthy elderly people over 80 years of age, indicating that TNF- α has a certain predictive effect on death.

According to recent research reports that there is an important relationship the between intestinal microbiota and inflammatory aging, Inflammation may be caused by decreased in the autoimmune tolerance and the composition of the intestinal microbiota caused by aging, leading to its abnormal immune activation (12). Increased release of gram-negative bacteria and lipopolysaccharide in the intestine leads to chronic inflammation throughout the body, which in turn induces the occurrence of various neurological diseases such as AD, PD, and amyotrophic lateral sclerosis (ALS) (12). The intestinal microbiota can also regulate host behaviour through the brain-gut axis, affect the host's blood-brain barrier function and basic neurodevelopmental processes such as the maturation of microglia, and participate in the regulation of brain functions (13). The intestinal microbiota participates in the process of aging mainly through regulating oxidative stress, the immune response, and metabolism (13, 14). Aging people have disorders of the intestinal microbiota. Studies have compared the fecal microbes of patients with progeria with their respective healthy siblings. There is a marked decline in the relative abundance of the family *Ruminococcaceae* in patients with progeria, while the families *Erysipelotrichaceae* and *Lachnospiraceae* are

enriched; these findings are consistent with the mouse model of progeria (15). When the researchers transplanted the intestinal microbiota of normal mice into progeria mice, the average lifespan increased (15). These results indicate that regulating and maintaining the balance of the intestinal microbiota of the elderly may be a means of preventing and treating aging-related diseases and delaying aging. Hence, this topic deserves further discussion and research.

As active microorganisms that are beneficial to human body, probiotics play a great part in maintaining the balance of microorganisms in the intestinal tract. Supplementing probiotics can facilitate the production of immunologically active factors and different types of immunoglobulins by regulating cellular and humoral immunity, participating in inflammation, improving the immune response, and promoting the proliferation of spleen cells (16). Therefore, our group screened probiotics from the faeces of seven centenarians of the Centenarian Village in Ganzhou, Jiangxi province, China. Based on this screening, we chose *Lactobacillus fermentum* SX-0718, *L. casei* SX-1107, *Bifidobacterium longum* SX-1326, and *B. animalis* SX-0582 to prepare a probiotic combination. Then we evaluated the anti-aging effects of this probiotic combination by using the senescence accelerated mouse prone 8 (SAMP8) mice model. Our findings provide a basis for the development of an anti-aging probiotic dietary supplement for elderly people.

MATERIALS AND METHODS

In Vitro Experiments Bacterial Strains

The research team screened the faeces of seven centenarians of the Centenarian Village in Ganzhou, Jiangxi province, China; their ages were 103, 107, 102, 105, 100, 101, and 100, respectively. First, the faecal microorganisms were extracted and subjected to serial dilutions. The various dilutions were spread aseptically on the selected culture medium and cultivated in aerobic and anaerobic environments for 24–48 h. According to the colony shape, size, colour, edge, gloss, and texture, 20–40 single colonies were picked and then activated and cultured on the corresponding liquid medium for 24–48 h. The genomic DNA of the activated bacteria was extracted and then sequenced to identify the types of bacteria by using the NCBI database. A total of more than 1,500 strains were screened, and four probiotics were selected to form a probiotic combination (all from Jiangxi Shanxing Biotechnology Co., Ltd, Nanchang, Jiangxi, PR China): *L. fermentum* SX-0718, *L. casei* SX-1107, *B. longum* SX-1326, and *B. animalis* SX-0582. The bacteria were cultivated in De Man-Rogosa-Sharpe (MRS) medium at 37°C under anaerobic conditions with a bacterial density of 1×10^9 colony-forming units (CFU)/mL.

Probiotic Evaluation of Isolates

For the acid resistance test, after activation, bacteria were centrifuged at 4500 g for 10 min at 4°C, and the cell pellet was resuspended in phosphate buffered saline (PBS). The cell

suspension was diluted in PBS with different pH (3, 5, 7 and 9) and incubated at 37°C, for 4 h. For the bile salt tolerance test, bacteria were inoculated in MRS medium containing different bile salts concentrations (0.0%-0.5% wt/wt) at 37°C for 4 h. After incubation, all bacteria were counted by the plate number method (17).

For antimicrobial testing, pathogenic microorganisms were selected, including *Salmonella typhimurium* ATCC 13311, *Shigella flexneri* ATCC 12022, *Propionibacterium acnes* ATCC 11827, *Sh. dysenteriae* 301, *Enterohemorrhagic coli* O157, *S. enteritidis* ATCC 13076, *Listeria monocytogenes* ATCC 19111, *Staphylococcus aureus* Cowan1 and *Candida albicans* SC531. They were cultured overnight and spread on the lysosomal broth (LB) (Hopbio, Hb0384-1, Qingdao) agar plate surface. Then, an Oxford cup was placed on the surface of the agar, and the bacterial supernatant (200 µL) was added. The size of the inhibition zone around the Oxford Cup was measured (18).

Experimental Design and Processing

The mice used in this experiment – SAMP8, a rapidly aging mouse model, and SAMR1, the corresponding normal aging model – were purchased from the Peking University Health Science Center. The 3-month-old male mice were maintained in a standard environment for 2 weeks before beginning the experiments. The standard environment for mouse breeding comprised a 12-h photoperiod, a temperature of $22 \pm 3^\circ\text{C}$, relative humidity of $50\% \pm 15\%$, and free access to food and water. Then, the mice were divided into four groups: (i) the control (C) group ($n = 10$), SAMR1 mice, daily gavage of normal saline (the same volume as used for the probiotic combination); (ii) the model (M) group ($n = 9$), daily gavage of normal saline daily (the same volume as used for the probiotic combination); (iii) the low-dose probiotic (L) group ($n = 10$), daily gavage of 1×10^7 CFU/mL *L. fermentum* SX-0718 + 1×10^7 CFU/mL *L. casei* SX-1107 + 1×10^7 CFU/mL *B. longum* SX-1326 + 1×10^7 CFU/mL *B. animalis* SX-0582 for 18 weeks; (iv) the high-dose probiotic (H) group ($n = 10$), daily gavage of 1×10^9 CFU/mL *L. fermentum* SX-0718 + 1×10^9 CFU/mL *L. casei* SX-1107 + 1×10^9 CFU/mL *B. longum* SX-1326 + 1×10^9 CFU/mL *B. animalis* SX-0582, for 18 weeks. After the probiotic treatment, all mice underwent behavioural testing. They were then anaesthetised and the brain and colon were collected (Supplementary Figure 1A).

Aging Score

Animals in each group were scored objectively for 11 indicators including fur gloss, fur roughness, the degree of hair loss, skin ulcers, eye damage, corneal turbidity, corneal ulcers, cataracts, kyphosis, reactivity, and the passive escape response. Each index is divided into 4-5 grades, and the score is calibrated. The higher the score an animal gets, the higher its degree of aging (19).

Behavioural Experiments

The pole test was used to detect motor dysfunction in mice. The apparatus is a metal rod with a diameter of 1 cm and a length of 50 cm. To prevent the mice from slipping, the metal rod was wrapped with bandage gauze, and the bottom of the metal rod

was placed in a cage. The mouse was placed face down on the top of the pole, and the latency for the mouse to fall freely to the cage (hind limbs touch the bottom of the cage) was recorded. Each mouse was tested three times, 15 min apart, and the average value was calculated.

The open field test was used to evaluate the changes in exploratory behaviour and anxiety of each mouse when exposed to a new environment. The apparatus is a square divided into 25 squares of equal area; the edge area and the central area are defined. The free movement of mice was recorded for 10 min. After each experiment, the experimental area was cleaned to remove any odour left by the previous mouse so that it would not affect the behaviour of the subsequent mouse.

The Barnes maze was used to test the spatial memory ability. The animals were placed individually in the target box of the target hole and allowed to adapt to the apparatus for 2 min the day before the start of the test. On day 1 of testing, a transfer device was used to place the animal in the centre of the maze. Then, each mouse was guided to the target hole, and the animals were permitted to stay in the box for 2 min. Each animal was observed for a maximum of 3 min at a time. During this period, if the animal could not find the target box, it was guided to the target box and allowed to stay there for 2 min. The animals were trained each day for 9 days. On the last day of probe test, count the incubation period of each group of mice, the stay time in the target area, the stay time in the reverse target area, and the correct number of holes.

Western Blot

One gram of tissue was homogenised in radioimmunoprecipitation assay (RIPA) buffer containing protease inhibitor cocktail and phenylmethylsulphonyl fluoride (PMSF) with electric homogeniser. The sample was centrifuged at 12000 g for 10 min at 4°C . The supernatant was removed and the protein concentration was determined with a BCA protein assay kit. The samples were then subjected to sodium dodecyl sulphate–polyacrylamide gel electrophoresis (SDS-PAGE) to separate protein. The wet transfer method was used to transfer the separated protein to a polyvinylidene fluoride membrane (PVDF). After the transfer, the membrane was blocked and then incubated with the appropriate primary and secondary antibodies according to the manufacturer's instructions. Finally, the membrane was incubated with a chemiluminescent substrate and the protein bands were visualised with an automatic gel imaging analyser. The primary antibodies used included: rabbit anti- β -actin (β -actin; 1:1000; Cell Signaling Technology; Cat# 4970S), rabbit anti-Bcl-2 associated X Protein (Bax, 1:1000; Cell Signaling Technology, Cat# 14796S), rabbit anti-B-cell lymphoma-2 (Bcl-2, 1:1000; Cell Signaling Technology, Cat# 3498S), rabbit anti-phosphorylated-AKT (p-AKT; 1:1000; Sangon Biotech, Cat# D151499), rabbit anti-AKT (1:1000; Sangon Biotech, Cat# D151621), rabbit anti-silent information regulator 1 (Sirt 1; 1:1000; Cell Signaling Technology, Cat#9475), mouse anti-Toll-like receptor 4 (TLR4; 1:1000; Santa Cruz Biotechnology, Cat# sc-293072), rabbit anti-myeloid differentiation primary response gene 88 (MyD88; 1:1000; Proteintech; Cat# 23230-1-AP), rabbit anti-phosphorylated-p65 (p-p65; 1:1000; Abcam; Cat# ab86299), rabbit

anti-p65 (p65 1:1000; Cell Signaling Technology; Cat# 8242S), rabbit anti-tight junction protein 1 (zona occludens 1, ZO-1; 1:5000; Proteintech; Cat# 21773-1-AP), and rabbit anti-Occludin (Occludin 1:1000; Proteintech; Cat# 13409-1-AP).

Immunofluorescence and Inflammatory Factor Detection

Brains were fixed in paraformaldehyde and then subjected to dehydration, clearing, wax immersion, and embedding. The embedded tissue was sliced continuously at a thickness of 5 μ m. The sections were deparaffinised and equilibrated to water, subjected to antigen retrieval, and incubated in 5% bovine serum albumin (BSA) for 30 min. The sections were then incubated with the appropriate primary and secondary antibodies. The nuclei were then stained with DAPI. After mounting the sections, they were viewed under an upright fluorescence microscope and images were captured. The number of NeuN-positive cells was counted by using the ImageJ software (National Institutes of Health). The average cell number/field of view was used for statistical analysis.

To detect inflammatory factors, protein was extracted from the brains following the same method described for western blot. The following kits were used to evaluate the levels of inflammatory factors in the hippocampus of mice, following the manufacturer's instructions: IL-1 β (Proteintech, Cat# KE10003), TNF- α (Proteintech, Cat# KE10002) and IL-6 (Proteintech, Cat# KE10007).

Bacterial DNA Extraction

For microbiota analysis, the faeces of each group of mice (n=8) were collected. A genomic DNA kit (Qiagen, Cat#51804) was used to extract fecal genomic DNA, following the product instructions. Then the NanoDrop spectrophotometer was used to determine the concentration and quality of the extracted DNA. Genomic DNA was re-extracted for samples that did not meet the quality requirements. The 16S ribosomal DNA (rDNA) V4 region was amplified by using the following primers: 515F, 5'-GTG CCA GCMGCC GCG GTAA-3'; 806R, 5'-GGA CTA CVS GGG TAT CTAAT-3'. The IlluminaHiSeq2000 platform was used for sequencing. The sequencing results have been deposited in GenBank (accession number PRJNA768326).

High-Throughput Sequencing

The data were subjected to sequence denoising or operational taxonomic unit (OTU) clustering by using the analysis process of the Vsearch software or QIIME2 DADA2 analysis. The Vsearch method (20) mainly includes de-priming, splicing, quality filtering, de-duplication, de-chimerism, clustering and other steps to obtain OTU. The DADA2 method mainly carries out the steps of depriming, quality filtering, de-noising, splicing and de-chimerism. Each deduplicated sequence generated after DADA2 quality control is called an amplicon sequence variant (ASV), or feature sequence (corresponding to a representative sequences of OTU). ASV and OTU were then used to analyse the species composition, alpha diversity, beta diversity, species difference analysis and symbol species, etc.

Statistical Analysis

GraphPad Prism 7 was used for statistical analysis. The data were expressed as the mean \pm standard deviation (SD). One-way analysis of variance (ANOVA) was used to determine a statistically significant difference ($p < 0.05$).

RESULTS

Probiotic Properties

First, we conducted acid tolerance, bile salt tolerance and antibacterial experiments to evaluate the probiotic characteristics of the selected strains. The four selected probiotics were tolerant to medium strong acid (**Figure 1A**) and survived in different bile salt concentrations (**Figure 1B**). As shown in **Figure 1A**, after 4 h in pH 3 PBS, the survival rates of *L. fermentum* SX-0718, *L. casei* SX-1107, *B. longum* SX-1326, and *B. animalis* SX-0582 were 80.2%, 92.4%, 99.0%, and 99.5%, respectively. As shown in **Figure 1B**, *L. fermentum* SX-0718 had low tolerance to bile salt. *B. longum* SX-1326 showed excellent bile salt tolerance: at a concentration of 0.5%, the survival rate was still 85.4%. In addition, the selected probiotics significantly inhibited the growth of the pathogens *S. typhimurium* ATCC 13311, *Sh. flexneri* ATCC 12022, *P. acnes* ATCC 11827, *Sh. dysenteriae* 301, *E. coli* O157, *S. enteritidis* ATCC 13076, *L. monocytogenes* ATCC 19111, *Staph. aureus* Cowan1 and *C. albicans* SC531, with a suppression area from 15.25 mm to 22.5 mm (**Figure 1C**).

The Probiotic Combination Improved Behaviour in SAMP8 Mice

The Barnes maze test was used to evaluate the effect of the probiotic combination on the spatial learning and memory abilities. Compared with C group, in daily training, mice in group M took significantly longer time to find the platform, while probiotic combination (group L and H) greatly reduced the escape latency, the latency period of searching for right foramen. On the probe test, the latency of the probiotic combination treatment was significantly shorter than that of the M group (L vs. M = 27.4 s vs. 48.19 s; $p < 0.001$; H vs. M = 20.34 s vs. 48.19 s; $p < 0.001$), and there was no significant difference between low-dose and high-dose probiotics (**Figure 2A**).

The pole test was conducted to observe the effect of the probiotic combination on the motor dysfunction of SAMP8 mice. As shown in **Figure 2**, compared with the C group, the M group showed significant motor retardation (M vs. C = 19.46 s vs. 8.877 s; $p < 0.001$), and treatment with either low or high concentrations of the probiotic combination significantly alleviated the motor dysfunction of SAMP8 mice (L vs. M = 13.78 s vs. 19.46 s; $p < 0.001$; H vs. M = 10.73 s vs. 19.46 s; $p < 0.001$).

The open field test was used to detect the behavioral and mental changes of mice to the new environment, such as exploratory behavior and anxiety. Experimental parameters showed that compared with mice in group M (distance = 4384 cm, number = 109, distance = 574.6), mice in groups C, L, and H had a longer total movement distance (distance =

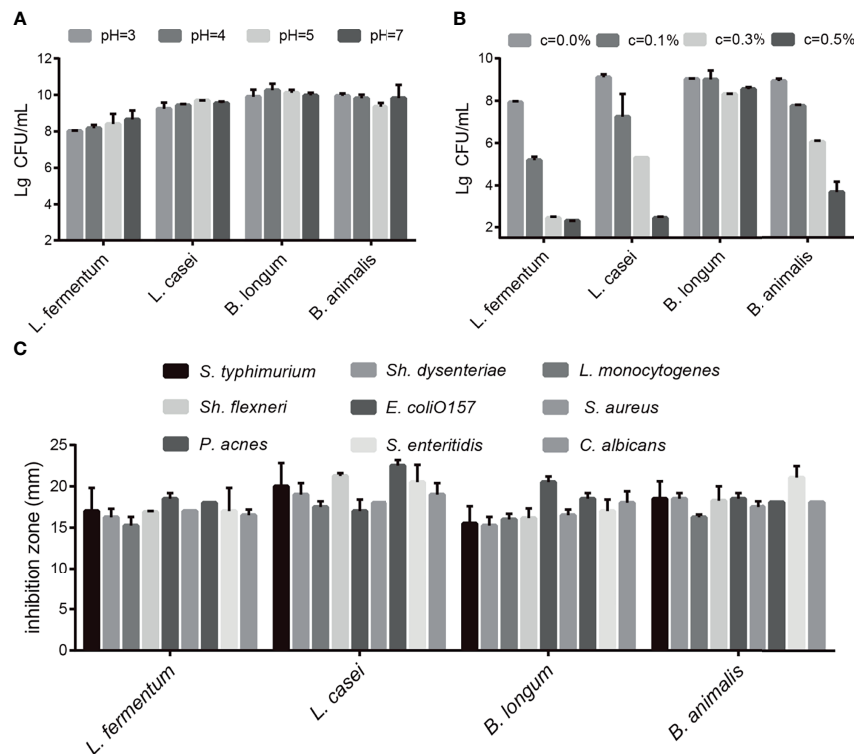


FIGURE 1 | Evaluation of the probiotic characteristics of *L. fermentum* SX-0718, *L. casei* SX-1107, *Bifidobacterium* SX-1326, and *B. animalis* SX-0582. **(A)** The acid tolerance of *L. fermentum* SX-0718, *L. casei* SX-1107, *B. longum* SX-1326 and *B. animalis* SX-0582. **(B)** The cholate tolerance of *L. fermentum* SX-0718, *L. casei* SX-1107, *B. longum* SX-1326 and *B. animalis* SX-0582. **(C)** Antibacterial activities of *L. fermentum* SX-0718, *L. casei* SX-1107, *B. longum* SX-1326 and *B. animalis* SX-0582 on *Salmonella typhimurium* ATCC 13311, *Shigella flexneri* ATCC 12022, *Propionibacterium acnes* ATCC 11827, *Sh. dysenteriae* 301, *Escherichia coli* O157, *S. enteritidis* ATCC 13076, *Listeria monocytogenes* ATCC 19111, *Staphylococcus aureus* Cowan1 and *Candida albicans* SC531.

5505 cm, distance = 5474 cm, distance = 5313 cm; C vs M, $P < 0.05$; L vs M, $p < 0.05$; H vs M, $p < 0.05$), more times to enter the central area (number = 59.33, number = 91.56, number = 104.8; C vs M, $p < 0.05$; L vs M, $p < 0.05$; H vs M, $p < 0.05$) and longer central movement distance (distance = 1379 cm, distance = 1187 cm, distance = 1416 cm; C vs M, $p < 0.05$; L vs M, $p < 0.05$; H vs M, $p < 0.05$). In addition, there was no dose-dependent in probiotics treatment.

The Probiotic Combination Reduced Neuronal Death and Prevented the Decrease of Sirt 1 Expression in the Hippocampus of SAMP8 Mice

The reduction in the number of hippocampal neurons in SAMP8 mice is closely related to the learning and memory declines. Therefore, we detected the number of neurons in the hippocampus of SAMP8 mice through NeuN immunostaining. Compared with C group, the M group had fewer hippocampal neurons; the probiotic combination protected hippocampal neurons compared with the M group (**Figure 3A**). Neuronal loss due to apoptosis – regulated by Bax and Bcl-2 – plays an important part in the occurrence and development of aging. The p-AKT can modulate apoptosis by regulating Bcl-2/Bax. We

evaluated the expression of Bax, Bcl-2, and p-AKT in the hippocampus of mice by using western blot. The results showed that the expression of pro-apoptotic protein Bax in group M mice was significantly higher than that in C mice, and the expression of anti-apoptotic protein Bcl-2 and p-AKT was significantly lower than that of the M group, while the pro-apoptotic protein expression in the L and H groups was significantly lower than that in M group, and the expression of apoptotic protein was notably higher than that of the M group. In addition, the expression of Sirt 1 in the C, L and H groups was prominently higher than that in the M group, indicated that probiotic combination could inhibit the decrease of Sirt 1 expression in aging mice.

The Probiotic Combination Inhibited TLR4/NF- κ B Signaling Pathway and Hippocampal Inflammation in SAMP8 Mice

Inflammation plays an important role in maintaining and promoting aging, and the TLR4/NF κ B pathway is closely related to inflammation. Hence, we evaluated the expression of proteins involved in the TLR4/NF κ B signalling pathway in the hippocampus by using western blot. Compared with the M group, the probiotic combination significantly reduced TLR4,

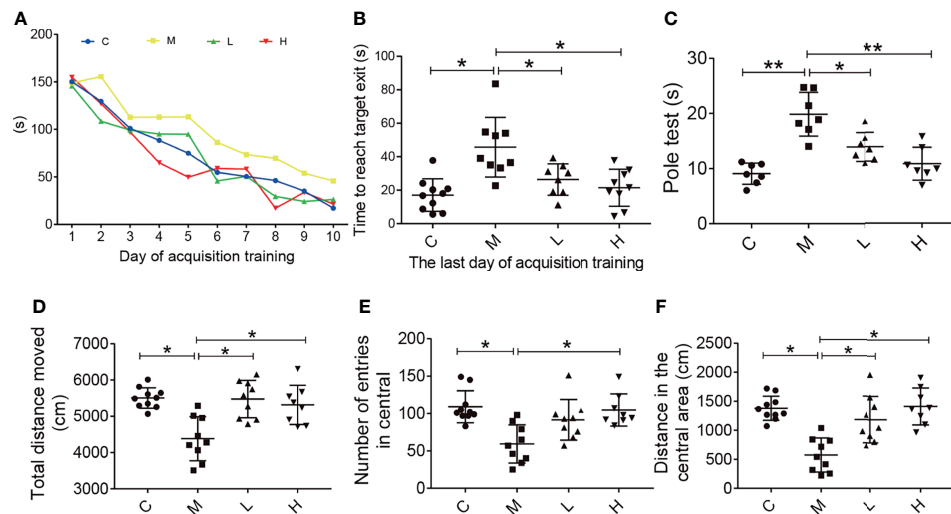


FIGURE 2 | The probiotic combination improved spatial memory, motor dysfunction, and exploratory behaviour in SAMP8 mice. **(A)** The time to reach the target exit during the training test (the Barnes maze). **(B)** The probiotic combination reduced time it took SAMP8 mice to reach the target exit during the probe test of the Barnes maze. **(C)** The probiotic combination improved the motor dysfunction in SAMP8 mice (the pole test). **(D)** The probiotic combination increased the total distance in SAMP8 mice moved in the open-field test. **(E)** The probiotic combination increased the number of entries SAMP8 mice made in central area of the open-field test. **(F)** The probiotic combination increased the distance SAMP8 mice moved in the central area of the open-field test. C: control group (n = 10), M: model group (n = 9), L: low-dose probiotic group (n = 8), H: high-dose probiotic group (n = 9). Data are presented as the means \pm SD. *p < 0.05 **p < 0.01.

MyD88 and p-65/p65 expression (Figure 4A, $p < 0.01$). In addition, the detection of inflammatory factor protein levels showed that probiotic combination significantly reduced the relative expression of the pro-inflammatory cytokine IL-1 β , IL-6 and TNF- α compared with the M group, (Figure 4B; $p < 0.01$). These results suggest that the probiotic combination modulates the upregulation of TLR4/NF κ B signalling pathway components to reduce inflammation in SAMP8 mice.

The Probiotic Combination Altered the Gut Microbiota Composition of SAMP8 Mice

The intestinal microbiota is closely related to the occurrence and development of senescence. We collected the faeces of mice and analysed their intestinal microbiota changes by using high-throughput sequencing. A total of 1,138,968 valid tags and 10,202 OTUs were obtained, with an average of 2550.25 per group (data not shown). To analyse the influence of the probiotic combination on the intestinal microbiota of SAMP8 mice, we carried out a diversity analysis of the microbiota. The Observed_species index represented the actual observed number of OTU, and the Chao1 index indicates the diversity of the microbiota. As shown in the Figure 5, the Observed_species index and Chao1 indexes of the M group of mice were reduced, while the probiotic combination increased the abundance and diversity of intestinal microbiota, although the changes were not significant (Figures 5A, B). The Venn diagram shows 441 common OTU among all the groups, with 47, 42, 69, and 57 unique OUT for the C, M, L, and H groups, respectively (Figure 5C). In addition, the principal co-ordinates analysis (PCoA) used to study the similarity of microbial communities showed that the points of the C group are

clustered together, the points of the M group are relatively scattered, and the samples of the C, L, and H groups have high similarity. These findings indicate that the probiotic combination alters the intestinal microbiota of aging mice to a pattern like that of normal mice (Figure 5D). We analysed the relative abundance of the top 20 bacterial genera among the different groups. There was notably increased the relative abundance of *Alisipes*, *Prevotella*, *Odoribacter*, *Lactobacillus* and *Oscillibacter*, and decreased the relative abundance of *Alloprevotella*, *Barnesiella* and *Akkermansia*. Compared with the M group, the probiotic combination reduced the relative abundance of *Alistipes* and *Prevotella*, and increased the relative abundance of *Alloprevotella*, *Acetatifactor*, and *Clostridium XIVa* (Figure 5E).

The Probiotic Combination Alleviated Colonic Inflammation and Decreased Tight Junction Protein Expression in SAMP8 Mice

Intestinal microbiota imbalance and intestinal inflammation can be causally related to each other. Therefore, haematoxylin and eosin (H&E) staining was used to detect the pathological changes in the mice colon, and the western blot were applied to detect the expression of key proteins in the TLR4/NF κ B inflammatory pathway and intestinal permeability-related proteins in mouse colon tissue. As shown in Figure 6, mucosal epithelial cells were shed and a small amount of the intestinal gland structure was destroyed in the colon of mice in the M group, while no mucosal epithelial cells were shed and the intestinal gland structure was maintained in the intestinal tissues of the C, L and H groups. In addition, we used western blot to examine the expression of key proteins in the TLR4/NF κ B inflammatory pathway as well as

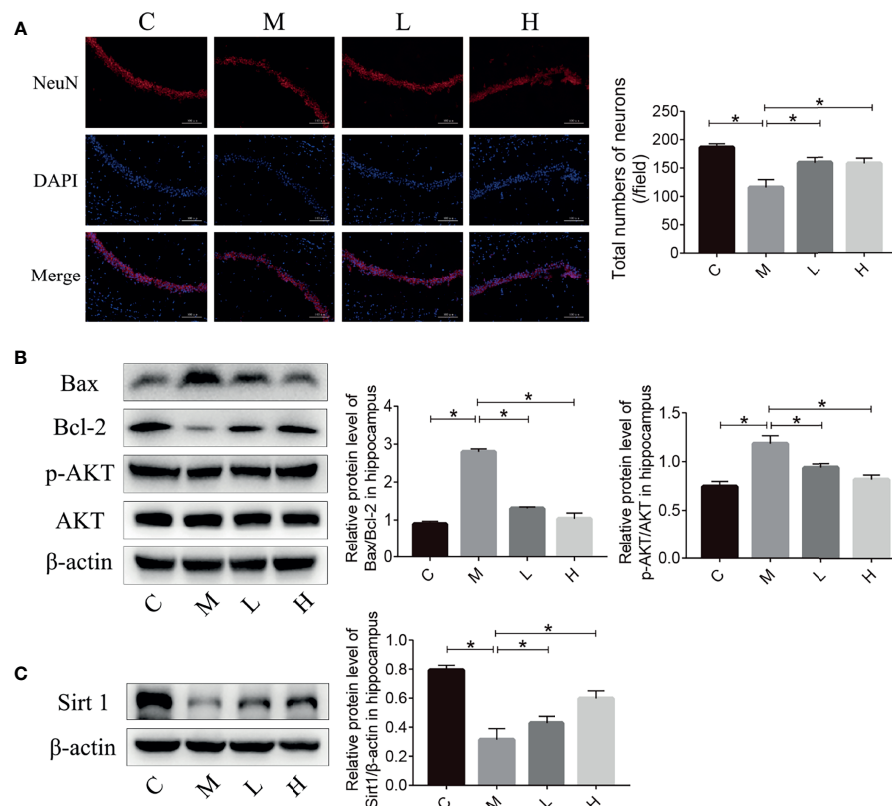


FIGURE 3 | The probiotic combination reduced neuronal death and prevented the decrease in Sirt1 expression in the hippocampus of SAMP8 mice. **(A)** Photomicrographs and quantitative analysis of the number of neurons in the hippocampus, analysed by NeuN immunostaining. **(B)** The effect of the probiotic combination on the expression levels of Bax, Bcl-2, p-AKT and AKT in the hippocampus. **(C)** The effect of the probiotic combination on the expression level of Sirt1 in the hippocampus. C: control group (n = 4), M: model group (n = 4), L: low-dose probiotics group (n = 4), H: high-dose probiotics group (n = 4). Data are presented as the means \pm SD. *p < 0.05.

proteins related to intestinal permeability. Compared with the C group, ZO-1 and Occludin expression decreased and TLR4, MyD88, and p-p65 expression increased in the M group. The probiotic combination significantly increased the expression of ZO-1 and Occludin – indicating increased integrity of the intestinal barrier – and reduced the expression of TLR4, MyD88, and p-p65 – indicating a modulation of intestinal inflammation (**Figures 6B, C**).

DISCUSSION

The aging of the population is a prominent global problem in today's society. Aging can lead to a series of physical changes and abnormal behaviours, such as hair loss, sagging skin, reduced mental ability, decreased memory and even dementia (21). The health problems caused by the aging are major challenges in the field of health care (12). There is currently no good way to prevent or treat aging. Therefore, research related to anti-aging treatments and aging-related diseases is needed urgently. The SAMP8 mouse exhibits rapid aging that is consistent with what happens in humans. It is mainly characterised

by reduced learning and memory, cognitive impairment and neurodegenerative changes. It is a common natural pathogenesis model to study dementia and aging (22).

In this research, the SAMP8 mice were used to evaluate the effects of a probiotic combination. First, we identified four probiotics (*L. fermentum* SX-0718, *L. casei* SX-1107, *B. longum* SX-1326, and *B. animalis* SX-0582; Jiangxi Shanxing Biotechnology Co., Ltd, Nanchang, Jiangxi, PR China) from the faeces of centenarians. *In vitro* experiments verified that they had good acid resistance, bile salt resistance and antibacterial properties (**Figure 1**). In addition, the probiotic combination could alleviate weight loss and reduce the aging score of SAMP8 mice (**Supplementary Figures 1B, C**). In behavioural tests, aging mice showed impaired spatial memory, motor dysfunction and decreased exploratory behaviour (**Figure 2**). The probiotic combination was able to ameliorate these changes, indicating that it may exert anti-aging effects.

Given the promising behavioural data, we studied the possible anti-aging mechanism of the probiotic combination. The hippocampus is involved in learning and memory and damage to this brain region can cause learning and memory impairment and spatial positioning disorders (23). Compared with the C

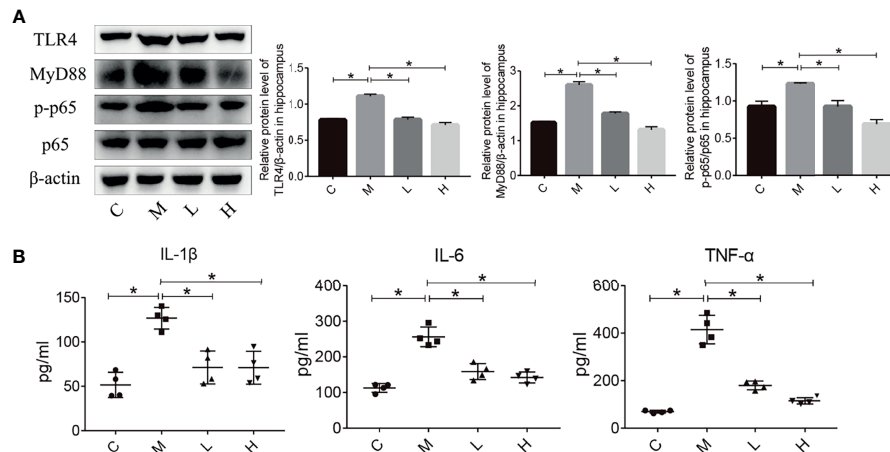


FIGURE 4 | The probiotic combination modulated the TLR4/NFκB signalling pathway and hippocampal inflammation in SAMP8 mice. **(A)** The effect of the probiotic combination on the expression levels of TLR4, MyD88, p-p65 and p65 in the hippocampus. **(B)** The probiotic combination reduced the levels of the pro-inflammatory cytokines IL-1β, IL-6 and TNF-α. C: control group (n = 4), M: model group (n = 4), L: low-dose probiotics group (n = 4), H: high-dose probiotics group (n = 4). Data are presented as the means ± SD. *p < 0.05.

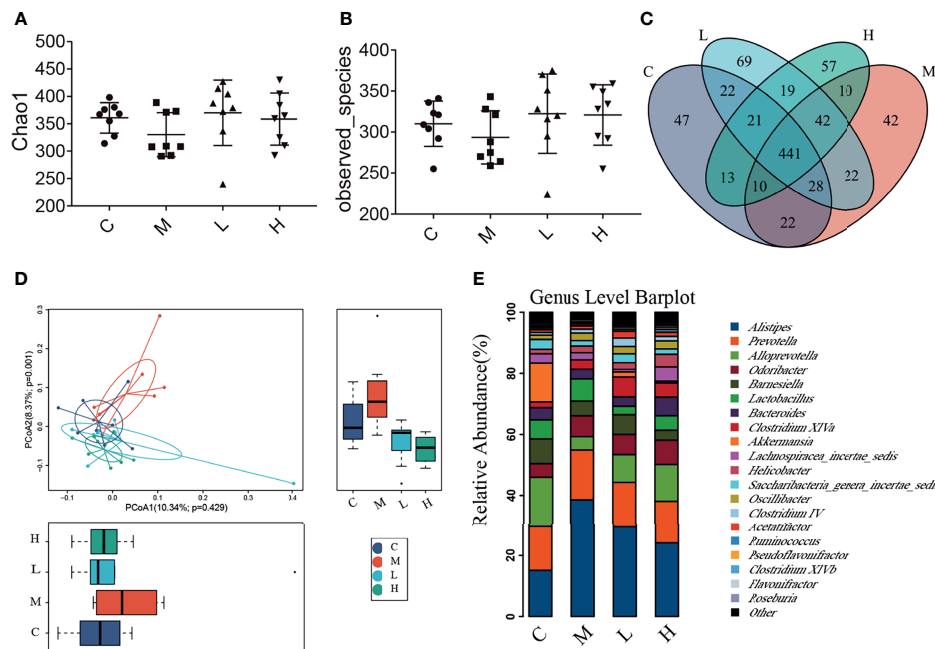


FIGURE 5 | The probiotic combination altered the gut microbiota composition of SAMP8 mice. **(A)** The Chao1 index. **(B)** The Observed_species index. **(C)** The Venn diagram. **(D)** The PCoA analysis. **(E)** Species abundance analysis at the genus level. C, control group (n = 8); M, model group (n = 8); L, low-dose probiotics group (n = 8); H, high-dose probiotics group (n = 8). Data are presented as the means ± SD.

group, there were fewer neurons in the hippocampus of the M group. The probiotic combination could alleviate the loss of neurons in SAMP8 mice (**Figure 3A**). Many studies have shown that the AKT signalling pathway plays a significant role in the apoptosis and metabolism of neurons. The AKT signalling

pathway improves cell survival by regulating forkhead transcription factor (FKHR), as well as mammalian target of rapamycin (mTOR) to increase protein synthesis and affect nerves. The growth of synapses and the development of synaptic plasticity ultimately affect learning and memory

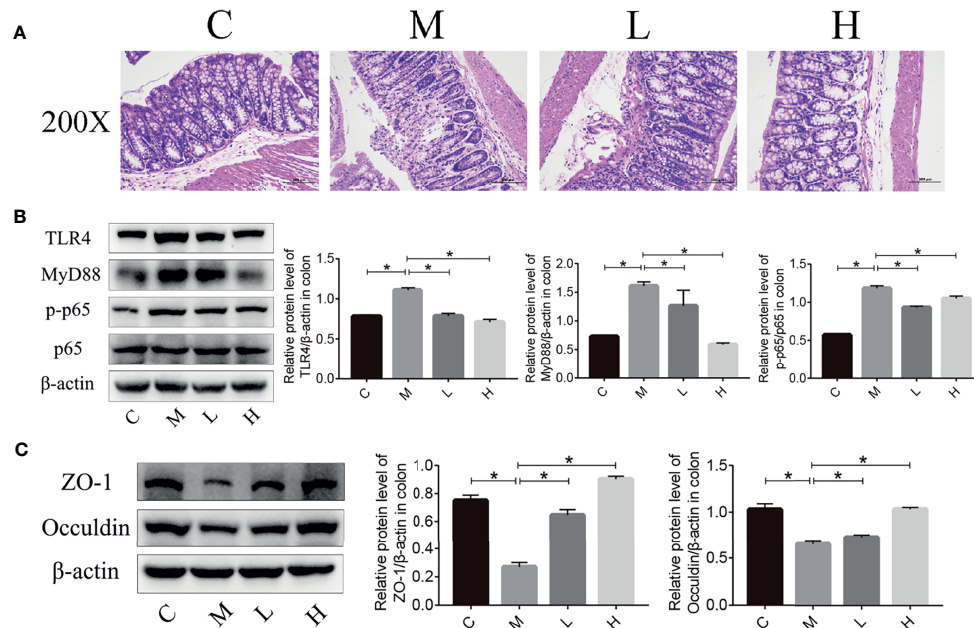


FIGURE 6 | The probiotic combination alleviated colonic inflammation and decreased tight junction protein expression in SAMP8 mice. **(A)** HE staining of the colon. **(B)** The effect of the probiotic combination on the expression levels of TLR4, MyD88, p-p65 and p65 in the colon. **(C)** The effect of the probiotic combination on the expression levels of ZO-1 and Occludin in the colon. C, control group (n = 4); M, model group (n = 4); L, low-dose probiotics group (n = 4); H, high-dose probiotics group (n = 4). Data are presented as the means \pm SD. *p < 0.05.

functions (24, 25). The p-AKT can directly regulate formation of the Bcl-2/Bax heterodimer through phosphoinositide 3-kinase (PI3K)-1 (26). Sirt 1 plays a significant role in the development of the brain and neurons as well as the pathogenesis of AD. Neurodegeneration and cognitive function are significantly improved after injection of a virus encoding Sirt 1 into the hippocampus (27). Research by Zhou et al. (28) also showed that blocking Sirt 1 with small interfering RNA (siRNA) can accelerate AD pathology and cognitive impairment. Moreover, there is an interaction between Sirt 1 and AKT. Histone acetyltransferase (HAT) can inhibit AKT phosphorylation, while Sirt 1 is a histone deacetylase (HDAC) that uses NAD to deacetylate AKT on lysine residues targeted by HAT (29). Sirt 6 is another NAD⁺ dependent deacetylase, Kawahara et al. (30) found that Sirt 6 can be recruited to the promoters of NF κ B downstream genes, reducing the level of promoter acetylation and inhibiting the expression of downstream genes related to apoptosis and cellular senescence. Studies have shown that overexpression of Sirt 6 can increase the healthy lifespan of mice by an average of 30% (31), so Sirt 6 may be another mechanism by which probiotics exert anti-aging effects, although this eventuality requires further study. The detection of NeuN-positive cells, apoptosis, proliferation-related proteins, and Sirt 1 in the hippocampus demonstrated that the probiotic combination can prevent hippocampal neuronal loss (Figure 3). The neuroprotective effect of the probiotic combination on hippocampal neurons may be through the regulation of the AKT signalling pathway and Sirt 1.

Neuroinflammation plays an important part in aging-related neurological diseases such as AD and PD (32). In these diseases, various inflammatory factors (food antigens, lipopolysaccharides, free fatty acids, reactive oxygen species, etc.) bind to TLR and activate NF κ B, an important factor in the immune system and the inflammatory process, after signal transduction. This phenomenon leads to the release of many pro-inflammatory factors (IL-1 β , IL-6, TNF- α , etc.), causing neuroinflammation, damage to the brain, and neuronal death (32, 33). Some drugs can alleviate the progression of neurodegenerative diseases such as AD and PD by modulating neuroinflammation (34, 35). In this study, compared with the M group, the levels of TLR4, MyD88, p-p65/p65, IL-1 β , TNF- α and IL-6 were significantly reduced in the L and H groups (Figure 4), indicating that the probiotic combination can inhibit neuroinflammation in aging mice and protect neurons.

The intestinal microbiota is closely related to human health. Under normal physiological conditions, the host and the intestinal microbiota maintain an ecological balance through synergistic antagonism. Local and continuous abnormal activities of intestinal microbes can cause inflammation of the intestinal mucosa. However, local inflammatory reactions often lead to the occurrence of chronic low-grade inflammation throughout the body. Chronic low-grade inflammation in the intestinal mucosa will result in the destruction of the intestinal barrier, and many harmful factors (lipopolysaccharides, pathogenic bacteria, etc.) will enter the body to induce neuroinflammation (14, 16, 32). We detected changes in the

intestinal microbes of mice by using high-throughput sequencing. Compared with the C group, the diversity and richness of the intestinal microbiota in the M group was decreased. The probiotic combination counteracted these changes in the intestinal microbiota and promoted the restoration of intestinal homeostasis (**Figures 5A, B**). Based on PCoA, we found that after treatment with the probiotic combination, the intestinal microbiota of the aging mice aggregated with the intestinal microbiota of the C group (**Figure 5D**), which indicates that the probiotic combination restores the intestinal microbiota of the aging mice to the composition of normal mice. Consistently with the findings of others, the abundance of *Akkermansia muciniphila* was decreased and the abundance of *Prevotella* was increased in aging mice (15). Moreover, the probiotic combination reduced the relative abundance of *Alistipes* and *Prevotella* (**Figure 5E**). *Akkermansia* can improve metabolism, exerts anti-inflammatory activity, and augments the efficacy of immunotherapy; it is also closely related to the intestinal barrier function. The decline in *Akkermansia* may cause damage to the intestinal barrier and lead to inflammation in the body (36). *Alistipes* is a gram-negative anaerobe and a facultative pathogen. The abundance of *Alistipes* increases in patients with depression (37). In the gut microbes of patients with intestinal irritability syndrome, *Alistipes* tends to increase, and this change may be one of the underlying causes of depression in such patients (38). Researchers have found that *Alistipes* can affect the use of tryptophan, impairing the balance of the serotonergic system in the intestine, and then inhibiting brain electrical activity, which may lead to cognitive dysfunction (37). *Prevotella* is a genus of essential bacteria in a healthy intestinal biota. However, studies have shown that *Prevotellaceae* bacteria increase in the intestinal microbiota of patients with schizophrenia (39). The abundance of *Prevotella* in the intestinal microbiota of patients with cerebral palsy and children with cerebral palsy and epilepsy increases significantly (40). The increased abundance of *Prevotella* may be related to diseases such as periodontitis, bacterial vaginosis, rheumatoid arthritis, metabolic disorders and low-grade systemic inflammation (41–43). This may be due to the intestinal colonisation of *Prevotella* leading to changes in the metabolism of the microbiota, reducing the production of IL-18, which intensifies intestinal inflammation and may lead to systemic autoimmunity (44).

Studies have shown that intestinal barrier dysfunction, and thus chronic inflammation from the intestine, plays an important role in aging (45). Therefore, we examined the pathological changes of colon in mice and detected the expression of components of the TLR4/NFκB inflammatory pathway (TLR4, MyD88 and p-p65) and tight junction proteins (ZO-1 and Occludin) in the colon. The mucosal epithelial cells in the colon of aging mice were shed and a small amount of intestinal gland structure was destroyed. The probiotic combination counteracted these changes (**Figure 6A**). Compared with the C group, the TLR4/NFκB signalling pathway was activated in the M group, with increased the expression of the inflammation-related proteins TLR4 and MyD88, which in turn increased the level of p-p65 (**Figure 6B**). At the same time,

Probiotics combination regulate the microbiota-gut-brain axis and alleviate aging in SAMP8 mice

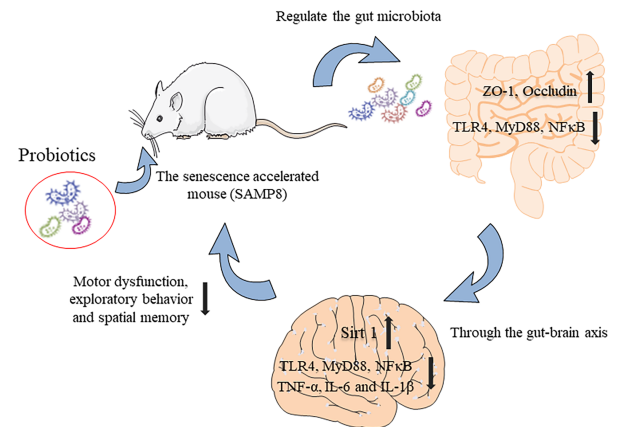


FIGURE 7 | Graphical summary of this study. The probiotic combination, determined by screening the faeces of centenarians, can increase the expression of intestinal permeability-related proteins ZO-1 and Occludin by regulating the intestinal microbiota. It also inhibits TLR4/NFκB-induced intestinal inflammation and then inhibits TLR4/NFκB-induced neuroinflammation through the gut-brain axis and up-regulates the expression of Sirt1 to protect hippocampal neurons. These changes underlie the improved spatial memory, motor function, and exploratory behaviour of aging mice.

the expression of ZO-1 and Occludin decreased significantly (**Figure 6C**). Treatment with the probiotic combination relieved the intestinal inflammation and increased the integrity of the intestinal barrier.

In summary, we have shown that the probiotic combination, developed by screening the faeces of centenarians, increases the expression of intestinal permeability-related proteins ZO-1 and Occludin by regulating the intestinal microbiota. It also inhibits TLR4/NFκB-induced intestinal inflammation and consequently, neuroinflammation through the gut-brain axis and upregulates the expression of Sirt1 to protect hippocampal neurons (**Figure 7**). These changes underlie improved spatial memory, motor function and exploratory behaviour of aging mice. Our research provides the basis for the probiotic combination to become a dietary supplement for anti-aging.

DATA AVAILABILITY STATEMENT

The data presented in the study are deposited in the GenBank repository, accession number PRJNA768326.

ETHICS STATEMENT

The animal study was reviewed and approved by the Laboratory Animal Ethics Committee of Nanchang Royo Biotech Co., Ltd (license No. RYE2020051401) on May 14, 2020.

AUTHOR CONTRIBUTIONS

XF and TC contributed to conception and design of the study. XZ, MY, and JW performed the experiments. YW, DH, and BW carried out data analysis. All authors participated in drafting of the manuscript and critical revision of the draft and contributed to the article and approved the submitted version.

FUNDING

This work was supported by grants from the National Natural Science Foundation of China (Nos. 82060638, 82060222), Science and Technology Plan of Jiangxi Health Planning Committee (Nos. 20195092), the Science and Technology Project of Jiangxi (Nos. 20194BCJ22032, 20192BBG70031),

Nanchang Hongcheng Project to TC, and double 10-thousand plan of Jiangxi Province (innovation and technology professionals as the high-end talent).

SUPPLEMENTARY MATERIAL

The Supplementary Material for this article can be found online at: <https://www.frontiersin.org/articles/10.3389/fimmu.2021.792746/full#supplementary-material>

Supplementary Figure 1 | The probiotic combination delayed the decrease in body weight and the increase in the aging score of SAMP8 mice. **(A)** The experimental design of this study. **(B)** Weekly body weight changes of SAMP8 mice during gavage of the probiotic combination. **(C)** The aging degree scores of SAMP8 mice after gavage of the probiotic combination. C: control group (n = 10), M: model group (n = 9), L: low-dose probiotics group (n = 8), H: high-dose probiotics group (n = 9). Data are presented as the means \pm SD. *p < 0.05 **p < 0.01.

REFERENCES

- Cano M, Guerrero-Castilla A, Nabavi SM, Ayala A, Argüelles S. Targeting Pro-Senescence Mitogen Activated Protein Kinase (Mapk) Enzymes With Bioactive Natural Compounds. *Food Chem Toxicol an Int J Published Br Ind Biol Res Assoc* (2019) 131:110544. doi: 10.1016/j.fct.2019.05.052
- Morelli N, Barelli S, Mayan M, Graffigna G. Supporting Family Caregiver Engagement in the Care of Old Persons Living in Hard to Reach Communities: A Scoping Review. *Health Soc Care Commun* (2019) 27:1363–74. doi: 10.1111/hsc.12826
- McHugh D, Gil J. Senescence and Aging: Causes, Consequences, and Therapeutic Avenues. *J Cell Biol* (2018) 217:65–77. doi: 10.1083/jcb.201708092
- Mattson MP, Arumugam TV. Hallmarks of Brain Aging: Adaptive and Pathological Modification by Metabolic States. *Cell Metab* (2018) 27:1176–99. doi: 10.1016/j.cmet.2018.05.011
- Nie X, Chen Y, Li W, Lu Y. Anti-Aging Properties of Dendrobium Nobile Lindl.: From Molecular Mechanisms to Potential Treatments. *J Ethnopharmacol* (2020) 257:112839. doi: 10.1016/j.jep.2020.112839
- Guedj A, Volman Y, Geiger-Maor A, Bolik J, Schumacher N, Künzel S, et al. Gut Microbiota Shape 'Inflamm-Ageing' Cytokines and Account for Age-Dependent Decline in DNA Damage Repair. *Gut* (2020) 69:1064–75. doi: 10.1136/gutjnl-2019-318491
- Michaud M, Balardy L, Moulis G, Gaudin C, Peyrot C, Vellas B, et al. Proinflammatory Cytokines, Aging, and Age-Related Diseases. *J Am Med Directors Assoc* (2013) 14:877–82. doi: 10.1016/j.jamda.2013.05.009
- Morshedi M, Hashemi R, Moazzen S, Sahebkar A, Hosseinfard ES. Immunomodulatory and Anti-Inflammatory Effects of Probiotics in Multiple Sclerosis: A Systematic Review. *J Neuroinflamm* (2019) 16:231. doi: 10.1186/s12974-019-1611-4
- López-Otin C, Blasco MA, Partridge L, Serrano M, Kroemer G. The Hallmarks of Aging. *Cell* (2013) 153:1194–217. doi: 10.1016/j.cell.2013.05.039
- Kalogeropoulos A, Georgiopoulos V, Psaty BM, Rodondi N, Smith AL, Harrison DG, et al. Inflammatory Markers and Incident Heart Failure Risk in Older Adults: The Health ABC (Health, Aging, and Body Composition) Study. *J Am Coll Cardiol* (2010) 55:2129–37. doi: 10.1016/j.jacc.2009.12.045
- Bruunsgaard H, Ladelund S, Pedersen AN, Schroll M, Jørgensen T, Pedersen BK. Predicting Death From Tumour Necrosis Factor-Alpha and Interleukin-6 in 80-Year-Old People. *Clin Exp Immunol* (2003) 132:24–31. doi: 10.1046/j.1365-2249.2003.02137.x
- Haran JP, McCormick BA. Aging, Frailty, and the Microbiome-How Dysbiosis Influences Human Aging and Disease. *Gastroenterol* (2021) 160:507–23. doi: 10.1053/j.gastro.2020.09.060
- Quigley EMM. Microbiota-Brain-Gut Axis and Neurodegenerative Diseases. *Curr Neurol Neurosci Rep* (2017) 17:94. doi: 10.1007/s11910-017-0802-6
- Wang HX, Wang YP. Gut Microbiota-Brain Axis. *Chin Med J* (2016) 129:2373–80. doi: 10.4103/0366-6999.190667
- Bárcena C, Valdés-Mas R, Mayoral P, Garabaya C, Durand S, Rodríguez F, et al. Healthspan and Lifespan Extension by Fecal Microbiota Transplantation Into Progeroid Mice. *Nat Med* (2019) 25:1234–42. doi: 10.1038/s41591-019-0504-5
- Bialecka-Dębek A, Granda D, Szmidi MK, Zielińska D. Gut Microbiota, Probiotic Interventions, and Cognitive Function in the Elderly: A Review of Current Knowledge. *Nutrients* (2021) 13:2514. doi: 10.3390/nu13082514
- Deng K, Chen T, Wu Q, Xin H, Wei Q, Hu P, et al. *In Vitro* and *In Vivo* Examination of Anticolonization of Pathogens by Lactobacillus Paracasei FJ861111.1. *J Dairy Sci* (2015) 98:6759–66. doi: 10.3168/jds.2015-9761
- Xia C, Cao X, Cui L, Liu H, Wang S, Chen T. Anti-Aging Effect of the Combination of Bifidobacterium Longum and B. Animalis in a D-Galactose-Treated Mice. *J Funct Foods* (2020) 69:103938. doi: 10.1016/j.jff.2020.103938
- Hosokawa M, Kasai R, Higuchi K, Takeshita S, Shimizu K, Hamamoto H, et al. Grading Score System: A Method for Evaluation of the Degree of Senescence in Senescence Accelerated Mouse (SAM). *Mech Ageing Dev* (1984) 26:91–102. doi: 10.1016/0047-6374(84)90168-4
- Rognes T, Flouri T, Nichols B, Quince C, Mahé F. VSEARCH: A Versatile Open Source Tool for Metagenomics. *PeerJ* (2016) 4:e2584. doi: 10.7717/peerj.2584
- da Costa JP, Vitorino R, Silva GM, Vogel C, Duarte AC, Rocha-Santos T. A Synopsis on Aging-Theories, Mechanisms and Future Prospects. *Ageing Res Rev* (2016) 29:90–112. doi: 10.1016/j.arr.2016.06.005
- Liu B, Liu J, Shi JS. SAMP8 Mice as a Model of Age-Related Cognition Decline With Underlying Mechanisms in Alzheimer's Disease. *J Alzheimer's Dis JAD* (2020) 75:385–95. doi: 10.3233/jad-200063
- Lazarov O, Hollands C. Hippocampal Neurogenesis: Learning to Remember. *Prog Neurobiol* (2016) 138–140:1–18. doi: 10.1016/j.pneurobio.2015.12.006
- Jo H, Mondal S, Tan D, Nagata E, Takizawa S, Sharma AK, et al. Small Molecule-Induced Cytosolic Activation of Protein Kinase Akt Rescues Ischemia-Elicited Neuronal Death. *Proc Natl Acad Sci USA* (2012) 109:10581–6. doi: 10.1073/pnas.1202810109
- Fournier NM, Lee B, Banasr M, Elsayed M, Duman RS. Vascular Endothelial Growth Factor Regulates Adult Hippocampal Cell Proliferation Through MEK/ERK- and PI3K/Akt-Dependent Signaling. *Neuropharmacol* (2012) 63:642–52. doi: 10.1016/j.neuropharm.2012.04.033
- Li H, Tang Z, Chu P, Song Y, Yang Y, Sun B, et al. Neuroprotective Effect of Phosphocreatine on Oxidative Stress and Mitochondrial Dysfunction Induced Apoptosis *In Vitro* and *In Vivo*: Involvement of Dual PI3K/Akt and Nrf2/HO-1 Pathways. *Free Radical Biol Med* (2018) 120:228–38. doi: 10.1016/j.freeradbiomed.2018.03.014
- Kim D, Nguyen MD, Dobbin MM, Fischer A, Sananbenesi F, Rodgers JT, et al. SIRT1 Deacetylase Protects Against Neurodegeneration in Models for Alzheimer's Disease and Amyotrophic Lateral Sclerosis. *EMBO J* (2007) 26:3169–79. doi: 10.1038/sj.emboj.7601758
- Zhou Y, Zhu F, Liu Y, Zheng M, Wang Y, Zhang D, et al. Blood-Brain Barrier-Penetrating siRNA Nanomedicine for Alzheimer's Disease Therapy. *Sci Advances* (2020) 6:7031. doi: 10.1126/sciadv.abc7031

29. Lin JY, Kuo WW, Baskaran R, Kuo CH, Chen YA, Chen WS, et al. Swimming Exercise Stimulates IGF1/ PI3K/Akt and AMPK/Sirt1/Pgc1 α Survival Signaling to Suppress Apoptosis and Inflammation in Aging Hippocampus. *Aging* (2020) 12:6852–64. doi: 10.18632/aging.103046
30. Kawahara TL, Michishita E, Adler AS, Damian M, Berber E, Lin M, et al. SIRT6 Links Histone H3 Lysine 9 Deacetylation to NF-kappaB-Dependent Gene Expression and Organismal Life Span. *Cell* (2009) 136:62–74. doi: 10.1016/j.cell.2008.10.052
31. Roichman A, Elhanati S, Aon MA, Abramovich I, Di Francesco A, Shahar Y, et al. Restoration of Energy Homeostasis by SIRT6 Extends Healthy Lifespan. *Nat Commun* (2021) 12:3208. doi: 10.1038/s41467-021-23545-7
32. Sampson TR, Debelius JW, Thron T, Janssen S, Shastri GG, Ilhan ZE, et al. Gut Microbiota Regulate Motor Deficits and Neuroinflammation in a Model of Parkinson's Disease. *Cell* (2016) 167:1469–80.e12. doi: 10.1016/j.cell.2016.11.018
33. Megur A, Baltrikienė D, Bukelskienė V, Burokas A. The Microbiota-Gut-Brain Axis and Alzheimer's Disease: Neuroinflammation Is to Blame? *Nutrients* (2020) 13:37. doi: 10.3390/nu13010037
34. Yang Q, Luo L, Sun T, Yang L, Cheng LF, Wang Y, et al. Chronic Minocycline Treatment Exerts Antidepressant Effect, Inhibits Neuroinflammation, and Modulates Gut Microbiota in Mice. *Psychopharmacol* (2020) 237:3201–13. doi: 10.1007/s00213-020-05604-x
35. Dong Y, Li X, Cheng J, Hou L. Drug Development for Alzheimer's Disease: Microglia Induced Neuroinflammation as a Target? *Int J Mol Sci* (2019) 20:558. doi: 10.3390/ijms20030558
36. Geerlings SY, Kostopoulos I, de Vos WM, Belzer C. Akkermansia Muciniphila in the Human Gastrointestinal Tract: When, Where, and How? *Microorganisms* (2018) 6:75. doi: 10.3390/microorganisms6030075
37. Ait-Belgnaoui A, Colom A, Braniste V, Ramalho L, Marrot A, Cartier C, et al. Probiotic Gut Effect Prevents the Chronic Psychological Stress-Induced Brain Activity Abnormality in Mice. *Neurogastroenterol Motil Off J Eur Gastrointestinal Motil Soc* (2014) 26:510–20. doi: 10.1111/nmo.12295
38. Hsiao EY, McBride SW, Hsien S, Sharon G, Hyde ER, McCue T, et al. Microbiota Modulate Behavioral and Physiological Abnormalities Associated With Neurodevelopmental Disorders. *Cell* (2013) 155:1451–63. doi: 10.1016/j.cell.2013.11.024
39. Grochowska M, Wojnar M, Radkowski M. The Gut Microbiota in Neuropsychiatric Disorders. *Acta Neurobiologiae Exp* (2018) 78:69–81. doi: 10.21307/ane-2018-008
40. Huang C, Li Y, Feng X, Li D, Li X, Ouyang Q, et al. Distinct Gut Microbiota Composition and Functional Category in Children With Cerebral Palsy and Epilepsy. *Front Pediatr* (2019) 7:394. doi: 10.3389/fped.2019.00394
41. Kovatcheva-Datchary P, Nilsson A, Akrami R, Lee YS, De Vadder F, Arora T, et al. Dietary Fiber-Induced Improvement in Glucose Metabolism Is Associated With Increased Abundance of Prevotella. *Cell Metab* (2015) 22:971–82. doi: 10.1016/j.cmet.2015.10.001
42. Randis TM, Ratner AJ. Gardnerella and Prevotella: Co-Conspirators in the Pathogenesis of Bacterial Vaginosis. *J Infect Dis* (2019) 220:1085–8. doi: 10.1093/infdis/jiy705
43. Arweiler NB, Netuschil L. The Oral Microbiota. *Adv Exp Med Biol* (2016) 902:45–60. doi: 10.1007/978-3-319-31248-4_4
44. Iljazovic A, Roy U, Gálvez EJC, Lesker TR, Zhao B, Gronow A, et al. Perturbation of the Gut Microbiome by Prevotella Spp. Enhances Host Susceptibility to Mucosal Inflammation. *Mucosal Immunol* (2021) 14:113–24. doi: 10.1038/s41385-020-0296-4
45. Kühn F, Adiliaghdam F, Cavallaro PM, Hamarneh SR, Tsurumi A, Hoda RS, et al. Intestinal Alkaline Phosphatase Targets the Gut Barrier to Prevent Aging. *JCI Insight* (2020) 5:134049. doi: 10.1172/jci.insight.134049

Conflict of Interest: The authors declare that the research was conducted in the absence of any commercial or financial relationships that could be construed as a potential conflict of interest.

Publisher's Note: All claims expressed in this article are solely those of the authors and do not necessarily represent those of their affiliated organizations, or those of the publisher, the editors and the reviewers. Any product that may be evaluated in this article, or claim that may be made by its manufacturer, is not guaranteed or endorsed by the publisher.

Copyright © 2021 Fang, Yue, Wei, Wang, Hong, Wang, Zhou and Chen. This is an open-access article distributed under the terms of the Creative Commons Attribution License (CC BY). The use, distribution or reproduction in other forums is permitted, provided the original author(s) and the copyright owner(s) are credited and that the original publication in this journal is cited, in accordance with accepted academic practice. No use, distribution or reproduction is permitted which does not comply with these terms.

Advantages of publishing in Frontiers



OPEN ACCESS

Articles are free to read
for greatest visibility
and readership



FAST PUBLICATION

Around 90 days
from submission
to decision



HIGH QUALITY PEER-REVIEW

Rigorous, collaborative,
and constructive
peer-review



TRANSPARENT PEER-REVIEW

Editors and reviewers
acknowledged by name
on published articles

Frontiers

Avenue du Tribunal-Fédéral 34
1005 Lausanne | Switzerland

Visit us: www.frontiersin.org

Contact us: frontiersin.org/about/contact



REPRODUCIBILITY OF RESEARCH

Support open data
and methods to enhance
research reproducibility



DIGITAL PUBLISHING

Articles designed
for optimal readership
across devices



FOLLOW US

@frontiersin



IMPACT METRICS

Advanced article metrics
track visibility across
digital media



EXTENSIVE PROMOTION

Marketing
and promotion
of impactful research



LOOP RESEARCH NETWORK

Our network
increases your
article's readership